BST

BioScience Trends

IRCA
BSSA

IACMHR

www.biosciencetrends.com

BioScience Trends is one of a series of peer-reviewed journals of the International Research and Cooperation Association for Bio & Socio-Sciences Advancement (IRCA-BSSA) Group and is published bimonthly by the International Advancement Center for Medicine & Health Research Co., Ltd. (IACMHR Co., Ltd.) and supported by the IRCA-BSSA and Shandong University China-Japan Cooperation Center for Drug Discovery & Screening (SDU-DDSC).

BioScience Trends devotes to publishing the latest and most exciting advances in scientific research. Articles cover fields of life science such as biochemistry, molecular biology, clinical research, public health, medical care system, and social science in order to encourage cooperation and exchange among scientists and clinical researchers.

BioScience Trends publishes Original Articles, Brief Reports, Reviews, Policy Forum articles, Case Reports, News, and Letters on all aspects of the field of life science. All contributions should seek to promote international collaboration.

BioScience Trends

Editorial and Head Office

Pearl City Koishikawa 603, 2-4-5 Kasuga, Bunkyo-ku,
Tokyo 112-0003, Japan

Tel: +81-3-5840-8764, Fax: +81-3-5840-8765
E-mail: office@biosciencetrends.com
URL: www.biosciencetrends.com

CONTENTS   *Volume 12, Number 3, 2018*

CONTENTS   (*Continued*)

Brief Report

Communication

Guide for Authors

Copyright

215

Policy Forum

Reducing the medical economic burden of health insurance in China: Achievements and challenges

Guanshen Dou[1], Qun Wang[2], Xiaohua Ying[1,*]

[1] *Department of Health Economics, School of Public Health, Fudan University, Shanghai, China;*
[2] *Faculty of Humanities and Social Sciences, Dalian University of Technology, Dalian City, Liaoning Province, China.*

Summary	The aims of this study were to describe health insurance reforms initiated by the Chinese government over the past two decades, to review their achievements in reducing the medical economic burden, and to summarize the challenges that still exist regarding a further reduction in out-of-pocket expenditures in this country. China has successfully attained the goal of providing health insurance coverage to almost the entire population by developing a mixed health insurance system, which consists of Urban Employees Basic Medical Insurance (UEBMI), Urban Resident Basic Medical Insurance (URBMI), New Rural Cooperative Medical Scheme (NCMS), and supplementary Catastrophic Health Insurance. Despite this achievement, China is still facing the challenges of a disparity in the medical economic burden by region and by health insurance scheme, relatively little protection from financial risk compared to developed countries, as well as low efficiency and quality of care under current payment systems. To further reduce the disparity in the medical economic burden and to increase the overall protection from financial risk in China, the Government should increase central government transfers to NCMS and URBMI enrollees in poor regions and increase the total amount of government subsidies to NCMS. In addition, China should improve the efficiency and quality of health insurance by further reforming the payment system.

Keywords: Out-of-pocket expenditure, health insurance, health care expenditure, China

1. Introduction

Between 1950 and 1980, the vast majority of Chinese residents were covered by urban or rural health insurance schemes. Since the late 1980s, however, the traditional rural health insurance scheme collapsed and traditional urban health insurance schemes were crippled due to the inefficiency and debt of state-owned enterprises. Since then, the Chinese population has been faced with considerable out-of-pocket (OOP) expenditures (*1*). From 1990 to 2001, OOP expenditures grew tenfold, and the share of OOP expenditures increased to 59.97% in 2001 (*2*). However, per capita income grew only five- or fourfold during the period (*3*). Such a large medical

*Address correspondence to:
Dr. Xiaohua Ying, Department of Health Economics, School of Public Health, Fudan University, No. 187 box, Yixueyuan Road No.138, Xuhui District, Shanghai 200032, China.
E-mail: xhying@fudan.edu.cn

economic burden resulted in a very large proportion of the population facing catastrophic expenditures and impoverishment due to OOP health expenses (*4*). Social health insurance has been as a primary focus of efforts to provide financial protection from illness-related costs for the Chinese population and populations in other low- and middle-income countries (*5*). Over the past two decades, the Chinese government has been working to reduce residents' medical economic burden through various health insurance reforms with the aim of achieving universal health coverage (UHC) by 2020. This paper will first describe health insurance reforms initiated by the Chinese government over the last two decades, and it will then summarize their achievements in reducing the medical economic burden. This paper will then focus on the challenges that still exist regarding a further reduction in OOP expenditures in China.

2. Health insurance reforms and their achievements in reducing the medical economic burden

Health insurance reforms over the last two decades have

Source: Statistical Yearbook of Health and Family Planning in China 2016

Figure 1. OOP expenditure share of health expenditure in China (%).

occurred in two major stages: establishing and initially developing health insurance schemes from 1994 to 2008, and further reforming health insurance schemes in a comprehensive manner from 2009 to the present.

The first stage of health insurance reforms started with a pilot project in Jiujiang and Zhenjiang to replace traditional urban health insurance schemes. Based on experiences in those two cities, the Chinese government formally established a mandatory social insurance program for urban employees - Urban Employees Basic Medical Insurance (UEBMI) - in 1998 (*6*). UEBMI is financed through payroll (8-14%), from both employer (6%) and employee (2%) contributions.

In late 2002, the Chinese government decided to establish the New Rural Cooperative Medical Scheme (NCMS) for rural residents in order to rebuild the rural health insurance scheme. In the NCMS, premiums come mainly from the central and local governments while the rest comes from individual contributions (*7*). As shown in Figure 1, the share of OOP expenditures out of total health care expenditures has decreased every year since 2002 as the number of participants in NCMS has increased.

After the implementation of UEBMI and NCMS, the only groups not covered by basic health insurance were children, students, the elderly, the disabled, and other unemployed populations in urban regions. Therefore, the Chinese government established Urban Resident Basic Medical Insurance (URBMI) for those groups in 2007 (*3,8*). URBMI is also mainly financed by the government, and urban families only contribute a small share of premiums (*2*).

Although the three basic insurance schemes covered 87% of the total population in 2008, the expense of seeing a doctor was a common problem at the time (*9*). The ratio of OOP expenditures per capita to household expenditures per capita dropped slightly (*10*). In addition, NCMS and URBMI offered relatively few

benefits compared to UEBMI in 2008. The inpatient reimbursement rate is 38% for NCMS, 44% for URBMI, and 67% for UEBMI, and the NCMS and URBMI schemes covered few outpatient services in 2008 (*11*). In light of the lack of financial protection from risk, the Chinese government initiated a new series of health sector reforms in 2009 that explicitly described the expansion of basic health insurance schemes as one of their primary objectives (*12*). Since then, the Chinese government has been committed to further reforming health insurance schemes in a comprehensive manner.

In the new series of health sector reform, the Chinese government first increased government subsidies to NCMS and URBMI to an unprecedented scale. In 2008, the Government provided 80 RMB/person/year to each participant in NCMS and URBMI, while in 2016 this amount rose to 420 RMB/person/year (*13*). Accordingly, benefits under the two insurance schemes were greatly increased. In 2012, the inpatient reimbursement rate and the outpatient reimbursement rate of the two insurance schemes both increased to 55% and 50%, respectively (*11*).

To further reduce the medical economic burden, the Government decided to launch Catastrophic Disease Insurance in 2012 (*14*). This scheme is financed by basic health insurance funds and is managed by commercial insurance companies. It provides the same coverage as that of basic health insurance, and its participants are covered by basic health insurance as well. Participants are allowed to receive extra reimbursements for medical expenses after they are reimbursed by basic health insurance. The specific reimbursement rate is defined at the local level, but the central government required that the rate of extra reimbursement be no less than 50%. In 2013, more than 200 million people participated in Catastrophic Disease Insurance (*15*). In 2015, the Catastrophic Disease Insurance scheme was fully implemented in China (*16*).
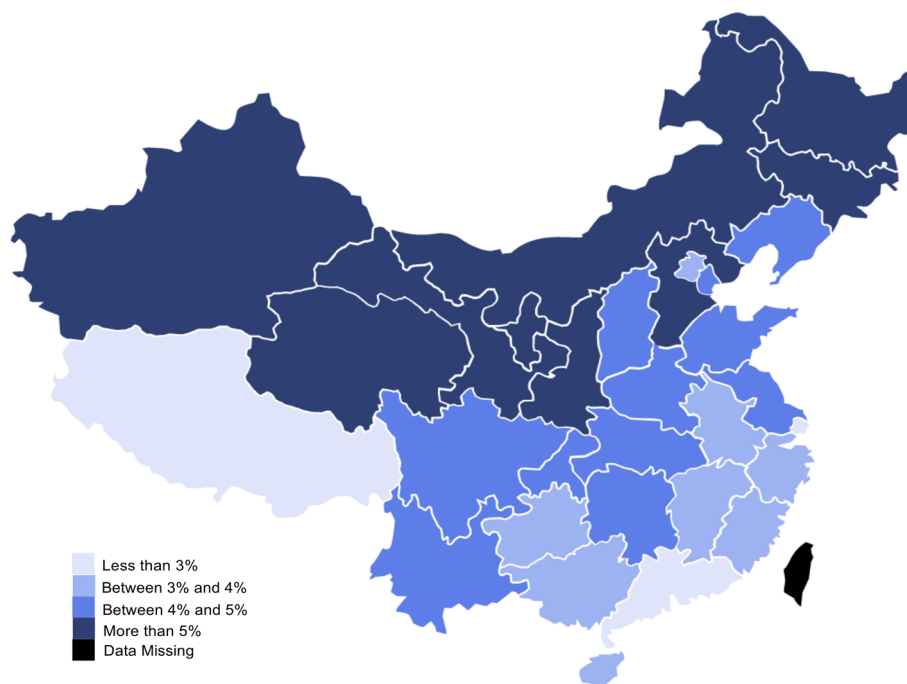
Source: Statistical Yearbook of Health and Family planning in China 2017, China Statistical Yearbook 2017

Figure 2. OOP per capita as percentage of average annual disposable income per capita of each province in 2015 (%).

Moreover, in 2009, the Chinese government began attempting to integrate NCMS and URBMI, which means unified funding pools, levels of benefits, and payment systems for NCMS and URBMI. Afterwards, many provinces or municipalities such as Tianjin, Chongqing, and Guangdong integrated NCMS and URBMI. In early 2016, the Chinese government announced that it was promoting the integration of NCMS and URBMI nationwide (*17*). In recent years, the integration of NCMS and URBMI has proceeded at a faster pace. This integration has received strong support from the Chinese population, and especially from rural residents (*18*). Suzhou, Shenzhen, Dongguan, and Zhongshan have gone even further by consolidating UEBMI, NCMS, and URBMI at the same time.

In addition, the payment mechanism also influences OOP expenditures (*19,20*). Fee-for-service (FFS) was previously the only common mechanism of payment in China. Under an FFS system, payment is made after care, so physicians are inclined to provide more services, which result in huge health care expenditures (*21*). In 2009, the Chinese government decided to replace FFS with other forms of prospective payment. In recent years, prospective payment systems such as the global budget payment system (GBPS) have been implemented in most provinces. In mid-2017, the Chinese government decided to fully implement a compound payment system based on DRGs and to further reduce the use of FFS, signaling the implementation of payment reform nationwide (*22*).

After more than two decades of considerable efforts, the three schemes (*i.e.* UEBMI, NCMS, and URBMI) combined have ensured coverage for almost the entire Chinese population, with rates currently approaching 95% (*2,23*). Moreover, the share of OOP expenditures out of total health care expenditures finally dropped to 29.27% in 2015, thus halving the share in 2001 (Figure 1).

3. Challenges still exist regarding a further reduction in OOP expenditures

Even though China has made startling achievements in extending health insurance coverage and in reducing OOP expenditures in such a short time, difficulties still exist regarding a further reduction in the medical economic burden and fully achieving the goal of UHC.

Regional disparities represent the greatest challenge. Eastern China has a much higher level of economic development than middle and western China, and middle China is less developed than western China. Figure 2 shows the percentage of OOP payments per capita with respect to the average annual disposable income per capita by province in 2015. Populations in Ningxia and Shaanxi Province respectively spend 6.46% and 6.24% of their annual disposable income per capita on OOP health expenses, and these figures are almost 2 times what the populations in Guangdong Province and the City of Shanghai spend. In general, the medical economic burden is much smaller in southeastern provinces than that in other regions. In addition, a higher percentage of individuals do not receive care due to financial reasons in middle and western regions than in other regions (Table 1). Thus, the level of economic development is inversely associated with the medical economic burden.

A disparity in the medical economic burden exists

Table 1. Reasons why individuals were not treated in 2013 (%)

Reason	Total	Urban				Rural			
		Total	East	Middle	West	Total	East	Middle	West
Self-healing	69.8	71.0	73.8	73.3	68.0	68.1	72.2	69.8	61.5
Economics	7.6	7.7	4.5	10.5	8.3	7.4	4.4	6.9	11.5
Inconvenience	5.2	5.6	6.8	5.0	5.1	4.6	5.3	4.8	3.6
No time	4.5	4.2	4.5	2.5	4.9	4.9	3.8	4.8	6.3
Other	13.0	11.6	10.4	8.7	13.7	15.0	14.3	13.8	17.1

Source: An Analysis Report of National Health Services Survey in China, 2013.

among the three basic insurance schemes. Studies have found that after the three health insurance schemes were consolidated, NCMS had an inpatient reimbursement rate of 52.5% and an outpatient reimbursement rate 56% in Suzhou in 2014, and these rates were about 20% lower than those of UEBMI and URBMI (*24*). This is because NCMS still provides fewer benefits than the other two health insurance schemes,.

In addition, China faces the challenge of relatively little protection from financial risk due to catastrophic medical expenditures despite a series of health insurance reforms (*25*). The share of OOP expenditures out of total health care expenditures in China is still much higher than that in higher income countries (*26*). According to a report by the World Health Organization on UHC worldwide in 2017, 17.7% of the Chinese population spent greater than 10% of their household budget on OOP health payments, which was much higher than that in OECD countries (*27*). Currently, more than 40% of the poor population is impoverished due to illness, and this rate has increased in recent years (*28*).

Moreover, the payment mechanisms currently used in China have led to difficulties in reducing OOP expenditures. GBPS and FFS are the two main payment systems in China, and local governments usually use a single payment system (*29*). FFS may lower the efficiency of health service utilization by providing unnecessary services (*21*). GBPS is proved to have a greater influence on total health care expenditures than on OOP expenditures (*30*). Moreover, GBPS could reduce the quality of medical services and hospital efficiency by rejecting critical patients and shortening the duration of hospitalization (*29,31-34*). In light of those circumstances, the Chinese government is promoting a compound payment system based on DRGs that has proven to be able to control expenditures without affecting the quality of medical services in other settings (*35*). Payment system reform is a challenge worldwide, and further studies are needed to evaluate the actual effects of the latest reform of payment systems in China.

4. Conclusion

Over the last two decades, the Chinese government has been devoted to reducing the medical economic burden through health insurance reforms. This started with the establishment of three health insurance schemes, *i.e.* UEBMI, URBMI, and NCMS. Health insurance has subsequently been reformed to attain the goal of UHC by 2020, including greater benefits under the three insurance schemes, establishment of catastrophic insurance, consolidating NCMS and URBMI, and transformation of the payment system. After more than two decades of efforts, the share of OOP expenditures out of total health care expenditures decreased to less than 30%, and more than 95% of population was covered by a health insurance scheme in 2015. However, China is still facing the challenges of a disparity in the medical economic burden by region and by health insurance scheme, relatively little protection from financial risk compared to other developing countries, as well as low efficiency and quality of care related to the current payment systems. In light of China's achievements in providing protection from financial risk, the most critical element of that effort's success is substantial government involvement. To further reduce the disparity in the medical economic burden and to increase the overall protection from financial risk in China, the Government should increase central government transfers to NCMS and URBMI enrollees in poor regions and increase the total amount of government subsidies to NCMS. In addition, China should improve the efficiency and quality of health insurance by further reforming the payment system.

References

1. Liu Y. Reforming China's urban health insurance system. Health Policy. 2002; 60:133-150.
2. National Health and Family Planning Commission of China. Statistical Yearbook of Health and Family Planning in China 2016. Union Medical University Press, 2016.
3. Cao Q, Shi L, Wang H, Dong K. Report from China: health insurance in China – Evolution, current status, and challenges. Int J Health Serv. 2012; 42:177-195.
4. Hsiao W, Li MQ, Zhang SF. Universal health coverage: The case of China, United Nations Research Institute for Social Development (UNRISD) Working Paper, No. 2014-15. *http://www.unrisd.org/80256B3C005BCCF9/ (httpAuxPages)/E15A4915BFDBEE8AC1257D9E0033 BACE/$file/Hsiao%20et%20al.pdf* (accessed March 29, 2018).
5. Doetinchem O, Carrin G, Evans D. World Health Report (2010): Thinking of introducing social health insurance? – Ten questions. *http://158.232.12.119/healthsystems/topics/*

financing/healthreport/26_10Q.pdf (accessed March 29, 2018).

6. Xin H. Experiences and lessons from urban health insurance reform in China. Popul Health Manag. 2016; 19:291-297.

7. The State Council of the Communist Party of China. Decisions on efforts to further enhance rural health. *http://www.gov.cn/gongbao/content/2002/content_61818.htm* (accessed March 29, 2018). (in Chinese)

8. Tang S, Tao J, Bekedam H. Controlling cost escalation of healthcare: Making universal health coverage sustainable in China. BMC Public Health. 2012; 12 Suppl 1:S8.

9. Center for Health Statistics and Information. Report on a 2008 national health services survey in China. *http://www.moh.gov.cn/cmsresources/mohwsbwstjxxzx/cmsrsdocument/doc9911.pdf* (accessed March 29, 2018). (in Chinese)

10. Long Q, Xu L, Bekedam H, Tang S. Changes in health expenditures in China in 2000s: Has the health system reform improved affordability? Int J Equity Health. 2013; 12:40.

11. Yip WC, Hsiao WC, Chen W, Hu S, Ma J, Maynard A. Early appraisal of China's huge and complex health-care reforms. Lancet. 2012; 379 :833-842.

12. Chen Z. Launch of the health-care reform plan in China. Lancet. 2009; 373:1322-1324.

13. China Financial and Economic News. Financial subsidy for residents will be increased to CNY 420 in 2016. *http://www.cfen.com.cn/cjxw/cz/201605/t20160506_1978932.html* (accessed March 29, 2018). (in Chinese)

14. National Development and Reform Commission. Guidance on efforts to provide catastrophic disease insurance to urban and rural residents *http://www.scio.gov.cn/32344/32345/32347/33156/xgzc33162/Document/1442272/1442272.htm.* (accessed March 29, 2018). (in Chinese)

15. Xiang L, Luo HQ, Pan Y, Li C, Zhang Y. Analysis of forms of compensation under catastrophic disease insurance and the effectiveness of compensation in the City of L. Chinese Journal of Health Policy. 2015; 8:29-33. (in Chinese)

16. The State Council of the Communist Party of China. Opinions on full implementation of catastrophic disease insurance for urban and rural residents. *http://www.gov.cn/xinwen/2015-08/02/content_2907531.htm* (accessed March 29, 2018). (in Chinese)

17. The State Council of the Communist Party of China. The State Council's opinions on integrating basic medical insurance systems for urban and rural residents. *http://www.gov.cn/zhengce/content/2016-01/12/content_10582.htm* (accessed March 29, 2018). (in Chinese)

18. Wang X, Zheng A, He X, Jiang H. Integration of rural and urban healthcare insurance schemes in China: An empirical research. BMC Health Serv Res. 2014; 14:142.

19. Huang Y, Liu Y, Yang X, Li J, Fang P. Global budget payment system helps to reduce outpatient medical expenditure of hypertension in China. Springerplus. 2016; 5:1877.

20. Gao C, Xu F, Liu GG. Payment reform and changes in health care in China. Soc Sci Med. 2014; 111:10-16.

21. Schroeder SA, Frist W. Phasing out fee-for-service payment. N Engl J Med. 2013; 368:2029-2032.

22. Guidance on further reform of the payment scheme for basic medical insurance. *http://www.gov.cn/zhengce/content/2017-06/28/content_5206315.htm* (accessed March 29, 2018). (in Chinese)

23. Yu H. Universal health insurance coverage for 1.3 billion people: What accounts for China's success? Health Policy. 2015; 119:1145-1152.

24. Li Y, Zhao Y, Yi D, Wang X, Jiang Y, Wang Y, Liu X, Ma S. Differences exist across insurance schemes in China post-consolidation. PLoS One. 2017; 12:e0187100.

25. Li YF. Analysis of the current state of and factors influencing poverty due to illness in rural areas. China Management Informationization. 2018; 21:188-190. (in Chinese)

26. World Bank Data. Out-of-pocket health expenditure (% of total expenditure on health). *https://data.worldbank.org/indicator/SH.XPD.OOPC.TO.ZS?locations=CN-XD* (accessed March 29, 2018).

27. World Bank. Tracking Universal Health Coverage 2017 Global Monitoring Report. 2017. *http://www.worldbank.org/en/topic/universalhealthcoverage/publication/tracking-universal-health-coverage-2017-global-monitoring-report* (accessed March 29, 2018).

28. China Net. Director of the Health and Family Planning Commission Bin Li's, response to "How to solve the problem of the vicious cycles of illness and poverty". *http://www.china.com.cn/news/2017-08/31/content_41507528.htm* (accessed March 29, 2018). (in Chinese)

29. Zhang Y, Tan HY, WU Y, Lai YH. The prominent problems of China's basic medical insurance payment system and the countermeasures. Chinese Health Economics. 2015; 34:23-25. (in Chinese, abstract in English)

30. He R, Miao Y, Ye T, Zhang Y, Tang W, Li Z, Zhang L. The effects of global budget on cost control and readmission in rural China: A difference-in-difference analysis. J Med Econ. 2017; 20:903-910.

31. Yu GJ, Zhao R, Zheng PY *et al*. Research on the effect of global budgeting in social health insurance towards the tertiary hospitals in Shanghai. Chinese Hospitals. 2013; 17:1-3. (in Chinese, abstract in English)

32. Kan K, Li SF, Tsai WD. The impact of global budgeting on treatment intensity and outcomes. Int J Health Care Finance Econ. 2014;14:311-337.

33. Liu SC, Luo ZY. Analysis of the current state of implementation of a prospective payment system for total medical expenses and its problems. Soft Science of Health. 2017; 31:40-42. (in Chinese)

34. Yang J, Li JS. Thinking on the implementation of total prepaid medical insurance reform. Chinese Hospital Management. 2013; 33:65-66. (in Chinese, abstract in English)

35. Babic U, Soldatovic I, Vukovic D, Milicevic MS, Stjepanovic M, Kojic D, Argirovic A, Vukotic V. Comparative analysis of the current payment system for hospital services in Serbia and projected payments under diagnostic related groups system in urology. Vojnosanit Pregl. 2015; 72:251-257.

Review

An update on Chinese herbal medicines as adjuvant treatment of anticancer therapeutics

Zhixue Wang[1], Fanghua Qi[1], Yangang Cui[2], Lin Zhao[1], Xiaogang Sun[3], Wei Tang[4], Pingping Cai[1,*]

[1] *Department of Traditional Chinese Medicine, Shandong Provincial Hospital affiliated to Shandong University, Ji'nan, China;*
[2] *Department of Chemotherapy, Shandong Provincial Hospital affiliated to Shandong University, Ji'nan, China;*
[3] *Department of Tumor Minimally Invasive Surgery, Shandong Provincial Hospital affiliated to Shandong University, Ji'nan, China;*
[4] *National Center for Global Health and Medicine, Tokyo, Japan.*

Summary	Numerous studies have indicated that in cancer treatment Chinese herbal medicines in combination with chemo-, radio-, or targeted-therapy can be used to enhance the efficacy of and diminish the side effects and complications caused by these therapies. Therefore, an understanding of Chinese herbal medicines is needed by physicians and other health care providers. This review provides an update on Chinese herbal medicines as adjuvant treatment of anticancer therapeutics. First, some Chinese herbal medicines (*e.g.* Astragalus, Ginseng, *Scutellaria barbata*, TJ-41, TJ-48, PHY906, Huachansu injection, and Kanglaite injection) that are commonly used for treating the cancer and/or reducing the toxicity induced by chemo-, radio-, or targeted-therapy are discussed. These Chinese herbal medicines have been shown to possess great advantages in terms of suppressing tumor progression, increasing the sensitivity of chemo-, radio-, or targeted-therapeutics, improving an organism's immune system function, and lessening the damage caused by these therapeutics. Second, some clinical trials using Chinese herbal medicines as adjuvant improving cancer treatment related side effects and complications are reviewed. Some Chinese herbal medicines have a significant effect on reducing cancer-related fatigue and pain, improving peripheral neuropathy and gastrointestinal side effects including diarrhea, nausea, and vomiting, decrease the incidence of bone marrow suppression, protecting anthracycline-induced cardiotoxicity and radiation-induced pneumonitis, and relieving EGFR-TKIs related acneiform eruptions and other side effects. This review of those medicines should contribute to an understanding of Chinese herbal medicines as adjuvant treatment for cancer and provide useful information for the development of more effective anti-cancer drugs. However, rigorously designed trials on potential Chinese herbal medicine must be further examined involving cancer treatment especially molecular targeted-therapy in the future.

Keywords: Chinese herbal medicine, adjuvant treatment, chemotherapy, radiotherapy, targeted therapy

1. Introduction

Cancer constitutes one of the leading causes of morbidity and mortality worldwide. Based on GLOBOCAN (a project of the International Agency for Research on Cancer) estimates, about 14.1 million new cancer cases and 8.2 million deaths occurred in 2012 worldwide (*1*). Because of the growth and aging of the population, as well as an increasing prevalence of established risk factors such as smoking, overweight, physical inactivity, and changing reproductive patterns associated with urbanization and economic development, the morbidity and mortality of cancer is predicted to be increased quickly in the next few decades worldwide, especially in low- and middle-income countries (*2*). It is projected that by 2030 an estimated 21.4 million new cases of cancer

Address correspondence to:
Dr. Pingping Cai, Department of Traditional Chinese Medicine, Shandong Provincial Hospital affiliated to Shandong University, No. 324, Jingwuweiqi Road, Ji'nan 250021, Shandong, China.
E-mail: pingpingcai@126.com

and 13.2 million cancer deaths will occur annually around the world, which brings an enormous burden on society (*3*).

Chemotherapy, radiotherapy, targeted therapy and immunotherapy are examples of anticancer therapies currently being utilized in patients with malignant tumors in middle and advanced stages for controlling tumor growth, prolonging survival time, and improving quality of life (QOL) to some extent. However, these therapies either alone or in combination have been shown to have numerous limitations and drawbacks including myelosuppression, gastrointestinal tract reaction, cardiac damage, liver and renal dysfunction, rash, hand-foot syndrome, or local radiation damage, and so on (*4,5*). In particular, with molecular-targeted drugs widely used, adverse effects of such treatments including acneiform eruptions, paronychia, xerosis, mucositis, and alopecia are thought to be less severe, but can still be significant (*6*). Not only can these toxicities severely affect patients' QOL, but in some specific instances, they can be associated with increased response to therapy (*7*). Therefore, it is of paramount importance that clinicians familiarize themselves with the basic management of the adverse effects caused by these drugs. More effective or adjunctive therapies must be soon developed for relieving adverse effects and complications of anticancer therapeutics.

With development of medicine and update of knowledge, cancer therapy has come into a diversified comprehensive treatment stage. Many scholars put forward the concept of "survival with cancer", and they insist controlling cancer and causing cancer cells to "be static" and "hibernate" for a long time, are better than striving to reduce the lump and completely kill all cancer cells (*5*). In the process of "survival with cancer", complementary and alternative medicine (CAM) might play an important role.

Traditional Chinese medicine (TCM) especially Chinese herbal medicines, as an important component of CAM, has evolved over thousands of years in China, Japan, and other Asian countries with its own unique system of theories, diagnostics and therapies. TCM has been increasingly used in the last decades and become well known for its significant role in preventing and treating cancer. It is widely used by TCM physicians and other health care providers to control the side effects and toxicities of cancer therapies, which improves the patient's QOL, prevents recurrence, and prolongs survival (*8*).

In our previous reviews of recent years, we have indicated that some Chinese herbal medicines as adjuvant treatment in combination with chemo- or radio-therapy were capable of enhancing the sensitivity of chemo- and radio-therapeutics, improving an organism's immune system function, and diminishing the side effects and complications caused by chemo- and radiotherapy (*3*), and we have also indicated that some Chinese herbal medicines as adjuvant treatment played important roles in different stages of cancer lesions including post-operation, radiotherapy or chemotherapy stages (*5*). Here an update of the new laboratory and clinical studies especially from 2015 to March 2018 on Chinese herbal medicines as adjuvant treatment especially on relieving adverse effects and complications of anticancer therapeutics will be focused. First, some Chinese herbal medicines that are commonly used on cancer patients to treat the cancer and/or reduce the toxicity induced by chemo-, radio-, or targeted-therapy are discussed. Second, clinical trials of Chinese herbal medicines as adjuvant cancer treatment to reduce side effects and complications during chemo-, radio-, or targeted-therapy are reviewed. This review should contribute to an understanding of Chinese herbal medicines as adjuvant treatment for cancer and provide useful information for development of more effective anti-cancer drugs.

2. Chinese herbal medicines commonly used as adjuvant treatment in cancer therapy

Chinese herbal medicines in current use are usually classified as single herbs, compound formulations (a combination of several herbs), and Chinese medicine preparations. The biological ingredients of herbal medicines are mainly extracted from plants, animal parts, shells, insects, and even stones and minerals. In recent decades, a large number of herbal medicines including single herbs, traditional herbal formulations, and Chinese medicine preparations have been widely used on cancer patients around the world especially in China for managing common cancer symptoms of fatigue, chronic pain, anorexia, insomnia, limbs edema, and constipation (*9*). Numerous basic and clinical studies have been conducted to identify effective anticancer agents in Chinese herbal medicines and ascertain their properties as related to the treatment of cancer. Several herbal medicines have been found to have potentially beneficial effects on cancer progression and may ameliorate chemo-, radio-, or targeted-therapy induced complications and side effects (*10,11*). Therefore, the anticancer pharmacology of the Chinese herbal medicines most commonly used as adjuvant treatment in cancer therapy must be understood.

2.1. *Single herbss*

Based on TCM classic theory, the formation of tumors are usually due to deficiency of vital energy (Qi and blood) in the body, combined with some pathogenic factors such as external evil invading, emotional abnormality, overeating and so on, leading to Qi stagnation, blood stasis and heat- and dampness-induced toxicity blocking in the body, and then forming lumps as time goes by (*5,12*). According to the above theory, TCMs which are used for cancer treatment usually fall

into three categories: the first one with properties of spiriting vital energy (Qi and blood), the second one with the properties of promoting blood stasis, and the third with properties of clearing heat and detoxifying. Thus, according to references and our clinical experience, we will choose some single herbs commonly prescribed by traditional Chinese physicians for cancer treatment and give them a brief introduction especially regarding clinical studies (Table 1).

2.1.1. *Some single Chinese herbal medicines with properties of spiriting vital energy*

Panax ginseng *Panax ginseng* (Ren-Shen in Chinese or Ginseng in Korea) is a well-known and popular Chinese herbal medicine, which is believed to be the king of the herbs in the Orient, particularly in China, Korea and Japan. It has been used for several thousand years with mysterious powers as a tonic, prophylactic and restorative agent (*13*). Much of the pharmacological research has shown that *Panax ginseng* has potent immune modulation, vasorelaxation, anti-oxidation, anti-inflammation, and anticancer properties (*14*). *Panax ginseng* contains many active components such as ginsenosides, peptides, essential oil and polysaccharides, among which, ginsenosides (*e.g.*, Rg3 and Rb1) are considered an excellent option for their anticancer property (*15*). Ginseng and its active components have been reported as an adjuvant treatment to synergistically enhance efficacy of conventional therapy (*e.g.*, chemo- and radio-therapeutics), reduce the risk of development and recurrence of some types of cancer (*e.g.*, stomach, liver, pancreas, and colon cancer), and improve host intrinsic response to cancer and quality of patients' life (*16*). An epidemiological study indicated that patients taking ginseng had a 50% lower risk of cancer recurrence compared to patients not taking ginseng (*17*). In the following, we emphasize some basic and clinical research in recent years about Ginseng and its active components.

A pilot study indicates that Ginseng has potential as an effective treatment for advanced cancer patients in improving response and survival rate (*18*). A phase III trial was developed by Mayo Clinic Rochester (Rochester, USA) to evaluate the efficacy of Ginseng on cancer-related fatigue and indicated that Ginseng showed great benefit for ameliorating cancer-related fatigue without any discernible toxicity (*19*). Moreover, Ginseng appears to be a promising radio-protector and is capable of attenuating the deleterious effects of radiation on human normal tissue, especially for cancer patients undergoing radiotherapy (*20*). It could improve radiation-induced liver injury, which might be associated with the modulation of oxidative stress, inflammatory reactions, and apoptosis (*21*).

Ginsenoside Rg3 is recognized to boost immune response and has anti-cancer activity against a majority

of carcinomas including non-small cell lung cancer (NSCLC). An *in vitro* study indicated Rg3 might be a new agent targeting programmed death ligand 1 (PD-L1) in chemotherapy refractory NSCLC (*22*). Moreover, a multicenter, large-sample, randomized clinical trial on improving the median survival time of advanced NSCLC by a combination of Ginsenoside Rg3 and chemotherapy was conducted by Zhang *et al*. They indicated that a combination of Ginsenoside Rg3 with chemotherapy could prolong the survival of patients with advanced NSCLC, improve patients' symptoms and reduce chemotherapy induced myelosuppression (*23*).

Although evidence of efficacy in relation to Ginseng and its active components use is obvious, well-designed clinical trials are required to provide more information for scientists and healthcare consumers. Furthermore, using cautions and adverse reactions of Ginseng are crucial for people. Ginseng should be avoided by children and used with some prudence by patients medicated with blood pressure medicines, blood-thinning medications, hormones, or insulin due to possible drug-herb interactions (recommendation performed by American Cancer Society) (*24*). Ginseng is relatively nontoxic but in high doses (*i.e.*, superior to 3 g ginseng root daily) can confer adverse symptoms such as insomnia, nervous excitation, headaches, and nausea. Ginseng may present steroid/hormone like effects, so in women who have breast or endometrial cancer special attention for its use is recommended (*25*).

Radix Astragali *Radix Astragali* (Huang-Qi in Chinese), the root of *Astragalus membranaceus* Bunge, is one of the most famous and frequently used herbal medicines and healthy food supplements used as a tonic. It has been widely used to treat cancer and other immune disorders in China and Southeast Asia for thousands of years (*26*). The chemical composition of *Radix Astragali* mainly includes triterpenoid saponins, polysaccharides, flavonoids, amino acids, and trace elements, of which triterpenoid saponins (*e.g.*, Astragaloside IV and Astragaloside II) represent the major beneficial constituents responsible for the bioactivities and efficacies of *Radix Astragali* on human health (*27*). *Radix Astragali* and its active constituents have been proposed as an adjuvant treatment to synergistically enhance efficacy and reduce toxicity of chemo-, radio-, or targeted-therapeutics on breast, gastric, liver, colon, and lung cancers and so on.

Multiple randomized clinical trials have suggested that *Radix Astragali*-based intervention can reduce symptoms, improve QOL and immunologic function, increase plasma nerve growth factor (NGF) levels, and delay the progression of chemotherapy-induced peripheral neuropathy (CIPN) (*28*). In addition, Huangqi injection combined with chemotherapy has an enhanced anti-tumor effect and can improve the short-term prognosis and clinical outcome in children with acute lymphoblastic leukemia (ALL) (*29*). It could reduce

Table 1. Single TCMs commonly prescribed by traditional Chinese physicians for cancer treatment

Common name	Other names	Efficacy according to TCM theory	Major active ingredients	Biological activity	Preclinical and/or clinical evidence of anticancer activity	Ref.
Panax ginseng	Ren-Shen in Chinese, Ginseng in Korea	As a tonic, prophylactic and restorative agent with the efficacy of spiriting vital energy	Ginsenosides, essential oil, peptidoglycans, polysaccharides, nitrogen-containing compounds, fatty acids and phenolic compounds	Antitumor, antioxidant, immunomodulation, anti-ulcer, anti-adhesive, antioxidant, hepatoprotective, hypoglycemic	Clinical: (i) Ren-Shen: Ameliorating cancer-related fatigue without any discernible toxicity; (ii) Ren-Shen: Improving radiation-induced liver injury; (iii) Ginsenoside Rg3: prolong the survival of patients with advanced NSCLC and reduce chemotherapy induced myelosuppression.	16-21,23
					Preclinical: Ginsenoside Rg3 a new agent targeting PD-L1 in chemotherapy refractory NSCLC.	22
Radix Astragali	Huang-Qi in Chinese	As a tonic with the efficacy of spiriting vital energy	Isoflavonoids, triterpenoid saponins, polysaccharides, amino butyric acids and various trace elements	Antitumor, antioxidant, hepatoprotective, anti-diabetic, antimicrobial, antiviral, immunomodulation	Clinical: (i) Improve gastrointestinal side effects, and ameliorate bone marrow suppression in colorectal cancer patients with chemotherapy; (ii) Delay the progression of CIPN; (iii) Decrease infectious rate in ALL children with chemotherapy.	28-30
					Preclinical: Astragaloside IV inhibit cancer cell invasion via Rac1/MAPK and PKC-α-ERK1/2-NF-κB pathway	31-33
Radix Codonopsis	Dang-Shen in Chinese	As a tonic with the efficacy strengthening spleen and nourishing lung	Polysaccharides, alkaloids, phenylpropanoids, triterpenes, and polyacetylenes	Antioxidant, antimicrobial, antitumor, immunomodulation	Clinical: (i) Reducing the immunosuppressive effect of radiotherapy; (ii) Improving chemotherapy induced CIN, reduce myelosuppression and/or enhance immune response of patients	37-39
Poria cocos	Fu-Ling in Chinese, Hoelen in Japanese	As a tonic with the efficacy of strengthening spleen	Triterpenes, polysaccharides, steroids, amino acids, choline, and histidine	Antitumor, anti-inflammatory, antioxidant, antiviral, immunomodulation	Clinical: Improve tumor response rate and alleviate chemotherapy-related adverse events.	46
					Preclinical: Combined with oxaliplatin: Inhibit the migration and invasion of gastric cancer cells via regulating the EMT process.	45
Angelicae Sinensis Radix	Dang-Gui in Chinese, Dong Quai in English, Toki in Japanese, or Tanggwi in Korea	With nourishing Yin, promoting blood circulation, and moisturizing dryness functions	Ligustilide, butylphthalide, senkyunolide A, phthalide dimers, ferulic acid, coniferyl ferulate, polyacetylenes	Antitumor, neuroprotective, immunomodulation, cardiovascular protective	Preclinical: Enhance radio-sensitivity of radiation in human liver cancer cells	54
Curcuma longa	Jiang-Huang in Chinese	With the efficacy of promoting blood circulation and removing blood stasis	Curcumin, demethoxycurcumin, and bisdemethoxycurcumin,	Antitumor, anti-inflammatory, antioxidant	Preclinical: Curcumin: (i) Modulates chemo-resistance and radio-resistance; (ii) Protects normal organs such as liver, kidney, oral mucosa, and heart from chemotherapy and radiotherapy induced toxicity.	58,59
Hedyotis diffusa willd	Bai-Hua-She-She-Cao in Chinese	With the efficacy of clearing eat and detoxifying	Triterpenes, polysaccharide and anthraquinones	Antitumor, chemopreventive, hepatoprotective, antiviral, antibacterial, antidiabetic, antioxidant, gastroprotective	Clinical: Enhance the overall survival of patients with GC.	62
					Preclinical: Suppress colorectal cancer growth through multiple cellular pathways including MAPK, STAT3, AKT and ERK signaling.	61-64
Scutellaria barbata	Ban-Zhi-Lian in Chinese, Banjiryun in Korea	With the efficacy of clearing heat and detoxifying	Phenolic acids, flavonoids, triterpene acids and sterol glucosides	Antitumor, anti-inflammatory	Preclinical: (i) Inhibit migration and invasion of colorectal cancer cells via suppression of PI3K/AKT and TGF-β/Smad signaling pathways; (ii) Inhibit 5-FU resistance in colorectal cancer by regulating PI3K/AKT pathway	66,67
					Clinical: Improve afatinib-induced paronychia in cancer patient.	69

Abbreviations: programmed death ligand 1 (PD-L1); chemotherapy-induced peripheral neuropathy (CIPN); epithelial-mesenchymal transition (EMT); gastric cancer (GC).

bone marrow suppression caused by chemotherapy drugs and increase neutrophil count during remission induction chemotherapy to reduce the incidence and duration of infection in children with ALL (*30*).

Astragaloside IV could inhibit breast cancer cell invasion by suppressing Vav3 mediated Rac1/MAPK signaling and inhibit lung cancer invasion *via* the PKC-α-ERK1/2-NF-κB pathway (*31,32*). Astragaloside IV also could inhibit progression of glioma *via* blocking MAPK/ERK signaling pathway (*33*). In addition, Astragaloside II could inhibit autophagic flux and enhance chemosensitivity of cisplatin in human cancer cells (*34*).

Radix Codonopsis   *Radix Codonopsis* (Dang-Shen in Chinese) is a famous traditional Chinese medicine and has long been used for replenishing energy deficiency, strengthening the immune system, lowering blood pressure and improving appetite in China, Japan and Korea (*35*). In many cases, it is utilized primarily as a substitute for the much more costly *Panax ginseng* and is therefore called the poor man's ginseng. Phytochemical studies indicate that polysaccharides, alkaloids, phenylpropanoids, triterpenes, and polyacetylenes are the main components of *Radix Codonopsis* (36). Recently, *Radix Codonopsis* and its active constituents have been proposed to have functions of antioxidant, antimicrobial, antitumor and improving immunity. They are reported as adjunctive cancer therapeutics with activities of immunomodulation, anti-proliferation and attenuation of adverse effects induced by cytotoxic therapy.

Radix Codonopsis was used as an adjuvant in cancer patients during radiotherapy. It could reduce the immunosuppressive effect of radiotherapy on delayed hypersensitive reaction, and the lymphocyte response to PHA and IL-2 (*37*). Some TCM decoctions of which *Radix Codonopsis* was a main ingredient could effectively improve clinical symptoms, signs and QOL of cancer patients. A modern agent Shenqi Fuzheng Injection, prepared from Codonopsis Radix and Astragali Radix, commonly used as a supplementary therapy for cancers, could reprogram the immunosuppressive microenvironment *in vivo* to enhance the cytotoxicity of tumor-infiltrating immune cells in melanoma (*38*). Combining oxaliplatin regimens with some TCM decoctions containing *Radix Codonopsis* in the management of colorectal cancer (CRC) could effectively improve chemotherapy induced CIN, reduce myelosuppression and/or enhance immune response of patients (*39*). In addition, polysaccharides from *Radix Codonopsis* exhibited significant inhibitory effects on tumor cell growth, invasion, and migration of human epithelial ovarian cancer cells (*40*). Polysaccharides from *Radix Codonopsis* also could inhibit melanoma metastasis *via* regulating integrin signaling (*41*).

Although *Radix Codonopsis* is commonly prescribed by traditional Chinese physicians for cancer treatment in the clinic, there are few clinical studies published currently in English. Thus, more rigorous trials are needed to confirm the efficacy of *Radix Codonopsis* and its active constituents on cancer therapy in the future.

Poria cocos   *Poria cocos* (Fu-Ling in Chinese or Hoelen in Japanese), is an important medicinal and edible fungus that grows in association with pine trees, and its dried sclerotium has been used as a traditional medicine in China for centuries (*42*). It is a well known Chinese herbal medicine used to treat diabetes, dysentery, chronic fatigue syndrome, diarrhea, dizziness, edema, insomnia, kidney problems, nervousness, urination problems, and weakness (*5*). The chemical composition of *Poria cocos* mainly includes triterpenes, polysaccharides, steroids, amino acids, choline, histidine, *etc*. (*43*). Recently, *Poria cocos* and its active constituents have been reported to have functions of anticancer, anti-inflammatory, antioxidant, antiviral and improved immunity (*44*). They have been proposed as an adjuvant treatment to synergistically enhance efficacy and reduce toxicity of chemo-, radio-, or targeted-therapeutics on leukemia, lung, and colorectal cancers and so on.

Poria cocos combined with oxaliplatin could significantly inhibit the migration and invasion of gastric cancer cells *via* regulating the epithelial-mesenchymal transition (EMT) process of gastric cancer (*45*). Moreover, *Poria cocos* as one of the most frequently used herbs combined with the FOLFOX4 chemotherapy regimen could effectively improve tumor response rate, one year survival and QOL of patients. It also could alleviate chemotherapy-related adverse events including neutropenia, nausea and vomiting, and neurotoxicity, compared to the FOLFOX4 chemotherapy regimen alone (*46*). In addition, Pachymic acid, a lanostane-type triterpenoid from *Poria cocos*, could induce apoptosis of human lung cancer cells through activation of the JNK and ER stress pathways (*47*), and induce apoptosis of bladder cancer cells *via* the mitochondrial apoptosis pathway (*48*). Triterpenes from *Poria cocos* also could suppress growth and invasiveness of pancreatic cancer cells through downregulation of MMP-7 (*49*).

Taken together, although *Poria cocos* and is its active constituents have been reported as an adjuvant treatment for cancer therapy, more rigorous trials are needed to confirm the efficacy of *Poria cocos* and its active constituents for cancer therapy in the future.

2.1.2. *Some single TCMs with properties of promoting blood circulation and removing blood stasis*

Angelicae Sinensis Radix   *Angelicae Sinensis Radix*, (Dang-Gui in Chinese, Dong Quai in English, Toki in Japanese, or Tanggwi in Korea), is a well-known Pharmacopoeia-recorded medical material in China with nourishing Yin, promoting blood circulation, and moisturizing dryness functions. It is usually used to strengthen heart, lung, and liver meridians, as well as lubricate the bowel (*5*). Furthermore, it has been called

"female ginseng" due to its superior efficacy in treating gynecological conditions including dysmenorrhea, pelvic pain, recovery from childbirth and menopausal symptoms (*50*). Over 70 compounds have been identified from *Angelicae Sinensis Radix*, including essential oils such as ligustilide, butylphthalide and senkyunolide A, phthalide dimers, organic acids and their esters such as ferulic acid, coniferyl ferulate, polyacetylenes, vitamins and amino acids (*51*). *Angelicae Sinensis Radix* and some of its active constituents have been reported to possess hematopoietic, antioxidant, immunoregulatory, anti-cancer, memory, radioprotective, and neuroprotective effects. Moreover, some reports indicated that *Angelicae Sinensis Radix* and some of its active constituents exhibited great anticancer effects in liver, oral, and lung cancers *via* inducing apoptosis, revising multidrug resistance or modulating lymphocyte activity and improving immunity (*52,53*). In addition, the decoction containing Radix Angelicae Sinensis could enhance radiosensitivity of radiation in human liver cancer cells by modulating caspase-dependent apoptosis protein (*54*).

Although *Angelicae Sinensis Radix* is commonly prescribed by traditional Chinese physicians for cancer treatment in the clinic, there are few clinical studies published currently in English. Thus, more rigorous trials are needed to confirm the efficacy of *Angelicae Sinensis Radix* and its active constituents for cancer therapy in the future.

Curcuma longa Curcuma longa (Jiang-Huang in Chinese), a member of the ginger family and commonly known as turmeric, is a culinary spice and therapeutic used in Asia for thousands of years to induce color and flavor in food as well as to treat a wide array of diseases such as diabetes, atherosclerosis, acne, jaundice, dysmenorrheal, as well as cancer (*5*). The major bioactive compounds of *Curcuma longa* contain curcumin, demethoxycurcumin, and bisdemethoxycurcumin, with curcumin being the most abundant ingredient (*55*). It has been shown that curcumin has a variety of pharmacological effects such as antioxidant, anti-cancer, anti-inflammatory, and anti-microbial activities. Anti-cancer effects of curcumin are involved in cell cycle arrest, apoptosis, angiogenesis and metastasis *via* a wide range of cellular and molecular pathways involved in cancer pathogenesis including NF-kB, MAPK, PTEN, P53, and microRNAs (miRNA) network (*56*). Curcumin has been widely used to fight against cisplatin-resistant cancer cells and decrease its unwanted side effects (*e.g.* ototoxicity, nephrotoxicity and neurotoxicity) (*57*). Curcumin might be a safe and effective inhibitor of P-glycoprotein (P-gp) to overcome multidrug resistance (MDR) in human cancer (*58*). In addition, some research has revealed that curcumin can sensitize tumors to different chemotherapeutic agents including doxorubicin, 5-FU, paclitaxel, vincristine, oxaliplatin, etoposide and so on in numerous cancers (*e.g.*, breast,colon, pancreas, gastric, liver, blood, lung, prostate, and ovary) (*59*).

Moreover, curcumin has also been shown to protect normal organs such as liver, kidney, oral mucosa, and heart from chemotherapy and radiotherapy induced toxicity (*5*).

However, since most of such findings have yet to be confirmed in clinical studies, its effect on humans is not clearly known. Thus, the future prospect of research on *Curcuma longa* and curcumin will be a very exciting field of research for the coming decades and will provide us with better mechanisms of utilizing them as adjuvant drugs against cancer in the near future.

2.1.3. *Some single TCMs with properties of clearing heat and detoxifying*

Hedyotis diffusa willd Hedyotis diffusa willd (Bai-Hua-She-She-Cao in Chinese) has been known as an ingredient of popular herbal teas and a famous TCM for a long time in the Orient and tropical Asia. It was recorded in Chinese pharmacopoeia (2015 edt) with the functions of inducing diuresis to reduce edema, clearing away the heat evil and detoxification, and promoting blood circulation to arrest pain. Up to now, 171 compounds have been reported from *Hedyotis diffusa willd*, including iridoids, flavonoids, anthraquinones, phenolics and their derivatives, volatile oils and miscellaneous compounds. *In vitro* and *in vivo* studies show these phytochemicals and plant extracts to exhibit a range of pharmacological activities of anti-cancer, antioxidant, anti-inflammatory, anti-fibroblast, immunomodulatory and neuroprotective effects (*60*). Recently, *Hedyotis diffusa willd* and some of its active constituents have gained increasing attention as an antitumor herb. Clinically, this herb has often been applied as a critical element in many TCM formulae for the treatment of various cancers, including gastric cancer (GC) and colorectal cancer (*61-64*). A latest retrospective matched-cohort study presented that *Hedyotis diffusa willd* was the most commonly prescribed single herb for treating GC patients and complementary TCM therapy enhanced the overall survival of patients with GC in Taiwan (*62*). It probably produced the therapeutic effects against GC by synergistically regulating many biological pathways, such as nucleotide excision repair, apoptosis, cell cycle, PI3K/AKT/mTOR signaling pathway, VEGF signaling pathway, and Ras signaling pathway (*61*). *Hedyotis diffusa willd* could suppress colorectal cancer growth through multiple cellular pathways including MAPK, STAT3, AKT and ERK signaling (*63*). It also could suppress metastasis in 5-FU-resistant colorectal cancer cells by regulating the TGF-β signaling pathway (*64*). Although *Hedyotis diffusa willd* is widely studied in laboratory and clinical studies, more rigorous trials are needed to confirm the efficacy of *Hedyotis diffusa willd* and its active constituents on cancer therapy in the future.

Scutellaria barbata Scutellaria barbata (Ban-Zhi-Lian in Chinese or Banjiryun in Korea), a herbal plant in Astragalus genus, is a well-known anti-inflammatory

and anti-cancer herb with the properties of clearing heat, activating blood and dissolving stasis according to TCM theory. It has been widely used for treatment of various kinds of cancer, such as colorectal, liver, breast and lung cancer in China and other Asian countries for many years (65). Chromatographic analysis has demonstrated that scutellarein, apigenin, baicalein and luteolin are main components of *Scutellaria barbata*. *Scutellaria barbata* was reported to process the effects of promoting apoptosis, and inhibiting cell proliferation and angiogenesis in human colon cancer cells. It could inhibit migration and invasion of colorectal cancer cells *via* suppression of PI3K/AKT and TGF-β/Smad signaling pathways (66). It also could inhibit 5-FU resistance in colorectal cancer by regulating PI3K/AKT pathway (67). Moreover, *Scutellaria barbata* could regulate immune function of Lewis-bearing C57BL/6 mice with a decrease of IL-17, IL-10, FOXP3, TGF-β1, RORγt, and IL-6 levels and increase of IL-2 and IFN-γ levels (68). In addition, a decoction of Ban-Zhi-Lian (*Scutellaria barbata*) with Bai-Hua-She-She-Cao (*Hedyotis diffusa Willd*) could effectively improve afatinib-induced paronychia in patients (69). However, there are few reports on the anticancer effects of the active constituents of *Scutellaria barbata*. A water-soluble polysaccharide SPS2p, isolated from the whole grass of *Scutellaria barbata*, could inhibit proliferation and EMT, and promote apoptosis of human colon cancer HT29 cells *via* PI3K/AKT pathway (70). In the future, more rigorous trials are needed to confirm the efficacy of *Scutellaria barbata* and its active constituents for cancer therapy.

3. Traditional Chinese herbal formulations commonly prescribed by traditional Chinese physicians for cancer treatment

Traditional Chinese herbal formulations, or Kampo in Japanese, are a combination of compatible herbs in fixed dosages, most of which come from classical or well known Chinese textbooks of medicine like "Shang Han Lun" and "Jin Gui Yao Lue" (5). Currently, several traditional Chinese herbal formulations, such as Bu-Zhong-Yi-Qi-Tang (TJ-41), have been found to have a potentially beneficial effect for treating various cancers. A brief outline of the anticancer pharmacology of some traditional Chinese herbal formulations commonly prescribed by traditional Chinese physicians for cancer treatment is presented below (Table 2).

3.1. *Bu-zhong-yi-qi-tang*

Bu-zhong-yi-qi-tang (Hochuekki-to or TJ-41 in Japanese, or Bojungikki-Tang in Korean) is a classical formulation widely used in China, Japan, and South Korea for a long time. It was recorded as a tonic for the treatment of weakness including fatigue, visceroptosis, gastrointestinal motility disorder, and rectal prolapse due

Table 2. Traditional Chinese herbal formulations commonly prescribed by traditional Chinese physicians for cancer treatment

Common name	Other names	Composition	Biological activity	Preclinical and/or clinical evidence of anticancer activity	Ref.
Bu-zhong-yi-qi-ang	Hochuekki-to or TJ-41 in Japanese; Bojungikki-Tang in Korean	Includes 7 herbs: *Pinellia tuber, Scutellaria baicalensis, Zingiberis rhizoma, Zizyphi fructus, Coptidis rhizoma, Glycyrrhiza radix, Panax ginseng*	Antitumor, immunomodulation	*Preclinical: (i)* Reversing cisplatin resistance through induction of apoptosis and autophagy in lung cancer cells; *(ii)*Inhibiting 5-FU-induced intestinal mucositis *via* the suppression of inflammatory cytokine up-regulation. *Clinical: (i)* Have protective effect of intestine and hematopoietic organs against radiation damage. *(ii)* Improving localized radiotherapy-induced immune deterioration; *(iii)* Improving cancer-related fatigue and QOL; *(iv)* Reducing radiation or chemotherapy induced side effects.	72,73 73-75
Shi-Quan-Da-Bu-Tang	Juzentaiho-to or TJ-48 in Japanese, Sipjeondaebo-tang in Korean	Includes 10 herbs: *Ginseng radix, Astragali radix, Angelicae radix, Rehmanniae radix, Atractylodis lanceae rhizoma, Cinnamomi cortex, Poria, Paeoniae radix, Ligustici rhizoma Glycyrrhizae radix*	Antitumor, immunomodulation	*Clinical: (i)* Regulating T cells through decreasing Foxp3+ Treg populations in advanced pancreatic cancer patients; *(ii)* Inhibiting B16 cell metastasis by inducing NK cell activity. *(iii)* Combined with anti-PD-1 antibody: increasing treatment response rates for B16 melanoma. *Preclinical:* Alleviating bone marrow suppression caused by TS-1 in mice.	77-79 5
Xiao-chai-hu-tang	Sho-sai-ko-to or TJ-9 in Japanese	Includes 7 herbs: *Bupleurum falcatum, Scutellaria baicalensis, Panax ginseng, Zizyphus jujube, Pinellia ternate, Zingiber officinale, Glycyrrhiza glabra*	Antitumor, anti-inflammatory antioxidant, immunomodulation, hepatoprotective, anti-hepatic fibrosis	*Preclinical:* Inhibiting cell proliferation and promoting apoptosis of HCC cells *via* regulating the expression of Bax, Bcl-2, CDK4 and cyclin-D1. *Clinical: (i)* Preventing the development of HCC from hepatitis C virus-associated liver cirrhosis (HCV-LC) in the HCV-LC patients; *(ii)* considered to be a useful method against stomatitis prevention and sharp pain mitigation from chemotherapy.	80 82,83
Huang-qin-tang	PHY906	Includes 4 herbs: *Scutellaria baicalensis Georgi, Paeonia lactiflora Pall, Glycyrrhiza uralensis Fisch, Ziziphus jujuba Mill*	Antitumor, anti-inflammatory	*Preclinical:* Enhancing the anti-tumor activity of Sorafenib in nude mice bearing HepG2 xenografts by targeting on the inflammatory state of microenvironment of tumor tissue. *Clinical:* Enhancing the antitumor efficacy of some anticancer drugs but also alleviating chemo- or targeted-therapy (*e.g.*, CTP-11) induced side effects.	85 86,87

to chronic diarrhea. Furthermore, it has been identified as an effective drug for the treatment of TCM spleen-qi deficiency in clinical practice in recent years. It contains 7 herbs including *Pinellia tuber*, *Scutellaria baicalensis*, *Zingiberis rhizoma*, *Zizyphi fructus*, *Coptidis rhizoma*, *Glycyrrhiza radix*, and *Panax ginseng* (*3*). Recently, much of the pharmacological research has shown that Bu-zhong-yi-qi-tang has potent immunomodulatory and anticancer properties.

A study was conducted by Li *et al*. to investigate the frequencies and patterns of Chinese herbal medicine treatment for lung cancer patients and the effect of Chinese herbal medicine on their survival probability in Taiwan (*71*). They indicated that the use of Chinese herbal medicine as an adjunctive therapy might reduce the mortality hazard ratio of lung cancer patients and Bu-zhong-yi-qi-tang was found to be the top formula prescribed by traditional Chinese physicians for lung cancer patients. Yu *et al*. found that co-treatment with Bu-zhong-yi-qi-tang and cisplatin might reverse cisplatin resistance through induction of apoptosis and autophagy in lung cancer cells (*72*). Moreover, Bu-zhong-yi-qi-tang could inhibit 5-FU-induced intestinal mucositis, and this effect might be due to the reduction in apoptosis and necrosis in intestinal mucosal epithelia *via* the suppression of inflammatory cytokine up-regulation (*73*). Bu-zhong-yi-qi-tang was reported to have a protective effect for intestine and hematopoietic organs against radiation damage. It also could effectively improve localized radiotherapy-induced immune deterioration *via* increasing the number of CD19+ B cells in patients with end stage cancer (*74*). In addition, Bu-zhong-yi-qi-tang might have beneficial effects on cancer-related fatigue and QOL in cancer patients, and it also could reduce the extent of side effects such as leucopenia and intestinal damage and fatigue occurring as a result of radiation or chemotherapy used to treat malignant tumors (*75*).

3.2. *Shi-Quan-Da-Bu-Tang*

Shi-quan-da-bu-tang (Juzentaiho-to or TJ-48 in Japanese, or Sipjeondaebo-tang in Korean) is a well-known Chinese herbal formulation first recorded in the Chinese Song Dynasty (about A.D. 1,200) and it comprises 10 herbs including *Ginseng radix*, *Astragali radix*, *Angelicae radix*, *Rehmanniae radix*, *Atractylodis lanceae rhizoma*, *Cinnamomi cortex*, *Poria*, *Paeoniae radix*, *Ligustici rhizoma* and *Glycyrrhizae radix* (*5*). It has been used for many years for the treatment of various kinds of diseases such as anemia, rheumatoid arthritis, atopic dermatitis, chronic fatigue syndrome, and ulcerative colitis. Recently, Shi-quan-da-bu-tang has been reported to have antitumor effects and to modulate immune responses. It could reduce the side effects of chemotherapy, radiation therapy and surgical treatment, and prevent various types of cancers (*e.g.*, breast, liver, brain and pancreatic cancer) or their metastasis according

to numerous preclinical and clinical studies.

A Pilot, randomized, double-blind, placebo-controlled trial (*n* = 32) was conducted to evaluate the efficacy and safety of Shi-quan-da-bu-tang for anorexia in patients with cancer (*76*). The results showed that 4 weeks of Shi-quan-da-bu-tang treatment effectively improved the QOL and anorexia in patients. As Shi-quan-da-bu-tang is commonly used by patients with lung cancer undergoing outpatient chemotherapy, a QOL questionnaire for cancer patients treated with anticancer drugs was conducted in patients (*n* = 16) with non-small cell lung cancer (*77*). Significant improvement was observed in the total QOL score, mainly owing to improvement in patients "physical condition." TJ-48 also could increase regulatory activities in T cells through decreasing Foxp3+ Treg populations in advanced pancreatic cancer patients, and this effect might lead to immune-augmentation for various combination therapies (*78*). Moreover, the effect of Shi-quan-da-bu-tang on natural killer (NK) cell activity and metastasis in combined treatments with anti-PD-1 antibody in a mouse model of melanoma metastasis was investigated (*79*). The data suggested that Shi-quan-da-bu-tang could inhibit B16 cell metastasis by inducing NK cell activity. Additionally, combination therapy with Shi-quan-da-bu-tang and anti-PD-1 antibody increased treatment response rates for B16 melanoma. In addition, TJ-48 was effective in alleviating bone marrow suppression caused by TS-1 (an oral anticancer drug containing a 5-FU derivative Tegafur) in mice (*5*).

3.3. *Xiao-chai-hu-tang*

Xiao-chai-hu-tang (Sho-sai-ko-to or TJ-9 in Japanese), a classical traditional Chinese herbal formulation originally recorded in "Shang Han Lun", has been used to treat liver diseases especially chronic hepatitis and liver cancer for thousands of years in China and Japan. It consists of seven medicinal herbs (*Bupleurum falcatum*, *Scutellaria baicalensis*, *Panax ginseng*, *Zizyphus jujube*, *Pinellia ternate*, *Zingiber officinale*, and *Glycyrrhiza glabra*) (*5*). Much pharmacological research has shownthat Xiao-chai-hu-tang has potent antiinflammation, antioxidation, immunomodulation, hepatoprotective, anti-hepatic fibrosis, and antitumor properties. Recently, many basic or clinical studies have been conducted to assess the beneficial effects and safety of Xiao-chai-hu-tang for cancer treatment. These studies have demonstrated that Xiao-chai-hu-tang treats cancer by enhancing immune regulation, anti-angiogenesis and apoptosis of tumor cells.

Xiao-chai-hu-tang could halt cell proliferation and promote apoptosis of human hepatocellular carcinoma (HCC) cells *via* regulating the expression of Bax, Bcl-2, CDK4 and cyclin-D1 (*80*). A cross-sectional analysis of the National Health Insurance Research Database in Taiwan was conducted to investigate the prescription frequency and patterns of Chinese herbal medicines for

HCC patients. They found that the herbal preparation of Xiao-chai-hu-tang was the most obviously increased and important Chinese herbal medicine being used for HCC patients (*81*). A cohort study that also used the Taiwanese National Health Insurance Research Database was conducted to investigate the effects of Chinese herbal medicine on HCC risk among patients with chronic hepatitis B. They suggested that the use of some Chinese herbal medicines including Xiao-chai-hu-tang was associated with a significantly reduced HCC risk in patients with chronic hepatitis B, which supports the integration of TCM into clinical practice to influence a favorable prognosis (*82*). In addition, Xiao-chai-hu-tang gargle as a gargling agent for patients receiving chemotherapy showed a significantly decreased incidence of stomatitis, and a painkilling effect compared to gargling with providone-iodine and amphotericin B. Thus, Xiao-chai-hu-tang gargle was considered to be a useful method against stomatitis prevention and sharp pain mitigation from chemotherapy (*83*).

3.4. *Huang-qin-tang*

Huang-qin-tang is a classical traditional Chinese herbal formulation with four herbs (*Scutellaria baicalensis Georgi*, *Paeonia lactiflora Pall*, *Glycyrrhiza uralensis Fisch*, and *Ziziphus jujuba Mill*), which was first recorded in "Shang Han Lun". It has been used for over 1800 years to treat a variety of gastrointestinal symptoms including diarrhea, nausea and vomiting, and abdominal cramps (*5*). PHY906 (KD018) is a modified pharmaceutical preparation derived from the traditional herbal formulation Huang-qin-tang and it consists of the same four herbs as Huang-qin-tang at a relative weight ratio of 3:2:2:2 (*3*). A series of preclinical and clinical studies to investigate the anticancer activities of PHY906 has been conducted in recent years. PHY906 not only enhances the antitumor efficacy of some anticancer drugs but also alleviates chemotherapy-induced side effects, such as diarrhea (*84*). PHY906 can serve as an adjuvant to Sorafenib, CTP-11, 5-FU, leucovorin (LV), and capecitabine in the treatment of advanced colorectal, pancreatic, and liver cancer (*85,86*).

According to a preclinical study, PHY906 was reported to enhance the anti-tumor activity of Sorafenib in nude mice bearing HepG2 xenografts by targeting the inflammatory state of the microenvironment of tumor tissue (*85*). PHY906 was also demonstrated to decrease toxicity from fractionated abdominal irradiation by promoting faster recovery of the intestine (*87*). Additional preclinical studies have shown that PHY906 could reduce the toxicity associated with CTP-11 treatment while increasing CTP-11's antitumor effects in metastatic colorectal cancer (*86*). Clinical studies indicated that PHY906 treatment could result in a significant decrease in patient's gastrointestinal toxicity, and no PHY906-associated toxicity has been observed (*84*).

4. Chinese medicine preparations commonly used in clinical practice for cancer treatment

Chinese medicine preparations are a form of Chinese herbal medicine that are isolated from single herbs or their active compounds or herbal formulations and prepared using modern advanced pharmaceutical technology (*3*). There are various dosage forms including injections, tablets, pills, capsules, and liquids. Compared to traditional decoctions, Chinese medicine preparations are safer, more effective, and easier to use (*5*). Thus, Chinese medicine preparations are becoming increasingly popular in China and are attracting worldwide attention.

Currently in China, some Chinese medicine preparations are derived from single TCMs or their active compounds or herbal formulations, which have properties of spiriting vital energy and their anticancer molecular mechanisms mainly by improving immunity (*e.g.*, Shenqi fuzheng injection and Kanglaite injection). Some Chinese medicine preparations are derived from single TCMs or their active compounds or herbal formulations, which have properties of clearing heat and detoxifying, promoting blood circulation and removing blood stasis and their anticancer molecular mechanisms involving apoptosis, cell cycle arrest, angiogenesis and metastasis, immune-regulation, and so on (*e.g.*, Huachansu injection and Brucea javanica injection). We want to stress that some TCMs and some natural compounds like Mylabris, Chansu, camptothecin derivatives, and vinca alkaloids are toxic. However, the application of these toxicants provides a magic power to deal with severe diseases like cancer, and this process might be described as "fighting fire with fire" (*88*). Thus, in the following, a brief outline of the oncologic pharmacology of the most commonly used Chinese medicine preparations including some toxicants that have been approved by the State Food and Drug Administration (FDA) of China are briefly presented below (Table 3).

4.1. *Shenqi fuzheng injection*

Shenqi fuzheng injection is an injectable traditional Chinese herbal formula comprised of two herbal medicines, *Radix Astragali* (Huang-Qi) and Codonopsis pilosula (Dang-Shen). The injection has been approved by China's FDA since the 1990s (*3*). It is used extensively throughout China to modify the immunological function of patients with chronic diseases including cancer and cerebrovascular diseases such as, angina, coronary heart disease, heart failure, and so on. Currently, many trials have studied the Shenqi fuzheng injection in combination with chemo- or radio-therapy in patients with lung, breast, and colorectal cancer; some have shown that the Shenqi fuzheng injection may play an important role in the treatment of advanced cancers by improving tumor response and reducing the toxicity of chemotherapy (*89-91*).

Table 3. Chinese medicine preparations commonly used clinically for cancer treatment

Common name	Source or composition	Biological activity	Preclinical and/or clinical evidence of anticancer activity	Ref.
Shenqi fuzheng injection	Comprised of 2 herbs: *Radix Astragali Codonopsis pilosula*	Antitumor, immunomodulation	*Clinical*: improve the chemotherapy efficacy and the quality of survival (KPS), strengthen cellular immune function, and decrease the chemotherapy and/or radiotherapy toxicities. *Preclinical*: attenuate cranial radiation therapy-induced brain injury in mice *via* inhibition of the NF-κB signaling pathway and microglial activation.	89-91 92
Kanglaite injection	Extracted from *Semen Coicis Yokuinin*	Antitumor	*Preclinical*: (*i*) Combined with Gefitinib: promoting apoptosis and increasing sensitivity to Gefitinib in human lung adenocarcinoma cells; (*ii*) Inhibiting TNF-α-mediated EMT in colorectal cancer cell lines *via* inhibition of NF-κB pathway. *Clinical*: (*i*) Combined with gemcitabine: demonstrated encouraging clinical evidence of anti-neoplastic activity and a well-tolerated safety profile; (*ii*) Combined with FOLFOX regimen: strengthen the overall response rate, improve the QOL, reduce nausea and vomiting, and reduce the incidence of leucopenia.	93,94 96,97
Huachansu injection	Extracted from the skin and parotid venom glands of the toad *Bufo bufo gargarizans* Cantor	Antitumor, Anti-HBV, immunomodulation	*Preclinical*: (*i*) Combined with doxorubicin: increase apoptosis of HCC cells through the Fas- and mitochondria-mediated pathways; (*ii*) Regulating cancer cell migration by matrix metalloproteinases of human breast carcinoma cells; (*iii*) inhibiting proliferation and inducing apoptosis in human bladder cancer cells by Fas/FasL and TNF-α/TNFR1 pathway. *Clinical*: (*i*) Improving objective tumor response and reducing chemotherapy-related side effects; (*ii*) Combined with TACE could significantly increase the objective response rate and 2-year survival rate; (*iii*) Reducing the quantity of pericardial effusion and improving the patient's QOL.	98-101 102-104
Brucea javanica oil emulsion injection	Extracted from *Brucea javanica* Merr.	Antitumor	*Clinical*: (*i*) Enhancing chemotherapeutic effect, improving QOL, and reducing adverse effects of platinum-contained chemotherapeutics; (*ii*) Intrapleural injection of chemotherapy drugs plus BJOEI has a better benefit of ORR for treating malignant pleural effusions and improves the QOL of malignant pleural effusions patients.	107-110

Abbreviations: epithelial mesenchymal transition (EMT); tumor necrosis factor-alpha (TNF-α); transcatheter arterial chemoembolization (TACE); Brucea javanica oil emulsion injection (BJOEI); overall response rate (ORR).

A meta-analysis indicated that Shenqi fuzheng injection combined with chemotherapy (*e.g.*, FOLFOX regimen and XELOX regimen) in treatment of colorectal cancer could improve chemotherapy efficacy and quality of survival (KPS), strengthen cellular immune function (CD3+, CD4+, CD4+/CD8+ and NK+), and reduce adverse events such as leukocytopenia, thrombocytopenia and gastrointestinal toxicity (*89*). Additional meta-analysis demonstrated that the Shenqi fuzheng injection intervention with conventional chemotherapy exhibited better therapeutic efficacy than the conventional chemotherapy group with a statistically significant higher objective tumor response in the treatment of lung, breast, and digestive cancers. Cotreatment with Shenqi fuzheng injection could enhance NK, CD3 +, CD4 + level, and CD4 +/CD8 + ratio compared with the conventional chemotherapy group (*90*). Moreover, Shenqi Fuzheng injection can improve the clinical efficacy and decrease the radiation toxicities in the NSCLC patients treated with radiation (*91*). In addition, Shenqi fuzheng injection could attenuate cranial radiation therapy-induced brain injury in mice *via* inhibition of the NF-κB signaling pathway and microglial activation (*92*).

4.2. *Kanglaite injection*

Kanglaite injection is an acetone extract of herbal medicine coix seed (Semen Coicis Yokuinin) prepared as an herbal medicine using modern advanced pharmaceutical technology. In August 1997, Phase III clinical trials were completed and Kanglaite injection was officially launched in China after final approval from the Ministry of Public Health (*5*). Since that time, over 1 million cancer patients have received Kanglaite injection. Kanglaite injection is mainly used for the treatment of NSCLC, liver cancer, gastric cancer, *etc*. It has been found to significantly decrease cancer load, improve QOL of cancer patients, and may ameliorate multiple drug resistance of cancers when combined with chemo-, radio-, or targeted-therapy in clinical use.

According to a preclinical study, Kanglaite injection combined with Gefitinib had an outstanding apoptosis promotion effect on A549 cell lines of lung adenocarcinoma, and Kanglaite injection could increase sensitivity of A549 cells of human lung adenocarcinoma to Gefitinib (*93*). Additionally, a recent study reported that Kanglaite injection could inhibit tumor necrosis factor-alpha-mediated epithelial mesenchymal transition (EMT) in colorectal cancer cell lines *via* inhibition of NF-κB pathway (*94*).

In clinical practice, Kanglaite injection was reported to provide objective evidence for lung cancer and significantly reduce the expression of miRNA-21 in patients with advanced lung cancer (*95*). Moreover, a randomized, open-label, safety and exploratory efficacy study of Kanglaite injection plus Gemcitabine versus Gemcitabine in patients with advanced pancreatic cancer

was published in 2017 by Schwartzberg *et al*. This multi-centered, randomized phase 2 trial indicated that Kanglaite injection (30 g/day) plus a standard regimen of gemcitabine demonstrated encouraging clinical evidence of anti-neoplastic activity and a well-tolerated safety profile (*96*). In addition, a network of meta-analysis involving 38 randomized controlled trials and 2,761 participants was conducted to compare which was the best Chinese herb injection based on the FOLFOX regimen for gastric cancer. Kanglaite injection exhibited greater effects than many other Chinese herb injections in clinical efficacy and safety for gastric cancer. It could strengthen the overall response rate, improve the QOL, reduce nausea and vomiting, and reduce the incidence of leukopenia (III-IV) (*97*).

4.3. *Huachansu injection*

Huachansu injection or Cinobufacini injection is a water-soluble preparation extracted from the skin and parotid venom glands of the toad (*Bufo bufo gargarizans* Cantor) which contains Chansu. It has been approved by China's FDA since the 1990s and widely used to treat patients with lung, liver, colon, and pancreatic cancers at oncology clinics in China (*3*). Cardiac glycosides including bufalin, resibufogenin, and cinobufagin are the three major active constituents to which the antitumor activity of Huachansu injection may be attributed. Huachansu injection exhibited significant effects on inhibition cell proliferation, induction of cell differentiation and apoptosis, disruption of the cell cycle, inhibition of cancer angiogenesis, reversal of multi-drug resistance, and regulation of the immune response in cancer cells (*5*). It also could effectively enhance physical immunity and improve the QOL with little toxicity in cancer patients.

Pre-clinical studies have shown that Huachansu effectively inhibits growth and induces apoptosis in human HCC. Combination of Cinobufacini and doxorubicin could increase apoptosis of HCC cells through the Fas- and mitochondria-mediated pathways (*98*). Additionally, recent studies reported that cinobufacini might be able to regulate cancer cell migration accelerated by matrix metalloproteinases of human breast carcinoma cell line MDA-MB-231 (*99,100*). Moreover, Huachansu could efficiently inhibit proliferation and induce apoptosis in human bladder cancer cells *in vitro* and *in vivo*, which was largely mediated by Fas/FasL and TNF-α/TNFR1 pathway (*101*).

A meta-analysis suggested that Huachansu could be a promising supplement to routine chemotherapy in treating advanced NSCLC. It could effectively improve objective tumor response of NSCLC patients and reduce chemotherapy-related side effects including leukocytopenia, thrombocytopenia, and nausea and vomiting and so on (*102*). Another meta-analysis demonstrated that cinobufacini combined

with transcatheter arterial chemoembolization (TACE) could significantly increase the objective response rate and 2-year survival rate compared with TACE only in patients with advanced HCC (*103*). In addition, Huachansu injection has been reported to be effective for treating malignant pericardial effusion, pleural effusions, and ascites by intracavitary injection. Huachansu injection could effectively relieve the patient's cardiac tamponade symptoms and improve the patient's QOL with the levels of CA-125 in pericardial effusion decreased and the quantity of pericardial effusion significantly reduced (*104*). Recently, a randomized phase II study demonstrated that Cinobufacin injection, when combined with gemcitabine, failed to improve the outcome of patients with locally advanced and/or metastatic pancreatic cancer (*105*). This is partly due to the insufficient efficacy of Cinobufacin injection in current formulation. Therefore, development of a more potent drug formulation demands a clear knowledge of the active components in Cinobufacin, and identification of their putative biomarkers.

4.4. *Brucea javanica oil emulsion injection*

Brucea javanica oil emulsion injection (BJOEI) is one of TCMs products, which takes Brucea Jen petroleum ether extracts as raw material and purified soybean lecithin as emulsifier (*106*). It is employed as adjunctive therapy in the treatment of lung carcinoma, brain metastasis of lung carcinoma, and gastrointestinal tumorigenesis.

The anticancer activity of BJOEI might be attributed to the following properties: inducing apoptosis, disturbing the cell cycle, disrupting cellular energy metabolism, and depressing expression of vascular endothelial growth factor (*107*). A great number of published studies have proved that BJOEI can perform a synergistic antitumor effect by improving tumor response, boosting KPS, reducing the incidence of adverse events and stimulating immunity during chemotherapy or radiotherapy (*108*).

A meta-analysis involving twenty-one studies and 2234 cases indicated that BJOEI could enhance the chemotherapeutic effect in NSCLC patients, improve the QOL, and reduce adverse effects of platinum-contained chemotherapeutics including nausea and vomiting and leucopenia, and thus it is worth referring to the clinic (*107*). Moreover, BJOE combined with chemotherapy could be considered as a safe and effective regimen in treating patients with advanced gastric cancer. A meta-analysis demonstrated that BJOEI combined with chemotherapy (*e.g.*, Potassium capsule, Cisplatin, 5-FU, and Oxaliplatin) for treating gastric cancer possessed the property of prominently relieving nausea and vomiting, diarrhea, neutropenia, neurotoxicity, and so on (*109*). In addition, intrapleural injection of traditional chemotherapy drugs plus BJOEI has a better benefit of overall response rate (ORR) for treating malignant pleural effusions and improves the QOL of malignant

pleural effusions patient, compared with traditional chemotherapy drugs alone (*110*). The participation of BJOEI could reduce the toxicity caused by chemotherapy drugs. However, more prospectively designed, large-sample, and multicenter rigorously randomized controlled trials (RCTs) should be needed for BJOEI in future studies.

5. Clinical trials of Chinese herbal medicines as adjuvant treatment in cancer therapy

In conventional Western medicine, chemotherapy, radiotherapy and targeted-therapy are major conventional cancer therapies and bring great benefit to the survival of patients; however, these treatments typically affect multiple organ systems including gastrointestinal tract, heart, liver, kidney, marrow, skins, peripheral nerves, blood vessels, and so on. Fatigue, pain, diarrhea, nausea, vomiting, hair loss, cardiac injury (*e.g.*, myocardial ischemia, hypertension, cardiomyopathy, and arrhythmia), bone marrow suppression, liver and kidney dysfunction, and peripheral neuropathy symptoms are common side effects and complications during chemo-, radio- or targeted-therapy (*5,9*). These complications and side effects inconvenience and cause discomfort to patients and they may also limit or prevent delivery of therapy at its optimal dose and time, potentially causing fatalities. Among them, febrile neutropenia is a life-threatening condition that requires immediate attention, especially in patients with chemotherapy-related neutropenia, and cardiovascular disease represents the most common potentially life-threatening late effects (*111,112*). Thus, more effective therapies to help prevent and control complications and side effects of conventional cancer therapies must soon be developed. Some TCMs have been found to be adjunctive in cancer therapies. Here we will give a brief outline on the use of TCMs to reduce some complications and side effects associated with conventional cancer therapies in clinical studies (Table 4).

5.1. *Fatigue*

Cancer-related fatigue is a highly prevalent, persistent and subjective sense of tiredness related to cancer disease or cancer treatment which cannot be relieved by sleep or rest (*5,113*). Regardless of cancer type and treatment modality, nearly all patients experience fatigue during cancer treatment and nearly a third report chronic fatigue that persists for years after treatment completion. It significantly interferes with patients' daily activities and decreases their QOL. Additionally, these symptoms can be accompanied by depression and impairment in cognition and sleep. However, it remains under-recognized and under-treated, partly because of limited understanding of its pathophysiology and lack of effective treatments. Traditional Chinese medical

comprehensive therapy might have its advantages in dealing with this condition.

A systematic review of randomized clinical trials involving 10 trials and 751 participants was conducted to analyze the effect of Chinese herbal medicine for cancer-related fatigue (*114*). The findings showed that Chinese herbal medicine plus chemotherapy or supportive care was superior to chemotherapy or supportive care in improving quality of life including relieving cancer-related fatigue and anxiety. In addition, a randomized, double-blind, placebo-controlled clinical trial was conducted to evaluate the efficacy of Shen-mai-san (a famous Traditional Chinese herbal formulation composed of processed Ginseng, Liriope spicata, and Schizandrae fructus) in patients with cancer who were undergoing chemotherapy or radiotherapy (*115*). Shenmai-san was found to be effective for treating cancer-related fatigue and had anti-fatigue activity as shown on a QOL questionnaire and laboratory data (*e.g.*, WBC, Hb, platelet, CEA, heart rate variability, and liver and renal functions). Furthermore, Bu-Zhong-Yi-Qi-Tang was reported to have beneficial effects on cancer-related fatigue and quality of life in cancer patients (*75*). Taken together, the findings from a limited number of trials suggest that Chinese herbal medicine seems to be effective and safe in the treatment of cancer-related fatigue. However, the current evidence is insufficient to draw a confirmative conclusion due to the poor methodological quality of included trials. Thus, conducting rigorously designed trials on potential Chinese herbal medicine is warranted.

5.2. *Chronic pain*

Pain is a common and burdensome symptom of cancer and the causes of pain can be the cancer itself (the tumor pressed on bones, nerves, or other organs) or its treatment (*e.g.*, surgery, chemotherapy, or radiotherapy). It was reported that 75-90% of cancer patients especially who have bone metastasis experienced pain during their illness (*5*). As indicated in current WHO guidelines, three step analgesic ladder therapies are the standard of care for cancer pain. However, up to 50% of cancer pain is still undertreated. In recent years, many clinical trials have suggested that some TCMs as adjunctive therapy increase the peripheral release of endogenous analgesic agents, reduce pain mediator secretion and induce central nervous system (CNS) analgesia. These studies demonstrated that the use of TCM to treat pain triggered by cancer is effective and economical and furthermore produces fewer side effects (*116*).

Wen Jing Zhi Tong Fang, is a Chinese herbal medicine first recorded in the Qing Dynasty and composed of evodia rutaecarpa (Wuzhuyu), semen sinapis (Baijiezi), ephedra sinica (Mahuang), and asarum sieboldii (Xixin). It is designed for cancer pain relief through dredging healthy *Qi* to warm and activate blood

Table 4. Clinical trials of Chinese herbal medicines as adjuvant treatment to reduce complications and side effects during chemotherapy

Chinese herbal medicines	Complications and side effects	Clinical trials of TCMs as adjuvant treatment in cancer therapy				
		Patients (*n*)	Experimental group	Control group	Outcomes	*Ref.*
TJ-41	Fatigue	*n* = 40	TJ-41	Nothing	Fatigue levels increased (experimental group vs. control group, p < 0.05)	*75*
Shen-mai-san	Fatigue	*n* = 60	Shen-mai-san	Placebo	QOL and laboratory data (e.g., CEA, heart rate variability, and liver and renal functions) improved	*115*
Wen Jing Zhi Tong Fang	Chronic pain	*n* = 62	Wen Jing Zhi Tong Fang + appropriate analgesic drug	Appropriate analgesic drug	Relieving cancer-related pain with reduced doses of analgesic drugs, less adverse reactions, and improved QOL.	*117*
Fufang E-Jiao Jiang	Bone marrow suppression	*n* = 64	Fufang E-Jiao Jiang + chemotherapy + rhIL-11 + rhG-CSF	Chemotherapy + rhIL-11 + rhG-CSF	Relieving the myelosuppression caused by GP regimen and increasing white cell and blood platelets counts	*119*
Elemene injection	Bone marrow suppression	*n* = 765	Elemene injection + radiation	Radiation	Reducing the incidence of bone marrow suppression and improving QOL	*120**
TJ-43	Gastrointestinal function	*n* = 60	TJ-43	Placebo	Reducing anorexia and maintaining food intake caused by cisplatin-including chemotherapy	*122*
PHY906	Gastrointestinal function	*n* = 24	PHY906 + chemotherapy	Chemotherapy	Some gastrointestinal side effects such as diarrhea, abdominal cramps, and vomiting were reduced	*5*
AC591	CIPN	*n* = 72	AC591 + chemotherapy	Chemotherapy	Preventing oxaliplatin-induced neuropathy without reducing its antitumor activity	*123*
Aidi injection	Radiation pneumonitis	*n* = 1,192	Aidi injection + radiotherapy	Radiotherapy	Alleviating the radiation pneumonitis, radiation esophagitis, and myelosuppression of radiotherapy	*128**
Zhi-Gan-Cao-Tang	Cardiotoxicity	A case report	Zhi-Gan-Cao-Tang + Anthracycline compounds	Anthracycline compounds	Chest X-ray: great improvements in pulmonary edema and cardiomegaly.	*131*
Xiao-chai-hu-tang (TJ-9)	Acneiform eruptions	A case report	TJ-9 + Gefitinib	Gefitinib	Exhibiting significant effects on acneiform eruptions induced by Gefitinib	*132*

*A systematic review and meta-analysis; Abbreviations: Bu-Zhong-Yi-Qi-Tang (TJ-41); Liu-jun-zi-tang (TJ-43); Huangqi Guizhi Wuwu decoction (AC591); Chemotherapy induced peripheral neuropathy (CIPN).

and by promoting circulation through the back meridians, which is considered to be the source of yang *Qi* (healthy *Qi*) and have broad connections with the viscera. The application of CMWC on back meridians combined with WHO 3-step analgesic ladder treatment was effective in relieving cancer-related pain with reduced doses, less adverse reactions, and improved QOL (*117*). Shuangbai San is a Chinese herb preparation used externally to treat pain. It contains 6 Chinese herbal medicines: Oriental Arborvitae, Rhubarb, Phellodendron amurense, Mint, Eupatorium japonicum, and Corydalis). A multicenter, randomized, double-blind, placebo-controlled trial indicated that the use of Shuangbai San could effectively relieve mild pain in liver cancer patients and improve their QOL (*118*). In all, TCM interventions appear to have beneficial effects on cancer-related pain. However, there are several limitations associated with the current

published studies on TCMs relieving pain such as indeterminate results, small sample sizes, and little examination of outcomes. Therefore, further research with rigorous design and larger sample size is needed to re-evaluate the effectiveness of TCMs in treating cancer related pain.

5.3. Bone marrow suppression

Bone marrow suppression is a reduction in the activity of bone marrow, resulting in decreased numbers of red blood cells, platelets, and white blood cells. One of the most common reasons for a patient to have this condition is chemotherapy treatment for cancer. While the bone marrow is functioning below normal levels, the patient is at risk, and needs to be monitored very closely. In some cases, hospitalization is recommended for people

with Bone marrow suppression until their bone marrow is functioning normally. In recent years, some TCMs have been reported to have beneficial effects on cancer therapy related bone marrow suppression.

Colla corii asini (or E-Jiao in Chinese), donkey-hide gelatin prepared by stewing and concentrating from Equus asinus L. donkey hide, is a health-care food and traditional Chinese medicine widely used in life-nourishing and clinical hematic antanemic therapy for more than 2,000 years in China (5). Many studies indicated that E-Jiao and its preparations such as Fufang E-Jiao Jiang could effectively promote the recovery of bone marrow hemopoietic function in cancer patients with myelosuppression. Fufang E-Jiao Jiang in combination with conventional interleukin-11 (rhIL-11) and recombinant human granulocyte colony stimulating factor (rhG-CSF) in cancer patients showed significant effects on relieving the myelosuppression caused by GP (Gemcitabine + DDP) chemotherapy regimen and increasing white cell and blood platelet counts compared to using rhIL-11 and rhG-CSF groups alone (119). In addition, the elemene injection combined radiotherapy in the treatment of lung cancer with brain metastases appears to improve the treatment response rate and alleviated symptoms. The combined treatment has showed positive impact to reduce the incidence of bone marrow suppression and improve QOL (120). Kushen injection combined with radiotherapy significantly improved the clinical effect and reduced the incidence of adverse events including bone marrow suppression, radiation pneumonia, and radiation esophagitis (121). In all, TCM interventions appear to have beneficial effects for alleviating myelosuppression caused by chemotherapy in cancer patients. However, there are several limitations associated with the current published studies of TCMs relieving myelosuppression such as indeterminate results, small sample sizes, and little examination of outcomes. Thus, conducting rigorously designed trials on potential Chinese herbal medicine are warranted.

5.4. Gastrointestinal side effects

Gastrointestinal side effects including loss of appetite, diarrhea, nausea, and vomiting are the most common symptoms occurring in cancer patients after surgery and/or receiving chemo-, radio-, or targeted-therapy. However, there is still no effective treatment to ameliorate these symptoms in cancer patients. Recently, many clinical trials have suggested that some TCMs may be effective for treating gastrointestinal side effects.

Liu-jun-zi-tang (TJ-43 or Rikkunshito in Japanese) is a famous Traditional Chinese herbal formulation including 6 herbs (*Ginseng Radix*, *Poria cocos*, *Rhizoma atractylodis macrocephalae*, *liquorice root*, *pinelliae tuber*, *pericarpium citri*,*common ginger*, and *Jujube*) (5). TJ-43 enhances digestive tract motility,

improves the gastric accommodation reflex, protects against gastric mucosal injury, and enhances appetite. Based on these mechanisms, TJ-43 has been used to treat various gastrointestinal tract diseases, such as functional dyspepsia, gastroesophageal reflux disease, and chemotherapy-induced nausea. A placebo-controlled, double-blind, randomized trial was conducted to evaluate the efficacy of TJ-43 for chemotherapy-induced anorexia (122). TJ-43 was shown to have the effect of reducing anorexia and maintaining food intake caused by cisplatin-including chemotherapy in patients with lung cancer. In addition, some clinical studies have shown that PHY906 enhances the therapeutic indices of a broad spectrum of anticancer agents such as Capecitabine, 5-FU and irinotecan in colorectal, liver, and pancreatic cancers. PHY906 could reduce chemotherapy-induced toxicities especially gastrointestinal side effects (5,86).

5.5. Peripheral neuropathy

Chemotherapy induced peripheral neuropathy (CIPN) is a common significant and debilitating side-effect resulting from the administration of neurotoxic chemotherapeutic agents. These pharmaco-chemotherapeutics can include taxanes, vinca alkaloids, platinum analogues, and others. Moderate to severe CIPN significantly decreases the quality of life and physical abilities of cancer patients. However, there are currently no effective drugs to prevent CIPN. Recently, many clinical trials have suggested that some TCMs may be effective at treating CIPN.

AC591 is a standardized extract of Huangqi Guizhi Wuwu decoction, an herbal formula recorded in "Synopsis of the Golden Chamber" for improving limb numbness and pain. AC591 could prevent oxaliplatin-induced neuropathy without reducing its antitumor activity, and might be a promising adjuvant to alleviate sensory symptoms in clinical practice (123). Goshajinkigan, a Japanese traditional herbal medicine (Kampo), is a promising drug which is widely used to treat diabetic neuropathy and CIPN in Japan. It could relieve the oxaliplatin-induced cold hyperalgesia and mechanical allodynia without affecting anti-tumor activity of oxaliplatin, and, therefore, might be useful for the oxaliplatin-induced neuropathy in clinical practice (124).

5.6. Radiation pneumonitis

Radiotherapy pneumonitis (RP) caused by radiation-induced lung toxicity is the most serious complication (125). It typically presents 1-6 months after radiation therapy. The clinical features usually include mild dry cough, mild fever, and mild dyspnea, but in some cases, severe respiratory failure appears and leads to death. The incidence of moderate to severe radiotherapy pneumonitis with radiotherapy is 10-20%. When RP

is left untreated for a long time, it may develop into pulmonary fibrosis, which has a high rate of mortality. However, there is a lack of drugs for prevention and treatment of this disease. In recent years, some TCMs have been reported to have beneficial effects on radiotherapy-related radiation pneumonitis.

A systematic review involving twenty-two RCTs and 1819 participants was conducted to evaluate the efficacy and safety of herbal medicines as adjunctive therapy for the prevention of radiation pneumonitis in patients with lung cancer who undergo radiotherapy (*126*). The findings showed that the herbal formulas used in combination with radiation therapy consisted mainly of those that tonify yin, tonify qi, and nourish blood. Among them, Ophiopogonis Radix is the most commonly used herb that nourishs yin, Astragali Radix is a typical herb with qi-tonifying effects, and *Angelicae Sinensis Radix* is a classic herb that nourishes blood for lung cancer as adjunctive therapy with radiotherapy. A recent systematic review reported that Astragalus-containing Chinese herbal medicines are effective at protecting against radiotherapy pneumonitis as adjunctive therapy during conservative radiotherapy (*127*). Aidi injection (Z52020236, China Food and Drug Administration (CFDA)) is an adjuvant chemotherapy drug commonly used in China, which is composed of the extracts from Astragalus, Eleutherococcus senticosus, Ginseng, and Cantharidin. Astragalus, Eleutherococcus senticosus, Cantharidin and Ginseng, and others are important traditional Chinese medicine, which appear to have antitumor activity, immunoregulation, and attenuation to the acute or subacute toxicity induced by chemotherapy (*128*). Aidi injection plus radiotherapy could significantly improve the clinical efficacy and QOL of patients with lung cancer. Aidi injection could alleviate the myelosuppression, radiation pneumonitis, and radiation esophagitis of radiotherapy. It had the attenuation and synergistic efficacy to radiotherapy. In all, there is some encouraging evidence that oral administration of herbal medicines combined with radiotherapy may benefit patients with thoracic cancer by preventing or minimizing radiation pneumonitis. However, due to the poor methodological quality of the identified studies, a definitive conclusion could not be drawn. To confirm the merits of this approach, further rigorously designed large scale trials are warranted.

5.7. Cardiotoxicity

Anthracycline compounds (*e.g.*, doxorubicin, epirubicin, and daunorubicin) are some of the most effective antineoplastic drugs in the treatment of both hematological malignancies and solid tumors (129). Moreover, anthracycline-based treatments are first-line chemotherapy agents used to treat breast cancer both in the adjuvant and neoadjuvant setting. Unfortunately, anthracycline-associated dose-dependent cardiotoxicity

is a limiting factor in clinical use. Extensive efforts have been devoted to identifying strategies to prevent anthracycline-induced cardiotoxicity. However, most cardioprotective agents have shown little effect in clinical trials. In recent years, some Chinese herbal medicines have been reported to have beneficial effects on anthracycline-induced cardiotoxicity.

Platycodon grandiflorum (Jie-Geng) is an herb that has been used in TCM for thousands of years to treat cardiovascular disease. In TCM theory, P. grandiflorum can nourish *Qi* and relieve symptoms, such as palpitations, shortness of breath, and chest pain. A randomized controlled trial indicated the cardioprotective effects and safety of P. grandiflorum in patients with early breast cancer receiving anthracycline-based chemotherapy (*130*). Zhi-Gan-Cao-Tang, an herbal formula recorded in "Shang-Han-Lun" to supplement Yang-*Qi*, nourish the Ying-blood, and strengthen the heart spirit as complementary medicines to relieve heart failure-related symptoms. It was reported that Zhi-Gan-Cao-Tang was the most frequent formula Chinese herbal formula prescribed by TCM practitioners for treating heart failure. A case was presented that anthracycline-induced cardiotoxicity resolved slowly following the administration of modified Zhi-Gan-Cao-Tang in an 18-year-old adolescent male with refractory acute lymphoblastic leukemia (ALL) (*131*). After 2 months of Zhi-Gan-Cao-Tang treatment, the follow-up chest X-ray showed great improvements in pulmonary edema and cardiomegaly.

5.8. Molecular-targeted drugs-related adverse effects

With molecular-targeted drugs especially epidermal growth factor receptor-tyrosine kinase inhibitors (EGFR-TKIs) (*e.g.*, Gefitinib and Afatinib) widely used, adverse effects of such treatments including acneiform eruptions, paronychia, xerosis, mucositis, and alopecia are thought to be less severe, but can still be significant (*6*). Not only can these toxicities severely affect patients' QOL, but in some specific instances, they can be associated with increased response to therapy. The incidence of acneiform eruptions is about 60-80% in patients using EGFR-TKIs. It usually appears within 1 to 3 weeks after EGFR-TKIs treatment and reaches a peak within 3 to 5 weeks. Li *et al*. reported that Xiao-chai-hu-tang exhibited significant effects on acneiform eruptions induced by Gefitinib (*132*). In addition, some Chinese herbal medicines with the properties of "clearing heat", "detoxifying" and "cooling blood" exhibited significant effects on acneiform eruptions induced EGFR-TKIs such as Cortex moutan, Radix paeoniae rubra, Fructus Kochiae, and so on (*133*). However, there are few reports on the effects of Chinese herbal medicines on molecular-targeted drugs-related adverse effects in English. Moreover, due to the poor methodological quality of the identified studies, a definitive conclusion could not be

drawn. To confirm the merits of this approach, further rigorously designed large scale trials are warranted.

6. Conclusion

In conclusion, Chinese herbal medicines substantially influence cancer therapy as adjuvant treatment. In cancer treatment, Chinese herbal medicines in combination with chemo-, radio-, and targeted-therapy are capable of enhancing the efficacy of and diminishing the side effects and complications caused by these therapies. Chinese herbal medicines have great advantages in terms of suppressing tumor progression, increasing the sensitivity of chemo-, radio-, and targeted-therapy, improving an organism's immune system function, and lessening the damage caused by these therapies. They have a significant effect on reducing cancer-related fatigue and pain, improving peripheral neuropathy and gastrointestinal side effects including diarrhea, nausea, and vomiting, decrease the incidence of bone marrow suppression, protecting anthracycline-induced cardiotoxicity and radiation-induced pneumonitis, and relieving EGFR-TKIs related acneiform eruptions and other side effects. This review of those medicines should contribute to an understanding of Chinese herbal medicines as adjuvant treatment for cancer and provide useful information for the development of more effective anti-cancer drugs. However, more rigorously designed trials on potential Chinese herbal medicine must be further examined involving cancer treatment especially molecular targeted-therapy in the future.

Acknowledgments

References

1. Torre LA, Bray F, Siegel RL, Ferlay J, Lortet-Tieulent J, Jemal A. Global cancer statistics, 2012. CA Cancer J Clin. 2015; 65:87-108.
2. Torre LA, Siegel RL, Ward EM, Jemal A. Global Cancer Incidence and Mortality Rates and Trends--An Update. Cancer Epidemiol Biomarkers Prev. 2016; 25:16-27.
3. Qi F, Li A, Inagaki Y, Gao J, Li J, Kokudo N, Li XK, Tang W. Chinese herbal medicines as adjuvant treatment during chemo- or radio-therapy for cancer. Biosci Trends. 2010; 4:297-307.
4. Macdonald JB, Macdonald B, Golitz LE, LoRusso P, Sekulic A. Cutaneous adverse effects of targeted therapies: Part I: Inhibitors of the cellular membrane. J Am Acad Dermatol. 2015; 72:203-218; quiz 219-220.
5. Qi F, Zhao L, Zhou A, Zhang B, Li A, Wang Z, Han J. The advantages of using traditional Chinese medicine as an adjunctive therapy in the whole course of cancer treatment instead of only terminal stage of cancer. Biosci Trends. 2015; 9:16-34.
6. Owczarek W, Słowińska M, Lesiak A, Ciążyńska M, Maciąg A, Paluchowska E, Marek-Józefowicz L, Czajkowski R. The incidence and management of cutaneous adverse events of the epidermal growth factor receptor inhibitors. Postepy Dermatol Alergol. 2017; 34:418-428.
7. Dai J, Belum VR, Wu S, Sibaud V, Lacouture ME. Pigmentary changes in patients treated with targeted anticancer agents: A systematic review and meta-analysis. J Am Acad Dermatol. 2017; 77:902-910.
8. Sun X, Zhang X, Nian JY, Guo J, Yin Y, Zhang GL, Yu MW, Zhang Y, Wang XM, Yang GW, Yang L, Cheng PY, Li JP. Chinese Herbal Medicine as Adjunctive Therapy to Chemotherapy for Breast Cancer: A Systematic Review and Meta-Analysis. Evid Based Complement Alternat Med. 2016; 2016:3281968.
9. Chung VC, Wu X, Lu P, Hui EP, Zhang Y, Zhang AL, Lau AY, Zhao J, Fan M, Ziea ET, Ng BF, Wong SY, Wu JC. Chinese Herbal Medicine for Symptom Management in Cancer Palliative Care: Systematic Review And Meta-analysis. Medicine (Baltimore). 2016; 95:e2793.
10. Wang CY, Bai XY, Wang CH.Traditional Chinese medicine: A treasured natural resource of anticancer drug research and development. Am J Chin Med. 2014; 42:543-559.
11. Liu ZL, Zhu WR, Zhou WC, Ying HF, Zheng L, Guo YB, Chen JX, Shen XH. Traditional Chinese medicinal herbs combined with epidermal growth factor receptor tyrosine kinase inhibitor for advanced non-small cell lung cancer: A systematic review and meta-analysis. J Integr Med. 2014; 12:346-358.
12. Ling CQ. My reviews on the etiology and pathogenesis of malignant cancer. Journal of Traditional Chinese Medicine. 2009; 50:952-953. (in Chinese)
13. Xiang YZ, Shang HC, Gao XM, Zhang BL. A comparison of the ancient use of Ginseng in traditional Chinese medicine with modern pharmacological experiments and clinical trials. Phytother Res. 2008; 22:851-858.
14. Sun YX. Structure and biological activities of the polysaccharides from the leaves, roots and fruits of *Panax ginseng* C.A. Meyer: An overview. Carbohydr Polym. 2011; 85:490-499.
15. Mohanan P, Subramaniyam S, Mathiyalagan R, Yang DC. Molecular signaling of ginsenosides Rb1, Rg1, and Rg3 and their mode of actions. J Ginseng Res. 2018; 42:123-132.
16. Xie J, Shao J, Lu Y, Chen J, Wang J, Yu S, Jia L. Separation of ginseng active ingredients and their roles in cancer metastasis supplementary therapy. Curr Drug Metab. 2013; 14:616-623.
17. Yun TK, Choi SY. Preventive effect of ginseng intake against various human cancers: A case-control study on 1,987 pairs. Cancer Epidemiol Biomarkers Prev. 1995; 4:401-408.
18. Lee JH, Kwon KR, Cho CK, Han SS, Yoo HS. Advanced cancer cases treated with cultivated wild ginseng phamacopuncture. J Acupunct Meridian Stud. 2010; 3:119-124.
19. Barton DL, Liu H, Dakhil SR, Linquist B, Sloan JA, Nichols CR, McGinn TW, Stella PJ, Seeger GR, Sood A, Loprinzi CL. Wisconsin Ginseng (Panax quinquefolius) to improve cancer-related fatigue: A randomized, double blind trial, N07C2. J Natl Cancer Inst. 2013; 105:1230-1238.

20. Lee TK, Johnke RM, Allison RR, O'Brien KF, Dobbs LJ Jr. Radioprotective potential of ginseng. Mutagenesis. 2005; 20:237-243.

21. Kim HG, Jang SS, Lee JS, Kim HS, Son CG. *Panax ginseng* Meyer prevents radiation-induced liver injury *via* modulation of oxidative stress and apoptosis. J Ginseng Res. 2017; 41:159-168.

22. Jiang Z, Yang Y, Yang Y, Zhang Y, Yue Z, Pan Z, Ren X. Ginsenoside Rg3 attenuates cisplatin resistance in lung cancer by downregulating PD-L1 and resuming immune. Biomed Pharmacother. 2017; 96:378-383.

23. Zhang Y, Wang XQ, Liu H, Liu J, Hou W, Lin HS. A multicenter, large-sample, randomized clinical trial on improving the median survival time of advanced non-small cell lung cancer by combination of Ginseng Rg3 and chemotherapy. Zhonghua Zhong Liu Za Zhi. 2018; 40:295-299. (in Chinese)

24. Rossi RE, Pericleous M, Mandair D, Whyand T, Caplin ME. The role of dietary factors in prevention and progression of breast cancer. Anticancer Res. 2014; 34:6861-6875.

25. Lopes CM, Dourado A, Oliveira R. Phytotherapy and Nutritional Supplements on Breast Cancer. Biomed Res Int. 2017; 2017:7207983.

26. Qi Y, Gao F, Hou L, Wan C. Anti-Inflammatory and Immunostimulatory Activities of Astragalosides. Am J Chin Med. 2017; 45:1157-1167.

27. Fu J, Wang Z, Huang L, Zheng S, Wang D, Chen S, Zhang H, Yang S. Review of the botanical characteristics, phytochemistry, and pharmacology of Astragalus membranaceus (Huangqi). Phytother Res. 2014; 28:1275-1283.

28. Deng B, Jia L, Cheng Z. *Radix Astragali*-Based Chinese Herbal Medicine for Oxaliplatin-Induced Peripheral Neuropathy: A Systematic Review and Meta-Analysis. Evid Based Complement Alternat Med. 2016; 2016:2421876.

29. Yan PH, Yan M, Wang XM, Wang SH. Effect of Huangqi injection on short-term prognosis in children with acute lymphoblastic leukemia.2014; 16:141-146. Zhongguo Dang Dai Er Ke Za Zhi. (in Chinese)

30. Zhang XJ, Yan M, Liu Y, Wang XM, Nuriding H. Effects of Huangqi injection on infection factors in children with acute lymphoblastic leukemia. Zhongguo Dang Dai Er Ke Za Zhi. 2014; 16:147-151. (in Chinese)

31. Cheng X, Gu J, Zhang M, Yuan J, Zhao B, Jiang J, Jia X. Astragaloside IV inhibits migration and invasion in human lung cancer A549 cells *via* regulating PKC-α-ERK1/2-NF-κB pathway. Int Immunopharmacol. 2014; 23:304-313.

32. Li B, Wang F, Liu N, Shen W, Huang T. Astragaloside IV inhibits progression of glioma *via* blocking MAPK/ERK signaling pathway. Biochem Biophys Res Commun. 2017; 491:98-103.

33. Jiang K, Lu Q, Li Q, Ji Y, Chen W, Xue X. Astragaloside IV inhibits breast cancer cell invasion by suppressing Vav3 mediated Rac1/MAPK signaling. Int Immunopharmacol. 2017; 42:195-202.

34. Yang C, Wu C, Xu D, Wang M, Xia Q. Astragaloside II inhibits autophagic flux and enhance chemosensitivity of cisplatin in human cancer cells. Biomed Pharmacother. 2016; 81:166-175.

35. Li CY, Xu HX, Han QB, Wu TS. Quality assessment of *Radix Codonopsis* by quantitative nuclear magnetic resonance. J Chromatogr A. 2009; 1216:2124-2129.

36. He JY, Ma N, Zhu S, Komatsu K, Li ZY, Fu WM. The genus Codonopsis (Campanulaceae): A review of phytochemistry, bioactivity and quality control. J Nat Med. 2015; 69:1-21.

37. Zeng XL, Li XA, Zhang BY. Immunological and hematopoietic effect of Codonopsis pilosula on cancer patients during radiotherapy. Zhongguo Zhong Xi Yi Jie He Za Zhi. 1992; 12:607-608, 581. (in Chinese)

38. Du J, Cheng BC, Fu XQ, Su T, Li T, Guo H, Li SM, Wu JF, Yu H, Huang WH, Cao H, Yu ZL. *In vitro* assays suggest Shenqi Fuzheng Injection has the potential to alter melanoma immune microenvironment. J Ethnopharmacol. 2016; 194:15-19.

39. Chen M, May BH, Zhou IW, Sze DM, Xue CC, Zhang AL. Oxaliplatin-based chemotherapy combined with traditional medicines for neutropenia in colorectal cancer: A meta-analysis of the contributions of specific plants. Crit Rev Oncol Hematol. 2016; 105:18-34.

40. Xin T, Zhang F, Jiang Q, Chen C, Huang D, Li Y, Shen W, Jin Y, Sui G. The inhibitory effect of a polysaccharide from Codonopsis pilosula on tumor growth and metastasis *in vitro*. Int J Biol Macromol. 2012; 51:788-793.

41. Liu Y, Zou X, Sun G, Bao Y. Codonopsis lanceolata polysaccharide CLPS inhibits melanoma metastasis *via* regulating integrin signaling. Int J Biol Macromol. 2017; 103:435-440.

42. Zhu W, Wei W, Zhang S, Zheng Y, Chen P, Xu X. The phosphatome of medicinal and edible fungus *Wolfi poria cocos*. Curr Microbiol. 2018; 75:124-131.

43. Sun Y. Biological activities and potential health benefits of polysaccharides from *Poria cocos* and their derivatives. Int J Biol Macromol. 2014; 68:131-134.

44. Ríos JL. Chemical constituents and pharmacological properties of *Poria cocos*. Planta Med. 2011; 77:681-691.

45. Wang N, Liu D, Guo J, Sun Y, Guo T, Zhu X. Molecular mechanism of *Poria cocos* combined with oxaliplatin on the inhibition of epithelial-mesenchymal transition in gastric cancer cells. Biomed Pharmacother. 2018; 102:865-873.

46. Chen M, May BH, Zhou IW, Xue CC, Zhang AL. FOLFOX 4 combined with herbal medicine for advanced colorectal cancer: A systematic review. Phytother Res. 2014; 28:976-991.

47. Ma J, Liu J, Lu C, Cai D.Pachymic acid induces apoptosis *via* activating ROS-dependent JNK and ER stress pathways in lung cancer cells. Cancer Cell Int. 2015 Aug 5;15:78.

48. Jeong JW, Lee WS, Go SI, Nagappan A, Baek JY, Lee JD, Lee SJ, Park C, Kim GY, Kim HJ, Kim GS, Kwon TK, Ryu CH, Shin SC, Choi YH. Pachymic Acid Induces Apoptosis of EJ Bladder Cancer Cells by DR5 Up-Regulation, ROS Generation, Modulation of Bcl-2 and IAP Family Members. Phytother Res. 2015; 29:1516-1524.

49. Cheng S, Eliaz I, Lin J, Thyagarajan-Sahu A, Sliva D. Triterpenes from *Poria cocos* suppress growth and invasiveness of pancreatic cancer cells through the downregulation of MMP-7. Int J Oncol. 2013; 42:1869-1874.

50. Wang X, Liu Y, Wang L, Han J, Chen S. A Nucleotide Signature for the Identification of *Angelicae Sinensis Radix* (Danggui) and Its Products. Sci Rep. 2016; 6:34940.

51. Chen XP, Li W, Xiao XF, Zhang LL, Liu CX. Phytochemical and pharmacological studies on Radix Angelica sinensis. Chin J Nat Med. 2013; 11:577-587.

52. Gong W, Zhou Y, Li X, Gao X, Tian J, Qin X, Du G.

Neuroprotective and Cytotoxic Phthalides from *Angelicae Sinensis Radix*. Molecules. 2016; 21(5). pii: E549.

53. Huang F, Li S, Lu X, Liu A, Du G, Shi G. Two glutathione S-transferase inhibitors from Radix Angelicae sinensis. Phytother Res. 2011; 25:284-289.

54. Kou W, Li YD, Liu K, Sun SB, Dong YM, Wu ZH. Radix Angelicae Sinensis and Radix Hedysari enhance radiosensitivity of 12C6+ radiation in human liver cancer cells by modulating apoptosis protein. Saudi Med J. 2014; 35:945-952.

55. Bar-Sela G, Schaffer M. An evidence-based perspective of *Curcuma longa* (Turmeric) for cancer patients. In: Cho WCS, editor. Evidence-based Anticancer Materia Medica. the Netherlands: Springer; 2011. pp. 225-243.

56. Mirzaei H, Masoudifar A, Sahebkar A, Zare N, Sadri Nahand J, Rashidi B, Mehrabian E, Mohammadi M, Mirzaei HR, Jaafari MR. MicroRNA: A novel target of curcumin in cancer therapy. J Cell Physiol. 2018; 233:3004-3015.

57. Rezaee R, Momtazi AA, Monemi A, Sahebkar A. Curcumin: A potentially powerful tool to reverse cisplatin-induced toxicity. Pharmacol Res. 2017; 117:218-227.

58. Lopes-Rodrigues V, Sousa E, Vasconcelos MH. Curcumin as a Modulator of P-Glycoprotein in Cancer: Challenges and Perspectives. Pharmaceuticals (Basel). 2016; 9(4). pii: E71.

59. Bordoloi D, Roy NK, Monisha J, Padmavathi G, Kunnumakkara AB. Multi-Targeted Agents in Cancer Cell Chemosensitization: What We Learnt from Curcumin Thus Far. Recent Pat Anticancer Drug Discov. 2016; 11:67-97.

60. Liu X, Wu J, Zhang D, Wang K, Duan X, Meng Z, Zhang X. Network Pharmacology-Based Approach to Investigate the Mechanisms of *Hedyotis diffusa Willd*. in the Treatment of Gastric Cancer. Evid Based Complement Alternat Med. 2018; 2018:7802639.

61. Chen R, He J, Tong X, Tang L, Liu M. The *Hedyotis diffusa Willd*. (Rubiaceae): A Review on Phytochemistry, Pharmacology, Quality Control and Pharmacokinetics. Molecules. 2016; 21(6). pii: E710.

62. Hung KF, Hsu CP, Chiang JH, Lin HJ, Kuo YT, Sun MF, Yen HR. Complementary Chinese herbal medicine therapy improves survival of patients with gastric cancer in Taiwan: A nationwide retrospective matched-cohort study. J Ethnopharmacol. 2017; 199:168-174.

63. Feng J, Jin Y, Peng J, Wei L, Cai Q, Yan Z, Lai Z, Lin J. *Hedyotis diffusa willd* extract suppresses colorectal cancer growth through multiple cellular pathways. Oncol Lett. 2017; 14:8197-8205.

64. Lai Z, Yan Z, Chen W, Peng J, Feng J, Li Q, Jin Y, Lin J. *Hedyotis diffusa Willd* suppresses metastasis in 5-fluorouracil-resistant colorectal cancer cells by regulating the TGF-β signaling pathway. Mol Med Rep. 2017; 16:7752-7758.

65. Tao G, Balunas MJ. Current therapeutic role and medicinal potential of *Scutellaria barbata* in Traditional Chinese Medicine and Western research. J Ethnopharmacol. 2016; 182:170-80.

66. Jin Y, Chen W, Yang H, Yan Z, Lai Z, Feng J, Peng J, Lin J. *Scutellaria barbata* D. Don inhibits migration and invasion of colorectal cancer cells *via* suppression of PI3K/AKT and TGF-β/Smad signaling pathways. Exp Ther Med. 2017; 14:5527-5534.

67. Lin J, Feng J, Yang H, Yan Z, Li Q, Wei L, Lai Z, Jin Y, Peng J. *Scutellaria barbata* D. Don inhibits 5-fluorouracil

68. Gong T, Wang CF, Yuan JR, Li Y, Gu JF, Zhao BJ, Zhang L, Jia XB, Feng L, Liu SL. Inhibition of Tumor Growth and Immunomodulatory Effects of Flavonoids and Scutebarbatines of *Scutellaria barbata* D. Don in Lewis-Bearing C57BL/6 Mice. Evid Based Complement Alternat Med. 2015; 2015:630760.

69. Yang PY, Tai CJ. Chinese Medicine Treatment for Afatinib-Induced Paronychia. Case Rep Oncol Med. 2017; 2017:7327359.

70. Sun P, Sun D, Wang X. Effects of *Scutellaria barbata* polysaccharide on the proliferation, apoptosis and EMT of human colon cancer HT29 Cells. Carbohydr Polym. 2017; 167:90-96.

71. Li TM, Yu YH, Tsai FJ, *et al*. Characteristics of Chinese herbal medicine usage and its effect on survival of lung cancer patients in Taiwan. J Ethnopharmacol. 2018; 213:92-100.

72. Yu N, Xiong Y, Wang C. Bu-Zhong-Yi-Qi Decoction, the Water Extract of Chinese Traditional Herbal Medicine, Enhances Cisplatin Cytotoxicity in A549/DDP Cells through Induction of Apoptosis and Autophagy. Biomed Res Int. 2017; 2017:3692797.

73. Gou H, Gu LY, Shang BZ, Xiong Y, Wang C. Protective effect of Bu-Zhong-Yi-Qi decoction, the water extract of Chinese traditional herbal medicine, on 5-fluorouracil-induced intestinal mucositis in mice. Hum Exp Toxicol. 2016; 35:1243-1251.

74. Lee AJ, Lee HJ, Kim JD, Jung HJ, Bae SH, Ryoo HM, Kim SG. Changes of peripheral blood lymphocyte subtypes in patients with end stage cancer administered localized radiotherapy and bojungikki-tang. Evid Based Complement Alternat Med. 2014; 2014:207613.

75. Jeong JS, Ryu BH, Kim JS, Park JW, Choi WC, Yoon SW. Bojungikki-tang for cancer-related fatigue: A pilot randomized clinical trial. Integr Cancer Ther. 2010; 9:331-338.

76. Cheon C, Yoo JE, Yoo HS, Cho CK, Kang S, Kim M, Jang BH, Shin YC, Ko SG. Efficacy and Safety of Sipjeondaebo-Tang for Anorexia in Patients with Cancer: A Pilot, Randomized, Double-Blind, Placebo-Controlled Trial. Evid Based Complement Alternat Med. 2017; 2017:8780325.

77. Ishiura Y, Shiba Y, Terasaki Y, Hayase H, Hamada M, Izawa K, Sugimoto A, Hirokami K, Segawa M, Kasahara K, Fujimura M. Effect of Japanese Traditional Medicine, TJ-48, on the Quality of Life of Patients with Non-Small Cell Lung Cancer Receiving Outpatient Chemotherapy. Gan To Kagaku Ryoho. 2016; 43:331-334. (in Japanese)

78. Ikemoto T, Shimada M, Iwahashi S, Saito Y, Kanamoto M, Mori H, Morine Y, Imura S, Utsunomiya T. Changes of immunological parameters with administration of Japanese Kampo medicine (Juzen-Taihoto/TJ-48) in patients with advanced pancreatic cancer. Int J Clin Oncol. 2014; 19:81-86.

79. Ishikawa S, Ishikawa T, Tezuka C, Asano K, Sunagawa M, Hisamitsu T. Efficacy of Juzentaihoto for Tumor Immunotherapy in B16 Melanoma Metastasis Model. Evid Based Complement Alternat Med. 2017; 2017:6054706.

80. Zhao J, Liu L, Zhang Y, Wan Y, Hong Z. The herbal mixture Xiao-chai-hu Tang (xcht) induces apoptosis of human hepatocellular carcinoma Huh7 cells *in vitro* and *in vivo*. Afr J Tradit Complement Altern Med. 2017; 14:231-241.

81. Ting CT, Kuo CJ, Hu HY, Lee YL, Tsai TH. Prescription frequency and patterns of Chinese herbal medicine for liver cancer patients in Taiwan: A cross-sectional analysis of the National Health Insurance Research Database. BMC Complement Altern Med. 2017; 17:118.

82. Tsai TY, Livneh H, Hung TH, Lin IH, Lu MC, Yeh CC. Associations between prescribed Chinese herbal medicine and risk of hepatocellular carcinoma in patients with chronic hepatitis B: A nationwide population-based cohort study. BMJ Open. 2017; 7:e014571.

83. Matsuoka H, Mizushima Y, Kawano M, Tachibana N, Sawada Y, Kato S, Nagakura H, Tanaka M, Suzuki K, Tadanobu K. Clinical availability of the herbal medicine, SYOUSAIKOTOU, as a gargling agent for prevention and treatment of chemotherapy-induced stomatitis. Gan To Kagaku Ryoho. 2004; 31:2017-2020. (in Japanese)

84. Chu E. Wedding Rigorous Scientific Methodology and Ancient Herbal Wisdom to Benefit Cancer Patients: The Development of PHY906. Oncology (Williston Park). 2018; 32:e20-e27.

85. Lam W, Jiang Z, Guan F, Huang X, Hu R, Wang J, Bussom S, Liu SH, Zhao H, Yen Y, Cheng YC. PHY906 (KD018), an adjuvant based on a 1800-year-old Chinese medicine, enhanced the anti-tumor activity of Sorafenib by changing the tumor microenvironment. Sci Rep. 2015; 5:9384.

86. Kummar S, Copur MS, Rose M, Wadler S, Stephenson J, O'Rourke M, Brenckman W, Tilton R, Liu SH, Jiang Z, Su T, Cheng YC, Chu E. A phase I study of the Chinese herbal medicine PHY906 as a modulator of irinotecan-based chemotherapy in patients with advanced colorectal cancer. Clin Colorectal Cancer. 2011; 10:85-96.

87. Rockwell S, Grove TA, Liu Y, Cheng YC, Higgins SA, Booth CJ. Preclinical studies of the Chinese Herbal Medicine formulation PHY906 (KD018) as a potential adjunct to radiation therapy. Int J Radiat Biol. 2013; 89:16-25.

88. Wang S, Wu X, Tan M, Gong J, Tan W, Bian B, Chen M, Wang Y. Fighting fire with fire: Poisonous Chinese herbal medicine for cancer therapy. J Ethnopharmacol. 2012; 140:33-45.

89. Xu R, Lin L, Li Y, Li Y. ShenQi FuZheng Injection combined with chemotherapy in the treatment of colorectal cancer: A meta-analysis. PLoS One. 2017; 12:e0185254.

90. Yang Y, Ting W, Xiao L, Shufei F, Wangxiao T, Xiaoying W, Xiumei G, Boli Z. Immunoregulation of Shenqi Fuzheng Injection combined with chemotherapy in cancer patients: A systematic review and meta-analysis. Evid Based Complement Alternat Med. 2017; 2017:5121538.

91. Jiang H, Zhang H1, Hu X, Ma J. A meta-analysis of Shenqi Fuzheng combined with radiation in the treatment of nonsmall cell lung cancer. J Cancer Res Ther. 2015; 11:C101-C103.

92. Zhang J, Tong F, Cai Q, Chen LJ, Dong JH, Wu G, Dong XR. Shenqi fuzheng injection attenuates irradiation-induced brain injury in mice *via* inhibition of the NF-κB signaling pathway and microglial activation. Acta Pharmacol Sin. 2015; 36:1288-1299.

93. Zhao N, Wei S, Hong L, Wang J, Shen F, Zhang F. Experimental study on effects of Kanglaite injection in gefitinib induction of A549 cell strain apoptosis in human adenocarcinoma of lung. Journal of Clinical Oncology. 2015; 1:1-7. (in Chinese)

94. Shi G, Zheng X, Zhang S, Wu X, Yu F, Wang Y, Xing

F. Kanglaite inhibits EMT caused by TNF-α *via* NF-κB inhibition in colorectal cancer cells. Oncotarget. 2017; 9:6771-6779.

95. Wu Y, Zhang J, Hong Y, Wang X. Effects of Kanglaite Injection on Serum miRNA-21 in Patients with Advanced Lung Cancer. Med Sci Monit. 2018; 24:2901-2906.

96. Schwartzberg LS, Arena FP, Bienvenu BJ, Kaplan EH, Camacho LH, Campos LT, Waymack JP, Tagliaferri MA, Chen MM, Li D. A randomized, open-label, safety and exploratory efficacy study of kanglaite injection (KLTi) plus gemcitabine versus gemcitabine in patients with advanced pancreatic cancer. J Cancer. 2017; 8:1872-1883.

97. Wang JC, Tian JH, Ge L, Gan YH, Yang KH. Which is the best Chinese herb injection based on the FOLFOX regimen for gastric cancer? A network meta-analysis of randomized controlled trials. Asian Pac J Cancer Prev. 2014; 15:4795-4800.

98. Xia J, Inagaki Y, Gao J, Qi F, Song P, Han G, Sawakami T, Gao B, Luo C, Kokudo N, Hasegawa K, Sakamoto Y, Tang W. Combination of cinobufacini and doxorubicin increases apoptosis of hepatocellular carcinoma cells through the Fas- and Mitochondria-Mediated Pathways. Am J Chin Med. 2017; 45:1537-1556.

99. Nakata M, Kawaguchi S, Oikawa A, Inamura A, Nomoto S, Miyai H, Nonaka T, Ichimi S, Fujita-Yamaguchi Y, Luo C, Gao B, Tang W. An aqueous extract from toad skin prevents gelatinase activities derived from fetal serum albumin and serum-free culture medium of human breast carcinoma MDA-MB-231 cells. Drug Discov Ther. 2015; 9:417-421.

100. Nakata M, Mori S, Kamoshida Y, Kawaguchi S, Fujita-Yamaguchi Y, Gao B, Tang W. Toad skin extract cinobufatini inhibits migration of human breast carcinoma MDA-MB-231 cells into a model stromal tissue. Biosci Trends. 2015; 9:266-269.

101. Yang T, Shi R, Chang L, Tang K, Chen K, Yu G, Tian Y, Guo Y, He W, Song X, Xu H, Ye Z. Huachansu suppresses human bladder cancer cell growth through the Fas/Fasl and TNF- alpha/TNFR1 pathway *in vitro* and *in vivo*. J Exp Clin Cancer Res. 2015; 34:21.

102. Zhou B, Wu F, Yuan L, Miao Z, Zhu S. Is Huachansu Beneficial in Treating Advanced Non-Small-Cell Lung Cancer? Evidence from a Meta-Analysis of Its Efficacy Combined with Chemotherapy. Evid Based Complement Alternat Med. 2015; 2015:408145.

103. Wu T, Sun R, Wang Z, Yang W, Shen S, Zhao Z. A meta-analysis of Cinobufacini combined with transcatheterarterial chemoembolization in the treatment of advanced hepatocellular carcinoma. J Cancer Res Ther. 2014; 10 Suppl 1:60-64.

104. Sun T, Zhang Y, Shen Y, Hu K, Zuo M. A case of advanced lung cancer with malignant pericardial effusion treated by intrapericardial Cinobufacini injection instillation. Biosci Trends. 2014; 8:235-239.

105. Meng Z, Garrett CR, Shen Y, Liu L, Yang P, Huo Y, Zhao Q, Spelman AR, Ng CS, Chang DZ, Cohen L. Prospective randomised evaluation of traditional Chinese medicine combined with chemotherapy: A randomised phase II study of wild toad extract plus gemcitabine in patients with advanced pancreatic adenocarcinomas. Br J Cancer. 2012; 107:411-416.

106. Lu YY, Huang XE, Cao J, Xu X, Wu XY, Liu J, Xiang J, Xu L. Phase II study on Javanica oil emulsion injection (Yadanzi®) combined with chemotherapy in treating patients with advanced lung adenocarcinoma. Asian Pac J

Cancer Prev. 2013; 14:4791-4794.

107. Xu W, Jiang X, Xu Z, Ye T, Shi Q. The Efficacy of Brucea javanica Oil Emulsion Injection as Adjunctive Therapy for Advanced Non-Small-Cell Lung Cancer: A Meta-Analysis. Evid Based Complement Alternat Med. 2016; 2016:5928562.

108. Wang Q, Wang M, He X, Gao T, Cao H, Dou W, Tian J. Meta-analysis on treatment of non-small cell lung cancer with brucea javanica oil emulsion in combination with platinum-contained first-line chemotherapy. Zhongguo Zhong Yao Za Zhi. 2012; 37:2022-2029. (in Chinese)

109. Wu JR, Liu SY, Zhu JL, Zhang D, Wang KH. Efficacy of Brucea javanica Oil Emulsion Injection Combined with the Chemotherapy for Treating Gastric Cancer: A Systematic Review and Meta-Analysis. Evid Based Complement Alternat Med. 2018; 2018:6350782.

110. Fuhong D, Xiang G, Haiying L, Jiangye W, Xueming G, Wenxiao C. Evaluation of efficacy and safety for Brucea javanica oil emulsion in the control of the malignant pleural effusions *via* thoracic perfusion. BMC Cancer. 2018; 18:411.

111. Babiker HM, McBride A, Newton M, Boehmer LM, Drucker AG, Gowan M, Cassagnol M, Camenisch TD, Anwer F, Hollands JM. Cardiotoxic effects of chemotherapy: A review of both cytotoxic and molecular targeted oncology therapies and their effect on the cardiovascular system. Crit Rev Oncol Hematol. 2018; 126:186-200.

112. Armanious MA, Mishra S, Fradley MG. Electrophysiologic toxicity of chemoradiation. Curr Oncol Rep. 2018; 20:45.

113. Yang L, Li TT, Chu YT, Chen K, Tian SD, Chen XY, Yang GW. Traditional Chinese medical comprehensive therapy for cancer-related fatigue. Chin J Integr Med. 2016; 22:67-72.

114. Su CX, Wang LQ, Grant SJ, Liu JP. Chinese herbal medicine for cancer-related fatigue: A systematic review of randomized clinical trials. Complement Ther Med. 2014; 22:567-79.

115. Lo LC, Chen CY, Chen ST, Chen HC, Lee TC, Chang CS. Therapeutic efficacy of traditional Chinese medicine, Shen-Mai San, in cancer patients undergoing chemotherapy or radiotherapy: Study protocol for a randomized, double-blind, placebo-controlled trial. Trials. 2012; 13:232.

116. Ling Y. Traditional Chinese medicine in the treatment of symptoms in patients with advanced cancer. Ann Palliat Med. 2013; 2:141-152.

117. Cai P, Li L, Hong H, Zhang L, He C, Chai X, Liu B, Chen Z. A Chinese medicine warm compress (Wen Jing Zhi Tong Fang), combined with WHO 3-step analgesic ladder treatment for cancer pain relief: A comparative randomized trial. Medicine (Baltimore). 2018; 97:e9965.

118. Ye X, Lu D, Chen X, Li S, Chen Y, Deng L. A Multicenter Randomized, Double-Blind, Placebo-Controlled Trial of Shuangbai San for Treating Primary Liver Cancer Patients With Cancer Pain. J Pain Symptom Manage. 2016; 51:979-986.

119. Fu L, Fu H, Liu LQ, Huo ZJ, Yu YH, Yu JM. Efficacy of donkey-hide gelatin mixture for gemcitabine and cisplatin chemotherapy regimen induced myelosuppression. Chinese Clinical Oncology. 2014; 19:739-742. (in Chinese)

120. Jiang X, Hidru TH, Zhang Z, Bai Y, Kong L, Li X. Evidence of elemene injection combined radiotherapy in lung cancer treatment among patients with brain metastases: A systematic review and meta-analysis. Medicine (Baltimore). 2017; 96:e6963.

121. Wang S, Lian X, Sun M, Luo L, Guo L. Efficacy of compound Kushen injection plus radiotherapy on nonsmall-cell lung cancer: A systematic review and meta-analysis. J Cancer Res Ther. 2016; 12:1298-1306.

122. Inoue T, Takagi H, Owada Y, *et al*. The efficacy of the Kampo medicine rikkunshito for chemotherapy-induced anorexia (RICH trial): Study protocol for a randomized controlled trial.Trials. 2017; 18:485.

123. Cheng X, Huo J, Wang D, Cai X, Sun X, Lu W, Yang Y, Hu C, Wang X, Cao P. Herbal Medicine AC591 Prevents Oxaliplatin-Induced Peripheral Neuropathy in Animal Model and Cancer Patients. Front Pharmacol. 2017; 8:344.

124. Hoshino N, Hida K, Ganeko R, Sakai Y. Goshajinkigan for reducing chemotherapy-induced peripheral neuropathy: Protocol for a systematic review and meta-analysis. Int J Colorectal Dis. 2017; 32:737-740.

125. Bledsoe TJ, Nath SK, Decker RH. Radiation Pneumonitis. Clin Chest Med. 2017; 38:201-208.

126. Kim KI, Jun JH, Baek H, Kim JH, Lee BJ, Jung HJ. Oral administration of herbal medicines for radiation pneumonitis in lung cancer patients: A systematic review and meta-analysis. PLoS One. 2018; 13:e0198015.

127. He H, Zhou X, Wang Q, Zhao Y. Does the course of astragalus-containing chinese herbal prescriptions and radiotherapy benefit to non-small-cell lung cancer treatment: A meta-analysis of randomized trials. Evid Based Complement Alternat Med. 2013; 2013:426207.

128. Xiao Z, Liang R, Wang CQ, Xu S, Li N, He Y, Tang F, Chen L, Ma H. Can Aidi injection alleviate the toxicity and improve the clinical efficacy of radiotherapy in lung cancer?: A meta-analysis of 16 randomized controlled trials following the PRISMA guidelines. Medicine (Baltimore). 2016; 95:e4517.

129. Early Breast Cancer Trialists' Collaborative Group (EBCTCG). Effect of chemotherapy and hormonal therapy for early breast cancer on recurrence and 15-year survival: An overview of the randomised trials. Lancet. 2005; 365:1687-717.

130. Hao W, Liu S, Qin Y, Sun C, Chen L, Wu C, Bao Y. Cardioprotective effect of Platycodon grandiflorum in patients with early breast cancer receiving anthracycline-based chemotherapy: Study protocol for a randomized controlled trial. Trials. 2017; 18:386.

131. Wu BY, Liu CT, Chen SY, Tsai MY. A case of chemotherapy-induced congestive heart failure successfully treated with Chinese herbal medicine. Complement Ther Med. 2015; 23:251-256.

132. Li S, Shen T, Zhu J, Xiao C, Liu Y, You FM. My opinion on Gefitinib rash treatment with traditional Chinese medicine. Journal of Sichuan of Traditional Chinese Medicine. 2016; 34:46. (in Chinese)

133. Hu MY, Chen PF. Research progress in therapy of EGFR-TKI associated rash by traditional Chinese medicine. Journal of Jiangxi University of TCM. 2016; 28:122-124. (in Chinese)

Original Article

Genotyping of single nucleotide polymorphisms using the SNP-RFLP method

Saifullah, Toshifumi Tsukahara[*]

Area of Bioscience and Biotechnology, School of Materials Science, Japan Advanced Institute of Science and Technology (JAIST), Nomi, Ishikawa, Japan.

Summary   **Genetic polymorphisms, including single nucleotide polymorphisms (SNPs), are responsible for inter-individual variability in susceptibility to cancer and other disorders. Both environmental factors (*e.g.*, smoking or carcinogen exposure) and genetic variation underlie the development of cancer; however, studies of twins suggest that genetic variation is more important. Hence, the identification of SNPs makes an important contribution to cancer research. In this study, 13 SNPs in 12 genes were genotyped in HEK 293 and HeLa cells using the simple and inexpensive SNP-RFLP method. Sanger sequencing was performed for one SNP to validate the SNP-RFLP results. Of the 13 SNPs, 10 were homozygous and three were heterozygous (rs10937405, rs12296850, and rs3814113) in HEK 293 cells, while 12 were homozygous and one was heterozygous (rs995030) in HeLa cells. The cells carried eight disease-associated risk alleles (32% of typed alleles), including rs2853677, rs995030, rs2736100, and rs6010620 in HEK 293 cells, and rs10937405, rs3814113, rs4767364, and rs6010620 in HeLa cells. Four SNP loci were homozygous for different alleles in each cell line, with HEK 293 cells having a CC genotype at rs2853677, GG at rs2736100 and rs4767364, and TT at rs3819197, while HeLa cells had TT genotypes at rs2853677 and rs2736100, AA at rs4767364, and CC at rs3819197. In conclusion, these results are potentially applicable for testing of novel gene therapeutic approaches in future experiments where the non-risk alleles of the eight identified risk alleles are substituted into HEK 293 or HeLa cells.**

Keywords: SNPs, carcinoma risk, RFLP, HEK 293 cells, HeLa cells

1. Introduction

Single nucleotide polymorphisms (SNPs), which are single base alterations at specific genome loci, are important, commonly bi-allelic, abundant (> 9 million), and the most frequent (1 in 1,000 bases) subtle genetic variation in the human genome (*1*). Depending on the location of a SNP within the genome, it can be associated with various phenomena at the level of gene expression. SNPs located in the 3'- or 5'-untranslated region (-UTR), or within introns, of genes can alter specific sequence motifs, including protein-binding sites, resulting in strong associations with various disorders, including

testicular neoplasms, glioma, and lung adenocarcinoma (*2-4*). SNPs in non-coding regions can also be useful as markers for population genetics and evolutionary studies (*5*) and may be associated with inherited susceptibility to cancer (*6*). Moreover, SNPs in the coding regions of genes have strong associations with other phenomena, such as alcohol consumption behavior (*7*), aero-digestive tract cancers (*8*), drug responses in pharmacogenomics (*9*), and inherited monogenic disorders (*10*), and are routinely analyzed for diagnostic purposes.

Single nucleotide polymorphism-restriction fragment length polymorphism (SNP-RFLP) is an enzymatic method of SNP genotyping in which a region containing a specific SNP allele is targeted and amplified by PCR and subsequently digested using an endonuclease enzyme. The results are interpreted based on length variation of the resulting digested PCR fragments, which are distinguished by gel electrophoresis. SNP-RFLP is a relatively simple, rapid, inexpensive, and convenient method for SNP genotyping, in contrast to more complex

---

*Address correspondence to:
Professor Toshifumi Tsukahara, Area of Bioscience and Biotechnology, School of Materials Science, Japan Advanced Institute of Science and Technology (JAIST), 1-1 Asahidai, Nomi, Ishikawa 923-1292, Japan.
E-mail: tukahara@jaist.ac.jp

SNP typing methods, such as sequencing, DNA chips, TaqMan assays, and hybridization, among others.

Cell lines are scientific tools that provide simplified models, allowing examination of the function of biological tissues under artificially regulated conditions, and without the ethical implications of experiments using whole organisms. Human embryonic kidney-derived epithelial cells (HEK 293) and the cervical cancer-derived epithelial cells (Henrietta Lacks; HeLa) are arguably the mammalian cell lines most extensively used in biological research, due to their rapid turnover time and ability to express heterologous proteins, including factors that undergo post-translational modifications (*11,12*). In this study, we characterized a number of disease-relevant SNPs in HEK 293 and HeLa genomic DNA using the simple and inexpensive SNP-RFLP method. The resulting information could assist other investigators performing SNP studies by providing control data for genome-wide association studies (GWAS) or laboratory diagnostic methods. In addition, the results will be of interest to other researchers for application in the development of new gene therapy, protein, or peptide-based drugs targeting these genetic variations.

2. Materials and Methods

2.1. *Cell culture*

HEK 293 cells and HeLa cells (RIKEN Cell Bank, Japan) were cultured in Dulbecco's modified Eagle's medium (DMEM, Nacalai Tesque, Inc., Japan) supplemented with 10% fetal bovine serum (Gibco, Life Technology, Canada). Cells were plated at a density of 2×10^6 per well in sterile 35×10 mm cell culture dishes (Falcon, USA) and cultured in an incubator at 37°C, 5% CO_2, and 95% humidity for 48-96 h, after which DNA samples were extracted.

2.2. *Genomic DNA extraction*

Extraction of genomic DNA from both HEK 293 and HeLa cell lines was performed using TRIzol reagent (Invitrogen, cat. no. 15596-018, USA), according to the manufacturer's instructions with minor modifications. Briefly, when cells were at 100% confluence, culture medium was removed and cells were rinsed with 1 mL of ice-cold PBS per 35×10 mm culture dish. Next, 1 mL of TRIzol reagent was added directly to the cells in the culture dish, followed by pipetting to lyse the cells, addition of 300 μL of chloroform, and centrifugation at $12,000 \times g$ for 15 min at 4°C. The bottom layer after centrifugation contained protein, the interface included the DNA, and the supernatant contained RNA. Supernatants were removed, then 400 μL of 100% ethanol was added to the interface and organic phase, and tubes were mixed by inversion several times,

followed by centrifugation at $2,000 \times g$ for 5 min at 4°C and the supernatant was removed (containing protein). Pellets were then washed twice with 1 mL of 0.1 M sodium citrate in 10% ethanol solution by incubation at room temperature for 30 min and centrifugation at $2,000 \times g$ for 5 min at 4°C. After discarding the wash solution, DNA pellets were precipitated with 1.8 mL of 75% ethanol, followed by incubation at room temperature for 10-20 min with periodic mixing and centrifugation at $2,000 \times g$ for 5 min at 2-8°C. Finally, the ethanol was removed, and DNA pellets were air dried for 5-10 min in an open tube and then dissolved in 100 μL of 8 mM NaOH for long term storage at -20°C for use in future experiments. DNA concentrations were measured by UV spectroscopy (SmartSpec™ 3000, USA).

2.3. *Primer design*

One of the most important factors in optimizing SNP-RFLP assays is primer design, which is critical for successful genotyping. Primers should be designed so that PCR amplicons will be 250-500 bp in total, and each primer should be at different distances from the SNPs site, so that products of different length will be easily distinguishable after restriction digestion. In this study, we first input target 500-600 bp genomic DNA sequences, including the SNP alleles of interest, into the online NCBI primer BLAST software. Next, one pair of 18-35 bp nucleotide sequences were selected as primers to amplify a 250-500 bp genomic DNA target, with each primer a different distance from the SNP site; factors considered when designing primers included melting temperature (Tm), percentage GC content (GC%), and self-complementarity. PCR primer pairs were designed to amplify only the target genomic sequence with no cross-reaction with homologous non-target regions.

2.4. *SNP-RFLP*

Thirteen pairs of SNPs significantly associated with carcinoma development, alcoholism, or other conditions, according to previous publications, and that include restriction sites for commercially available enzymes, were selected from the NCBI SNP database (Table 1).

2.4.1. *PCR amplification*

PCR reactions were performed in a total volume of 20 μL using a thermo cycler (GeneAmp PCR System 9700, Singapore). Reaction mixtures contained 8.3 μL of autoclaved MilliQ water, 4 μL of 5 × Gold Taq buffer (Promega, USA), 2 μL of 2 mM dNTPs, 2 μL of 25 mM $MgCl_2$, 2 μL of 91 ng/μL genomic DNA template, 0.8 μL (10 pmol) of each primer, and 0.1 μL of *Taq* polymerase (Promega, USA). PCR conditions were as

Table 1. SNPs used in this study

SNP no.	SNP site	Accession number	Gene	Chromosome: position	Molecular consequence [risk allele]	Phenotype; possible risks
1	CATACACT[A/G]AAGTGAAA	rs671	*ALDH2*	12:111803962	c.1510G>A (p.Glu504Lys); missense [A]	alcohol consumption behavior; cardiovascular diseases (7)
2	TATAATCT[C/T]GTGTTCAA	rs10937405	*TP63*	3:189665394	g.189665394C>T; intron variant [C]	lung adenocarcinoma (4)
3	GAGACCCG[C/T]CTGGTGCA	rs2853677	*TERT*	5:1287079	g.12969C>T; intron variant [C]	lung adenocarcinoma (4)
4	GGGCTTAC[A/G]GCTATTGA	rs12296850	*SLC17A8*	12:100426307	g.100820085A>G; downstream gene variant [G]	lung squamous cell carcinoma (15)
5	CAAATGGT[A/G]CATGCAGT	rs995030	*KITLG*	12:88496894	g.88496894A>G; 3'-UTR variant [G]	testicular neoplasms (2)
6	TCCATATC[C/T]TCTGGACC	rs3814113	*BNC2*	9:16915023	g.16915021T>C; intergenic variant [T]	serous ovarian cancer (16)
7	GTGTTTCT[G/T]TAGCTTTG	rs2736100	*TERT*	5:1286401	g.13647G>T; intron variant [G]	idiopathic pulmonary fibrosis (21)
8	AAAAGCCA[G/T]GGGAACTA	rs4295627	*CCDC26*	8:129673211	g.129673211T>G; intron variant [G]	glioma (3)
9	GCTCTTGG[C/T]CCAGGAGA	rs498872	*PHLDB1*	11:118606652	g.118606652C>T; 5'-UTR variant [T]	glioma (3)
10	TGACTCAA[C/T]TTGTTTTCT	rs1494961	*HELQ*	4:83453327	g.83453327C>T; missense [C]	aero-digestive tract cancers (8)
11	TGGGGTAC[A/G]TATACTCC	rs4767364	*NAA25*	12:112083644	g.112083644G>A; intron variant [A]	aero-digestive tract cancers; type 1 diabetes (8)
12	TCCTTCCA[C/T]CTTTTCAT	rs3819197	*ADH1A*	4:99279352	g.99279352C>T; intron variant [none]	alcohol consumption behavior (17)
13	GGAGGAGC[A/G]CCTGCTTT	rs6010620	*RTEL1*	20:63678486	g.63678486A>G; intron variant [G]	glioma; atopic dermatitis (3)

follows: pre-denaturation at 95°C for 3 min; followed by 23-28 cycles of 95°C for 30 s, 58-63°C for 30 s, and 72°C for 30 s; and a final extension at 72°C for 7 min. Polyacrylamide gel electrophoresis (PAGE) was used to analyze PCR amplicons.

2.4.2. *RFLP*

For rapid detection of SNP sites, PCR products were cleaved using specific restriction enzymes (NEB, Takara, and Thermo Scientific™). The restriction endonucleases for SNP-RFLP were chosen using two online tools, Watcut (*13*) and SnapGene Viewer software (*14*). RFLP reaction mixtures contained 6 μL of autoclaved MilliQ water, 10 μL of PCR product, 1 μL of bovine serum albumin, 2 μL of 10 × reaction buffer, and 1 μL of endonuclease enzyme. Reactions were carried out at 37°C for 2 h.

2.4.3. *PAGE*

PCR amplicons and products of restriction enzyme cleavage were analyzed by PAGE; gels consisted of autoclaved MilliQ water (6 mL), 40% acrylamide/bis mixed solution (1.2 mL), 10 × tris borate EDTA stock solution (0.8 mL), 10% ammonium persulfate (120 μL), and TEMED (8 μL). PCR amplicons and cleaved fragments were run alongside a 100 kb ladder marker at 200 V, 2.0 A, for 30 min. Gel staining was performed with SYBR Green dye (Lonza, Cat. 50513, USA) for 25 min. Gel images were obtained using a LAS-3000 Image Analyzer (Fujifilm, Japan).

2.4.4. *Mechanism of SNP-RFLP*

The SNP-RFLP method for genotyping used in this study is exemplified by SNP No. 10 (Accession No. rs1494961) where the target SNP (T/C), was designated position 0; comparatively, the forward primer was designed at -241 bp upstream and the reverse primer +100 bp downstream, to amplify a 341 bp genomic DNA region flanking the target SNP. Following PCR, amplicons were treated using the MunI restriction endonuclease. Where the sequence 5′-CAATTG-3′ was included among the amplicons, MunI cleaved it to produce fragments of 100 and 241 bp. No other MunI recognition sites were included in the 341 bp fragment, other than the target SNP within it. Product length variation was subsequently analyzed by PAGE.

2.5. *Sanger sequencing*

To validate the PCR-RFLP results, SNP No. 13 (Accession No. rs6010620) was also analyzed by Sanger sequencing using a 3130XL Genetic Analyzer (Applied Biosystems, Japan). The thermocycling reactions for direct sequencing comprised 10 μL, containing 5 μL of

Table 2. Primer sequences and optimum PCR conditions

SNP no.	Accession no.	Primers (5' to 3')	[a]PCR conditions
1	rs671	[1] GATGTGTTTGGAGCCCAGTC [2] AGCAGACCCTAAATCCCTGG	63°C[b], 23[c]
2	rs10937405	[1] ACTTATGCTACGGTTCAGGGA [2] CCATCCTCTGCATGTTAGGTTT	63°C[b], 23[c]
3	rs2853677	[1] TCTGGCCTAATTTTCAACACTTTTA [2] GATCAACACACACTCGGCAG	63°C[b], 23[c]
4	rs12296850	[1] TGCTGCCAGTCAGAATCATATC [2] TAGAGGTGCTCGTTACAGGTG	58°C[b], 28[c]
5	rs995030	[1] GCTGACATGTTGCCAAATCC [2] AACTTGCATGGAGCAGGACT	63°C[b], 23[c]
6	rs3814113	[1] ACCGTGTTAGGATGGTCTCG [2] CCAGTTGGAGGTGAGTTCGT	63°C[b], 23[c]
7	rs2736100	[1] TTGCTACCCTTGTCCTGAGC [2] ACGTTGCTGTCACTCACTGG	63°C[b], 23[c]
8	rs4295627	[1] TGGCTATTTTGGAAGGAAAAGTG [2] TCCTCACTTGGCAATCTGGT	63°C[b], 23[c]
9	rs498872	[1] AGATTGGGAGATGGAGGCAG [2] AGGCTTTCTGCTCCTTCCTT	63°C[b], 23[c]
10	rs1494961	[1] GGAATGGAAGGGGCTGAG [2] GACTGGAAATGCGAAGGC	63°C[b], 23[c]
11	rs4767364	[1] AGCTGGTGCTGAATTGCAC [2] CGGTTTTCTAACTCAAAGACAAAAT	63°C[b], 23[c]
12	rs3819197	[1] TGGCTTCAGCACAATAGGAA [2] CCCAAAACTTGTGGCTGATT	63°C[b], 23[c]
13	rs6010620	[1] TCCTCGACCCACAGTGATCC [2] AGTGTGTGCTGCTCCTCTCA	63°C[b], 23[c]

[1]Forward primer; [2]Reverse primer; [a]Optimal conditions, denaturation at 95°C for 30 s, extension at 72°C for 30 s, 91 ng/µL concentration genomic DNA template, 0.8 µL of 10 pmol/µL each primer; [b]Primer annealing temperature; [c]Cycles.

water, 1.5 µL of 5 × Big Dye buffer, 1 µL of 2.5 × Big Dye version 1.1, 3.1 (Applied Biosystems, USA), 0.5 µL of 3.2 pmol/µL reverse primer, and 2 µL of purified PCR fragment from agarose gel. The thermocycling conditions were as follows: pre-denaturation at 96°C for 1 min; followed by 25 cycles of 96°C for 10 s, 50°C for 5 s, and 72°C for 4 min; and then a hold step at 4°C for an indefinite period. Reaction products were ethanol precipitated and resuspended in HiDi formamide (Applied Biosystems, USA). Products were denatured at 95°C for 3 min followed by chilling on ice for 3 min. Then, samples were mounted on the Genetic Analyzer system to extract nucleotide sequence information by capillary electrophoresis. Finally, results were analyzed using Seq_Scanner software (Applied Biosystems, Japan).

3. Results

3.1. *DNA extraction*

Genomic DNA was isolated from HEK 293 and HeLa cell lines, and sample concentrations were 1,520 and 704 ng/µL, with purity ratios (absorbance at 260 nm divided by that at 280 nm) of 1.83 and 1.77, respectively.

3.2. *Primer sequences*

The primer sequences used in this genotyping study

and their optimum PCR conditions are presented in Table 2. These data could be useful to other researchers to facilitate convenient genotyping of these SNPs by enzymatic methods.

3.3. *SNP-RFLP*

Images of PAGE separated PCR and products of restriction digestion are shown in Figure 1. The results of genotyping of the 13 SNPs in 12 genes in genomic DNA from both cell lines are presented in Table 3. In HEK 293 cells, 10 SNPs were homozygous, while three (rs10937405, rs12296850, and rs3814113) were heterozygous; among the homozygous SNPs, eight comprised alleles cut by the specific endonucleases, whereas two were the uncut allele. In HeLa cells, 12 SNPs were homozygous and one (rs995030) was heterozygous; among the homozygous SNPs, five comprised alleles containing specific endonuclease sites and seven were the uncut alleles. Although both cell types had similar allele distributions, some distinct alleles were observed at a number of SNP positions; for example, HEK 293 cells had a CC genotype at rs2853677, GG at rs2736100 and rs4767364, and TT at rs3819197, whereas HeLa cells had TT genotypes at rs2853677 and rs2736100, AA at rs4767364, and CC at rs3819197. These variations may reflect the different origins of the cells; HEK 293 cells are an embryonic cell line originating from the Netherlands, while HeLa cells are mature cancerous cells derived from
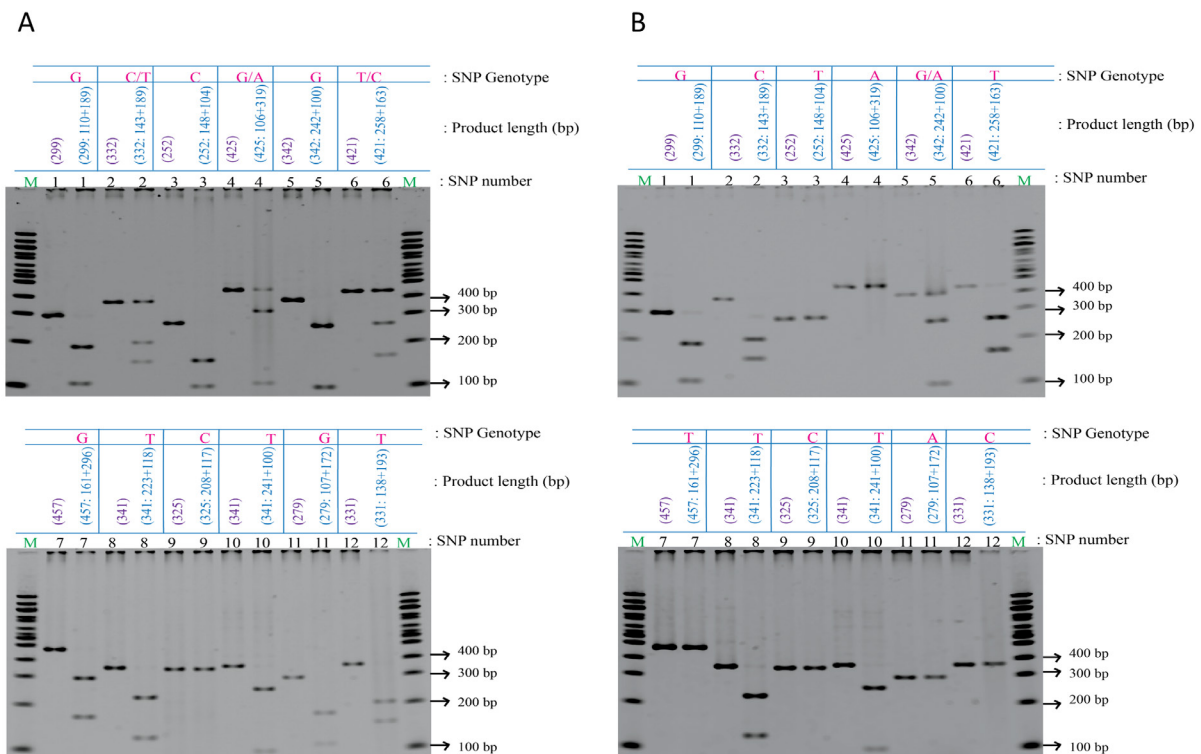
Figure 1. PAGE images for SNP genotyping of (A) HEK 293 cells and (B) HeLa cells by SNP-RFLP. Samples were run in pairs with PCR products to the left of restriction digest reactions; for example, 'SNP No. 1 (299)', PCR products for SNP No. 1; and 'SNP No. 1 (299:110 + 189)', restriction digestion reaction (RFLP) for the same SNP.

Table 3. Results of SNP-RFLP analysis for SNP genotyping in both cell lines

SNP no.	Accession no.	Gene	Endonuclease	Recognition site	Product (restriction fragment) length (bp)	HEK 293 genotype		HeLa genotype	
						Cut/uncut	Genotype	Cut/uncut	Genotype
1	rs671	*ALDH2*	AcuI	CTGAAGN16^	299 (110 + 189)	+	GG	+	GG
2	rs10937405	*TP63*	BssSαI	C^ACGAG	332 (143 + 189)	+/-	C/T	+	CC
3	rs2853677	*TERT*	MvaI	CC^WGG	252 (148 + 104)	+	CC	-	TT
4	rs12296850	*SLC17A8-NR1H4*	BceAI	ACGGCN12^	425 (106 + 319)	+/-	G/A	-	AA
5	rs995030	*KITLG*	SphI	GCATG^C	342 (242 + 100)	+	GG	+/-	G/A
6	rs3814113	*BNC2*	MboII	GAAGAN8^	421 (258 + 163)	+/-	T/C	+	TT
7	rs2736100	*TERT*	BfmI	C^TRYAG	457 (161 + 296)	+	GG	-	TT
8	rs4295627	*CCDC26*	NcoI	C^CATGG	341 (223 + 118)	+	TT	+	TT
9	rs498872	*PHLDB1*	PfoI	T^CCNGGA	325 (208 + 117)	-	CC	-	CC
10	rs1494961	*HELQ*	MunI	C^AATTG	341 (241 + 100)	+	TT	+	TT
11	rs4767364	*NAA25*	Hpy166II	GTN^NAC	279 (107 + 172)	+	GG	-	AA
12	rs3819197	*ADH1A*	BccI	CCATCN4^	331 (138 + 193)	+	TT	-	CC
13	rs6010620	*RTEL1-TNFRSF6B*	BspMI	ACCTGCN4^	284 (242 + 42)	-	GG	-	GG

'+', cut; '-', uncut; 'W', A or T; 'R', A or G; 'Y', C or T.

an American woman. Identified SNP risk alleles are presented in Table 1 ("phenotype; possible risks").

3.4. *Validation of SNP-RFLP by Sanger sequencing*

Sanger sequencing of one marker (SNP No. 13; Accession No. rs6010620) was performed to validate the SNP-RFLP results. The sequencing results for both cell lines indicated that they carried the G rather than the A allele at this locus (Figure 2B-C), consistent with the results of SNP-RFLP analysis (rs6010620 in Table 3; Figure 2A). These data indicate that the PCR-RFLP

results were correct, supporting the conclusion that the generated SNP-RFLP results confirm the genotypes of 13 SNPs in 12 different genes. These results have the potential to assist other researchers and inform clinical diagnostics to identify SNPs associated with cancer risk using a convenient enzymatic method.

4. Discussion

In this study, we profiled 13 SNPs associated with disease risk in 12 genes in the HEK 293 and HeLa cell lines using the cost-effective SNP-RFLP method. Across

Figure 3. Allele distribution chart for the 13 SNPs typed in this study.
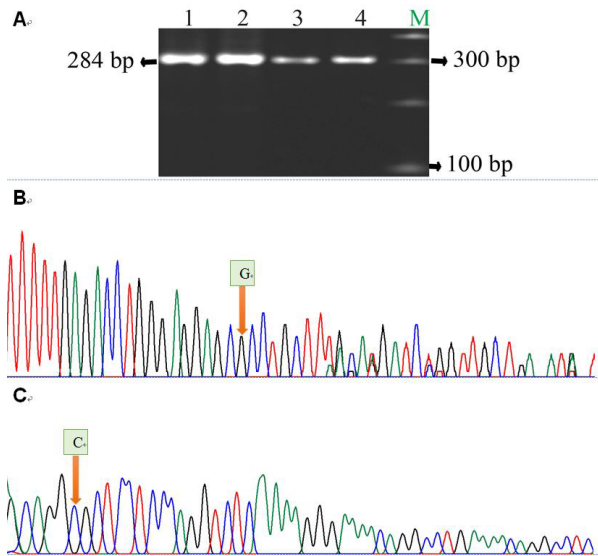
Figure 2. Sequencing validation results for SNP-RFLP of SNP No. 13 (Accession No. rs6010620). A: Image of PAGE of SNP No. 13 genotyping; 1: HEK 293 cells PCR product, 2: HEK 293 cells RFLP, uncut, G allele; 3: HeLa cells PCR product; 4: HeLa cells RFLP, uncut, G allele; M: marker. **B:** Sequencing electropherogram results for SNP rs6010620 in HEK 293 cells; G allele is indicated by an arrow. **C:** Sequencing electropherogram results for SNP rs6010620 in HeLa cells; G allele (reverse primer 5'-AGTGTGTGCTGCTCCTCTCA-3' was used) was also present.

the two cell lines, 22 alleles contributed to homozygous genotypes, and four were in the heterozygous state (Figure 3). Eight risk alleles associated with disease, comprising 32% of typed alleles, were identified at the following SNPs: rs2853677, rs995030, rs2736100, and rs6010620 in HEK 293 cells and rs10937405, rs3814113, rs4767364, and rs6010620 in HeLa cells. We identified heterozygosity at three SNPs, rs10937405, C/T; rs12296850, G/A; and rs3814113, T/C, in HEK 293 cells; and one in HeLa cells (rs995030, G/A).

Takeuchi *et al.*, 2011, genotyped the SNP, rs671, in the Japanese population and found a strong association with alcoholism and subsequently also with cardiovascular diseases, particularly for individuals with the AA genotype at this locus (*7*). Here, we found that both cell lines were GG homozygotes (wild-type) for rs671. Shiraishi *et al.*, 2012, and Li Xiaoting *et al.*, 2016, reported that lung adenocarcinoma is associated with rs10937405 in the *TP63* gene, and rs2853677 and rs2736100 in *TERT*, in Japanese and Chinese populations (*4,6*). One study identified rs12296850, in the *SLC17A8-NR1H4* gene, as significantly associated with the risk of lung squamous cell carcinoma at the genome-wide significance level (*15*). Rapley *et al.*, 2009, studied men with infertility and found an association with the genetic variant, rs995030, in *KITLG*, with testicular germ cell tumors in a UK population (*2*). Song *et al.*, 2009, and Shete *at al.*, 2009, genotyped rs3814113 for ovarian cancer, rs4295627, rs498872, and rs6010620 for glioma in populations from the UK, the USA, and France (*3,16*). MacKay *et*
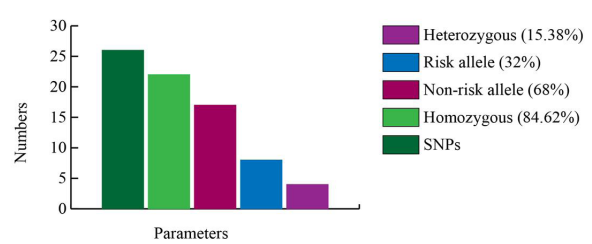
al., 2011, studied upper aero-digestive tract cancer and identified associations with rs1494961 and rs4767364, while Han *et al.*, 2007, reported an association of rs3819197 with alcoholism (*8,17*). These GWAS indicate that SNPs can be associated with susceptibility to certain diseases, even when the variant is in a non-coding, intronic, or 3'/5'-UTR region.

All of the SNPs mentioned above were characterized using BeadChip, TaqMan, or pyrosequencing methods. By contrast, we used the simple and cost-effective SNP-RFLP method to conduct SNP genotyping. SNP-RFLP is an accurate method for SNP genotyping, useful for small basic research studies of complex genetic variation, such as HLA allele typing or ABO blood group determinants (*18*). One disadvantage of this method is that target SNP nucleotide sequences may not always span commercially available endonuclease enzyme recognition sites. Another limitation is that sequences may contain too many palindromic recognition sites to allow a single endonuclease cleavage.

The findings presented here could be useful for the development of new gene therapy techniques, which could be tested directly in HEK 293 or HeLa cell lines as model mammalian expression systems. For example, Liu *et al.*, 2017, developed A to I editing (the conversion of A.T to G.C base pairs in DNA) at the genomic level by combining the dCas9 and TadA enzyme systems (*19*). We may apply this system in future to replace the pathogenic A allele with a G nucleotide (I) at the rs4767364 SNP, using HeLa cells as a test system. Furthermore, these data could be useful for the preparation of allele-specific probes for the development of probes-on-carrier DNA chips (*20*) for SNP genotyping.

In summary, in the present study 13 SNPs in 12 genes were genotyped in HEK 293 and HeLa cells using the SNP-RFLP technique. We detected eight risk alleles and four distinguish loci in both cell lines. HEK 293 cells were heterozygous at three loci, while there was a single heterozygous locus in HeLa cells. Further profiling of other carcinoma-related SNPs in HEK 293 and HeLa cells will be necessary to facilitate the study of the relationship between SNPs and cancer, to enable the development of gene therapy for treatment of those disorders. These findings will also assist mechanistic

studies of the functions of these SNPs in HEK 293 or HeLa cell models in the near future.

References

1. Kim S, Misra A. SNP genotyping: Technologies and biomedical applications. Annu Rev Biomed Eng. 2007; 9:289-320.
2. Rapley EA, Turnbull C, Al Olama AA, *et al*. A genome-wide association study of testicular germ cell tumor. Nat Genet. 2009; 41:807-810.
3. Shete S, Hosking FJ, Robertson LB, *et al*. Genome-wide association study identifies five susceptibility loci for glioma. Nat Genet. 2009; 41:899-904.
4. Shiraishi K, Kunitoh H, Daigo Y, *et al*. A genome-wide association study identifies two new susceptibility loci for lung adenocarcinoma in the Japanese population. Nat Genet. 2012; 44:900-904.
5. Jorde LB, Watkins WS, Bamshad MJ, Dixon ME, Ricker CE, Seielstad MT, Batzer MA. The distribution of human genetic diversity: A comparison of mitochondrial, autosomal, and Y-chromosome data. Am J Hum Genet. 2000; 66:979-988.
6. Li X, Xu X, Fang J, Wang L, Mu Y, Zhang P, Yao Z, Ma Z, Liu Z. Rs2853677 modulates Snail1 binding to the TERT enhancer and affects lung adenocarcinoma susceptibility. Oncotarget. 2016; 7:37825-37838.
7. Takeuchi F, Isono M, Nabika T, Katsuya T, Sugiyama T, Yamaguchi S, Kobayashi S, Ogihara T, Yamori Y, Fujioka A, Kato N. Confirmation of ALDH2 as a Major locus of drinking behavior and of its variants regulating multiple metabolic phenotypes in a Japanese population. Circ J. 2011; 75:911-918.
8. McKay JD, Truong T, Gaborieau V, *et al*. A genome-wide association study of upper aerodigestive tract cancers conducted within the INHANCE consortium. PLoS Genet. 2011; 7:e1001333.
9. Jittikoon J, Mahasirimongkol S, Charoenyingwattana A, Chaikledkaew U, Tragulpiankit P, Mangmool S, Inunchot W, Somboonyosdes C, Wichukchinda N, Sawanpanyalert P, He Y, McLeod HL, Chantratita W. Comparison of genetic variation in drug ADME-related genes in Thais with Caucasian, African and Asian HapMap populations. J Hum Genet. 2015; 61:119-127.
10. Syvänen A-C. Accessing genetic variation: Genotyping single nucleotide polymorphisms. Nat Rev Genet. 2001; 2:930-942.
11. Thomas P, Smart TG. HEK293 cell line: A vehicle for the expression of recombinant proteins. J Pharmacol Toxicol Methods. 2005; 51:187-200.
12. Moorhead J. Henrietta Lacks: The mother of modern medicine. The Guardian 2010. *https://www.theguardian.com/science/2010/jun/23/henrietta-lacks-cells-medical-advances* (accessed May 2, 2018).
13. Palmer M. WutCut: A web application for restriction analysis and related tasks. University of Waterloo. *http://watcut.uwaterloo.ca/template.php?act=snp_new* (accessed May 2, 2018).
14. SnapGene® software (from GSL Biotech; available at snapgene.com). *http://www.snapgene.com/products/snapgene_viewer/* (accessed May 2, 2018).
15. Dong J, Jin G, Wu C, *et al*. Genome-wide association study identifies a novel susceptibility locus at 12q23.1 for lung squamous cell carcinoma in Han Chinese. PLoS Genet. 2013; 9:e1003190.
16. Song H, Ramus SJ, Tyrer J, *et al*. A genome-wide association study identifies a new ovarian cancer susceptibility locus on 9p22.2. Nat Genet. 2009; 41:996-1000.
17. Han Y, Gu S, Oota H, Osier MV, Pakstis AJ, Speed WC, Kidd JR, Kidd KK. Evidence of positive selection on a class I ADH locus. Am J Hum Genet. 2007; 80:441-456.
18. Ota M, Fukushima H, Kulski JK, Inoko H. Single nucleotide polymorphism detection by polymerase chain reaction-restriction fragment length polymorphism. Nat Protoc. 2007; 2:2857-2864.
19. Gaudelli NM, Komor AC, Rees HA, Packer MS, Badran AH, Bryson DI, Liu DR. Programmable base editing of A•T to G•C in genomic DNA without DNA cleavage. Nature. 2017; 551:464-471.
20. Tsukahara T, Nagasawa H. Probe-on-carriers for oligonucleotide microarrays (DNA chips). Sci Technol Adv Mater. 2004; 5:359-362.
21. Mushiroda T, Wattanapokayakit S, Takahashi A, Nukiwa T, Kudoh S, Ogura T, Taniguchi H, Kubo M, Kamatani N, Nakamura Y. A genome-wide association study identifies an association of a common variant in TERT with susceptibility to idiopathic pulmonary fibrosis. J Med Genet. 2008; 45:654-656.

Expression of glucocorticoid receptor shows negative correlation with human B-cell engraftment in PBMC-transplanted NOG-hIL-4-Tg mice

Toshiro Seki[1], Asuka Miyamoto[2,3], Shino Ohshima[2], Yusuke Ohno[2], Atsushi Yasuda[1], Yutaka Tokuda[3], Kiyoshi Ando[4], Yoshie Kametani[2,5,*]

[1] *Department of Internal Medicine, Division of Nephrology, Endocrinology and Metabolism, Tokai University School of Medicine, Isehara, Kanagawa, Japan;*

[2] *Department of Molecular Life Science, Division of Basic Medical Science, Tokai University School of Medicine, Isehara, Kanagawa, Japan;*

[3] *Department of Breast and Endocrine Surgery, Tokai University School of Medicine, Isehara, Kanagawa, Japan;*

[4] *Department of Hematology and Oncology, Tokai University School of Medicine, Isehara, Kanagawa, Japan;*

[5] *Institute of Advanced Biosciences, Tokai University, Hiratsuka, Kanagawa, Japan.*

Summary   **The humanized mouse system is a promising tool for analyzing human immune responses *in vivo*. Recently, we developed a new humanized mouse system using the severely immunodeficient NOD/Shi-*scid*-IL2rγ^*null* (NOG)-hIL-4-Tg mouse, which enabled us to evaluate the human humoral immune response after peripheral blood mononuclear cell (PBMC) transplantation. However, the mechanism by which hIL-4 enhances antigen-specific IgG production in these mice is not clear. In this study, we analyzed the relationship between human lymphocyte subsets and the expression level of the glucocorticoid receptor (GR) to clarify the humoral immune condition in human PBMC-transplanted NOG-hIL-4 mice. The results showed that the human GR mRNA level was significantly lower in NOG-hIL-4-Tg splenocytes than in conventional NOG splenocytes after immunization. Whereas no obvious difference of the proportion of T helper-cell subsets was observed between the NOG and NOG-hIL-4-Tg mouse strains, the B-cell proportion and antigen-specific IgG concentration in plasma showed strong negative correlations with the GR mRNA level. These results suggest that the GR expression level was changed in PBMCs in the humanized NOG-hIL-4-Tg mice, which may support B-cell survival and function in the mouse system.**

Keywords: Humanized mouse, IL-4, Th subset, glucocorticoid receptor

1. Introduction

The humanized immune system mouse model is a promising tool in personalized medicine because the system can be used to anticipate the efficiency of each treatment before the actual drug administration (*1*). There are three main systems to reconstruct human immunity in the immunodeficient mice (*2-7*). The human immune cells used for transplantation are categorized as hematopoietic stem cells (*8-10*), peripheral blood mononuclear cells (*11-13*), and immune-related tissues, *i.e.*, bone marrow, thymus and/ or fetal liver (*14,15*). Severely immunodeficient mice transplanted with human peripheral blood mononuclear cells (PBMCs) are affected by graft-versus-host disease (GVHD) within a short period (*12*). Previously, we developed NOD/Shi-*scid*-IL2rγ^*null* (NOG)-hIL-4-transgenic (Tg) mice, which systemically express human interleukin-4 (hIL-4) in the NOG mouse (*16*). This mouse strain suppressed GVHD after PBMC transplantation. In these mice, human lymphocytes

were engrafted for a longer period without GVHD symptoms. Moreover, use of this mouse system enabled the induction of antigen-specific IgG production after immunization. The detailed mechanism of enhancing antibody production in hIL-4 Tg mice has not been clarified, but IL-4 was reported to support expansion of plasmablasts (*17*) and modify the proportion of T helper (Th)-cell subsets, especially Th2 and T follicular helper (Tfh) cells (*18*). While Th2 cells have been believed to function mainly in specific antibody production, Tfh, a subset existing in the germinal centers, has recently been shown to be necessary for the production of high-affinity IgG antibodies (*19-21*). Furthermore, the increase in regulatory T (Treg), which suppresses the immune reaction, may be observed to suppress the onset of GVHD (*22,23*).

The glucocorticoid receptor (GR), a steroid hormone receptor (*24-26*), is expressed in lymphocytes and is well known as a powerful immune regulator that can control GVHD symptoms (*27-29*). Therefore, glucocorticoid (GC) might play an important role in the suppression of GVHD symptoms in NOG and NOG-hIL-4-Tg mice transplanted with human PBMCs. On the other hand, GC is reported to suppress B-cell survival (*30*) or class switching by the suppression of activation-induced cytidine deaminase (AID) expression (*31*). This finding suggests that the highly expressed GC may inhibit specific IgG production in the NOG-based humanized mouse. Moreover, the effect of GC is still controversial on Treg- or Tfh-cell development (*29,32*).

In this study, we examined the correlation between GR expression level and lymphocyte cellularity to contribute to the clarification of the mechanism of enhancement of antibody production and suppression of GVHD in the NOG-hIL-4-Tg mouse system.

2. Materials and Methods

2.1. *Ethical approval*

Human PBMCs from healthy volunteer donors were obtained after receiving written informed consent based on Institutional Review Board-approved protocols according to institutional guidelines. This work was approved by the Tokai University Human Research Committee (12R-002) and Central Institute for Experimental Animals (CIEA) Human Research Committee (08-01). These studies were conducted in accordance with the Declaration of Helsinki protocols and all Japanese federal regulations required for the protection of human subjects. The use of immunodeficient mice for xenotransplantation studies was approved in compliance with the Guidelines for the Care and Use of Laboratory Animals, and all animal studies were approved by the committees of CIEA and the Tokai University School of Medicine.

2.2. *Mouse strains*

NOD/Shi-scid-IL2rγ^{null} (NOG; formal name, NOD. Cg-*Prkdc^{scid}il2rγ^{tm1Sug}*/ShiJic) mice (*3*) were purchased from InVivo Science, Inc. (IVS, Kawasaki, Japan). NOG-hIL-4 Tg (formally, NOD.Cg-*Prkdc^{scid}il2rγ^{tm1Sug}*/ ShiJic *Tg(CMV-IL4)3-2*/Jic) mice (*16*) were previously generated by CIEA and maintained at Tokai University School of Medicine under specific-pathogen-free (SPF) conditions. The offspring with the inserted transgene were selected as reported previously (*16*).

2.3. *ELISA/EIA*

Peripheral blood (PB) samples were collected from the orbital venous plexus of 4- to 6-week-old mice using heparin (Novo-heparin; Mochida Pharmaceutical Co., Tokyo, Japan)-coated capillaries (Drummond Scientific, Broomall, PA, USA) under anesthesia. The level of human IL-4 protein was measured using a Human IL-4 ELISA Set BD OptEIA^{TM} (BD OptEIA^{TM}, BD Biosciences, San Diego, CA, USA) according to the manufacturer's instructions. Corticosterone was measured using a YK240 Corticosterone EIA kit (Yanaihara Institute Inc, Shizuoka, Japan) according to the manufacturer's instructions. The protocol for specific IgG antibody detection has been previously described (*33*). Briefly, microwells in microtiter plates (Sumiron, Tokyo, Japan) were coated with CH401MAP peptide (1 µg/mL) diluted in carbonate buffer (pH 9.5), and the antigens were adsorbed to the microwells overnight at 4°C. The wells were washed with phosphate-buffered saline (PBS)-Tween (0.05%, v/v) and blocked with 3% bovine serum albumin (BSA)-PBS at room temperature (RT) for 2 h. After three washes with PBS-Tween, 10-fold serial dilutions of mouse plasma were added to the wells and incubated for 2 h at RT. The plates were washed three times before addition of biotin-conjugated mouse anti-human IgG monoclonal antibody (mAb) (BD Pharmingen, San Diego, CA, USA) (1:3,000, v/v). After a 2 h incubation at 37°C, the plates were washed 3 times, followed by the addition of streptavidin-horseradish peroxidase (1:50,000, v/v; BD Pharmingen). The plates were incubated for 1 h at RT, and unbound conjugates were removed by washing. EIA substrate kit solution (Bio-Rad Laboratories, Hercules, CA, USA) was then added to each well. The reaction was stopped with 10% HCl, and the absorbance was measured at 450 nm.

2.4. *Preparation and transplantation of human PBMCs into NOG mice and NOG-IL-4-Tg mice*

The healthy donors (HD) enrolled in the experiments and all of mice transplanted with HD PBMC are listed in Table 1. A total of 7.5 mL of PB from healthy donors was drawn into Vacutainer ACD tubes (NIPRO Corporation,

Table 1. List of NOG and NOG-IL-4-Tg mice transplanted with HD PBMCs (The percentage was estimated by FCM-analyzed lymphocyte-gated data)

Mouse No.	Donor	Cell No. (×10^6)	hIL-4 (pg/mL)	GC (ng/mL)	GR (relative amount)	Specific Antibody (ng/mL)	CD19+ (%)	% of CD45			% of CD4				
								CD3+ (%)	CD8+ (%)	CD4+ (%)	Th1 (%)	Th2 (%)	Th17 (%)	Tfh (%)	Treg (%)
PBS-NOG-hIL-4-Tg															
#1	HD1	230	221	91	0.118	1.6	0.9	99.1	75.9	20.3	38.6	0.98	0.13	0.89	4.63
#2	HD2	62	240	12	0.061	1	1.0	99.00	64.5	30.2	15.9	1.41	0.14	1.01	5.82
#3	HD3	110	251	131	0.123	14.6	12.9	87.1	13.5	68.3	31.4	1.13	0.18	1.91	5.46
#4	HD3	91	431	140	0.034	1.6	9.9	90.1	21.9	62.6	24.0	0.54	0.07	0.90	3.50
#5	HD4	46	404	286	0.114	29.5	11.4	88.8	14.7	60.1	6.9	0.25	0.02	0.16	3.68
#6	HD5	200	157	9	0.056	—*	7.5	92.5	38.0	50.7	48.1	0.91	0.18	0.35	1.56
CH401MAP-NOG-hIL-4-Tg															
#7	HD1	230	220	131	0.074	40.2	22.9	77.1	11.4	60.2	43.2	0.34	0.03	0.95	4.10
#8	HD2	120	181	64	0.114	7.6	12.5	87.5	35.8	47.8	40.0	0.52	0.08	1.03	2.92
#9	HD3	45	268	112	0.152	9.6	14.6	85.4	17.6	58.7	25.4	0.75	0.13	1.59	5.23
#10	HD3	74	494	137	0.063	—	21.7	78.2	20.3	55.2	31.6	0.65	0.12	0.88	4.16
#11	HD4	69	402	181	0.051	15.2	21.5	79.1	2.20	69.9	10.3	0.17	0.01	0.65	2.46
#12	HD5	120	196	82	0.069	—	13.3	86.7	16.0	59.6	30.6	0.44	0.04	1.59	8.31
PBS-NOG															
#13	HD1	130	nd**	188	0.462	—	1.1	98.9	33.2	58.7	22.6	1.25	0.04	1.19	3.77
#14	HD1	63	nd	188	0.041	32.3	3.7	96.4	37.4	47.1	25.3	0.26	0.08	1.43	5.46
#15	HD3	71	nd	195	0.187	22	1.3	98.7	36.8	53.6	20.3	5.55	0.64	0.40	1.25
#16	HD4	200	nd	162	0.110	11	0.6	99.4	16.3	78.1	42.4	0.52	0.12	1.03	2.78
CH401MAP-NOG															
#17	HD1	95	nd	157	0.247	—	2.4	97.7	48.3	35.8	26.8	1.02	0.05	0.24	3.88
#18	HD2	29	nd	75	0.183	1.5	0.6	99.4	48.4	35.2	24.8	1.15	0.12	0.43	3.97
#19	HD3	46	nd	69	0.165	8	7.3	92.7	14.0	74.5	34.4	0.10	0.03	1.90	1.74
#20	HD4	88	nd	187	0.095	32.1	12.6	87.4	11.0	72.0	43.5	0.53	0.07	2.07	6.21

* Not determined. The measurement failed because of nonspecific cross-reactivity. ** Not detected.

Osaka, Japan) containing heparin. The collected PB was immediately placed in 10 mL of Ficoll-Hypaque (Sigma-Aldrich, London, UK), and mononuclear cells were isolated by density centrifugation (500 × g, 30 min, 20°C). The cells were washed with PBS for 5 min at 300 × g, 4°C. Numbers of PBMCs ranging from 2.5 to 5 × 10^6 were intravenously transplanted into 8- to 12-week-old NOG or NOG-hIL-4-Tg mice. Two mice from each strain were transplanted with the same donor PBMCs, to use one for peptide immunization and the other for negative control (PBS and Freund's adjuvant).

2.5. Peptide immunization

A CH401 peptide, which includes the epitope sequence of the anti-human epidermal growth factor receptor 2 (HER2) mAb, was determined using multiple antigen peptides (MAP) with a partial amino acid sequence of HER2/neu previously (*34*). The peptide was synthesized using a Rink amide resin (0.4-0.7 mmol/g), an ACT357 peptide synthesizer (Advanced Chemtech, Louisville, KY, USA) and a multiple antigen peptide named CH401MAP, a 20-mer peptide of the HER2 molecule that was synthesized as an antigen peptide. The HER2 peptide was emulsified with complete Freund's adjuvant (CFA) (Wako Pure Chemical Industries, Ltd, Osaka, Japan) (50 μg/head, 100 μL, 1:1, v/v) and administered intraperitoneally to the PBMC-transplanted NOG-hIL-4-Tg mice in which the hIL-4 level was greater than 100 pg/mL in the plasma. For the negative control, an equal volume of PBS was emulsified and injected into PBMC-transplanted NOG-hIL-4-Tg mice. Boosters were performed using incomplete Freund's adjuvant (IFA) (Wako Pure Chemical Industries, Ltd) at 2 weeks after the first immunization. Two weeks after the booster, the mice were sacrificed for analyses.

2.6. Analysis of engrafted human cells in human PBMC-transplanted mice

At 4 weeks after transplantation, the mice were euthanized for analysis. PB was collected in the presence of heparin *via* retro-orbital bleeding under inhalation anesthesia at 4 weeks after transplantation. The mice were sacrificed and analyzed for human T- and B-cell development and antibody production. Engraftment and differentiation of human cells in the spleen cells were analyzed by flow cytometry (FCM) staining with anti-human antibodies as described below. Fluorochrome-conjugated anti-human mAbs were used to identify human immune cells. The cells were incubated with appropriate dilutions of fluorescently labeled mAbs for 15 min at 4°C and were then washed with PBS containing 1% (w/v) BSA. The cells were analyzed using FACS Fortessa, Verse, or Canto (BD Bioscience, Franklin Lakes, NJ, USA). For each analysis, the live gate with white blood cells or lymphocytes was

further gated based on hCD45 expression. The mouse anti-human mAbs used in this study are listed in Table S1 (*http://www.biosciencetrends.com/action/getSupplementalData.php?ID=24*).

2.7. Real time RT PCR

A total of 5 × 10^5 cells from NOG or NOG-IL-4-Tg mouse spleens were collected, stored in TRIzol (Invitrogen, Carlsbad, CA, USA) at –80°C and extracted according to the manufacturer's instructions. The total RNA concentration was determined by measuring absorbance at 260 nm. The purity was estimated by the relative ratio of the absorbance at 260/280 nm. Integrity was assayed by agarose gel electrophoresis. The purity and integrity were greater than 95%. cDNA was synthesized from the total RNA (2 μg) using a High Capacity cDNA Reverse Transcription Kit (Life Technologies, CA, USA). TaqMan probes for human common GR and β-actin (Thermo Fisher Scientific Co., Ltd., MA, USA), were used and RT-PCR was conducted by Applied Biosystems Step One Plus Real-Time PCR Systems in all analyses. A commercially available Taqman Fast Universal PCR Master mix (Thermo Fisher Scientific) was used for PCR amplification and detection of GR (Hs00353740_m1). All samples were assessed in triplicate. Quantification of the expression of the target gene in relation to the respective housekeeping gene was carried out employing the comparative (ΔΔ) Ct method.

2.8. Statistics

Statistical analysis was performed with Microsoft Excel (Microsoft, Redmond, WA, USA). The data are shown as the mean ± SD. Significant differences between groups were determined by two-sided Student's *t*-test analysis.

3. Results

3.1. Correlation between human IL-4 and Th and B cell proportions in humanized NOG-hIL-4-Tg mice

First, we purified donor PBMCs and transplanted them into 2 to 3 NOG and NOG-hIL-4-Tg mice. After the transplantation, CH401MAP, a breast cancer vaccine candidate that is a part of the HER2 molecule (*34,35*), emulsified with FCA was injected into the mice, and a booster was administered after 2 weeks. A mouse transplanted with PBMCs from the same donor as those transplanted into the CH401MAP-vaccinated mouse was injected with PBS/FCA and used as a control mouse. After 4 weeks, mice were sacrificed, and spleen cells were obtained as shown in Figure 1A and Table 1. The mean spleen cell number was 1.23 ± 0.69 (× 10^8) in PBS-NOG-hIL-4-Tg mice, 1.10 ± 0.60 (× 10^8) in CH401-NOG-hIL-4-Tg mice, 1.16 ±
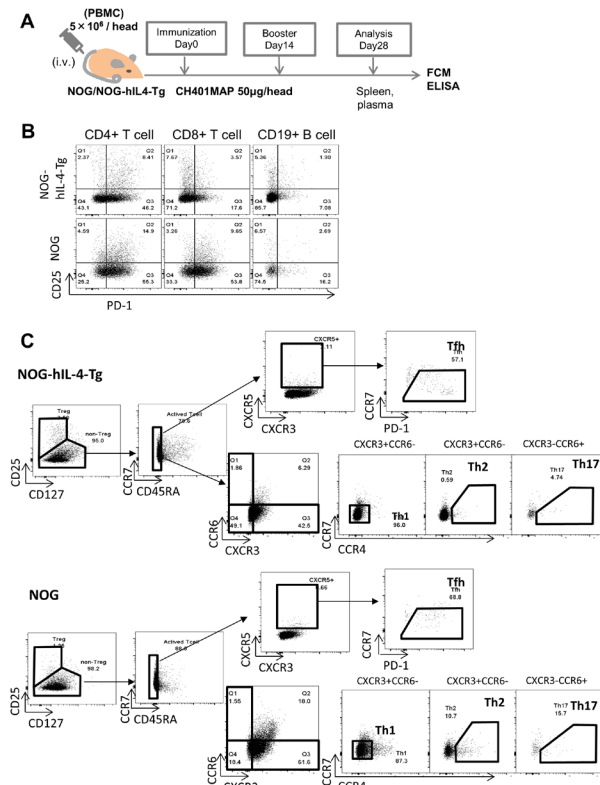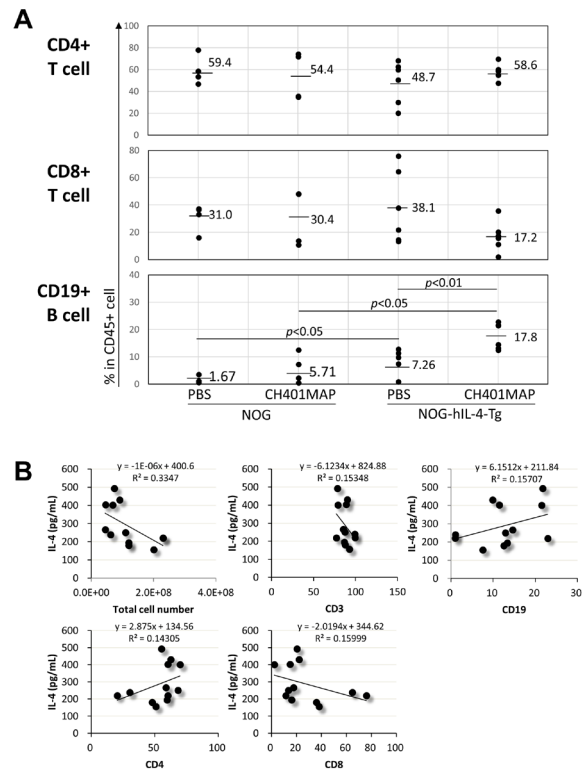
Figure 1. Characterization of human lymphocyte subsets in PBMC-transplanted humanized mice. (A) Protocol for analysis of the human PBMC-transplanted humanized mouse. **(B)** FCM analysis of CD25 and PD-1 expression in human CD4+ and CD8+ T cells and B cells in spleens of NOG-hIL-4-Tg and NOG mice at 4 weeks after PBMC transplantation. **(C)** FCM analysis of human Th subsets in spleens of NOG-hIL-4-Tg and NOG mice at 4 weeks after PBMC transplantation. Representative data from 12 NOG-hIL-4-Tg and 8 NOG are shown.

Figure 2. Relationship between the human IL-4 level and lymphocyte subsets in PBMC-transferred humanized mice. (A) The percentage of human CD4+ and CD8+ T cells and B cells in CD45+ cells in spleen cells from NOG-hIL-4-Tg and NOG mice at 4 weeks after PBMC transplantation. PBS; the mice treated with adjuvant alone. CH401MAP; the mice treated with CH401MAP emulsified with Freund's adjuvant. PBS-NOG ($n = 4$), CH401MAP-NOG ($n = 4$), PBS-NOG-hIL-4-Tg ($n = 6$), CH401MAP-NOG-hIL-4-Tg ($n = 6$). **(B)** Comparison of the correlation between the plasma hIL-4 level and total cell number and proportions of CD3+ T cells, CD19+ B cells, CD4+ T cells, and CD8+ T cells in CD45+ cells in NOG-hIL-4-Tg mice. PBS-NOG-hIL-4-Tg ($n = 6$), CH401MAP-NOG-hIL-4-Tg ($n = 6$). Correlation equations and R2 are shown in each panel.

0.55 ($\times 10^8$) in PBS-NOG mice and 6.45 ± 0.28 ($\times 10^7$) in CH401-NOG mice as shown in Table 1. Thus, the spleen cell number in the CH401MAP-immunized NOG mouse was significantly lower than that in the other three groups. In the NOG-hIL-4-Tg mice, the IL-4 concentration in the plasma showed a negative correlation with total spleen cell number (Figure 2B, upper left panel).

These results suggest that IL-4 expression affects the cell number in the transplanted mouse spleen and that this effect may be maintaining the splenic cell number after immunization.

3.2. *Flow cytometry analysis of human lymphocytes transplanted into NOG and NOG-hIL-4-Tg mice*

To compare the lymphocyte subsets of the mice, we conducted multicolor-flow cytometry using the antibodies shown in Table S1 (*http://www.biosciencetrends.com/ action/getSupplementalData.php?ID=24*). At first, we analyzed human CD4+ and CD8+ T cells, B cells and expression of CD25, an activation/regulatory marker in the spleen of NOG and NOG-hIL-4-Tg mice. As shown in Figure 1B and Figure 2A (upper two panels), no

significant difference was observed in the proportions of CD4+ T cells and CD8+ T cells between NOG and NOG-hIL-4 Tg mice with or without immunization, whereas CD19+ B cell levels were significantly higher in NOG-hIL-4-Tg mice than in conventional NOG mice (Figure 2A, lower panel). This result was consistent with our previous report (*16*). On the other hand, immunized NOG-hIL-4-Tg mice possessed the highest proportion of B cells (17.8%).

Next, we compared the mean fluorescent intensity (MFI) of the programmed death-1 (PD-1) molecule on CD4+ T cells between immunized and nonimmunized mouse spleen cells because PD-1 is an activation/ exhaustion marker of lymphocytes (Figures 1B and S1, *http://www.biosciencetrends.com/action/ getSupplementalData.php?ID=24*). As a result, in the NOG-hIL-4-Tg mouse, the PD-1 MFI was higher in CD4+ T cells than in adjuvant-alone CD4+ T cells ($p < 0.05$), while in the conventional NOG mouse, no significant difference was observed between the

adjuvant-alone and peptide-immunized CD4+ T cells (Figure S1, upper panel, *http://www.biosciencetrends. com/action/getSupplementalData.php?ID=24*). For CD8+ T cells, while PD-1 expression was lower than that in CD4+ T cells overall, PD-1 MFI tended to increase after peptide immunization, but the expression was lower in the NOG-hIL-4-Tg mouse than in the conventional NOG mouse ($p < 0.01$) (Figure S1, lower panel, *http://www.biosciencetrends.com/action/ getSupplementalData.php?ID=24*). These results suggest that the NOG-hIL-4-Tg mouse possessed a higher number of B cells, but the CD4+ T cells and CD8+ T cells are not significantly different compared with those of the conventional NOG mouse. The activation/exhaustion of T cells was indicated after antigen-immunization in the NOG-hIL-4-Tg mouse.

The total spleen cell number was compared with the IL-4 level in the plasma of the NOG-hIL-4-Tg mice. As a result, IL-4 expression was shown to have a negative correlation with the number of splenic cells in the NOG-hIL-4-Tg mice, irrespective of the treatment (Table 1 and Figure 2B, upper left panel). When the proportions of T cells and B cells were compared with IL-4 expression, the total T-cell proportion showed a weak and negative correlation ($R^2 = 0.15348$) to the plasma IL-4 level (Figure 2B, upper middle panel), while the B-cell proportion showed a weak and positive correlation ($R^2 = 0.15707$) with the plasma IL-4 level (Figure 2B, upper right panel). In the T-cell subsets, CD4+ T cells showed a positive correlation ($R^2 = 0.14305$), but CD8+ T cells showed a negative correlation ($R^2 = 0.15999$) (Figure 2B, lower panels). These results suggest that the proportion of CD4+ T cells but not CD8+ T cells may be increased along with GR expression and influence B-cell survival and/or function.

3.3. *Flow cytometry of human Th cells transplanted into NOG and NOG-hIL-4-Tg mice*

Since the Th-cell proportion increase was dependent on IL-4 expression, we analyzed the Th-cell subset proportion and examined the correlation to IL-4 concentration in plasma. To compare the Th-cell subsets of the mice, we defined the subsets using the antibodies shown in Table S1 (*http://www.biosciencetrends.com/ action/getSupplementalData.php?ID=24*. As shown in Figure 1C, we analyzed the Th-cell subsets (Th1, Th2, Th17, Tfh and Treg) developed in the mice (*36*).

After the transplantation of human PBMCs into the NOG and NOG-hIL-4-Tg mouse models, the proportion of human Th-cell subsets was examined with/without peptide stimulation. Th1 cells were dominant in both NOG and NOG-hIL-4-Tg mice transplanted with human PBMCs as shown in Table 1, Figure 1C and Figure 3A. Th2 cells did not increase in NOG-hIL-4-Tg mice compared with NOG mice, irrespective of peptide
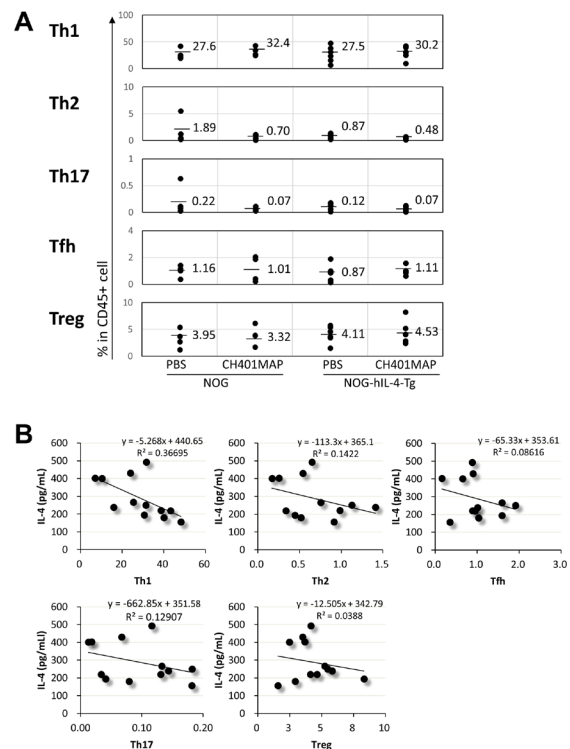

Figure 3. Relationship between human IL-4 level and Th subsets in PBMC-transferred humanized mice. (A) The percentage of Th-cell subsets in the spleen cells of NOG-hIL-4-Tg and NOG mice at 4 weeks after PBMC transplantation. The same mice described in Figure 2 were used. PBS-NOG (*n* = 4), CH401MAP-NOG (*n* = 4), PBS-NOG-hIL-4-Tg (*n* = 6), CH401MAP-NOG-hIL-4-Tg (*n* = 6). **(B)** Comparison of the correlation between plasma hIL-4 level and the proportions of Th1, Th2, Tfh, Th17, and Treg cells in CD45+ cells in NOG-hIL-4-Tg mice. PBS-NOG-hIL-4-Tg (*n* = 6), CH401MAP-NOG-hIL-4-Tg (*n* = 6). Correlation equations and R2 are shown in each panel.

immunization. In addition, Th17, Treg, and Tfh cells did not increase in either NOG or NOG-hIL-4-Tg mice. These results indicated that the proportion of Th-cell subsets are not affected by the plasma IL-4 level in the NOG-hIL-4-Tg mice.

Next, we examined the correlation between plasma IL-4 concentration and Th-cell subset. All the Th-cell subsets showed a negative correlation with IL-4 concentration (Figure 3B). For example, Th1, Th2 and Th17 proportions showed moderate correlations with IL-4 plasma concentration (Slope = –5.268, R2 = 0.36695 for Th1; Slope = –113.3, $R^2 = 0.1422$ for Th2; Slope = –662.85, $R^2 = 0.12907$ for Th17). Other Th-cell subsets had no correlation, while the B-cell proportion showed a moderate positive correlation with IL-4 ($R^2 = 0.15707$) (Figure 2B, upper right panel).

These results suggest that human IL-4 expressed in the NOG-hIL-4-Tg mouse was not sufficient for induction of Th2 cells or enhancement of Tfh cells but was sufficient to decrease Th1 cells. Therefore, the increase in B-cell number did not appear to be directly correlated with enhanced Th2 or Tfh cells.
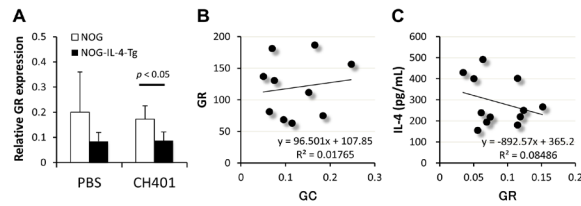
Figure 4. GR expression in PBMC-transferred humanized mice. (A) Relative GR expression in the spleen cells of the mice was shown. White bars represent NOG mice, and black bars represent NOG-hIL-4-Tg mice. Student's *t*-test was performed, and the significant difference (p < 0.05) is shown. PBS-NOG (*n* = 4), CH401MAP-NOG (*n* = 4), PBS-NOG-hIL-4-Tg (*n* = 6), CH401MAP-NOG-hIL-4-Tg (*n* = 6). **(B)** Comparison of the correlation between GC in the plasma and GR expression in the spleen cells of CH401MAP–NOG and CH401MAP-NOG-hIL-4-Tg mice were further analyzed. CH401MAP-NOG (*n* = 4), CH401MAP-NOG-hIL-4-Tg (*n* = 6). **(C)** The correlation between human IL-4 concentration in plasma and GR expression in the spleen cells of PBS-NOG-hIL-4-Tg and CH401MAP-NOG-hIL-4-Tg were analyzed. PBS-NOG-hIL-4-Tg (*n* = 6), CH401MAP-NOG-hIL-4-Tg (*n* = 6). Correlation equations and R2 are shown in each panel.

3.4. *Glucocorticoid receptor expression negatively correlates with B cells*

As GC signal is important for T-cell regulation (*29,32*), we hypothesized that IL-4 affected the decrease in GC signal. Therefore, we measured the concentration of GC and the expression of the GR in human lymphocytes, which affects GC signaling in T cells and B cells.

Spleen cells were collected from PBMC-transplanted and immunized mice, mRNA was purified and the GR mRNA was measured by real-time PCR. The results showed that GR expression tended to be low in immunized NOG-hIL-4-Tg mice compared with that in conventional NOG mice in the nonimmunized group, but a significant difference was not observed (Figure 4A). However, a significant difference was observed between immunized NOG and NOG-hIL-4 Tg mice, as shown in Figure 4A. In the immunized group, NOG-hIL-4-Tg mouse GR expression was significantly lower than that in conventional NOG mouse. However, the plasma corticosterone (representative of mouse GC, selected as the GC in the humanized mouse mainly produced by mouse tissues) level neither was significantly different nor showed a correlation with GR expression (Table 1 and Figure 4B).

These results demonstrated that humanized NOG mouse lymphocytes produce GR, which is suppressed by human IL-4. However, IL-4 expression and GR expression showed no correlation in NOG-hIL-4-Tg mice (Figure 4C).

3.5. *Correlation of GR with Th and B cells*

As GR expression was significantly different between the NOG and NOG-hIL-4-Tg mice and no correlation was observed between the difference and the level of corticosterone produced by the mice, we tried to
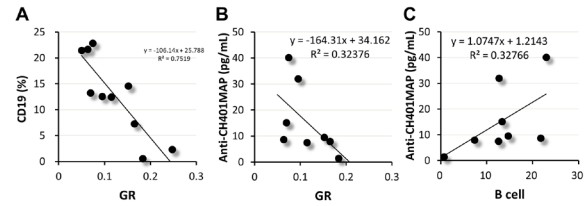
Figure 5. Relationship between GR expression and antibody production in PBMC-transferred humanized mice. (A) Comparison of the correlation between CD19+ B cells (% in CD45+ cells) and relative GR expression in the spleen cells of CH401MAP-NOG (*n* = 4) and CH401MAP-NOG-hIL-4-Tg mice (*n* = 6). **(B)** The correlation between anti-CH401MAP IgG antibody in plasma and GR expression in the spleen cells of CH401MAP-NOG (*n* = 3) and CH401MAP-NOG-hIL-4-Tg (*n* = 5) mice. **(C)** Comparison of the correlation between CD19+ B cells (% in CD45+ cells) and anti-CH401MAP IgG antibody in the plasma of CH401MAP-NOG (*n* = 3) and CH401MAP-NOG-hIL-4-Tg (*n* = 5) mice. Correlation equations and R2 are shown in each panel.
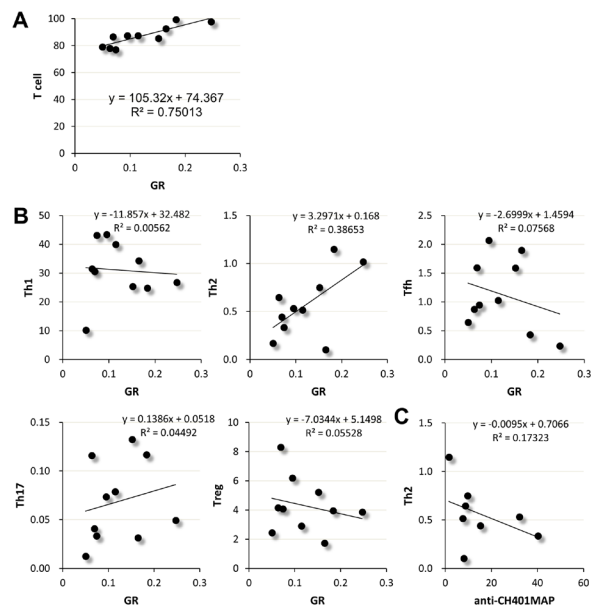
Figure 6. Relationship between GR expression and Th subsets in PBMC-transferred humanized mice. (A) Comparison of the correlation between CD3+ T cells (% in CD45+ cells) and relative GR expression in the spleen cells of CH401MAP-NOG (*n* = 4) and CH401MAP-NOG-hIL-4-Tg (*n* = 6) mice. **(B)** The correlation between each Th cell subset (Th1, Th2, Tfh, Th17, and Treg) and GR expression. **(C)** The correlation between Th2 cells and anti-CH401MAP IgG antibody. Correlation equations and R2 are shown in each panel.

analyze whether the difference was correlated with the lymphocyte subset differentiation/survival.

As spleen B-cell number was increased with IL-4 expression (Figure 2B, upper right panel), we analyzed the specific IgG production in the mouse. PB was collected from these mice, and the plasma was subjected to anti-CH401MAP IgG ELISA. The result indicated that GR expression showed a strong inverse correlation with the proportion of B cells (R^2 = 0.75192) (Figure 5A) and anti-CH401MAP IgG level (R^2 = 0.32376) (Figure 5B). The slope on a graph was not significantly

different between the NOG and NOG-hIL-4-Tg mouse models (Slope of NOG; –72.441, NOG-IL-4-Tg; –77.183) (Figure S2, *http://www.biosciencetrends. com/action/getSupplementalData.php?ID=24*). As the specific IgG and the B cell proportion also showed a strong correlation (R^2 = 0.32776) (Figure 5C), it is suggested that GR expression suppresses B-cell survival or differentiation into antibody-secreting effector cells.

Next, we examined the correlation between GR and Th-cell subsets. The total number of T cells showed a high positive correlation (R^2 = 0.75013) with GR (Figure 6A). Surprisingly, among the five Th-cell subsets (Th1, Th2, Th17, Treg and Tfh), a significant high positive correlation was observed only between Th2 and GR (R^2 = 0.38653) (Figure 6B, upper middle panel). As shown in upper right panel of Figure 6B, GR and Tfh, a subset known to be important for germinal center reaction and highly specific IgG production, showed no correlation (R^2 = 0.07568), suggesting that the development/ maintenance of Tfh is not involved in the GR effect.

These results suggest that the suppression of GR expression increased the B cell ratio, not the Tfh ratio, in the spleen of NOG-hIL-4-Tg mice, and eventually the specific IgG concentration is increased in the plasma.

4. Discussion

The NOG-hIL-4-Tg mouse model, which was developed by our group recently, enabled us to suppress GVHD after human PBMC transplantation and to produce specific anti-IgG production after immunization (*16*). This mouse system is promising for the evaluation of human vaccines. However, it has not been clarified how human IL-4 enables specific IgG production or suppresses GVHD in the mouse system. We hypothesized that GR expression may affect the humoral immunity of the humanized mouse, as GVHD is controlled by the glucocorticoid signal. Our results showed that GR expression was significantly lower in NOG-hIL-4-Tg spleen cells after CD401 immunization, and a strong negative correlation with the proportion of B cells and strong positive correlation with that of T cells were observed. Moreover, after the detailed analysis, a high negative correlation between specific IgG production and GR level was obtained, while a correlation with Tfh was not observed. These results suggest that the GR signal is decreased in the NOG-hIL-4-Tg mouse, which makes it difficult to inhibit B-cell function by GC.

IL-4 and GC crosstalk was reported previously, but according to the report, GC administration induced Th2 differentiation (*37*). However, our observation was that systemic expression of human IL-4 suppressed the GR expression of transplanted human PBMCs. It is curious that systemic expression of a high level of IL-4 suppressed GR expression, which may cause a decrease in Th2 differentiation, while GC concentration

in plasma was not correlated with GR expression (R^2 = 0.01765) (Figure 4B). This mechanism should be clarified in the future.

There have been many reports involving GC and/or GR expression and immune suppression, mainly with T-cell differentiation and function (*29,38*). Meanwhile, the effects of B-cell differentiation and function are not as well investigated and are less controversial. While a report suggests that GC function showed a negative correlation to B-cell survival and proliferation, another group reports that GC does not show a correlation with B-cell survival and proliferation but affects class-switch from IgM to other isotypes by modifying AID expression (*31*). GC is also reported to increase Treg cells, but another group reported that it does not (*29,32*). Occasionally, GC is used as an anti-inflammatory drug after anticancer treatment, as reported for leukemia (*39*). Thus, the function and the mechanism are not clear, but in our results, GC clearly affects B-cell number and antigen-specific antibody production negatively. Therefore, it shows promise to become important evidence for improving the humanized mouse system based on our model. Moreover, it will become a good model animal to investigate how GC affects the regulation of human antibody production.

Between the NOG and NOG-hIL-4-Tg mouse systems, no significant difference in the proportion of Th-cell subsets was detected. However, the proportion of the Th1 subset also showed a negative correlation with IL-4, which was consistent with a previous report (*40*). Although it is well known that the *in vitro* treatment of high-dose IL-4 induced Th2-cell differentiation (*41,42*), our result demonstrated that the proportion of the Th2 subset did not increase in NOG-hIL-4 Tg mice. As we reported previously (*17*), PMA-Ionomycin (PMA/Io) stimulation induced high expression levels of IL-4 in human CD4+ T cells engrafted in NOG-hIL-4-Tg mice. This contradiction might be resolved by analysis of the differences between the mice with and without *in vivo* stimulation. Kumar *et al*. and Murray *et al*. demonstrated that high-affinity and/or high numbers of antigen signals were polarized into Th1 cells, even in an IL-4-abundant environment (*43,44*). Similar to these reports, our CH401MAP peptide/Freund's adjuvant or Freund's adjuvant alone used to immunize NOG-hIL-4 Tg mice strongly activated human T cells; hence, the majority of T cells might be shifted to Th1 cells in the present study. Further analysis is required to determine the Th status in NOG-hIL-4 Tg mice.

In our results, there was a very low correlation between IL-4 in the plasma and the GR expression level, although NOG-hIL-4-Tg mice showed a lower GR level than conventional NOG mice. Therefore, it may be possible that the concentration of 100 pg/mL in the plasma is sufficient for the suppression of GR expression and that higher concentrations do not affect

the GR expression level further. While GR expression is reported to be increased by dexamethasone, which mimics GC induction *via* the hypothalamic-pituitary-adrenal axis against inflammatory signals such as TNF-α and/or IL-1β (*45*), sufficient IL-4 may suppress the release of these inflammatory cytokines in the blood, resulting in the suppression of GR expression. As spleen B cells are highly sensitive to GC (*30*), suppression of GR and GC signals may be highly beneficial to B-cell survival.

In conclusion, GR expression is decreased in NOG-hIL-4-Tg mice transplanted with human PBMCs. The decrease in GR expression shows a correlation with the increase in B-cell number and specific IgG production.

Acknowledgements

References

1. Kametani Y, Miyamoto A, Seki T, Ito R, Habu S, Tokuda Y. The significance of humanized mouse models for the evaluation of the humoral immune response against cancer vaccines. Personalized Medicine Universe. 2018. Doi. org/10.1016/j.pmu.2018.04.002

2. Shultz LD, Lang PA, Christianson SW, Gott B, Lyons B, Umeda S, Leiter E, Hesselton R, Wagar EJ, Leif JH, Kollet O, Lapidot T, Greiner DL. NOD/LtSz-Rag1null mice: An immunodeficient and radioresistant model for engraftment of human hematolymphoid cells, HIV infection, and adoptive transfer of NOD mouse diabetogenic T cells. J Immunol. 2000; 164:2496-2507.

3. Ito M, Hiramatsu H, Kobayashi K, Suzue K, Kawahata M, Hioki K, Ueyama Y, Koyanagi Y, Sugamura K, Tsuji K, Heike T, Nakahata T. NOD/SCID/gamma$_c^{null}$ mouse: An excellent recipient mouse model for engagement of human cells. Blood. 2002; 100:3175-3182.

4. Shultz L, Ishikawa F, Greiner D. Humanized mice in translational biomedical research. Nat Rev Immunol. 2007; 7:118-130.

5. Bouaziz J, Yanaba K, Tedder T. Regulatory B cells as inhibitors of immune responses and inflammation. Immunol Rev. 2008; 224:201-214.

6. Shultz L, Brehm M, Garcia-Martinez J, Greiner D. Humanized mice for immune system investigation: Progress, promise and challenges. Nat Rev Immunol. 2012; 12:786-798.

7. Ito R, Takahashi T, Katano I, Ito M. Current advances in humanized mouse models. Cell Mol Immunol. 2012; 9:208-214.

8. Watanabe Y, Takahashi T, Okajima A, Shiokawa M, Ishii N, Katano I, Ito R, Ito M, Minegishi M, Minegishi N, Tsuchiya S, Sugamura K. The analysis of the functions of human B and T cells in humanized NOD/shi-scid/γc^{null} (NOG) mice (hu-HSC NOG mice). Int Immunol. 2009; 21:843-858.

9. Danner R, Chaudhari S, Rosenberger J, Surls J, Richie T, Brumeanu T, Casares S. Expression of HLA class II molecules in humanized NOD.Rag1KO.IL2RgcKO mice is critical for development and function of human T and B cells. PLoS One. 2011; 6:e19826.

10. Suzuki M, Takahashi T, Katano I, Ito R, Ito M, Harigae H, Ishii N, Sugamura K. Induction of human humoral immune responses in a novel HLA-DR-expressing transgenic NOD/Shi-scid/γc^{null} mouse. Int Immunol. 2012; 24:243-252.

11. van Rijn R, Simonetti E, Hagenbeek A, Hogenes M, de Weger R, Canninga-van Dijk M, Weijer K, Spits H, Storm G, van Bloois L, Rijkers G, Martens A, Ebeling S. A new xenograft model for graft-versus-host disease by intravenous transfer of human peripheral blood mononuclear cells in RAG2$^{-/-}$γc$^{-/-}$ double-mutant mice. Blood. 2003; 102:2522-2531.

12. King M, Pearson T, Shultz L, *et al*. A new Hu-PBL model for the study of human islet alloreactivity based on NOD-*scid* mice bearing a targeted mutation in the IL-2 receptor gamma chain gene. Clin Immunol. 2008; 126:303-314.

13. Ito R, Katano I, Kawai K, Hirata H, Ogura T, Kamisako T, Eto T, Ito M. Highly sensitive model for xenogenic GVHD using severe immunodeficient NOG mice. Transplantation. 2009; 87:1654-1658.

14. Wege A, Melkus M, Denton P, Estes J, Garcia J. Functional and phenotypic characterization of the humanized BLT mouse model. Curr Top Microbiol Immunol. 2008; 324:149-165.

15. Covassin L, Jangalwe S, Jouvet N, Laning J, Burzenski L, Shultz L, Brehm M. Human immune system development and survival of non-obese diabetic (NOD)-*scid IL2rγ^{nul}*l (NSG) mice engrafted with human thymus and autologous haematopoietic stem cells. Clin Exp Immunol. 2013; 174:372-388.

16. Kametani Y, Katano I, Miyamoto A, Kikuchi Y, Ito R, Muguruma Y, Tsuda B, Habu S, Tokuda Y, Ando K, Ito M. NOG-hIL-4-Tg, a new humanized mouse model for producing tumor antigen-specific IgG antibody by peptide vaccination. PLoS ONE. 2017; 12:e0179239.

17. Fairfax K, Everts B, Amiel E, Smith A, Schramm G, Haas H, Randolph G, Taylor J, Pearce E. IL-4-secreting secondary T follicular helper (Tfh) cells arise from memory T cells, not persisting Tfh cells, through a B cell-dependent mechanism. J Immunol. 2015; 194:2999-2930.

18. Glatman Zaretsky A, Taylor J, King I, Marshall F, Mohrs M, Pearce E. T follicular helper cells differentiate from Th2 cells in response to helminth antigens. J Exp Med. 2009; 206:991-999.

19. Breitfeld D, Ohl L, Kremmer E, Ellwart J, Sallusto F, Lipp M, Förster R. Follicular B helper T cells express CXC chemokine receptor 5, localize to B cell follicles, and support immunoglobulin production. J Exp Med. 2000; 192:1545-1552.

20. Schaerli P, Willimann K, Lang A, Lipp M, Loetscher P, Moser B. CXC chemokine receptor 5 expression defines follicular homing T cells with B cell helper function. J Exp Med. 2000; 192:1553-1562.

21. Kim C, Rott L, Clark-Lewis I, Campbell D, Wu L, Butcher E. Subspecialization of CXCR5+ T cells: B helper activity is focused in a germinal center-localized subset of CXCR5+ T cells. J Exp med. 2001; 193:1373-1381.

22. Di Ianni M, Falzetti F, Carotti A, *et al*. Tregs prevent GVHD and promote immune reconstitution in HLA-haploidentical transplantation. Blood. 2011; 117:3921-3928.

23. Malard F, Bossard C, Brissot E, Chevallier P, Guillaume T, Delaunay J, Mosnier J, Moreau P, Grégoire M, Gaugler B, Mohty M. Increased Th17/Treg ratio in chronic liver GVHD. Bone Marrow Transplant. 2014; 49:539-544.

24. Beato M, Herrlich P, G S. Steroid Hormone Receptors: Many Actors in Search of a Plot. Cell 1995; 83:851-857.

25. Ratman D, Vanden Berghe W, Dejager L, Libert C, Tavernier J, Beck I, De Bosscher K. How glucocorticoid receptors modulate the activity of other transcription factors: A scope beyond tethering. Mol Cell endocriol. 2013; 380:41-54.

26. Taves M, Hamden J, Soma K. Local glucocorticoid production in lymphoid organs of mice and birds: Functions in lymphocyte development. Hormones and Behavior. 2017; 88:4-14.

27. Avivi I, Stroopinsky D, Rowe J, Katz T. A subset of CD8+ T cells acquiring selective suppressive properties may play a role in GvHD management. Transplant Immunol. 2013; 28:57-61.

28. Taves M, Plumb A, Korol A, Van Der Gugten J, Holmes D, Abraham N, Soma K. Lymphoid organs of neonatal and adult mice preferentially produce active glucocorticoids from metabolites, not precursors. Brain, Behavior, and Immunity. 2016; 57:271-281.

29. Ugor E, Preneka L, Papa R, Bertab G, Ernsztc D, Najbauera J, Németha P, Boldizsára F, Berkia T. Glucocorticoid hormone treatment enhances the cytokine production of regulatory T cells by upregulation of Foxp3 expression. Immunobiology. 2018; 223:422-431.

30. Gruver-Yates A, Quinn M, Cidlowski J. Analysis of glucocorticoid receptors and their apoptotic response to dexamethasone in male murine B cells during development. Endocrinology. 2014; 155:463-474.

31. Benko A, Olsen N, Kovacs W. Glucocorticoid inhibition of activation-induced cytidine deaminase expression in human B lymphocytes. Mol Cell Endocrinol 2014; 382:881-887.

32. Pandolfi J, Baz P, Fernández P, Discianni Lupi A, Payaslián F, Billordo L, Fainboim L, Arruvito L. Regulatory and effector T-cells are differentially modulated by Dexamethasone. Clin Immunol. 2013; 149:400-410.

33. Kametani Y, Shiina M, Katano I, *et al*. Development of human-human hybridoma from anti-Her-2 peptide-producing B cells in immunized NOG mouse. Exp Hematol. 2006; 34:1240-1248.

34. Miyako H, Kametani Y, Katano I, Ito R, Tsuda B, Furukawa A, Saito Y, Ishikawa D, Ogino K, Sasaki S, Imai K, Habu S, Makuuchi H, Tokuda Y. Antitumor effect of new HER2 peptide vaccination based on B cell epitope. Anticancer Res. 2011; 31:361-3368.

35. Ishida T, Tsujisaki M, Hinoda Y, Imai K, Yachi A. Establishment and characterization of mouse-human chimeric monoclonal anitbody to *erbB-2* product. Jpn J Cancer Res. 1994; 85:172-178.

36. Jing He J, Zhang X, Wei Y, *et al*. Low-dose interleukin-2 treatment selectively modulates CD4+ T cell subsets in patients with systemic lupus erythematosus. Nature Med. 2016; 22:991-995.

37. Tamada K, Harada M, Abe K, Li T, Nomoto K. IL-4-producing NK1.1+ T cells are resistant to glucocorticoid-induced apoptosis: Implications for the Th1/Th2 balance. J Immunol. 1998; 161:1239-1247.

38. Herold M, McPherson K, Reichardt H. Glucocorticoids in T cell apoptosis and function. Cell Mol Life Sci 2006; 63:60-72.

39. Chan L, Müschen M. B-cell identity as a metabolic barrier against malignant transformation. Exp Hematol. 2017; 53:1-6.

40. Blotta M, DeKruyff R, Umetsu D. Corticosteroids inhibit IL-12 production in human monocytes and enhance their capacity to induce IL-4 synthesis in CD4+ lymphocytes. J Immunol. 1997; 158:5589-5595.

41. Ramírez F, Fowell D, Puklavec M, Simmonds S, Mason D. Glucocorticoids promote a Th2 cytokine response by CD41 T cells *in vitro*. J Immunol. 1996; 156:2406-2412.

42. Nakayama T, Hirahara K, Onodera A, Endo Y, Hosokawa H, Shinoda K, Tumes D, Okamoto Y. Th2 Cells in Health and Disease. Annu Rev Immunol. 2017; 35:53-84.

43. Kumar V, Bhardwaj V, Soares L, Alexander J, Sette A, Sercarz E. Major histocompatibility complex binding affinity of an antigenic determinant is crucial for the differential secretion of interleukin 4/5 or interferon gamma by T cells. Proc Natl Acad Sci U S A. 1995; 92:9510-9514.

44. Murray J, Pfeiffer C, Madri J, Bottomly K. Major histocompatibility complex (MHC) control of CD4 T cell subset activation. II. A single peptide induces either humoral or cell-mediated responses in mice of distinct MHC genotype. Eur J Immunol. 1992; 22:559-565.

45. Rhen T, Cidlowski J. Antiinflammatory action of glucocorticoids – new mechanisms for old drugs. N Engl J Med. 2005; 353:1711-1723.

Sargassum serratifolium attenuates RANKL-induced osteoclast differentiation and oxidative stress through inhibition of NF-κB and activation of the Nrf2/HO-1 signaling pathway

Hong Jae Kim[1,§], Cheol Park[2,§], Gi-Young Kim[3], Eui Kyun Park[4], You-Jin Jeon[3], Suhkmann Kim[5], Hye Jin Hwang[6], Yung Hyun Choi[1,7,*]

[1] Anti-Aging Research Center, Dongeui University, Busan, Korea;
[2] Department of Molecular Biology, College of Natural Sciences, Dongeui University, Busan, Korea;
[3] Department of Marine Life Sciences, Jeju National University, Jeju, Korea;
[4] Department of Oral Pathology and Regenerative Medicine, School of Dentistry, Institute for Hard Tissue and Biotooth Regeneration, Kyungpook National University, Daegu, Korea;
[5] Department of Chemistry, College of Natural Sciences, Center for Proteome Biophysics and Chemistry Institute for Functional Materials, Pusan National University, Busan, Korea;
[6] Department of Food and Nutrition, College of Natural Sciences and Human Ecology, Dongeui University, Busan, Korea;
[7] Department of Biochemistry, Dongeui University College of Korean Medicine, Busan, Korea.

Summary *Sargassum serratifolium* C. Agardh is a marine brown alga that has long been used as an ingredient for food and medicine by many people living along Asian coastlines. Recently, various beneficial effects of extracts or compounds isolated from *S. serratifolium* have been reported, but their efficacies against bone destruction are unclear. Therefore, in this study, we investigated the inhibitory property of an ethanol extract of *S. serratifolium* (EESS) on osteoclast differentiation by focusing on the receptor activator of nuclear factor-κB ligand (RANKL)-stimulated osteoclastogenesis model using RAW 264.7 macrophages. Our results demonstrated that EESS reduced RANKL-induced osteoclast differentiation in RAW 264.7 cells, by inhibiting tartrate-resistant acid phosphatase (TRAP) activity and destroying the F-actin ring formation. EESS also attenuated RANKL-induced expressions of key osteoclast-specific genes, such as nuclear factor of activated T cells cytoplasmic 1 (NFATC1), TRAP, cathepsin K and matrix metalloproteinase-9. These effects were mediated by impaired nuclear translocation of nuclear factor (NF)-κB and suppression of IκB-α degradation. In addition, EESS effectively inhibited the production of reactive oxygen species (ROS) by RANKL, which was associated with enhanced expression of nuclear translocation of nuclear factor-erythroid 2-related factor 2 (Nrf2) and heme oxygenase-1 (HO-1). Overall, our findings provide evidence that EESS suppresses RANKL-induced osteoclastogenesis and oxidative stress through suppression of NF-κB and activation of Nrf2/HO-1 signaling pathway, indicating that *S. serratifolium* has a potential application the prevention and treatment of osteoclastogenic bone disease.

Keywords: Sargassum serratifolium, osteoclasts, RANKL, NF-κB, Nrf2/HO-1

1. Introduction

Bone remodeling or bone metabolism is a physiological process involving bone resorption and synthesis by osteoclasts and osteoblasts, respectively. Osteoclasts are specialized multinucleated cells that differentiate from hematopoietic stem cells to induce bone resorption (*1,2*). Under normal physiological conditions, they play an important role in the maintenance of calcium homeostasis and normal bone remodelling (*3,4*). However, excessive bone resorption compared to bone formation causes an imbalance in

§These authors contributed equally to this work.
Address correspondence to:
Dr Yung-Hyun Choi, Department of Biochemistry, College of Korean Medicine, Dongeui University, Busan 47227, Republic of Korea.
E-mail: choiyh@deu.ac.kr

bone remodeling. This may occur due to menopause, aging, oxidative and inflammatory stress. The net result may be a progression to a variety of metabolic bone diseases, such as osteoporosis, autoimmune arthritis, hypercalcemia, and Paget's disease (*5-7*). Currently, hormones and anti-resorptive therapies are commonly used to treat them. However, long-term use of estrogen after menopause may increase the risk of various types of cancer in addition to blood clotting (*8-10*). In addition, specific inhibitors of osteoclastic activity such as bisphosphonates, which are widely used as reabsorption therapies, can cause serious side effects including hypocalcemia and osteonecrosis (*9-11*). Therefore, the discovery of substances capable of inhibiting osteoclast differentiation is a useful strategy for developing therapeutic agents for bone resorption-related diseases.

Receptor activator of nuclear factor-κB (NF-κB) ligand (RANKL) and macrophage colony-stimulating factor (M-CSF) are known to be essential cytokines that play key roles in osteoclast differentiation and maturation (*12,13*). RANKL, a member of the tumor necrosis factor (TNF) superfamily, is a critical regulator for signaling to induce osteoclast differentiation and to facilitate the activation of precursor cells through interaction with its receptor RANK (*13,14*). On the other hand, M-CSF secreted from osteoclasts is involved in the survival and proliferation of osteoclast precursors and induction of RANK expression (*12,15*). Activation of RANK by RANKL stimulates transcriptional activation of osteoclast-specific factors, which are involved in osteoclast differentiation and osteoclastic activity through activation of various intracellular signal transduction pathways, thereby increasing bone resorption (*16-18*).

Oxidative stress caused by excessive production of reactive oxygen species (ROS) has been reported to inhibit osteoblast survival and function, thereby inhibiting bone formation (*19,20*). Excessive ROS can also cause bone destruction by exerting oxidative damage to all cellular biomolecules such as proteins, lipids and nucleic acids (*21,22*). In addition, the overproduction of ROS has been demonstrated to increase the expression of RANKL by osteoclasts, thereby activating osteoclasts and enhancing bone resorption capacity, indicating that ROS play an important role in osteoclastogenesis (*19,23,24*). Most cells have endogenous defense strategies to eliminate damage caused by excessive ROS production. Among them, the nuclear transcription factor erythroid-2-like factor 2 (Nrf2) is one of the critical antioxidant systems involved in the maintenance of the redox state (*25,26*). More importantly, many studies have shown that Nrf2 is a key regulator of bone homeostasis, because activation of Nrf2 signaling can promote the endogenous antioxidant response to ROS (*26-28*).

Recently, there has been a growing interest in marine resources for prevention and treatment of various diseases. Among them, seaweeds are abundant as active substances with various pharmacological actions, which may have the potential to prevent bone loss through inhibition of osteoclastogenesis (*29-34*). Sargassum is a genus of marine brown algae (Phaeophyceae) that is found in most seas around the world, and many coastal people, especially in Korea, Japan, and China, use it as a source for food and medicine (*35*). Recently, extracts or compounds isolated from *Sargassum siliquastrum*, *S. fusiforme* and *S. micracanthum* belonging to *Sargassum* spp. have been demonstrated to have potent inhibitory activities against osteoclast differentiation (*33,36-38*). For example, Komai *et al*. (*38*) reported that plastoquinones and chromene derivatives isolated from *S. micracanthum* contribute to inhibition of bone resorption by inhibiting the differentiation of osteoclast progenitors into osteoclast-like cells. In addition, sargachromanol G, a plastoquinone isolated from *S. siliquastrum*, was reported to have anti-osteoclastogenic effects while inhibiting the activity of NF-κB and mitogen-activated protein kinases by RANKL and interleukin-1β (*36,37*). However, up to now, the effectiveness of *S. serratifolium* in osteoclast formation has not been investigated. Therefore, this study was designed to examine the effects of an ethanol extract of *S. serratifolium* (EESS) on RANKL-induced osteoclast differentiation and oxidative responses, using RAW 264.7 cells as osteoclast precursor cells.

2. Materials and Methods

2.1. *Preparation of EESS*

The EESS used in this study was provided by the National Marine Biodiversity Institute of Korea (Seocheon, Republic of Korea). For the preparation of EESS, *S. serratifolium* was collected from offshore Jeju island, Republic of Korea in March 2016. Authentication of the brown algae was established by Dr. Dae-Sung Lee, National Marine Biodiversity Institute of Korea. Collected *S. serratifolium* was washed with tap water to remove slats, epiphytes, and sand attached to the surface of the samples, and then lyophilized. The dried sample of *S. serratifolium* (170 g) was pulverized, and extracted with 70% EtOH (1 : 10 w/v) for 1 h (five times) by sonication. The *S. serratifolium* extract (EESS) was obtained by evaporation under vacuum. Voucher specimen (AARC-2016-18) is deposited at the Anti-Aging Research Center, Dongeui University (Busan, Republic of Korea). The extract was dissolved in dimethylsulfoxide (DMSO, Sigma-Aldrich Chemical Co., St. Louis, MO, USA), before use in the experiment.

2.2. *Cell culture*

The murine macrophage RAW 264.7 cell line was

obtained from the American Type Culture Collection (Manassas, VA, USA). The cells were cultured in Dulbecco's modified Eagle's medium (WelGENE Inc., Daegu, Republic of Korea), containing 10% fetal bovine serum (WelGENE Inc.) and 100 U/mL penicillin and streptomycin (WelGENE Inc.) at 37℃ in humidified air with 5% CO_2, and were subcultured every three days.

2.3. *Cell viability assay*

For the cell viability study, RAW 264.7 cells were cultured in 96-well plates at a density of 5×10^4 cells per well. After a 24-h-incubation, the cells were treated with various concentrations of EESS for 48 h. Afterward, the medium was removed, 0.5 mg/mL of 3-(4,5-dimethylthiazol-2-yl)-2,5-diphenyltetrazolium bromide (MTT, Sigma-Aldrich Chemical Co.) was added to each well and incubated at 37℃ for 3 h. The supernatant was then replaced with dimethyl sulfoxide (DMSO) to dissolve the blue formazan crystals. After 10 min, the optical density was measured at a wavelength of 540 nm, with an enzyme-linked immunosorbent assay (ELISA) microplate reader (Dynatech Laboratories, Chantilly, VA, USA).

2.4. *Flow cytometry assay*

For flow cytometry analysis, cells cultured under the same conditions as in the MTT assay were resuspended in phosphate-buffered saline (PBS) and fixed in 75% (v/v) ethanol at 4℃ for 1 h. After washing with PBS, the cells were incubated in cold propidium iodide solution (50 μg/mL, Sigma-Aldrich Chemical Co.) containing RNase A (0.1 mg/mL) in PBS (pH 7.4) in the dark for 30 min. The relative DNA contents of stained cells were analyzed by fluorescence intensities using a flow cytometer (BD Biosciences, San Jose, CA, USA), and cells belonging to the sub-G1 phase were calculated as apoptotic cells.

2.5. *Tartrate-resistant acid phosphatase (TRAP) staining and activity assay*

RAW 264.7 cells were seeded in 48-well plates at a density of 1×10^5 cells per well, to investigate the effect of EESS on osteoclast differentiation. After 24-h-culture, 100 ng/mL RANKL (Abcam, Cambridge, MA, USA) with or without EESS (25 and 50 μg/mL) was added and further cultured for 5 days. The medium containing the relevant reagents was changed every three days within this period. After completion of the experiment, the cells were fixed with 4% paraformaldehyde (Sigma-Aldrich Chemical Co.) for 10 min and washed twice with PBS. The fixed cells were then permeabilized with 0.1% Triton X-100 for 1 min and stained for TRAP activity using a commercial kit (Sigma-Aldrich Chemical Co.), according to the manufacturer's instructions. TRAP-positive multinucleated cells containing three or more nuclei were classified as osteoclasts, counted and captured by a light microscope (Carl Zeiss, Oberkochen, Germany). At the same time, the culture medium was collected, and the activity of TRAP was measured using a TRAP assay kit (Sigma-Aldrich Chemical Co.) at 450 nm with an ELISA microplate reader. TRAP activity was calculated as a percentage of the untreated control, as previously described (*39*).

2.6. *F-actin ring formation assay*

The effect of EESS on the formation of F-actin rings was investigated in accordance with the methods of a previous study (*40*). Briefly, after treatment, the culture medium was replaced with a solution of 4% paraformaldehyde to fix the cells for 20 min at room temperature. The cells were then stained with fluorescein isothiocyanate (FITC)-phalloidin solution (Thermo Scientific, Waltham, MA, USA) for 45 min after 5 min treatment with a 0.1% Triton X-100 solution to permeabilize the cells. Nuclei were sequentially stained with 2.5 μg/mL 4′,6-diamidino-2-phenylindole (DAPI, Sigma-Aldrich Chemical Co.) solution for 15 min and images were captured using a fluorescence microscope (Carl Zeiss).

2.7. *Protein isolation and Western blot analysis*

To extract whole-cell proteins, the cells were collected, washed twice with ice-cold PBS, and then lysed using the cell lysis buffer [25 mM Tris-Cl (pH 7.5), 250 mM NaCl, 5 mM ethylenediaminetetraacetic acid, 1% Nonidet-P40, 1 mM phenylmethylsulphonyl fluoride, and 5 mM dithiothreitol] for 1 h before cell debris was removed by centrifugation. The cytosolic and nuclear extracts were prepared using an NE-PER Nuclear and Cytoplasmic Extraction Reagents kit (Pierce Biotechnology, Rockford, IL, USA) in accordance with the instructions of the manufacturer. The same amounts of protein (30-50 μg) were separated by electrophoresis on sodium dodecyl sulfate (SDS)-polyacrylamide gels and transferred to polyvinylidene difluoride membranes (Schleicher and Schuell, Keene, NH, USA). The membranes were blocked with 5% non-fat dry milk for 1 h at room temperature and subsequently probed with primary antibodies overnight with gentle agitation at 4℃. After washing three times with Tris-buffered saline containing 0.1% Tween-20 for 5 min, the membranes were incubated with the corresponding horseradish-peroxidase-linked secondary antibodies (Amersham Biosciences, Westborough, MA, USA) for 2 h at room temperature. The membranes were visualized by enhanced chemiluminescence (ECL) solution (Amersham Biosciences) and exposed to X-ray films.

2.8. *Detection of the intracellular ROS levels*

The production of intracellular ROS was monitored using a cell-permeable fluorogenic probe, 5,6-carboxy-2',7'-dichlorofluorescein diacetate (DCF-DA). Briefly, the collected cells were stained with 10 μM DCF-DA (Sigma-Aldrich Chemical Co.) in the dark at 37°C for 15 min. The cells were then rinsed twice with PBS, and 10,000 events were immediately analyzed using a flow cytometer (BD Biosciences, San Jose, CA, USA), with an excitation wavelength of 480 nm and an emission wavelength of 525 nm (*41*). To observe the degree of ROS production by fluorescence microscopy, the cells attached to the glass coverslips were stimulated with RANKL in the presence or absence of EESS. The cells were stained with 10 μM DCF-DA at 37°C for 15 min, washed twice with PBS, and then fixed with 4% paraformaldehyde (pH 7.4) for 20 min. The fixed cells were washed twice with PBS and analyzed using a fluorescence microscope (Carl Zeiss).

2.9. *Statistical analysis*

All the experiments reported in this study were replicated in three independent experiments. The results are presented as the mean ± SD. Statistical significance was assessed by one-way analysis of variance. A *p* value of < 0.05 was considered statistically significant.
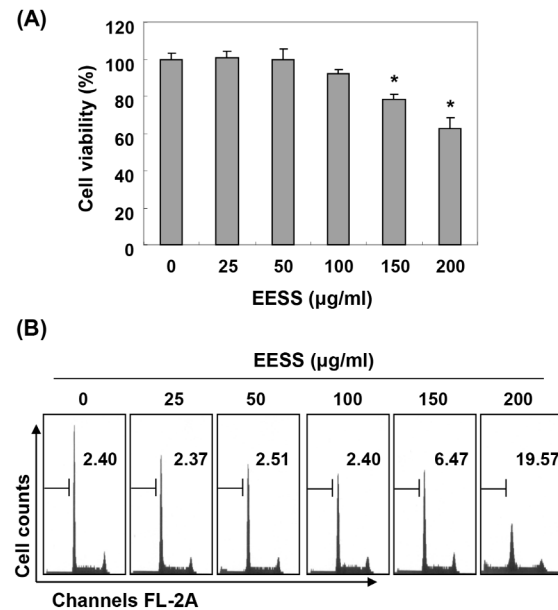
3. Results

3.1. *Effects of EESS on RAW 264.7 cell viability*

RAW 264.7 cell viabilities were measured following treatment with various concentrations of ESS for 48 h, to assess the results under current experimental conditions. The cytotoxic effect of EESS, as shown in Figure 1A, was not induced at concentrations up to 100 μg/mL of the agent, but the cell viabilities were gradually reduced in the treatment groups with larger concentrations (≥150 μg/mL) of EESS compared to the control cells. Flow cytometry analysis showed no significant difference in the frequencies of cells of the sub-G1 phase, which means the presence of apoptosis in the groups treated with ≤100 μg/mL of EESS compared to the control group (Figure 1B). Therefore, the highest concentration of EESS was chosen as 50 μg/mL for subsequent studies.

3.2. *EESS inhibits osteoclast differentiation in RANKL-stimulated RAW 264.7 cells*

RAW 264.7 cells were treated with 25 and 50 μg/mL EESS, respectively, in the presence of RANKL and stained with TRAP, to determine the inhibitory effect of EESS on osteoclast differentiation. In the RANKL-alone treatment group, typical osteoclast

Figure 1. Effect of EESS on the cell viability in RAW 264.7 cells. Cells were treated with various concentrations of EESS for 48 h. **(A)** Cell viability was assessed by the MTT assay. The results are the means ± SD obtained from three independent experiments (*$p < 0.05$ compared with the control group). **(B)** To quantify the degree of apoptosis induced by EESS, the cells were evaluated by a flow cytometer to determine sub-G1 DNA content, which represents the cells undergoing apoptotic DNA degradation. The results are expressed as the mean of two different experiments.

morphological changes, in which many cells were aggregated and bundled, and an increased activation of TRAP were observed, suggesting that RAW 264.7 cells differentiated completely into osteoclasts (Figure 2A). However, EESS significantly reduced multinucleated osteoclast-like cell formation and TRAP activity in RANKL-stimulated RAW 264.7 cells in a concentration-dependent manner. In addition, RANKL-induced osteoclast differentiation was completely suppressed in the osteoprotegerin (OPG)-treated cells, as a positive control (Figure 2).

3.3. *EESS disrupts the formation of F-actin ring structure in RANKL-stimulated RAW 264.7 cells*

To confirm the inhibitory effect of EESS on RANKL-induced osteoclastogenesis, the influence of EESS on formation of F-actin ring structures, known to beessential for bone resorption to occur (*42,43*), was investigated in this study. As shown in Figure 3, RANKL-treated RAW 264.7 cells showed the actin ring cytoskeletal structure; however, the size of the ring structure was markedly reduced in cells exposed to EESS compared with cells treated with RANKL alone, suggesting that EESS effectively inhibited osteoclast differentiation.

3.4. *EESS alleviates RANKL-induced NF-κB nuclear translocation and IκBα degradation in RAW 264.7 cells*
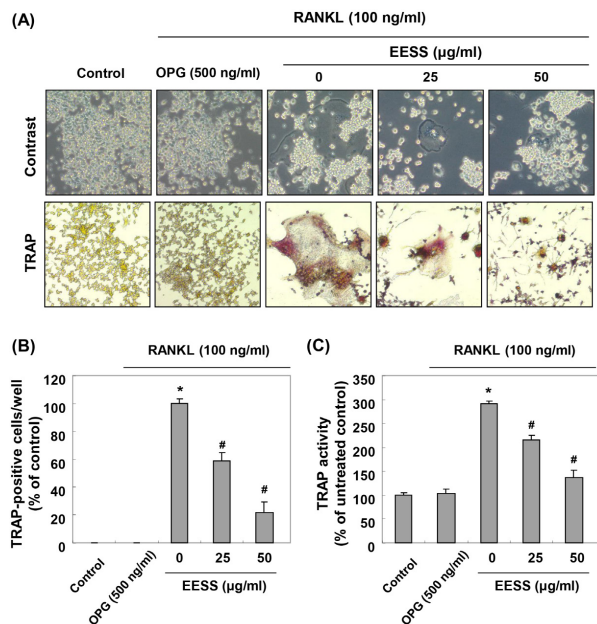
**Figure 2. Inhibition of RANKL-induced osteoclast differentiation by EESS in RAW 264.7 cells.** Cells were stimulated with 100 ng/mL RANKL in the presence or absence of EESS (25 and 50 µg/mL) for 5 days. Osteoprotegerin (OPG) was used as a positive control. **(A)** The fixed cells were stained for TRAP and identified using a microscope. **(B)** TRAP-positive multinucleated cells were counted to determine osteoclast numbers. **(C)** Supernatants were collected, and the TRAP activity was measured by an ELISA reader. **(B** and **C)** Each point represents the mean ± SD of three independent experiments (*$p < 0.05$ *vs.* the untreated control; #$p < 0.05$ *vs.* the RANKL-treated cells).
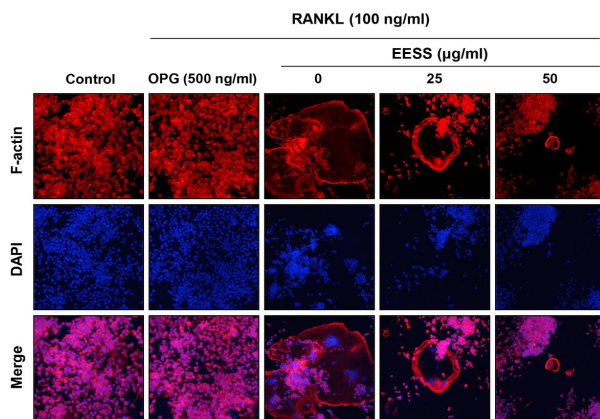
Figure 3. Suppression of F-actin ring formation by EESS in RANKL-stimulated RAW 264.7 cells. The cells were incubated with 100 ng/mL RANKL in the presence or absence of the indicated concentrations of EESS for 5 days. The cells were fixed and stained for F-actin ring with a FITC-phalloidin solution. Subsequently, the cells stained with DAPI solution and then imaged with a fluorescence microscope. OPG was used cells as a positive control.

We next determined whether EESS could attenuate RANKL-induced activation of NF-κB, which is critical for RANKL-mediated osteoclastogenesis (*13,14*). Immunoblotting data, using cytoplasmic and nuclear extracts, showed that the expression of the NF-κB p65 subunit in the nucleus was greatly increased after a
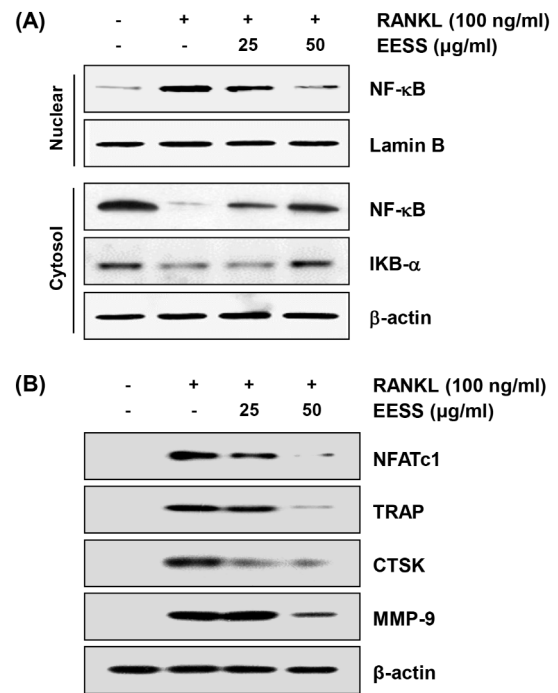
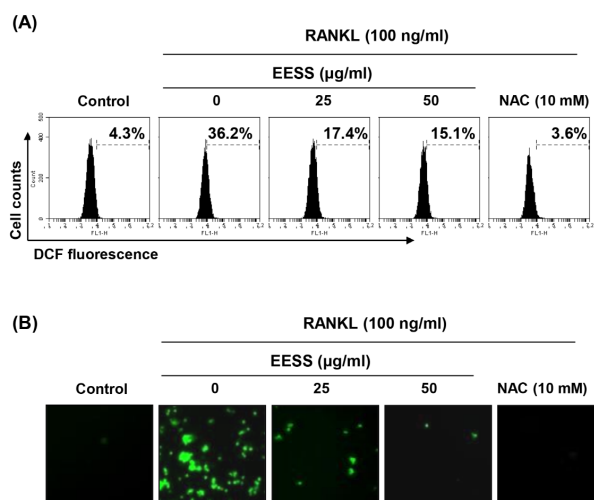**Figure 4. Effects of EESS on RANKL-induced activation of NF-κB and expression of osteoclast-specific genes in RAW 264.7 cells. (A)** After 100 ng/mL RANKL treatment with or without EESS for 5 days, the nuclear and cytosolic proteins were isolated, and the expression of NF-κB and IκB-α was determined by Western blot analysis using an ECL detection system. Lamin B and β-actin were used as internal controls for the nuclear and cytosolic fractions, respectively. **(B)** The cellular proteins were isolated from cells cultured under the same conditions, and the expression of osteoclast-specific proteins was assessed by Western blot analysis. β-actin was used as an internal control. The results shown are representative of three independent experiments.

RANKL challenge, whereas there was a reduction in its expression in the cytoplasm. In addition, the expression of IκBα was reduced in the cytoplasm, indicating that NF-κB was activated by RANKL treatment (Figure 4A). However, the shift of NF-κB p65 to the nucleus induced by RANKL and the degradation of IκBα were abolished in a concentration-dependent manner in the presence of EESS, suggesting that EESS could inhibit the activation of NF-κB by RANKL.

3.5. *EESS suppresses the RANKL-induced expression of osteoclastogenesis-associated genes in RAW 264.7 cells*

We further investigated the effect of EESS on the expression of osteoclastic markers for the study of mechanisms involved in the inhibition of osteoclastogenesis by EESS. When RAW 264.7 cells were treated with RANKL, immunoblotting revealed that the major osteoclastogenesis factors, including nuclear factor of activated T cells cytoplasmic 1 (NFATC1), TRAP, cathepsin K (CTSK) and matrix metalloproteinase-9 (MMP-9), were dramatically upregulated in the cells (Figure 4B). However, the increased levels of these genes by RANKL were

Figure 5. Effects of EECC on the RANKL-induced ROS generation in RAW 264.7 cells. The cells were treated with 100 ng/mL RANKL in the presence or absence of EESS (25 and 50 μg/mL). **(A)** The cells were incubated with DCF-DA, and DCF fluorescence was measured by flow cytometry. The values represent the means of two independent experiments. **(B)** After staining with DCF-DA, images were obtained using a fluorescence microscope. These images are representative of at least three independent experiments.

reduced by addition of EESS in a concentration-dependent manner.

3.6. EESS attenuates RANKL-induced ROS production in RAW 264.7 cells

As oxidative stress also plays a critical role in the osteoclast differentiation and bone resorption (*19,20*), we then investigated whether EESS could suppress RANKL-induced generation of ROS. Our flow cytometry results indicated that the level of ROS markedly increased in RANKL-stimulated cells; however, the increase in ROS content was reduced in a concentration-dependent manner by addition of EESS. Moreover, as expected, the co-treatment of N-acetyl cysteine (NAC), a ROS scavenger, completely blocked ROS production by RANKL (Figure 5A). The effect of preventing ROS formation was confirmed in our studies using a fluorescence microscope. Consistent with the results from flow cytometry, the increase in DCF-DA fluorescence intensity observed in the cells treated with RANKL was greatly weakened by pretreatment of EESS, as shown in Figure 5B.

3.7. EESS enhances the expression of Nrf2 and HO-1 in RAW 264.7 cells

Furthermore, the effect of EESS on the expression of Nrf2 and its regulatory gene heme oxygenase-1 (HO-1) was investigated because it is well known that activation of the Nrf2/HO-1 signaling pathway plays an important role in antioxidant activity for bone homeostasis (*26,44*). The immunoblotting results
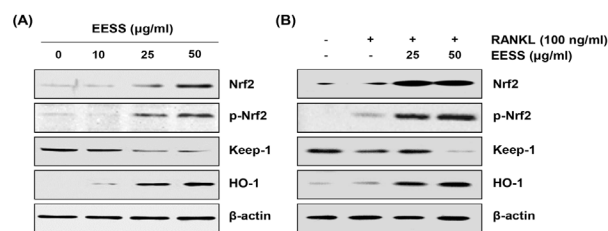
Figure 6. Effects of EECC on the expression on Nrf2 and its regulatory proteins in RAW 264.7 cells. The cells were treated with the indicated concentrations of EESS for 5 days **(A)** or treated with 100 ng/mL RANKL in the presence or absence of EESS (25 and 50 μg/mL) for 5 days **(B)**. The cellular proteins were probed with the indicated antibodies and were visualized using an ECL detection system. Equal protein loading was confirmed by analysis of β-actin. The results shown are representative of three independent experiments.

showed that the expression of Nrf2 and HO-1 protein gradually increased in a concentration-dependent manner on EESS treatment, but conversely, Kelch-like epichlorohydrin-associated protein 1 (Keap1) expression decreased with EESS treatment (Figure 6A). Phosphorylation at serine 40, in particular, is important for activation and stabilization of Nrf2, also increased with EESS treatment, demonstrating that EESS activated Nrf2/HO-1 signaling in RAW 264.7 cells. In addition, the expression and phosphorylation of Nrf2 in RANKL-treated cells were not increased or induced to a lower level than untreated control cells, its phosphorylation, as well as expression, were markedly elevated in cells co-treated with EESS and RANKL (Figure 6B). Furthermore, HO-1 expression was also much increased in treated cells compared to cells treated with EESS, and expression of Keap1 was further reduced, suggesting that the antioxidant effect of EESS may be related to Nrf2/HO-1 axis activation.

4. Discussion

In the current study, murine macrophage RAW 264.7 cell line was used to evaluate the effect of ethanol extract of *S. serratifolium* (EESS) on RANKL-induced osteoclast differentiation. We demonstrated that EESS could effectively attenuate RANKL-induced osteoclast differentiation by inhibiting TARP activity and F-actin ring formation accompanied by suppression of RANKL-induced expression of osteoclast-associated marker genes through inhibition of nuclear translocation of NF-κB. In addition, EESS abolished RANKL-induced oxidative stress by inhibiting ROS production related to the activation of Nrf2/HO-1 signaling pathway.

The destruction of metabolic balance of the bone is due to increase of bone resorption by osteoclasts rather than new bone formation by osteoblasts. RANKL is a key pro-osteoclastogenic cytokine that plays an essential role in the induction of osteoclast differentiation from hematopoietic cells of monocyte-macrophage lineage (*12,13*). Terminal differentiation into osteoclasts by

RANKL involves the following steps: 1) activation of TRAP, a representative osteoclast marker involved in bone resorption, and 2) formation of multinuclear osteoclasts by combining TRAP-positive cells with actin ring formation. To perform bone resorption by activated TRAP of mature osteoclasts, formation and maintenance of actin rings on the bone surface must be continued (*45,46*). Results of this study revealed that EESS could inhibit TRAP activation and F-actin ring formation by RANKL, suggesting that EESS might be able to inhibit bone resorption through blocking early stages of differentiation from precursor cells to osteoclasts.

As noted in many studies, NF-κB is a key transcription factor that plays a role in RANKL-induced osteoclast differentiation (*12,14*). Normally, NF-κB is retained in the cytoplasm in an inactive form coupled with IκB-α, an inhibitory subunit. When IκB-α is phosphorylated and degraded by a ubiquitin-dependent pathway upon binding of RANKL and RANK, NF-κB translocates from the cytosol into the nucleus and triggers transcriptional activation of several osteoclastogenesis-related genes (*13,14*). Results of the current study indicated that NF-κB translocation to the nucleus and cytoplasmic degradation of IκB-α were increased by RANKL stimulation. However, EESS reduced these changes. Therefore, blockade of nuclear translocation of NF-κB, an essential step in NF-κB activation, can be proposed as one of the mechanisms involved in EESS-mediated anti-osteoclastogenic effect.

Transcription factor NFATc1 as a master regulator in osteoclastogenesis. It also plays an important role in regulating the expression of osteoclast-specific genes upon RANKL signaling. Its expression is enhanced by binding to transcription factors including NF-κB on the promoter at early stage of osteoclast differentiation (*16,17*). Thus, genes regulated by NFATc1 including TRAP, CTSK, and MMP-9 are highly expressed at RANKL-induced terminal differentiation stage, thereby promoting bone resorption (*25,47*). Our results showed that RANKL-induced expression of NFATc1 was significantly suppressed by EESS in a concentration-dependent manner. Expression levels of most osteoclast-related marker genes were also reduced by EESS. Although further studies should be conducted to determine whether NF-κB plays a direct role in the regulation of NFATc1 expression, these results suggest that EESS-mediated blockade of NFATc1 expression associated with inhibition of NF-κB activation might play a central role in inhibiting osteoclast differentiation and bone resorption activity.

Up to date, targets of ROS that arise during osteoclast differentiation by RANKL signaling remain unclear. However, they certainly play important signaling roles in the process of osteoclastogenesis (*21,22*). Many previous studies have shown that ROS accumulation can increase the expression of RANKL in osteoclasts and enhance their survival and proliferation (*19,23,24*). In addition,

ROS can act as upstream molecules for activation of NF-κB and NFATc1 to promote transcription of osteoclast-specific genes at the onset of osteoclastogenesis. On the other hand, excessive production of ROS will inhibit the differentiation of osteoblasts and induce death of osteocytes as well as osteocytes, leading to bone formation imbalance (*19,20*). Therefore, inhibiting or eliminating ROS production can prevent pathological causes of various diseases associated with functional activation of osteoclasts by oxidative stress. As can be seen from results of the present study, EESS could significantly weaken RANKL-induced accumulation of ROS. The strong ROS scavenging ability of EESS might be another mechanism involved in its inhibitory effect on osteoclast differentiation.

Accumulated evidence suggests that Nrf2 signaling pathway plays a critical role in protecting cells from oxidative damage by promoting the expression of antioxidant enzymes in most cells. It is also an attractive target in bone metabolism homeostasis (*26,44*). Under physiological conditions, Nrf2 binds to Keap1 and becomes sequestered in the cytoplasm. However, under a situation in response to oxidative stress, Nrf2 is disassociated from Keap1 and then translocates to the nucleus. In this process, phosphorylation of Nrf2 is accompanied. It is an essential step for transcriptional activation of its target genes. HO-1 is one of cytoprotective enzymes that act as a rate-limiting enzyme. It is regulated by Nrf2 and catalyzes the degradation of heme to biliverdin, carbon oxide, and iron (*44,48*). Previous studies have shown that increased expression of HO-1 by transcriptional activation of Nrf2 plays a central role in the removal of ROS generation by RANKL (*26,44*). In the present study, expression and phosphorylation of Nrf2 were significantly increased in cultured cells co-treated with RANKL and EESS compared to those in cells treated with EESS alone while the expression of Keap1 was reversely decreased. Moreover, the expression of HO-1 was significantly upregulated in RANKL and EESS co-treatment cells, indicating that EESS could activate the Nrf2/HO-1 antioxidant pathway. Although further experiments are needed to determine the inhibition of ROS production and activation of Nrf2/HO-1 axis, results of this study show that the Nrf2/HO-1 signaling pathway might contribute to the protective ability of EESS against RANKL-mediated oxidative stress.

In summary, our data demonstrate that EESS can suppress RANKL-induced osteoclast differentiation through inactivation of NF-κB and inhibition of NFATC-1 expression. EESS also attenuated RANKL-induced oxidative stress associated with activation of Nrf2/HO-1 signaling pathway. Results of the current study suggest that EESS might have therapeutic potential for treating bone loss-related disorders. However, additional experiments such as reassessment of the anti-osteoclastogenic potential of EEES using

animal models and validation of major bioactive components of EESS are required.

References

1. Kikuta J, Ishii M. Osteoclast migration, differentiation and function: Novel therapeutic targets for rheumatic diseases. Rheumatology (Oxford). 2013; 52:226-234.
2. Teitelbaum SL, Ross FP. Genetic regulation of osteoclast development and function. Nat Rev Genet. 2003; 4:638-649.
3. Ralston SH, Layfield R. Pathogenesis of Paget disease of bone. Calcif Tissue Int. 2012; 91:97-113.
4. Kagiya T, Nakamura S. Expression profiling of microRNAs in RAW264.7 cells treated with a combination of tumor necrosis factor alpha and RANKL during osteoclast differentiation. J Periodontal Res. 2013; 48:373-385.
5. Lu B, Jiao Y, Wang Y, Dong J, Wei M, Cui B, Sun Y, Wang L, Zhang B, Chen Z, Zhao Y. A FKBP5 mutation is associated with Paget's disease of bone and enhances osteoclastogenesis. Exp Mol Med. 2017; 49:e336.
6. Galson DL, Roodman GD. Pathobiology of Paget's disease of bone. J Bone Metab. 2014; 21:85-98.
7. Mundy GR. Osteoporosis and inflammation. Nutr Rev. 2007; 65:S147-151.
8. Weitzmann MN, Pacifici R. Estrogen deficiency and bone loss: An inflammatory tale. J Clin Invest. 2006; 116:1186-1194.
9. El Osta L, El Osta N, El Osta H. Benefits and potential risks of bisphosphonate therapy A narrative review. J Med Liban. 2016; 64:228-237.
10. Rodan GA, Martin TJ. Therapeutic approaches to bone diseases. Science. 2000; 289:1508-1514.
11. Reid IR. Pharmacotherapy of osteoporosis in postmenopausal women: Focus on safety. Expert Opin Drug Saf. 2002; 1:93-107.
12. Ono T, Nakashima T. Recent advances in osteoclast biology. Histochem Cell Biol. 2018; 149:325-341.
13. Park JH, Lee NK, Lee SY. Current understanding of RANK signaling in osteoclast differentiation and maturation. Mol Cells. 2017; 40:706-713.
14. Honma M, Ikebuchi Y, Kariya Y, Suzuki H. Regulatory mechanisms of RANKL presentation to osteoclast precursors. Curr Osteoporos Rep. 2014; 12:115-120.
15. Asagiri M, Takayanagi H. The molecular understanding of osteoclast differentiation. Bone. 2007; 40:251-264.
16. Bi H, Chen X, Gao S, Yu X, Xiao J, Zhang B, Liu X, Dai M. Key Triggers of osteoclast-related diseases and available strategies for targeted therapies: A review. Front Med (Lausanne). 2017; 4:234.
17. Kuroda Y, Matsuo K. Molecular mechanisms of triggering, amplifying and targeting RANK signaling in osteoclasts. World J Orthop. 2012; 3:167-174.
18. Sundaram K, Nishimura R, Senn J, Youssef RF, London SD, Reddy SV. RANK ligand signaling modulates the matrix metalloproteinase-9 gene expression during osteoclast differentiation. Exp Cell Res. 2007; 313:168-178.
19. Domazetovic V, Marcucci G, Iantomasi T, Brandi ML, Vincenzini MT. Oxidative stress in bone remodeling: Role of antioxidants. Clin Cases Miner Bone Metab. 2017; 14:209-216.
20. Almeida M, O'Brien CA. Basic biology of skeletal aging: Role of stress response pathways. J Gerontol A Biol Sci Med Sci. 2013; 68:1197-1208.
21. Banfi G, Iorio EL, Corsi MM. Oxidative stress, free radicals and bone remodeling. Clin Chem Lab Med. 2008; 46:1550-1555.
22. Ziskoven C, Jäger M, Zilkens C, Bloch W, Brixius K, Krauspe R. Oxidative stress in secondary osteoarthritis: From cartilage destruction to clinical presentation? Orthop Rev (Pavia). 2010; 2:e23.
23. Lee NK, Choi YG, Baik JY, Han SY, Jeong DW, Bae YS, Kim N, Lee SY. A crucial role for reactive oxygen species in RANKL-induced osteoclast differentiation. Blood. 2005; 106:852-859.
24. Srinivasan S, Koenigstein A, Joseph J, Sun L, Kalyanaraman B, Zaidi M, Avadhani NG. Role of mitochondrial reactive oxygen species in osteoclast differentiation. Ann N Y Acad Sci. 2010; 1192:245-252.
25. Collins JA, Diekman BO, Loeser RF. Targeting aging for disease modification in osteoarthritis. Curr Opin Rheumatol. 2018; 30:101-107.
26. Marchev AS, Dimitrova PA, Burns AJ, Kostov RV, Dinkova-Kostova AT, Georgiev MI. Oxidative stress and chronic inflammation in osteoarthritis: An NRF2 counteract these partners in crime? Ann N Y Acad Sci. 2017; 140:114-135.
27. Bak SU, Kim S, Hwang HJ, Yun JA, Kim WS, Won MH, Kim JY, Ha KS, Kwon YG, Kim YM. Heme oxygenase-1 (HO-1)/carbon monoxide (CO) axis suppresses RANKL-induced osteoclastic differentiation by inhibiting redox-sensitive NF-κB activation. BMB Rep. 2017; 50:103-108.
28. Sun YX, Xu AH, Yang Y, Li J. Role of Nrf2 in bone metabolism. J Biomed Sci. 2015; 22:101.
29. Ueno M, Cho K, Isaka S, Nishiguchi T, Yamaguchi K, Kim D, Oda T. Inhibitory effect of sulphated polysaccharide porphyran (isolated from *Porphyra yezoensis*) on RANKL-induced differentiation of RAW264.7 cells into osteoclasts. Phytother Res. 2018; 32:452-458.
30. Ihn HJ, Kim JA, Cho HS, Shin HI, Kim GY, Choi YH, Jeon YJ, Park EK. Diphlorethohydroxycarmalol from *Ishige okamurae* suppresses osteoclast differentiation by downregulating the NF-κB signaling pathway. Int J Mol Sci. 2017; 18:E2635.
31. Kim KJ, Lee YJ, Hwang YH, Kang KY, Yee ST, Son YJ. *In vitro* and *in vivo* effects of *Gracilaria verrucosa* extracts on osteoclast differentiation. J Clin Med. 2017; 6:E32.
32. Kim YW, Baek SH, Lee SH, Kim TH, Kim SY. Fucoidan, a sulfated polysaccharide, inhibits osteoclast differentiation and function by modulating RANKL signaling. Int J Mol Sci. 2014; 15:18840-18855.
33. Koyama T. Extracts of marine algae show inhibitory activity against osteoclast differentiation. Adv Food Nutr Res. 2011; 64:443-454.

34. Das SK, Ren R, Hashimoto T, Kanazawa K. Fucoxanthin induces apoptosis in osteoclast-like cells differentiated from RAW264.7 cells. J Agric Food Chem 2010; 58:6090-6095.

35. Vadalà M, Palmieri B. From algae to "functional foods". Clin Ter. 2015; 166:e281-300.

36. Yoon WJ, Heo SJ, Han SC, Lee HJ, Kang GJ, Yang EJ, Park SS, Kang HK, Yoo ES. Sargachromanol G regulates the expression of osteoclastogenic factors in human osteoblast-like MG-63 cells. Food Chem Toxicol. 2012; 50:3273-3279.

37. Yoon WJ, Kim KN, Heo SJ, Han SC, Kim J, Ko YJ, Kang HK, Yoo ES. Sargachromanol G inhibits osteoclastogenesis by suppressing the activation NF-κB and MAPKs in RANKL-induced RAW 264.7 cells. Biochem Biophys Res Commun. 2013; 434:892-897.

38. Komai E, Miyahara T, Mori J, Obi N, Ochiai H, Saito H, Hayashi T. Inhibitory activities of plastoquinones and chromene derivative from a brown alga *Sagassum micracanthum* on bone resorption. Biol Pharm Bull. 2006; 29:1980-1982.

39. Yoo HS, Chung KH, Lee KJ, Kim DH, An JH. Melanin extract from *Gallus gallus domesticus* promotes proliferation and differentiation of osteoblastic MG-63 cells *via* bone morphogenetic protein-2 signaling. Nutr Res Pract. 2017; 11:190-197.

40. Yuan FL, Xu RS, Jiang DL, He XL, Su Q, Jin C, Li X. Leonurine hydrochloride inhibits osteoclastogenesis and prevents osteoporosis associated with estrogen deficiency by inhibiting the NF-κB and PI3K/Akt signaling pathways. Bone. 2015; 75:128-137.

41. Salimi A, Talatappe BS, Pourahmad J. Xylene induces oxidative stress and mitochondria damage in isolated human lymphocytes. Toxicol Res. 2017; 33:233-238.

42. Kong X, Yang Y, Wu W, Wan H, Li X, Zhong M, Su X, Jia S, Lin N. Triterpenoid saponin W3 from *Anemone flaccida* suppresses osteoclast differentiation through inhibiting activation of MAPKs and NF-κB pathways. Int J Biol Sci. 2015; 11:1204-1214.

43. Hong S, Huh JE, Lee SY, Shim JK, Rhee SG, Jeong W. TRP14 inhibits osteoclast differentiation *via* its catalytic activity. Mol Cell Biol. 2014; 34:3515-3524.

44. Loboda A, Damulewicz M, Pyza E, Jozkowicz A, Dulak J. Role of Nrf2/HO-1 system in development, oxidative stress response and diseases: An evolutionarily conserved mechanism. Cell Mol Life Sci. 2016; 73:3221-3247.

45. Soysa NS, Alles N. Osteoclast function and bone-resorbing activity: An overview. Biochem Biophys Res Commun. 2016; 476:115-120.

46. Hayman AR. Tartrate-resistant acid phosphatase (TRAP) and the osteoclast/immune cell dichotomy. Autoimmunity. 2008; 41:218-223.

47. Kim JH, Kim N. Regulation of NFATc1 in osteoclast differentiation. J Bone Metab. 2014; 21:233-241.

48. Kang KA, Hyun JW. Oxidative stress, Nrf2, and epigenetic modification contribute to anticancer drug resistance. Toxicol Res. 2017; 33:1-5.

Heterozygous deletion of *LRP5* gene in mice alters profile of immune cells and modulates differentiation of osteoblasts

Lisha Li[1,2,3], Yan Wang[1,2,3], Na Zhang[1,2,3], Yang Zhang[4], Jing Lin[1,2,3], Xuemin Qiu[1,2,3], Yuyan Gui[1], Feifei Wang[1,2,3], Dajin Li[1,2,3], Ling Wang[1,2,3,5,*]

[1] *Obstetrics and Gynecology Hospital of Fudan University, Shanghai, China;*
[2] *The Academy of Integrative Medicine of Fudan University, Shanghai, China;*
[3] *Shanghai Key Laboratory of Female Reproductive Endocrine-related Diseases, Shanghai, China;*
[4] *First Affiliated Hospital of Heilongjiang University of Chinese Medicine, Harbin, China;*
[5] *Laboratory for Reproductive Immunology, Hospital & Institute of Obstetrics and Gynecology, IBS, Fudan University Shanghai Medical College, Shanghai, China.*

Summary	Skeletal homeostasis is dynamically influenced by the immune system. Low density lipoprotein receptor-related protein-5 (*LRP5*) is a co-receptor of the Wnt signaling pathway, which modulates bone metabolism in humans and mice. Immune disorders can lead to abnormal bone metabolism. It is unclear whether and how LRP5 alters the balance of the immune system to modulate bone homeostasis. In this study, we used primary osteoblast to detect the differentiation of osteoblasts *in vitro*, the immune cells of spleen and bone marrow of 6-month old *LRP5* heterozygote (HZ) and wild-type (WT) mice were analyzed by Flow cytometry. We found that LRP5^{+/-} could influence the differentiation of osteoblasts by decreasing the mRNA level of *Osterix*, and increasing the mRNA level of *Runx2* and the ratio of receptor activator for nuclear factor-κB ligand/osteoprotegerin (*RANKL/OPG*). In the *LRP5*^{+/-} mice, percentages of NK cells, CD3e^{+} cells, and CD8a^{+} T cells were increased in both spleen and bone marrow, and percentages of CD106^{+} cells and CD11c^{+} cells were increased in spleen while decreased in bone marrow, conversely, CD62L^{+} cells were decreased in spleen while increased in bone marrow compared to the WT mice. Percentages of CD4^{+} cells, CD14^{+} cells, and CD254^{+} cells were increased in the spleen, and CTLA4^{+} cells were increased in the bone marrow of the *LRP5*^{+/-} mice. The mRNA level of Wnt signaling molecules such as β-catenin, and c-myc were decreased and APC was increased in spleen lymphocytes and bone marrow lymphocytes, and the mRNA level of Wnt3a was decreased in spleen lymphocytes while no change in bone marrow lymphocytes was seen with silencing LRP5 by specific small interfering RNA. In conclusion, heterozygous deletion of the *LRP5* gene in mice could alter the profile of the immune cells, influence the balance of immune environment, and modulate bone homeostasis, which might present a potential mechanism to explore the Wnt signaling pathway in the modulation of the immune system.

Keywords: Low density lipoprotein receptor-related protein-5, osteoblast, RANKL, OPG, T cells, NK cells, CD254

1. Introduction

Osteoporosis is a bone disorder which is characterized

by reduced bone strength and increased bone fragility. Patients with osteoporosis usually show an increase in bone transformation, leading to imbalance of absorption and bone formation (*1,2*). The differentiation of osteoblasts from bone marrow stromal cells is under control of multiple factors, including Wnt family proteins (*3*). Wnt ligands play a central role in development and homeostasis of various organs and activate two signaling pathways, the β-catenin-dependent canonical and β-catenin-independent noncanonical pathways.

Low density lipoprotein receptor-related protein-5 (LRP5) is a transmembrane low-density lipoprotein receptor that shares a similar structure with LRP6 and acts as a co-receptor with LRP6 and the Frizzled protein family members for transducing signals by Wnt proteins through the canonical Wnt pathway. In the activated canonical Wnt/β-catenin pathway, Wnt-protein ligands such as Wnt1 and Wnt 3a can bind to a Frizzled family receptor to dissociate the degradation complex consisting of Axin, adenomatous polyposis coli (APC) and glycogen synthase kinase 3β (GSK3β), then promote the accumulation of β-catenin and its nuclear translocation to regulate expression of various critical genes such as cyclin D1 and c-Myc (*4*). LRP5 is closely related to osteoblast differentiation, bone density and/or osteoporotic fracture, which plays a key role in skeletal homeostasis (*5*). In recent years, much attention has been paid to the role of the Wnt/β-catenin pathway and LRP protein in the pathomechanism of osteoporosis, indicating a possible contribution of polymorphic variants of the candidate LRP5 gene in disease development (*6,7*). The bone mass regulation mechanism of LRP5 provides new therapeutic targets for osteoporosis and other diseases. The finding that LRP5 mutations lead to abnormalities in bone growth in humans has led to attempts to generate animal models for bone defects (*8*).

The viewpoint of osteoimmunology is that the immune system and immune factors play an important role in the development of osteoporosis. In the bone-tumor micro-environment, immune cells such as dendritic cells, monocytes/macrophages, myeloid-derived suppressor cells, regulatory T cells, T helper cells, neutrophils, CD4^{+} T lymphocytes, CD8^{+} cytotoxic T lymphocytes, and natural killer cells, could cooperate with bone cells and tumor cells to enhance bone metastasis and tumor progression (*9-11*). The current hypothesis of the immune system regulating bone formation and bone resorption is linked to discovery of RANK and its ligand RANKL. These molecules were originally thought to be secreted by T lymphocytes and dendritic cells. T lymphocytes secrete inflammatory factors and Wnt ligands to promote bone formation and absorption (*12-14*).

The Wnt signaling cascade plays an important role in development and differentiation of immune cells, in the tumor microenvironment, loss of co-receptors LRP5 and LRP6 in dendritic cells results in reduced tumor growth with enhanced antitumor immune responses (*15*). Although the *LRP5* gene is well-recognized for regulating bone metabolism, its role on the immune system in the bone microenvironment has not been revealed. In this study, we examined the influence of *LRP5*^{+/-} to explore whether immune cells participate in the effect of LRP5 on bone metabolism. The findings suggest that heterozygous deletion of the *LRP5* gene could inhibit the differentiation of osteoblasts and alter the balance of immune cells, indicating that LRP5 plays

an important role in osteoimmunology influencing bone homeostasis.

2. Materials and Methods

2.1. Animals

8-week-old *LRP5*^{+/-} mice with a body mass of between 20 and 30 g were purchased from the Jackson Laboratory. The genotype of the *LRP5*^{+/-} mice was identified by the standard protocol provided by the Jackson Laboratory, and the identified primer sequences are listed in Table 1. The experiments were performed in accordance with the guidelines for the Care and Use of Laboratory Animals published by the US National Institutes of Health and approved by the local ethics committee. Throughout the study period, the mice were housed in a temperature- (23 ± 0.5°C) and humidity-controlled (43 ± 8%) environment under a 12 h light-dark cycle with food and water ad libitum.

2.2. Primary osteoblast isolation and induced differentiation culture

Primary osteoblast cultures were prepared from post-natal hippocampi (P0-P1) mouse pups as previously described (*16*). Briefly, cells were collected from the calvaria of newborn HZ or WT mice and extracted and digested in α-MEM which contained 0.1% collagenase and 0.2% dispase. The osteoblasts of each mouse were seeded in 6-well culture plates at a density of 5×10^5 living cells into serum-free and phenol red-free α-MEM which contained 10 μg/mL streptomycin and 10 units/mL penicillin. The osteogenic differentiation medium, containing serum-free and phenol red-free α-MEM, 20 mM ascorbic acid, 1 M β-glycerophosphate disodium salt hydrate, and 1 mM dexamethasone, was used to induce the differentiation of osteoblasts until the cells reached 80% confluence.

2.3. Lymphocyte culture, LRP5 siRNA transfection

Spleens were harvested from 8-weeks-old WT mice, using aseptic scissors to cut into small pieces gently and then passed through cell strainers. Red blood cells were lysed to gain spleen lymphocytes. The femur and tibia were removed from mice and cleaned of muscle and

Table 1. Summary of oligonucleotide primers for *LRP5*^{+/-} mice genotyping

Oligonucleotide	Sequence* (5'-3')
Common forward primer	CACTGCATGGATGCCAGTGAGGTG
Wild-type reverse primer	GCTGCCACTCATGGAGCCTTTATGC
Mutant reverse primer	CGCTACCGGTGGATGTGTGGAATGTGT

*The oligonucleotide sequences for genotyping were obtained from the Jackson Laboratory website: *https://www.jax.org/search?q=+005823*

Table 2. The primers used in the study

Gene	Forward Primer	Forward Primer
LRP5	CTGTGCTGATGGGTCTGATG	CTGTGCTGATGGGTCTGATG
Collagen1	TGACTGGAAGAGCGGAGAGTA	TGACTGGAAGAGCGGAGAGTA
Runx2	GACAGTCCCAACTTCCTGTG	GACAGTCCCAACTTCCTGTG
Osterix	GCTCGTAGATTTCTATCCTC	GCTCGTAGATTTCTATCCTC
OPG	CCTTGCCCTGACCACTCTTAT	CCTTGCCCTGACCACTCTTAT
RANKL	CAAGATGGCTTCTATTACCTGT	CAAGATGGCTTCTATTACCTGT
Wnt3a	CTCCTCTCGGATACCTCTTAGT	CTCCTCTCGGATACCTCTTAGT
β-cateinin	ATCACTGAGCCTGCCATCTG	ATCACTGAGCCTGCCATCTG
C -myc	CAGCTGCTTAGACGCTGGATT	CAGCTGCTTAGACGCTGGATT
APC	TTGTGGAATCTCTCAGCAAGAA	TTGTGGAATCTCTCAGCAAGAA
GAPDH	GTTGTCTCCTGCGACTTCA	GTTGTCTCCTGCGACTTCA

LRP5: low density lipoprotein receptor-related protein-5; *Runx2*: runt-related transcription factor 2; *OPG*: osteoprotegerin; *RANKL*: nuclear factor-κ B ligand; *APC*: *Adenomatous Polyposis Coli.*

connective tissue. The ends of the bones were cut, and bone marrow (BM) cells were flushed out with media using a needle attached to a syringe. Red blood cells were lysed to obtain BM lymphocytes. BM-derived lymphocytes were seeded in 6-well culture plates at a density of 10^6 cells/mL and cultured in RPMI 1640 supplemented with 10% fetal calf serum (FCS), 1x penicillin/streptomycin/neomycin, and 10 mM HEPES buffer. A double-stranded small interfering RNA (siRNA) against the LRP5 transcript or the negative control (Shanghai GenePharma Co., Ltd., Shanghai, China) was transfected into lymphocytes in six-well cluster plates using EntransterTM-R4000 transfection reagent (Engreen Biosystem, Beijing, China) in accordance with the manufacturer's instructions. Transfected cells were harvested for extraction of mRNA after 24 h.

2.4. *RNA extraction, reverse transfection, and real-time RT-PCR*

For PCR analysis, total RNA was isolated with an RNA extraction Kit (Axygen, CA, USA) according to the manufacturer's protocol, and the concentration of total RNA was measured with a NanoDrop 2000c (Thermo, Fisher, MA, USA). RNA (1 μg) was converted into cDNA using reverse transcriptase (Promega, Madison, USA). RT-PCR was performed using SYBR Premix Ex Taq (Takara Bio, Tokyo, Japan). The cDNA levels were determined using the housekeeping gene GAPDH, which was amplified in parallel with the gene to be analyzed and used to normalize the results. The threshold cycle (Ct) values were calculated using software supplied by the Applied Biosystems 7900 Real-time PCR system. Primer sequences are listed in Table 2.

2.5. *Quantitative detection of alkaline phosphatase (ALP) activity*

5×10^5 primary osteoblasts were seeded into 6-well culture plates and cultured until they reached 90% confluence. The cells were digested with pancreatin and collected into a 1.5 mL EP tube. The ALP kit was used to detect the ALP activity with the supernatant from the cells handled by cell lysate according to the reagent instructions.

2.6. *Reagents*

Flow cytometry antibodies FITC-conjugated anti-pan-NK/CD103/CD106/TCRgd, APC-conjugated anti-cytotoxic T lymphocyte antigen-4 (CTLA-4)/CD62L, PE-conjugated anti-CD4/CD14/CD19/CD254, PEcy5.5-conjugated anti-CD3e/CD11c, APC-efluor780-conjugated anti-CD8a, and their corresponding isotypes were purchased from Biolegend (San Diego, CA, USA).

2.7. *Flow cytometry analysis*

Splenocytes and bone marrow cells were obtained and 1×10^6 cells of each sample were incubated with chosen antibodies for 30 minutes on ice, then washed and resuspended in PBS which contained 0.1% sodium azide and 1% bovine serum albumin. The non-specific signal was identified by rat FITC- and PE-conjugated IgG isotype controls. Approximately 50,000 stained cells in each sample were analyzed by a CyAN ADP flow cytometer (Beckman Coulter, Brea, CA, USA), and each sample was examined twice. Data are expressed as the percentage of positive cells.

2.8. *Statistical analysis*

All data are presented as the mean ± SEM, and the means were statistically analyzed using Student's *t*-test as appropriate. All assays were repeated at least three times. Significance levels were noted as follows: $*p < 0.05$, $**p < 0.01$, and $***p < 0.001$.

3. Results

3.1. *The identification of LRP5$^{+/-}$ mice*

The transgene identification of *LRP5$^{+/-}$* mice was confirmed by the standard protocol provided by the
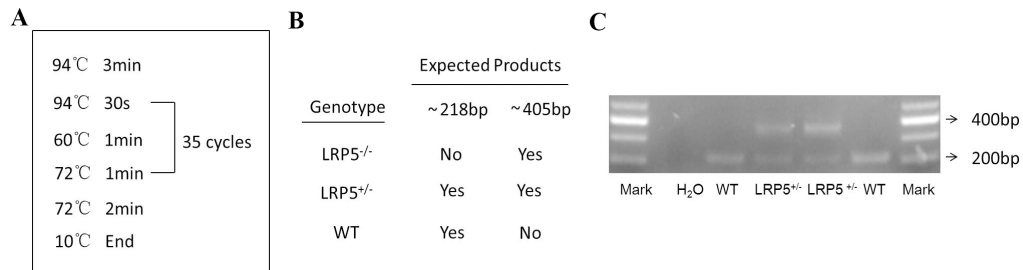
Figure 1. The gene identification of *LRP5*^{+/-} mice. (A) The master protocol details provided by the Jackson Laboratory. **(B)** The expected results of mice. Mutant = 405 bp, Heterozygote = 218 bp and 405 bp, Wild type = 218 bp. **(C)** The gel image of PCR products.
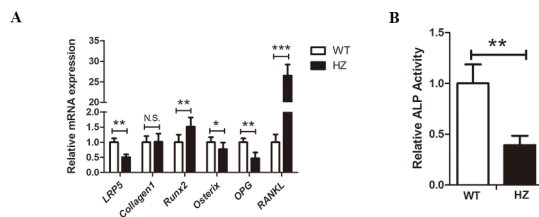
Figure 2. Heterozygous deletion of *LRP5* gene impaired the viability of osteoblasts and inhibited the differentiation of osteoblasts in vitro. (A) *LRP5*^{+/-} affected mRNA expression of osteoblastogenesis-related genes, including *Runx2, Osterix, Collagen I, OPG*, and **RANKL. (B)** The ALP activity of osteoblasts was determined after 7 days of culture. *$p < 0.05$. All results are expressed as the mean ± SEM, and data are representative of at least three experiments.

Jackson Laboratory (Stock Number 005823, Strain Name: B6.129P2-Lrp5 tm1Dgen /J). The expected products' sizes of heterozygote were 218bp and 405bp (Figure 1). The mRNA expression level of LRP5 was lower in the HZ mice than in the WT mice (Figure 2A).

3.2. Heterozygous deletion of LRP5 gene decreased ALP activity and inhibited the differentiation of osteoblasts in vitro

WT and HZ mice were used and the mRNA expression level of *Runx2* and *Osterix* were detected as important transcriptional molecules in differentiation of osteoblasts. The mRNA levels of the *Osterix* gene was inhibited while the *Runx2* gene was increased in *LRP5*^{+/-} mice (Figure 2A). Heterozygous deletion of the *LRP5* gene could increase the mRNA expression levels of *RANKL* and decrease the mRNA levels of *OPG*, while it showed no effect on the modulation of collagen1 (Figure 2A). After 7 days of cell differentiation culture to analyze vitality, the result showed that the ALP activity of HZ mice was decreased compared with WT mice (Figure 2B).

3.3. Heterozygous deletion of LRP5 gene in mice modulated the innate immune cells

Myeloid progenitors for osteoclasts can also differentiate

into dendritic cells (DC) and macrophages, suggesting a close relationship of osteoclasts to cells of the innate immune system. Then we explored whether heterozygous deletion of *LRP5* gene could modulate the profile of innate immune cells in the spleen and bone marrow. Compared with WT mice, the percentage of NK cells increased in the HZ mice (Figure 3A and 3B), while the percentage of γδT cells showed no difference in the two groups in both spleen and bone marrow (Figure 3C). The proportion of CD14⁺ cells increased in the spleen of HZ mice while there was no significant change in the bone marrow (Figure 3D and 3E). In HZ mice, we found that the CD11c⁺ cells were increased in the spleen, while decreased in the bone marrow (Figure 3F and 3G).

3.4. Heterozygous deletion of the LRP5 gene in mice regulated the balance of T cells while had no effect on B cells

Skeletal homeostasis is dynamically influenced by the immune system. Bone destruction is attributable to excessive bone resorption by osteoclasts, the formation of which is directly and indirectly regulated by T cells. We found that heterozygous deletion of the *LRP5* gene could increase the percentage of CD4⁺ T cells in the spleen, and increase CD8a⁺ cells in both spleen and bone marrow (Figure 4A-4D). Further analysis of the immunophenotype of *LRP5*^{+/-} mice showed that the CD62L⁺ cells decreased in the spleen while increased in the bone marrow in HZ mice (Figure 4E-4G), and the CD3e⁺ cells increased in both spleen and bone marrow in HZ mice compared to WT mice (Figure 4H, 4I). B cells are the main source of OPG in the bone marrow, but our result found no significant change in both spleen and bone marrow after heterozygous deletion of the *LRP5* gene (Figure 4J).

3.5. Heterozygous deletion of LRP5 gene in mice regulated the functional immune cells to modulate osteoimmunology

RANK and its ligand (RANKL; also known as CD254, OPGL, and TRANCE) are key regulators of bone
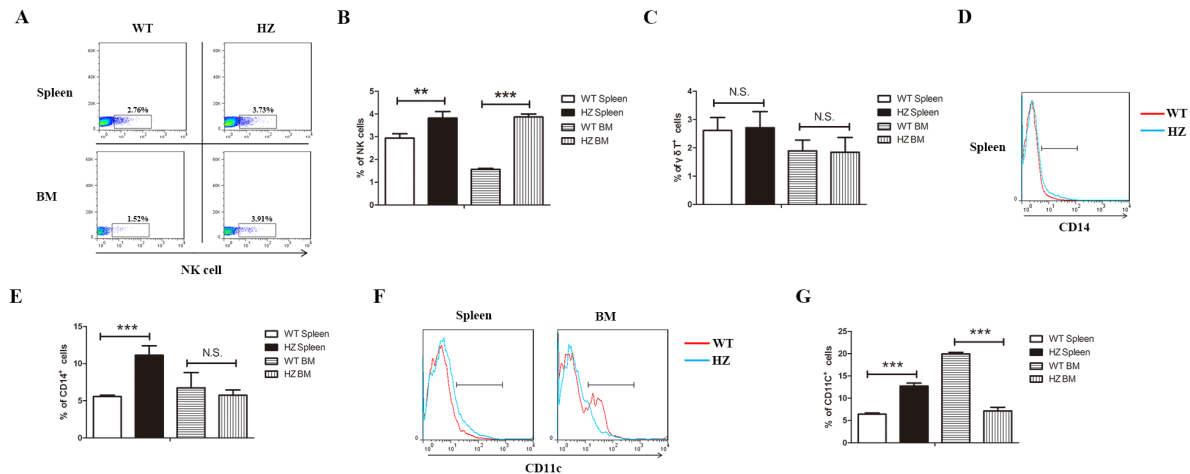
Figure 3. Proportion of innate immune cells in the spleen and bone marrow of *LRP5*$^{+/-}$ mice. (A) Flow cytometry of NK cells from each group. **(B)** Frequency of NK cells in mice as in A. **(C)** Frequency of γδT cells in each group. **(D)** Flow cytometry of CD14$^+$ cells from spleen. **(E)** Frequency of CD14+ cells in each group. **(F)** Flow cytometry of CD11c$^+$ cells from each group. **(G)** Frequency of CD11c$^+$ cells in mice as in **F.** *$p < 0.05$. All results are expressed as the mean ± SEM, and data are representative of at least three experiments.
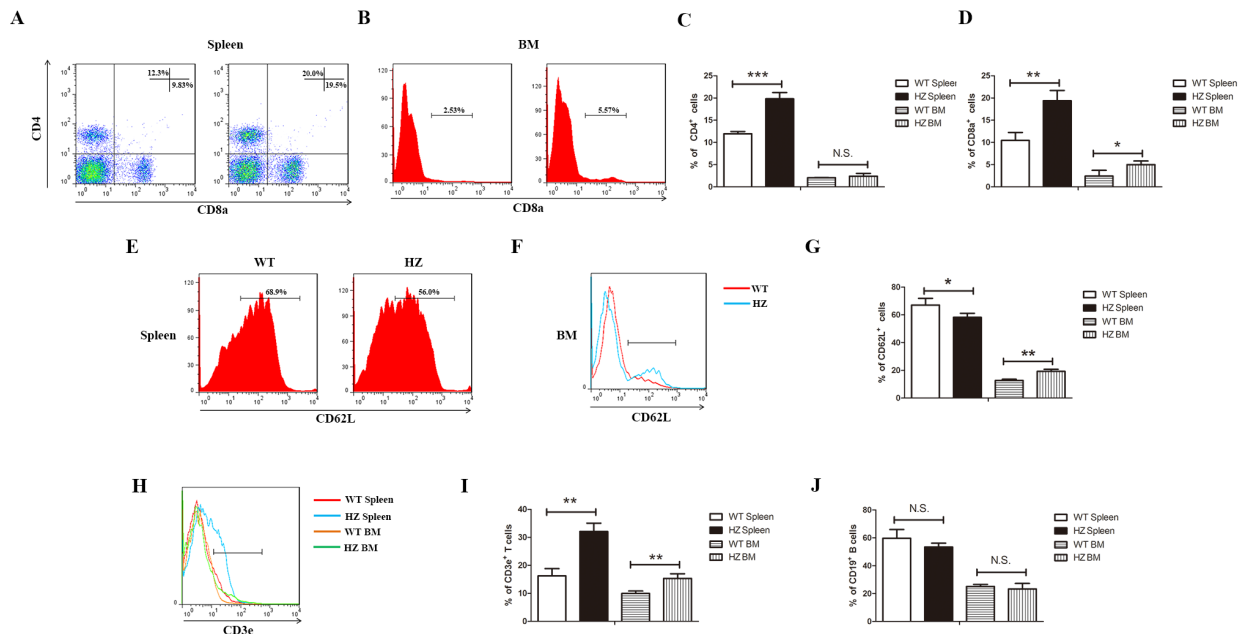

Figure 4. Heterozygous deletion of *LRP5* gene regulated the balance of T cells. (A) Flow cytometry of CD4$^+$ and CD8$^+$ T cells in spleen from HZ mice and WT mice. **(B)** Flow cytometry of CD8$^+$ T cells in bone marrow from HZ mice and WT mice. **(C,D)** Frequency of CD4$^+$ and CD8$^+$ T cells in mice as in A and B. **(E,F)** Flow cytometry of CD62L$^+$ cells from each group. **(G)** Frequency of CD62$^+$ cells in mice as in E and F. **(H)** Flow cytometry of CD3e$^+$ cells from each group. (I) Frequency of CD3e$^+$cells in mice as in H. **(J)** Frequency of CD19$^+$ B cells from each group. *$p < 0.05$. All results are expressed as the mean ± SEM, and data are representative of at least three experiments.

remodeling, mammary gland formation, lymph node development, and T-cell/dendritic cell communication. Here we found that the percentage of CD254$^+$ cells was increased in the spleen, while there was no significant change in the bone marrow in HZ mice (Figure 5A and 5B). As CD106 is a novel mediator of bone marrow mesenchymal stem cells *via* NF-κB in the bone marrow of acquired aplastic anemia, we also found the CD106$^+$ cells increased in the spleen while they decreased in the bone marrow in HZ mice compared to WT mice

(Figure 5C and 5D). The enhanced osteogenesis of mesenchymal stem cells (MSCs) modified by cytotoxic T lymphocyte-associated antigen 4 (CTLA4) has been shown in previous studies. The heterozygous deletion of the *LRP5* gene could evidently increase CTLA4$^+$ cells in bone marrow (Figure 5E). CD103 is a representative molecular of dendritic cells as well as a hallmark of tumor-infiltrating regulatory T cells and modulates immune inflammatory disease. In this study we found there was no significant difference of the CD103$^+$ cells
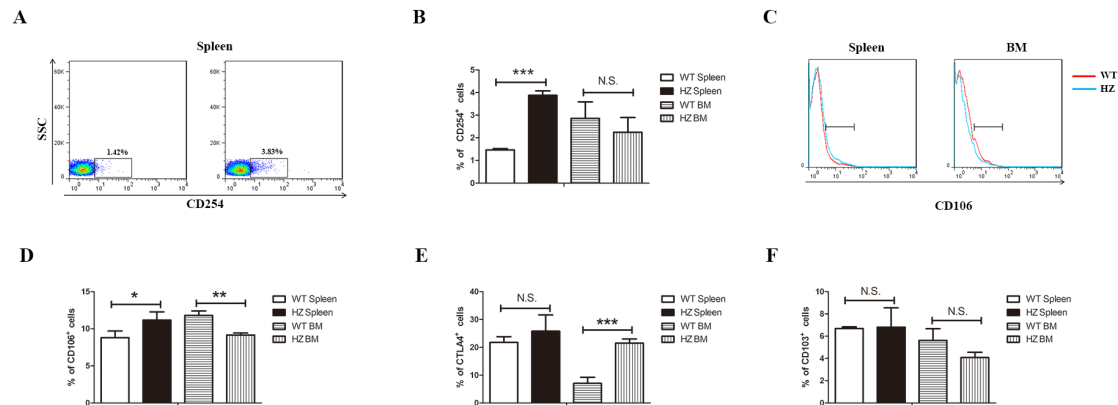
Figure 5. Heterozygous deletion of the *LRP5* gene regulated the functional immune cells. (A) Flow cytometry of CD254^{+} T cells in the spleen from HZ mice and WT mice. **(B)** Frequency of CD254^{+} from each group. **(C)** Flow cytometry of CD106^{+} cells from each group. **(D)** Frequency of CD254^{+} cells in mice as in C. **(E,F)** Frequency of CTLA4^{+} cells and CD103^{+} from each group. *$p < 0.05$. All results are expressed as the mean ± SEM, and data are representative of at least three experiments.
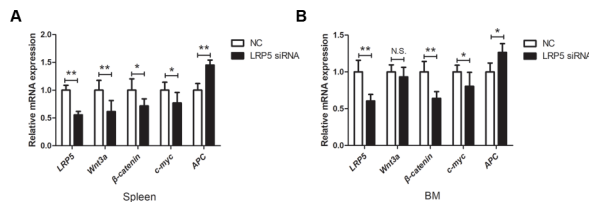
Figure 6. Silencing *LRP5* by specific small interfering RNA regulated Wnt signaling molecules of lymphocytes. The mRNA expression levels of Wnt3a, β-catenin, c-myc and APC in the WT spleen **(A)** and the bone marrow **(B)** lymphocytes treated with LRP5 siRNA or NC. *$p < 0.05$. All results are expressed as the mean ± SEM, and data are representative of at least three experiments.

in two groups of mice (Figure 5F).

3.6. Wnt signaling pathway involved in the modulation of immune system with silencing of LRP5 by specific small interfering RNA

As *LRP5* gene plays the part of co receptor in the Wnt signal, we examined whether the Wnt signaling pathway is involved in the regulation of immune system with low expression of LRP5. We found the mRNA levels of Wnt3a, β-catenin, and c-myc were decreased and the mRNA level of APC was increased in spleen lymphocytes treated with LRP5 siRNA compared with NC (Figure 6A). The mRNA levels of β-catenin, and c-myc were also decreased and the mRNA level of APC was increased in the bone marrow lymphocytes treated with LRP5 siRNA compared with NC, while the mRNA level of Wnt3a had no significant change (Figure 6B).

4. Discussion

The immune system and skeletal system share a variety of molecules, including cytokines, chemokines, hormones, receptors, and transcription factors. Bone

cells interact with immune cells under physiological and pathological conditions (*17*). In the present study, we found *LRP5*^{+/-} could inhibit the differentiation of osteoblasts and then investigated the immune cells in the spleen and bone marrow in *LRP5* HZ mice, the findings can be summarized as follows: heterozygous deletion of the *LRP5* gene can modulate the balance of T cells and innate immune cells in spleen and bone marrow congruously, such as increasing CD8^{+} T cells, CD4^{+} T cells, NK cells, total CD3e^{+} cells, CD14^{+} cells, CD106^{+} cells, CD11c^{+} cells and CD254^{+} cells in spleen; and there are some other change trends in bone marrow, with increasing the percentage of NK cells and CD3e^{+} cells, CD8^{+} cells and CD62L^{+} cells, while decreasing the percentage of CD106^{+} cells, CD11c^{+} cells; and there is no effect on the levels of B cells in both spleen and bone marrow.

LRP5 is the key mediator of β-catenin dependent Wnt signaling. However, very little is known about their specific roles in regulating bone-metabolism gene expression in osteoblasts. The OPG/RANKL/RANK system plays an important role in regulating the balance of osteoblast and osteoclast activity, preventing bone loss and ensuring normal bone regeneration (*18,19*). Both Runx2 and Osterix are important transcription factors in the process of osteoblast differentiation, Runx2 is expressed in the early stages of osteoblast differentiation, while Osterix is expressed in the late stage (*20*). The results that the mRNA expression of Runx2 was increased while Osterix was decreased in the *LRP5*^{+/-} mice revealed that heterozygous deletion of the *LRP5* gene could induce the differentiation disorder in the late stage. The results that the activity of ALP in *LRP5*^{+/-} mice was inhibited and the osteoblast differentiation related-genes were changed indicates that LRP5 participates in the modulation of Osteoporosis.

In previous studies, osteoimmunology was created as a new interdisciplinary field in large part to highlight

the shared molecules and reciprocal interactions between the two systems in both health and disease (*21*). The ratio of NK cells in *LRP5*^{+/-} mice is higher suggesting that NK cells are in an activation form and have the ability to produce an immune response, while NK cells may play a role in bone formation and bone loss. Myeloid progenitors for osteoclasts can also differentiate into DCs and macrophages, suggesting a close relationship of osteoclasts to cells of the innate immune system (*22*). Previous studies have implicated that γδ T cells can be activated and inhibit osteoclast differentiation and absorptive activity in animal models of rheumatoid arthritis (RA). Interestingly, both human and mouse CD11c^{+} DC can differentiate into osteoclasts *in vitro* and mouse DC can contribute to osteoclast formation *in vivo* (*23,24*). As we found CD11c^{+} cells were increased in spleen and decreased in bone marrow, while the γδ T cells had no influence on the *LRP5*^{+/-} mice, this indicated the *LPR5* gene may modulate osteoclast formation but have no effect on the differentiation of osteoblasts.

The stimulation and inhibition roles of T cells to osteoblasts and osteoclasts are closely related to the subsets of T cells, cytokines and local factors. The activation of CD8^{+} T cells in bone and the immune system plays a key role in maintaining the balance of osteoclasts-osteogenesis (*25,26*). Activation of CD4^{+} T cells can directly secrete soluble RANKL, TNF-α or IL-1, IL-6 and IL-17 to promote the formation of osteoclasts in inflammation diseases, such as rheumatoid arthritis, periodontitis, congenital adrenocortical hyperplasia and osteoporosis (*27,28*). Part of the TCR-CD3 complex present on the T-lymphocyte cell surface plays an essential role in the adaptive immune response (*29*). In our study, we found that *LRP5*^{+/-} increased the proportion of CD4^{+} T cells, CD8^{+} T cells and CD3e^{+} cells, while there was no effect on B cells, this change in *LRP5*^{+/-} mice may indicate that LRP5 could disturb the balance of T cells to promote the development of OP.

Neutrophilia is a normal response of an organism during inflammation. Various mechanisms are involved in the appearance of this response, including release of neutrophils from the bone marrow as well as demargination. Down-regulation of the CD62L antigen is regarded as a possible mechanism for neutrophilia during inflammation (*30,31*). We found the expression of CD62L was decreased in spleen and increased in bone marrow, indicating *LRP5*^{+/-} might influence the inflammatory reaction to promote the OP.

The current hypothesis of the immune system regulating bone formation and bone resorption is linked to the discovery of RANK and its ligand RANKL (also known as CD254). RANKL and RANK increase the rolls of DCs, stimulate the proliferation of initial T cells, and improve the survival of DCs (*32,33*). We found the CD254^{+} cells were increased in spleen in
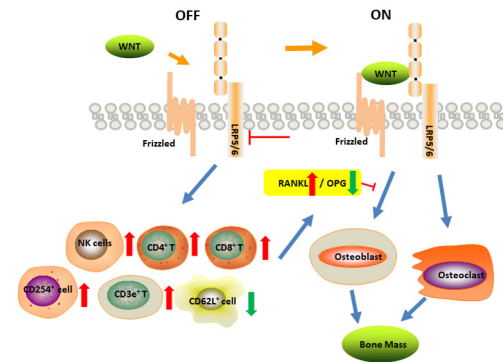
Figure 7. Schematic diagram of heterozygous deletion of the *LRP5* gene. Inhibition of the Wnt signal by heterozygous deletion of the *LRP5* gene influences the formation of bone mass through influencing the differentiation of osteoblasts, accompanied by disturbance of the balance of immune cells with an increased percentage of NK/CD3e^{+}/CD14^{+}/CD106^{+}/CD11c^{+}/CD4^{+}/CD254^{+}/CD8a^{+} cells and decreased CD62L^{+} cells in the spleen.

LRP5^{+/-} mice, indicating that *LRP5*^{+/-} could impact bone resorption. CD106 is a marker of placental chorionic mesenchymal stem cells with strong immune-modulatory function, and mesenchymal stem cells can differentiate into osteoblasts (*34*). It has been suggested that activation of the immune system by T cells has a negative impact on the reconstruction of bone within bone defects. As a vital co-inhibitory molecule expressed on activated T cells, CTLA4 can block the B7-CD28 co-stimulatory pathway to induce immune tolerance (*35*). CD103^{+} dendritic cells can combine with CD4^{+} T cells to initiate the classical RANKL/RANK osteoclast signaling pathway and participate in the formation of osteoporosis (*36*). In our study, *LRP5*^{+/-} could disturb the percentage of CD106^{+} cells in spleen and bone marrow, and increase the CTLA4^{+} cells while having no effect on CD103^{+} cells. These functional immune cells may participate in osteoimmunology by modulated LRP5.

Increasing evidence indicates that Wnt/β-catenin signaling promotes some disease progression such as cancer and autoimmune disease by regulating dendritic cells, T cells, NK cells and tumor cells. Modulating the expression of LRP5 could influence the Wnt signal and the balance of immune cells directly. We propose that targeting Wnt/β-catenin signaling would potentially modulate the immune system to regulate bone metabolic disease.

In summary, we report in the present study that *LRP5*^{+/-} can influence the differentiation of osteoblasts and disturb the balance of immune cells by modulating the Wnt signing pathway. This induction involves an increased percentage of NK/CD3e^{+}/CD14^{+}/CD106^{+}/CD11c^{+}/CD4^{+}/CD254^{+}/CD8a^{+} cells in the spleen of *LRP5*^{+/-} mice (Figure 7). Thus, the role of LRP5 should be investigated further to examine the pathogenesis of osteoimmunology.

References

1. Minisola S, Cipriani C, Occhiuto M, Pepe J. New anabolic therapies for osteoporosis. Intern Emerg Med. 2017; 12:915-921.
2. Salamanna F, Giardino R, Fini M. Spontaneous osteoclastogenesis: Hypothesis for gender-unrelated osteoporosis screening and diagnosis. Med Hypotheses. 2017; 109:70-72.
3. Karner CM, Long F. Wnt signaling and cellular metabolism in osteoblasts. Cell Mol Life Sci. 2017; 74:1649-1657.
4. Grainger S, Willert K. Mechanisms of Wnt signaling and control. Wiley Interdiscip Rev Syst Biol Med. 2018: e1422.
5. Weivoda MM, Ruan M, Hachfeld CM, Pederson L, Howe A, Davey RA, Zajac JD, Kobayashi Y, Williams BO, Westendorf JJ, Khosla S, Oursler MJ. Wnt Signaling Inhibits Osteoclast Differentiation by Activating Canonical and Noncanonical cAMP/PKA Pathways. J Bone Miner Res. 2016; 31:65-75.
6. Gao F, Xu F, Wu D, Cheng J, Xia P. Identification of novel genes associated with fracture healing in osteoporosis induced by Krm2 overexpression or Lrp5 deficiency. Mol Med Rep. 2017; 15:3969-3976.
7. Wolski H, Drwęska-Matelska N, Seremak-Mrozikiewicz A, Łowicki Z, Czerny B. The role of Wnt/β-catenin pathway and LRP5 protein in metabolism of bone tissue and osteoporosis etiology. Ginekol Pol. 2015; 86:311-314.
8. Fahiminiya S, Majewski J, Roughley P, Roschger P, Klaushofer K, Rauch F. Whole-exome sequencing reveals a heterozygous LRP5 mutation in a 6-year-old boy with vertebral compression fractures and low trabecular bone density. Bone. 2013; 57:41-46.
9. Qiu X, Gui Y, Xu Y, Li D, Wang L. DHEA promotes osteoblast differentiation by regulating the expression of osteoblast-related genes and Foxp3^{+} regulatory T cells. Biosci Trends. 2015; 9:307-314.
10. Weitzmann MN, Vikulina T, Roser-Page S, Yamaguchi M, Ofotokun I. Homeostatic Expansion of CD4^{+} T Cells Promotes Cortical and Trabecular Bone Loss, Whereas CD8^{+} T Cells Induce Trabecular Bone Loss Only. J Infect Dis. 2017; 216:1070-1079.
11. Xiao Y, Palomero J, Grabowska J, Wang L, de Rink I, van Helvert L, Borst J. Macrophages and osteoclasts stem from a bipotent progenitor downstream of a macrophage/osteoclast/dendritic cell progenitor. Blood Adv. 2017; 1:1993-2006.
12. Weitzmann MN. Bone and the Immune System. Toxicol Pathol. 2017; 45:911-924.
13. Okamoto K, Nakashima T, Shinohara M, Negishi-Koga T, Komatsu N, Terashima A, Sawa S, Nitta T, Takayanagi H. Osteoimmunology: The Conceptual Framework Unifying the Immune and Skeletal Systems. Physiol Rev. 2017; 97:1295-1349.
14. Sutton KM, Hu T, Wu Z, Siklodi B, Vervelde L, Kaiser P. The functions of the avian receptor activator of NF-κB ligand (RANKL) and its receptors, RANK and osteoprotegerin, are evolutionarily conserved. Dev Comp Immunol. 2015; 51:170-184.
15. Hong Y, Manoharan I, Suryawanshi A, Shanmugam A, Swafford D, Ahmad S, Chinnadurai R, Manicassamy B, He Y, Mellor AL, Thangaraju M, Munn DH, Manicassamy S. Deletion of LRP5 and LRP6 in dendritic cells enhances antitumor immunity. Oncoimmunology. 2015; 5:e1115941.
16. Gui Y, Duan Z, Qiu X, Tang W, Gober HJ, Li D, Wang L. Multifarious effects of 17-β-estradiol on apolipoprotein E receptors gene expression during osteoblast differentiation *in vitro*. Biosci Trends. 2016; 10:54-66.
17. Takahashi S, Fukuda M, Mitani A, Fujimura T, Iwamura Y, Sato S, Kubo T, Sugita Y, Maeda H, Shinomura T, Noguchi T. Follicular dendritic cell-secreted protein is decreased in experimental periodontitis concurrently with the increase of interleukin-17 expression and the Rankl/Opg mRNA ratio. J Periodontal Res. 2014; 49:390-397.
18. Park KH, Gu DR, Jin SH, Yoon CS, Ko W, Kim YC, Lee SH. Pueraria lobate Inhibits RANKL-Mediated osteoclastogenesis *via* downregulation of CREB/PGC1β/c-Fos/NFATc1 signaling. Am J Chin Med. 2017; 45:1725-1744.
19. He XF, Zhang L, Zhang CH, Zhao CR, Li H, Zhang LF, Tian GF, Guo MF, Dai Z, Sui FG. Berberine alleviates oxidative stress in rats with osteoporosis through receptor activator of NF-kB/receptor activator of NF-kB ligand/osteoprotegerin (RANK/RANKL/OPG) pathway. Bosn J Basic Med Sci. 2017; 17:295-301.
20. Zhang N, Zhang Y, Lin J, Qiu X, Chen L, Pan X, Lu Y, Zhang J, Wang Y, Li D, Wang L. Low-density lipoprotein receptor deficiency impaired mice osteoblastogenesis *in vitro*. Biosci Trends. 2018; 11:658-666.
21. Criscitiello C, Viale G, Gelao L, Esposito A, De Laurentiis M, De Placido S, Santangelo M, Goldhirsch A, Curigliano G. Crosstalk between bone niche and immune system: osteoimmunology signaling as a potential target for cancer treatment. Cancer Treat Rev. 2015; 41:61-68.
22. Ponzetta A, Benigni G, Antonangeli F, Sciumè G, Sanseviero E, Zingoni A, Ricciardi MR, Petrucci MT, Santoni A, Bernardini G. Multiple Myeloma Impairs Bone Marrow Localization of Effector Natural Killer Cells by Altering the Chemokine Microenvironment. Cancer Res. 2015; 75:4766-4777.
23. Phalke SP, Chiplunkar SV. Activation status of γδ T cells dictates their effect on osteoclast generation and bone resorption. Bone Rep. 2015; 3:95-103.
24. Ruef N, Dolder S, Aeberli D, Seitz M, Balani D, Hofstetter W. Granulocyte-macrophage colony-stimulating factor-dependent CD11c-positive cells differentiate into active osteoclasts. Bone. 2017; 97:267-277.
25. Kiesel JR, Buchwald ZS, Aurora R. Cross-presentation by osteoclasts induces FoxP3 in CD8^{+} T cells. J Immunol. 2009; 182:5477-5487.

26. Xu X, Li R, Zhou Y, Zou Q, Ding Q, Wang J, Jin W, Hua G, Gao J. Dysregulated systemic lymphocytes affect the balance of osteogenic/adipogenic differentiation of bone mesenchymal stem cells after local irradiation. Stem Cell Res Ther. 2017; 8:71.

27. Brincat SD1, Borg M, Camilleri G, Calleja-Agius J. The role of cytokines in postmenopausal osteoporosis. Minerva Ginecol. 2014; 66:391-407.

28. Alnaeeli M, Penninger JM, Teng YT. Immune interactions with CD4^{+} T cells promote the development of functional osteoclasts from murine CD11c^{+} dendritic cells. J Immunol. 2006; 177:3314-3326.

29. Chia LY, Walsh NC, Martin TJ, Sims NA. Isolation and gene expression of haematopoietic-cell-free preparations of highly purified murine osteocytes. Bone. 2015; 72:34-42.

30. Lobach AR, Uetrecht J. Clozapine promotes the proliferation of granulocyte progenitors in the bone marrow leading to increased granulopoiesis and neutrophilia in rats. Chem Res Toxicol. 2014; 27:1109-1119.

31. Zhang D, Chen G, Manwani D, Mortha A, Xu C, Faith JJ, Burk RD, Kunisaki Y, Jang JE, Scheiermann C, Merad M, Frenette PS. Neutrophil ageing is regulated by the microbiome. Nature. 2015; 525:528-32.

32. Akbar MA, Nardo D, Chen MJ, Elshikha AS, Ahamed R, Elsayed EM, Bigot C, Holliday LS, Song S. Alpha-1 antitrypsin inhibits RANKL-induced osteoclast formation and functions. Mol Med. 2017; 23.

33. Wisitrasameewong W, Kajiya M, Movila A, Taubman MA, Kawai T. DC-STAMP Is an Osteoclast Fusogen Engaged in Periodontal Bone Resorption. J Dent Res. 2017; 96:685-693.

34. Lu S, Ge M, Zheng Y, Li J, Feng X, Feng S, Huang J, Feng Y, Yang D, Shi J, Chen F, Han Z. CD106 is a novel mediator of bone marrow mesenchymal stem cells *via* NF-κB in the bone marrow failure of acquired aplastic anemia. Stem Cell Res Ther. 2017; 8:178.

35. Iwamoto N, Kawakami A. [The regulation of CTLA4-Ig in bone and cartilage destruction of rheumatoid arthritis]. Clin Calcium. 2015; 25:1817-23.

36. Habbeddine M, Verthuy C, Rastoin O, Chasson L, Bebien M, Bajenoff M, Adriouch S, den Haan JMM, Penninger JM, Lawrence T. Receptor Activator of NF-κB Orchestrates Activation of Antiviral Memory CD8 T Cells in the Spleen Marginal Zone. Cell Rep. 2017; 21:2515-2527.

Original Article

Mongolian Medicine echinops prevented postmenopausal osteoporosis and induced ER/AKT/ERK pathway in BMSCs

Yan Liu[1,2,§], Xiongyao Wang[3,§], Hong Chang[2], Xiaoming Gao[2], Chongyang Dong[3], Zimu Li[3], Jingtao Hao[3], Jiuhe Wang[4], Qiaoling Fan[1,*]

[1] *School of Basic Medical Science, Nanjing University of Chinese Medicine, Nanjing, China;*
[2] *Department of Traditional Chinese Medicine, Affiliated Hospital of Inner Mongolia Medical University, Hohhot, China;*
[3] *College of Traditional Chinese Medicine, Inner Mongolia Medical University, Hohhot, China;*
[4] *Department of Cardiology, Inner Mongolia Autonomous Rengion Hospital of Traditional Chinese Medicine, Hohhot, China.*

Summary   Hormone replacement medicine such as traditional Chinese medicine has proven to be effective in decreasing the risk of osteoporosis. Mongolian medicine echinops prevents osteoporosis, but its mechanism remains unclear. In this study, we explored the mechanism underlying echinops prevents and treats postmenopausal osteoporosis. Osteoporosis model was established by ovariectomy in rats. Rats were treated to Echinops (16.26, 32.5, or 65 mg/kg/day) by oral gavage for 3 months. Bone mineral density (BMD) was detected by micro-CT detection of left proximal medial metaphyseal tibia. Hematoxylin and eosin (H&E) and toluidine blue O staining were also performed. Serum levels of E2, ALP and testosterone were examined. Bone marrow-derived bone marrow stem cells (BMSCs) were isolated and treated with echinops-containing serum. Estrogen receptors (ER) including ERα and ERβ in bone specimens and BMSCs were detected by qRT-PCR. Cell viability and colon formation of BMSCs were detected. Expressions of ERα, ERβ, AKT, p-AKT, ERK, and p-ERK in BMSCs were detected by western blot. Results showed that echinops significantly increased trabecular interconnectivity, thickness of trabeculae, and connection of trabecula. Echinops significantly increased BMD and E2, but significantly reduced ALP and testosterone in dose-dependent manners. Echinops induced ERα and ERβ in both bone specimens and BMSCs. Echinops enhanced cell viability and ability of colony formation of BMSCs, and increased ERα, ERβ, p-AKT, and p-ERK. Thus, Mongolian echinops reduced bone loss and delayed the occurrence and development of osteoporosis, and increased ERα, ERβ, p-AKT, and P-ERK in BMSCs. These results provide experimental basis for clinical prevention and treatment of postmenopausal osteoporosis by echniops.

Keywords: Osteoporosis, echinops, ERα, ERβ, AKT/ERK pathway

1. Introduction

Osteoporosis (OP) is a metabolic bone disease characterized by low bone mass and the destruction of the microstructure of bone tissue, leading to increased bone fragility and easy to fracture (*1,2*). OP is the sixth

most common chronic diseases in humans (*3*). It was divided into two types: primary OP and secondary OP (*4,5*). Primary OP can be divided into two subtypes, namely Type I and Type II. Type I is postmenopausal osteoporosis (PMOP), which occurs in postmenopausal women (*6,7*). Type II is senile osteoporosis, most commonly seen in the elderly over 60 years old. About 200 million people worldwide suffer from osteoporosis, of which postmenopausal women account for 1/3 (*8,9*). The overall incidence of OP in Chinese population over 60 is 22.6%, with 15% for males and 28.6% for females, with a trend of increasing year by year (*10*). The incidence of OP in the United States is also quite high, about 20,000 cases of OP fractures, and 65,000 cases

died due to OP each year (*11*).

PMOP occurs in 5 to 10 years after menopause in women, most of whom have an increased bone turnover rate, due to fluctuations or gradually reduced in the level of estrogen. In post-menopausal 5-7 years, women lose about 20% of the bone mass (*12*). Although most osteoporosis does not directly cause death, its greatest risk is fractures, with high morbidity and disability (*6,11*). Estrogen deficiency caused by postmenopausal ovarian hypofunction is recognized as an important cause of postmenopausal osteoporosis (*13-15*). Estrogen replacement therapy is the preferred method of treatment for PMOP, which can enhance bone mineral density (BMD) and systemic bone mineral content, and effectively treat postmenopausal osteoporosis (*16-18*). However, the long-term use of estrogen increases the risk of breast cancer, endometrial cancer, cardiovascular accident and vascular embolism (*19*). In recent years, the prevention and treatment of PMOP by traditional Chinese medicine is attracting more and more attention (*20,21*). It is of great significance to find an estrogen replacement medicine for the prevention and treatment of postmenopausal osteoporosis in traditional medicine.

Mongolian medicine echinops was introduced in the canon of Mongolian Medical "Wisdom Ancientmirror". It functions as strengthening bone, reuniting bone, and callus (*22*). In recent year, it was showed that echinops decreased the serum level of bone Glp protein and inhibited osteoporosis in ovariectomized (OVX) rats (*23*). Post-surgery 90 days, the OVX rats were filled the stomach with echinops for 90 days and then the serum level of alkaline phosphatase (ALP) were significantly increased and serum level of interleukin-1 was significantly reduced (*24*). After successes of the osteoporosis, OVX rats were feed 90 days and then filled the stomach with echinops for 90 days, then BMD and the maximum deflection of bone were increased compared with OVX rats (*25*). These results implied that Mongolian echinops can inhibit the bone absorption and promote the bone formation, decreasing bone turnover, reducing bone loss, delaying the occurrence and development of PMOP. However, the mechanism underlying echinops prevents and treats PMOP is still unclear.

In this study, we aimed to explore the roles of estrogen receptors (ER; ERα and ERβ), p-AKT, and p-ERK in BMSCs during echinops prevents and treats postmenopausal osteoporosis.

2. Materials and Methods

2.1. *Animals and treatments*

A total of 84 SPF healthy female Wistar rats (250 ± 20 g, 4 months) were purchased from the animal research center of Inner Mongolia University, China (certification number: SCXK (Mongolia) 2012-0001). The rats received ad libitum access to standard chow pellets and water in 24°C, 50-60% humidity. This study was approved by animal ethics committee of Inner Mongolia University. After 7 days in new environment, the rats were anesthetized by intraperitoneal injection of 40 mg/kg pentobarbital sodium (P3761, SIGMA-ALDRICH, USA), shaved off the hair on the bilateral dorsal regions for OVX surgery (*26*). The ovaries were exposed by a 2 mm incision and resected with surgical scissors. Then, other exposed tissues were repositioned and incision was sutured with 3.0 silk threads in a routine fashion. Intraperitoneal injection of penicillin was administrated. Rats in sham groups was incision without ligation of ovaries artery.

Post-surgery 3 months (*26*), animals were treated to echinops (16.26, 32.5, or 65 mg/kg/day) by oral gavage for 3 months as previously reported (*25*). Echinops was prepared as below: weigh 500 g of dried echinops at 75°C, mixed with 10-time water, decocted for 1 h and filtrated; the slag was decocted with same volume water and filtrated again; the two filtration solutions were collected and concentrated to 500 ml to obtain 1g/mL echinops stock solution. The rats in OVX and sham groups received PBS daily. E2 treatment (E2758, SIGMA-ALDRICH) was set as positive control. After 3 months, the rats were euthanized by intraperitoneal injection of 40 mg/kg pentobarbital sodium, whole blood was collected from the heart through cardiac puncture, and the femur medial malleolus specimens were selected at 1 mm under the epiphyseal plate. After centrifuged at 3,000 rpm for 10 min, serum samples were collected, filtered with 0.22 μm filter, and stored at -20°C for subsequent experiments.

2.2. *Hematoxylin and eosin (H&E) and toluidine blue O staining*

The femur bones were fixed in 10% neutral buffered formalin solution for 48 h, dehydrated in graded ethanol (70-100%, cleared in xylene, embedded in paraffin, and sectioned into 5 μm. For H&E staining, sections were stained with hematoxylin for 3-8 min and eosin for 1-3 min. For toluidine blue O staining, sections were rinsed in toluidine blue O solution for 1 min. The images were observed by Olympus BX51 light microscopy (Olympus, Japan).

2.3. *Micro-computed tomography (micro-CT) detection*

Micro-CT of left proximal medial metaphyseal tibia were acquired using Scanco Mct35 scanner (Scanco, Switzerland) at 70 KVp, 114 μA for 800 ms. Bone mineral density was evaluated based on the micro-CT results.

2.4. *Serum levels of E2, ALP, and testosterone*

After centrifuged at 3,000 rpm for 10 min, serum samples

were collected and stored at -20°C until enzyme-linked immunosorbent assay (ELISA) detection. The levels of E2 (CSB-E05108h, CUSABIO), ALP (A059-2, Nanjing Jiancheng Bioengineering Institute), and testosterone (05099h, CUSABIO) were determined by commercially ELISA kits according to manufacturer's instruction using an Multiskan microplate reader (Thermo, USA).

2.5. *qRT-PCR detection*

Total RNA from bone specimens were extracted using Trizol (Takara, Japan). The RNA quality and quantity were examined using Nanodrop 1000 spectrophotometer (NanoDrop, USA). RT reaction was performed using Bestar qPCR RT kit (ABI, USA) according to manufacturer's instruction on ABI9700 PCR system (ABI, USA). The PCR reaction was performed using DBI Bestar® SybrGreen qPCRmasterMix (ABI, USA) on Stratagene Mx3000P Real time PCR system (Agilent, USA) according to manufacturer's instruction. The primer was listed below (5'-3'): R-GADPH Forward CCTCGTCTCATAGACAAGATGGT, reversed GGGTAGAGTCATACTGGAACATG; ERα Forward AAGAAGAATAGCCCCGCCC, reversed GCCAGGTTGGTCAATAAGCC; ERβ Forward ATGCCCTGGTCTGGGTGAT, reversed CCCCGAGATTGAGGACTTGT. Glyceraldehyde 3-phosphate dehydrogenase (GAPDH) was used as internal control. Relative expression was calculated using $2^{-\Delta\Delta Ct}$ method and normalized to sham group.

2.6. *Bone marrow-derived bone marrow stem cell (BMSC) isolation and flow cytometry identification*

The rat femur was rinsed in PBS containing 1% penicillin-streptomycin. After removal of both ends in joints, the bone was rinsed in DMEM with low glucose by a syringe until the bone pale. The mediums were collected and centrifuged at 800 rpm for 5 min. Cells were resuspended into DMEM with low glucose and cultured in incubator at 37°C, 5%CO2. After 48 h, cells were stained with primary antibodies of CD29 (ab179471, Abcam, USA), CD90 (ab216449, Abcam), CD45 (ab10558, Abcam), CD11b (ab128797, Abcam), and FITC-conjugated secondary antibody (ab6717, Abcam) in the darker for 30 min. The CD29, CD90, CD45, CD11b positive cells were analyzed using Epics-XL II flow cytometry (Beckman Coulter, USA).

2.7. *Cell viability and colon formation*

Cell viability was detected with a cell counting-8 kit (CCK-8, Beyotime, China). Cells (5x105 cells) were seeded in 96-well plates and incubated with echinops-containing serum for 24, 48 and 72h. Then, CCK-8 was added and the absorbance was detected at 450 nm on microplate reader. For colon formation assay, cells

were seeded in 6-well plates at 8×10^4 cells/well with echinops-containing serum for 13 days. Then, cells were fixed with 4% paraformaldehyde and stained with 0.1% crystal violet.

2.8. *Western blotting*

Protein was extracted using RIPA (Beyotime, China) with PMSF (1:100) at 4°C for 30 min, and quantified by BCA assay (#23227, Thermo, USA). 30 μg protein was separated by 8%SDS-PAGE and transferred to PVDF membranes (IPVH00010, Millipore, USA). The membrane was incubated with 5% non-fat milk for 30 min, and incubated with primary antibodies ERα (1:2,000), ERβ (1:4,000), AKT (1:1,500), p-AKT (1:1,000), ERK (1:1,000), p-ERK (1:2,000), and GAPDH (1:10,000) antibody at room temperature for 1 h, and then incubated with HRP goat anti-rabbit IgG secondary antibody (1:20,000, BOSTER, China) at room temperature for 40 min. The blots were detected using Immobilon Western CHEMILUM HRP Substrate (WBKLS0500, Millipore, USA), and light-producing reactions are captured with X-ray film.

2.9. *Statistical analysis*

Data were expressed as mean ± standard deviation, and compared using one-way analysis of variance (ANOVA) followed by Tukey's multiple comparison test. Statistical analyses were performed using the SPSS 10.0 software (SPSS, USA). Significance was considered at $p < 0.05$.

3. Results

3.1. *Echinops increased BMD and E2, but reduced ALP and testosterone in dose-dependent manners*

BMD at 90 days post-treatment was analyzed by micro-CT (Figure 1A). Compared with sham group, a significant reduction in BMD of cortical bone in OVX group was observed ($p < 0.01$). 16.25 mg/kg echinops not significantly increased the trabecular BMD, whereas 32.5 mg/kg ($p < 0.05$), 65 mg/kg ($p < 0.001$) and E2 significantly increased the BMD of trabecular bone in comparison to the untreated OVX rats.

The rats in OVX group showed lower level of E2 ($p < 0.01$, Figure 1B), and higher levels of ALP ($p < 0.01$, Figure 1C) and testosterone ($p < 0.01$, Figure 1D) than sham group. 16.26 mg/kg echinops not significantly changed the levels of E2 and testosterone, but significantly inhibited ALP level ($p < 0.01$) in comparison to the OVX group. 32.5 mg/kg and 65 mg/kg echinops significantly increased E2 level but decreased levels of ALP and testosterone in OVX rats (Figure 1B-D). There was not significant difference in ALP level between 32.5 mg/kg and 65 mg/kg treatment groups (Figure 1C).

Thus, echinops increased BMD and level of E2, but decreased levels of ALP and testosterone in concentration- dependent manners.
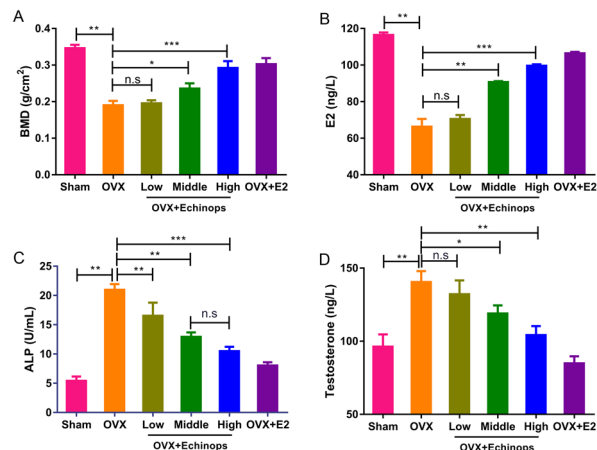
3.2. Echinops induced expression of ERα and ERβ

To detect the role of echinops on ERα and ERβ expression, qRT-PCR assays were performed (Figure 2). Compared with sham group, a significant decrease in ERα and ERβ mRNA expressions were shown in OVX

rats (Figure 2A and B). Echinops administrated at 16.26, 32.5 and 65 mg/kg significantly increased ERα and ERβ expressions in comparison to OVX group, showing a dose-dependent manner (Figure 2A and B).

3.3. Echinops inhibited osteopenia induced by OVX

After surgery for 90 days (*26*), rats in sham and OVX group were treated with echinops (32.5 mg/kg) or E2 for 90 days. Then, rats were euthanized and bones were collected. HE and toluidine blue O stainings showed a typical osteopenia with widened intertrabecular spaces, loss of trabecular bone thickness and interconnectivity in OVX group, compared with sham group (Figure 3). Echinops or E2 treatment significantly increased trabecular interconnectivity, thickness of trabeculae, and connection of trabecula, compared with OVX group, suggesting echinops inhibited the osteopenia induced by OVX (Figure 3).

3.4. Isolation and identification of BMSCs

To explore the mechanism in echinops treated osteoporosis, BMSCs were isolated and identified by flow cytometry of CD29, CD90, CD45, and CD11b. There were 90.6% isolated-cells positively expressed CD29 (Figure 4A), 93.8% positively expressed CD90 (Figure 4B), but only 4.5% positively expressed CD45 (Figure 4C), only 1.3% positively expressed CD11b (Figure 4D). These results suggested the isolated cells were almost BMSCs.

3.5. Echinops enhanced cell viability and ability of colony formation of BMSCs

To evaluate role of echinops in cell proliferation of BMSCs, cell viability (Figure 5A) and colony formation (Figure 5B and C) were performed. Echinops-containing serum (65 mg/kg) significantly increased cell viability (Figure 5A). Moreover, echinops-containing serum significantly increased colony formation of BMSCs in a dose-dependent manner ($p < 0.01$ at 16.26 and 32.5 mg/kg, and $p < 0.001$ at 65 mg/mg, Figure 5B). These

Figure 1. Micro-CT detection of bone mineral density (BMD) and Elisa detection of E2, ALP, testosterone levels. After surgery for 90 days and treatment for 90 days, **(A)** micro-CT was performed. Serum E2 **(B)**, ALP **(C)**, and testosterone **(D)** levels were detected by ELISA. Low: 16.26 mg/kg; middle: 32.5 mg/kg; high: 65 mg/kg. *$p < 0.05$, **$p < 0.01$, ***$p < 0.001$, n.s: not significant by ANOVA test.
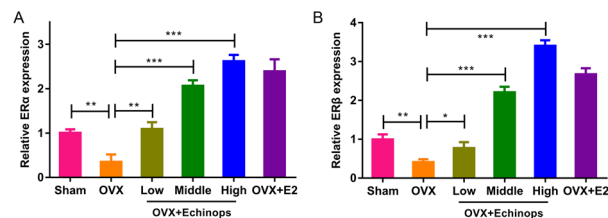
Figure 2. Effects of echinops on ERα and ERβ expression. After surgery for 90 days and treatment for 90 days, qRT-PCR detection of ERα mRNA **(A)** and ERβ mRNA **(B)**. Low: 16.26 mg/kg; middle: 32.5 mg/kg; high: 65 mg/kg. *$p < 0.05$, **$p < 0.01$, ****$p < 0.001$ by ANOVA test.

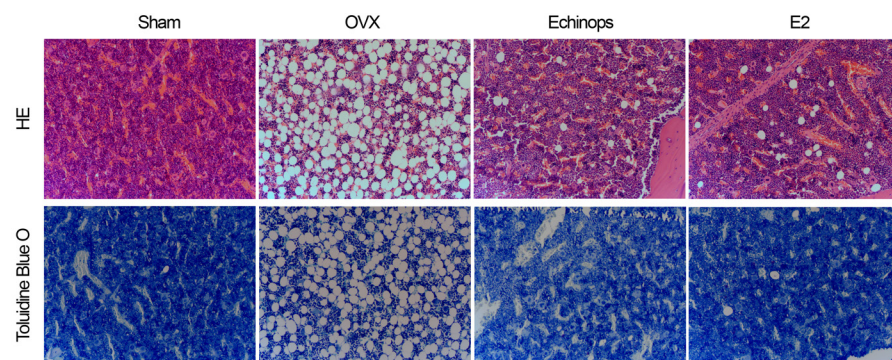**Figure 3. Echinops inhibited osteopenia induced by OVX.** After surgery for 90 days, rats were treated with echinops (32.5 mg/kg) or E2 for 90 days. HE and toluidine blue O staining were performed. 200X; arrow heads: loss of interconnectivity; arrow: trabecular bones.
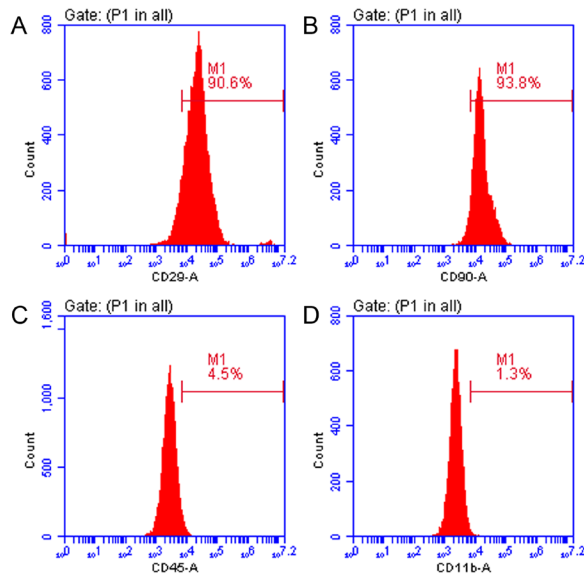
Figure 4. Identification of BMSCs isolated from rats. Flow cytometry detection of **(A)** CD29, **(B)** CD90, **(C)** CD45 and **(D)** CD11b on isolated cells were performed.

results suggested echinops-containing serum induced cell proliferation of BMSCs in a dose-dependent manner.

3.6. *Echinops increased ERα, ERβ, p-AKT, and P-ERK in BMSCs*

To explore the mechanism in echinops treated osteoporosis, expressions of ERα, ERβ, AKT, p-AKT, ERK, and p-ERK in BMSCs after echinops-containing serum treatment were examined (Figure 6). After treatment of Echniops-containing serum, ERα and ERβ levels were significantly increased compared with control BMSCs (Figure 6A and B). Moreover, the phosphorylations of AKT and ERK were significantly induced in a dose-dependent manner (Figure 6C and D).

4. Discussion

In this study, it was demonstrated that echinops functions like estrogen. It can effectively prevent and treat PMOP. Administrating echinops to ovariectomy-induced PMOP model, the BMD and serum level of E2 were increased, serum levels of ALP and testosterone were decreased. Echinops induced expression of ERα and ERβ in OVX rats. The mechanism in echinops prevented PMOP was explored by treating isolated BMSCs with echinops-containing serum. Echinops-containing serum significantly increased cell viability and colony formation of BMSCs, and increased ERα, ERβ, p-AKT, and P-ERK in BMSCs.

Rats are the most used model animal in the studies of osteoporosis so far (*14,27*). After ovariectomy in female rats, bone turnover accelerated, bone loss and bone strength decreased, which was similar to that of people after menopause (*28*). Using OVX model, it is
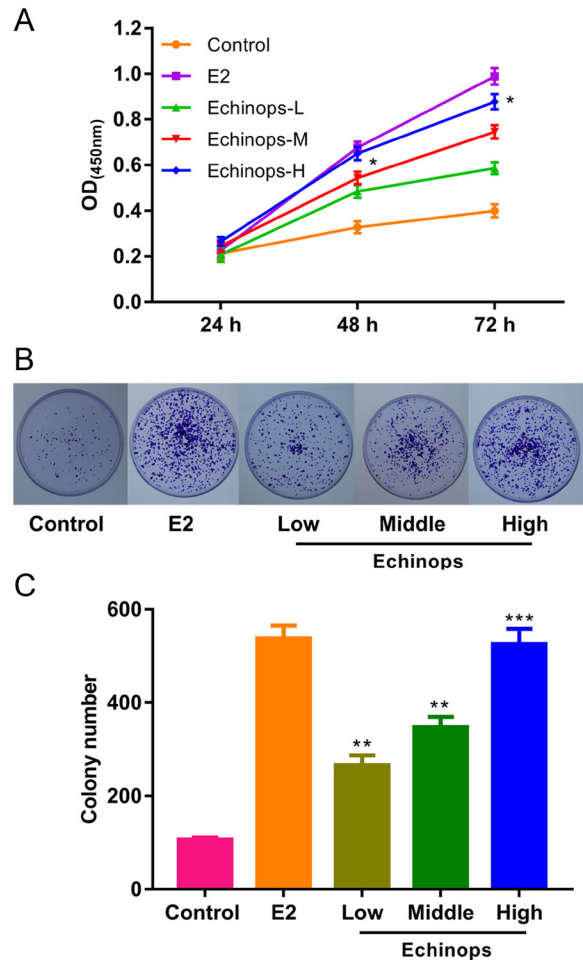
Figure 5. Effects of echinops-containing serum on cell viability and colony formation. BMSCs were treated with Echniops-containing serum that collected from rats administrated with 16.26 (low), 32.5 (middle), and 65 (high) mg/kg echinops. **(A)** Cell viability. **(B, C)** Colony formation. *$p < 0.05$, **$p < 0.01$, ***$p < 0.001$ *vs*. control.
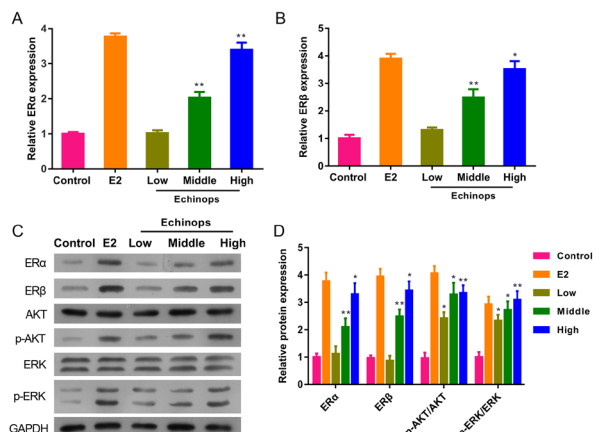
Figure 6. Effects of echinops-containing serum on expressions of ERα, ERβ, AKT, p-AKT, ERK, and P-ERK in BMSCs. BMSCs were treated with Echniops-containing serum that collected from rats administrated with 16.26 (low), 32.5 (middle), and 65 (high) mg/kg echinops. **(A)** ERα mRNA. **(B)** ERβ mRNA. **(C)** ERα, ERβ, AKT, p-AKT, ERK, and p-ERK. **(D)** Quantification of western bolts. *$p < 0.05$, **$p < 0.01$ *vs*. control.

easy to observe the effect of aging on bone tissue, the distribution and reconstruction of cancellous bone in rats and trabecular bone reconstruction of lamellar bone that similar to human (*28*). In the present study, a PMOP animal model was established in ovariectomized rats. The ovaries were artificially removed and the estrogen deficiency was induced in rats. The ERα and ERβ levels were also decreased. After 3 months, osteoporosis model was successfully replicated in OVX rats as previously described (*26*).

Estrogen is recognized drug in the prevention and treatment of PMOP, and diethylstilbestrol (E2) is a synthetic non-steroidal estrogen which can produce pharmacological and therapeutic effect similar to natural estradiol, and significantly reduce the ovariectomy-induced high bone turnover and -reduced bone resorption (*29,30*). Therefore, this study selected E2 as a positive control drug to validate the mechanism of Mongolian medicine echinops in PMOP treatment. Similar effects to E2 was demonstrated in this study.

After menopause, women's estrogen levels decreased significantly, estrogen through the estrogen receptor (ER) directly effect on the osteoblast and osteoclasts, lead to imbalance of bone resorption and bone formation, resulting in reduced bone mass and BMD, increased bone fragility and the occurrence of osteoporosis (*31,32*). The decrease of estrogen level and the decrease of the expression of ER in bone tissue are one of the most important pathogenesis. Estrogen can directly stimulate osteoblasts formation, inhibit osteoclasts activity, and regulate and control the balance of bone formation and bone resorption through ER. ER is expressed in both osteoblasts and osteoclasts (*33,34*). Osteoclasts is a very active metabolic giant multinucleated cells, recruited in the bone surface, and played important role in bone resorption and formation of lacuna through release of enzyme and acidic substances such as ALP to dissolve the bone matrix (*34,35*). Osteoblasts can synthesize the basic bone material, induces the formation of bone (*33*). The combination of estrogen and ER in osteoclasts induces the apoptosis of osteoclasts and osteoclasts precursors, reduces the number of osteoclasts. On the other hand, the combination of estrogen and ER in osteoclasts inhibited the recruitment and differentiation of osteoclasts precursors. In addition, estrogen regulated by osteoprotegerin/osteoprotegerin ligand (OPG/OPGL) system (*36*). The decline in estrogen levels results in a dysregulated ratio of osteoprotegerin/osteoprotegerin ligands leading to PMOP (*37*).

It was demonstrated that echinops decreased the serum level of bone Glp protein, interleukin-1, but increased serum level of ALP, increasing BMD, and inhibiting osteoporosis in ovariectomized (OVX) rats (*23-25*). Activation of ERK/PI3K plays important role in ER-mediated cell proliferation (*38*). Daidzein stimulated osteogenesis was mediated by both ERα and ERβ, and activation of ERK/PI3K pathway (*39*). Consistently, the

findings in this study showed echinops reduced ALP and testosterone serum levels in OVX rats, increased BMD and inhibited osteoporosis. In isolated BMSCs, echinops induced cell proliferation, increased ERα, ERβ, p-AKT, and P-ERK. This might associate with the enhancement of osteoblasts differentiation from BMSCs, inhibiting bone absorption and promote bone formation.

In conclusion, Mongolian echinops reduced bone loss and delayed the occurrence and development of PMOP, and increased ERα, ERβ, p-AKT, and p-ERK in BMSCs. These results provide experimental basis for clinical prevention and treatment of PMOP by echniops.

Acknowledgements

References

1. Zeng Y, Wu J, He X, Li L, Liu X, Liu X. Mechanical microenvironment regulation of age-related diseases involving degeneration of human skeletal and cardiovascular systems. Prog Biophys Mol Biol. 2017; pii: S0079-6107(17)30175-X. doi: 10.1016/j.pbiomolbio.2017.09.022
2. Aggarwal L, Masuda C. Osteoporosis: A quick update. J Fam Pract. 2018; 67:59-65.
3. Sobieszczańska M, Jonkisz J, Tabin M, Laszkiszcząchor K. Osteoporosis: genetic determinants and relationship with cardiovascular disease. Adv Clin Exp Med. 2013; 22:119-124.
4. Chang Y, Huang C, Hwang J, Kuo J, Lin K, Huang H, Bagga S, Kumar A, Chen F, Wu C. Fracture liaison services for osteoporosis in the Asia-Pacific region: current unmet needs and systematic literature review. Osteoporos Int. 2018; 29:779-792.
5. Lems WF, Raterman HG. Critical issues and current challenges in osteoporosis and fracture prevention. An overview of unmet needs. Ther Adv Musculoskelet Dis. 2017; 9:299-316.
6. McMillan LB, Zengin A, Ebeling PR, Scott D. Prescribing Physical Activity for the Prevention and Treatment of Osteoporosis in Older Adults. Healthcare (Basel). 2017; 5. pii: E85.
7. Peng L, Luo Q, Lu H. Efficacy and safety of bazedoxifene in postmenopausal women with osteoporosis: A systematic review and meta-analysis. Medicine (Baltimore). 2017; 96:e8659.
8. Lello S, Sorge R, Surico N. Osteoporosis's Menopausal Epidemiological Risk Observation (O.M.E.R.O.) study. Gynecol Endocrinol. 2015; 31:992-998.
9. Lo SS. Bone health status of postmenopausal Chinese women. Hong Kong Med J. 2015; 21:536-541. (in Chinese)
10. Mendoza N, Sanchez-Borrego R, Villero J, et al. 2013 Update of the consensus statement of the Spanish Menopause Society on postmenopausal osteoporosis. Maturitas. 2013; 76:99-107.
11. Forstein DA, Bernardini C, Cole RE, Harris ST, Singer A. Before the breaking point: reducing the risk of

osteoporotic fracture. J Am Osteopath Assoc. 2013; 113:S5-24; quiz S25.

12. Brynin R. Soy and its isoflavones: A review of their effects on bone density. Altern Med Rev. 2002; 7:317-327.

13. Fan JZ, Yang L, Meng GL, Lin YS, Wei BY, Fan J, Hu HM, Liu YW, Chen S, Zhang JK, He QZ, Luo ZJ, Liu J. Estrogen improves the proliferation and differentiation of hBMSCs derived from postmenopausal osteoporosis through notch signaling pathway. Mol Cell Biochem. 2014; 392:85-93.

14. Gambacciani M, Levancini M. Management of postmenopausal osteoporosis and the prevention of fractures. Panminerva Med. 2014; 56:115-131.

15. Miyamoto T. Mechanism Underlying Post-menopausal Osteoporosis: HIF1alpha is Required for Osteoclast Activation by Estrogen Deficiency. Keio J Med. 2015; 64:44-47.

16. Fontenot HB, Harris AL. Pharmacologic management of osteoporosis. J Obstet Gynecol Neonatal Nurs. 2014; 43:236-245.

17. Maichuk E, Voevodina IV, Mitrokhina TV, Makarova IA, Iureneva SV. The risk of atherosclerosis and osteoporosis development in post-ovariectomy syndrome women during hormone replacement therapy. Ter Arkh. 2014; 86:75-79. (in Russian)

18. Tella SH, Gallagher JC. Prevention and treatment of postmenopausal osteoporosis. J Steroid Biochem Mol Biol. 2014; 142:155-170.

19. Wuttke W, Jarry H, Haunschild J, Stecher G, Schuh M, Seidlova-Wuttke D. The non-estrogenic alternative for the treatment of climacteric complaints: Black cohosh (Cimicifuga or Actaea racemosa). J Steroid Biochem Mol Biol. 2014; 139:302-310.

20. Ge JR, Xie LH, Chen J, Li SQ, Xu HJ, Lai YL, Qiu LL, Ni CB. Liuwei Dihuang Pill treats postmenopausal osteoporosis with Shen (Kidney) yin deficiency *via* Janus kinase/signal transducer and activator of transcription signal pathway by up-regulating cardiotrophin-like cytokine factor 1 expression. Chin J Integr Med. 2016; doi: 10.1007/s11655-016-2744-2.

21. Shuai B, Shen L, Zhu R, Zhou P. Effect of Qing'e formula on the *in vitro* differentiation of bone marrow-derived mesenchymal stem cells from proximal femurs of postmenopausal osteoporotic mice. BMC Complement Altern Med. 2015; 15:250.

22. Parhat R, Makabel B, Nurhabek U, Tohonrbek A, Hayni, Song FF, Baysanbek A, Yang HY, Ding G, Zou ZM. Overview of application and research of Echinops genus in Chinese medicine. China Journal of Chinese Materia Medica. 2014; 39:3865. (in Chinese)

23. Liu Y, Ya-Bo JU, Chang H, Tcm DO, Hospital A. Laboratory study of the effects of mongolian echinops on bgp and ct of postmenopausal osteoporosis in experimental rat. Journal of Inner Mongolia Medical University. 2014; 36(S1): 7-11. (in Chinese)

24. Gao X, Guan L. Effect of Mongolian Blue Thorn on Serum Alkaline Phosphatase and Interleukin-1 of Ovariectomized Rats. Chinese Archives of Traditional Chinese Medicine. 2016; 34(12):2924-2926. (in Chinese)

25. Gao XM, Chang H, Ding CH. Effect of Mongolian Blue Thorn on Bone Mineral Density and the Maximum Deflection of Bone in Ovariectomized Rats. Guiding Journal of Traditional Chinese Medicine & Pharmacy. 2016; 22(24):16-19. (in Chinese)

26. Shahrezaee M, Oryan A, Bastami F, Hosseinpour S, Shahrezaee MH, Kamali A. Comparative impact of systemic delivery of atorvastatin, simvastatin, and lovastatin on bone mineral density of the ovariectomized rats. Endocrine. 2018; 60:138-150.

27. Peng J, Lai ZG, Fang ZL, Xing S, Hui K, Hao C, Jin Q, Qi Z, Shen WJ, Dong QN, Bing ZH, Fu DL. Dimethyloxalylglycine prevents bone loss in ovariectomized C57BL/6J mice through enhanced angiogenesis and osteogenesis. PLoS One. 2014; 9:e112744.

28. Compston JE. Sex steroids and bone. Physiol Rev. 2001; 81:419-447.

29. Li L, Chen X, Lv S, Dong M, Zhang L, Tu J, Yang J, Zhang L, Song Y, Xu L, Zou J. Influence of exercise on bone remodeling-related hormones and cytokines in ovariectomized rats: A model of postmenopausal osteoporosis. PLoS One. 2014; 9:e112845.

30. Parker SE, Troisi R, Wise LA, Palmer JR, Titus-Ernstoff L, Strohsnitter WC, Hatch EE. Menarche, menopause, years of menstruation, and the incidence of osteoporosis: the influence of prenatal exposure to diethylstilbestrol. J Clin Endocrinol Metab. 2014; 99:594-601.

31. Imai Y. Regulation of bone metabolisms by estrogen/ estrogen receptors signaling. Clin Calcium. 2013; 23:1621-1626. (in Japanese)

32. Xu B, Lovre D, Mauvais-Jarvis F. Effect of selective estrogen receptor modulators on metabolic homeostasis. Biochimie. 2016; 124:92-97.

33. Denger S, Reid G, Gannon F. Expression of the estrogen receptor during differentiation of human osteoclasts. Steroids. 2008; 73:765-774.

34. Sjogren K, Lagerquist M, Moverare-Skrtic S, Andersson N, Windahl SH, Swanson C, Mohan S, Poutanen M, Ohlsson C. Elevated aromatase expression in osteoblasts leads to increased bone mass without systemic adverse effects. J Bone Miner Res. 2009; 24:1263-1270.

35. Park K, Ju WC, Yeo JH, Kim JY, Seo HS, Uchida Y, Cho Y. Increased OPG/RANKL ratio in the conditioned medium of soybean-treated osteoblasts suppresses RANKL-induced osteoclast differentiation. Int J Mol Med. 2014; 33:178-184.

36. Su X, Liao EY, Peng J, Wu XP. The effects of 17 β-estradiol on the expression of osteoprotegerin, the ligand of osteoprotegerin and related cytokines in osteosarcoma MG63 cells. Zhonghua Nei Ke Za Zhi. 2003; 42:800-803. (in Chinese)

37. Ikeda T, Utsuyama M, Hirokawa K. Expression profiles of receptor activator of nuclear factor kappaB ligand, receptor activator of nuclear factor kappaB, and osteoprotegerin messenger RNA in aged and ovariectomized rat bones. J Bone Miner Res. 2001; 16:1416-1425.

38. Wang Y, Wang WL, Xie WL, Li LZ, Sun J, Sun WJ, Gong HY. Puerarin stimulates proliferation and differentiation and protects against cell death in human osteoblastic MG-63 cells *via* ER-dependent MEK/ERK and PI3K/Akt activation. Phytomedicine. 2013; 20:787-796.

39. Jin X, Sun J, Yu B, Wang Y, Sun WJ, Yang J, Huang SH, Xie WL. Daidzein stimulates osteogenesis facilitating proliferation, differentiation, and antiapoptosis in human osteoblast-like MG-63 cells *via* estrogen receptor-dependent MEK/ERK and PI3K/Akt activation. Nutr Res. 2017; 42:20-30.

Original Article

Serum containing Buyang Huanwu decoction prevents age-associated migration and invasion of human vascular smooth muscle cells by up regulating SIRT1 expression

Li Zhang[1,§,*], Chunshan Wei[2,§], Yunjun Ruan[3], Yanan Zhang[4], Yuliang Zhou[1], Da Lei[1,*]

[1] *Department of Cardiology, The First Affiliated Hospital of Guangdong Pharmaceutical University, Guangzhou, China;*
[2] *Department of Liver Disease, Shenzhen Hospital Affiliated to Guangzhou University of Chinese Medicine, Shenzhen, China;*
[3] *Department of Cardiology, Guangzhou General Hospital of Guangzhou Military Command, Guangzhou, China;*
[4] *Veterinary medicine, Northeast Agricultural University, Haerbin, China.*

Summary	The migration and invasion of vascular smooth muscle cells (VSMCs) caused by advanced aging play an important role in diffuse intimal thickening, facilitate adverse arterial remodeling and contribute to the initiation and progression of cardiovascular diseases. The inhibitory function of Buyang Huanwu decoction (BYHWD) has been found on aortic intimal hyperplasia and VSMC proliferation, but its effect on age-associated migration and invasion remains unknown. Here, we used an *in vitro* angiotensin II (Ang II)-induced senescence model to study the effects of serum containing BYHWD (BYHWS) on the migratory and invasive capacities, matrix metalloprotease type 2 (MMP-2) expression and modulation of sirtuin1 (SIRT1) signaling in human aorta VSMCs (HA-VAMCs). Our results showed that BYHWS was able to inhibit Ang II-induced migration and invasion, with down-regulation of MMP-2. In addition, manipulation of SIRT1 by either over-expression or siRNA knockdown ameliorated or promoted cellular migration and invasion, respectively. Moreover, BYHWS reversed senescence-mediated decrease of SIRT1 levels and SIRT1 was required for BYHWS regulation on migration and invasion of senescent HA-VAMCs. In summary, our data demonstrated that BYHWS suppressed the migration and invasion of age-associated VSMC *via* an increase of the SIRT1 level, which provides novel insights for the therapy of age-associated cardiovascular diseases.

Keywords: Buyang Huanwu decoction, vascular smooth muscle cells, senescence, migration/invasion, matrix metalloprotease type 2, sirtuin1 (SIRT1)

1. Introduction

Vascular aging has been viewed as a specific risk factor of cardiovascular diseases (CVD), such as atherosclerosis and hypertension (*1-4*). A complex series of events are involved in remodeled arterial wall with advanced aging, including migration and invasion of

abnormal vascular smooth muscle cells (VSMC), which significantly contribute to diffuse intimal thickening and the onset and progression of CVD (*2,3*). Previous data on interventions in age-associated VSMC migration and invasion indicated modulation of decrease and delay of the occurrence of severe CVD (*4*). New classes of drugs are currently being tested for CVD prevention, including glitazones and rimonabant. However, adverse effects such as heart failure and depression were found during the application of these treatments (*5*). Therefore, novel therapy remains to be developed.

It has been implicated that traditional Chinese Medicine (TCM) exerts a regulatory effect on the inhibition of aging, as well as the migration and invasion of VSMCs in diseased arteries (*6-9*). However, little is known about the effects of Buyang Huanwu decoction

(BYHWD) on aging. BYHWD, a classic TCM formulation featured as Qi-tonifying, stasis-eliminating, and has been used for therapy of stroke for centuries (*10,11*). Interestingly, cumulative evidence revealed that one of the mechanisms of BYHWD on various diseases represents a target to vascularity (*10,11*). For example, BYHWD shows a protective effect on cerebral arteries, coronary arteries and pulmonary arteries, *etc.* (*11*), the underlying molecular mechanisms of which relies on its pharmacological role in anti-inflammation, anti-oxidative, anti-apoptosis and anti- angiotensin II (Ang II) (*12-14*). Of note, it has been shown that BYHWD could inhibit VSMC proliferation caused by injury- or platelet-derived growth factor (*15,16*). In this scenario, there is potential role for BYHWD to control age-associated migration and invasion of serum containing BYHWD (VSMCs).

Age-associated VSMC migration/invasion represents a complex process and is regulated by multiple factors. Ang II is a major inductor of VSMCs senescence, and has been shown to potently simulate VSMCs migration and invasion (*17-21*). In addition, inhibition of Ang II pathways has been shown to substantially reduce age-associated arterial remodeling (*3,4*). The basement membrane which surrounds VSMC is cleaved by matrix metalloprotease (MMP) and restructured for age-associated migration and invasion (*2,3,22*). Exposure of new VSMCs to Ang II *via* activation of MMP- 2 increases the invasive capacity of old cells whereas MMP inhibitor reverses this effect (*23,24*). Emerging evidence points to sirtuin1 (SIRT1) as a contributer to the regulation of health and lifespan (*25,26*). It has been demonstrated that over-expression of SIRT1 and an activator of SIRT1 (*e.g.* resveratrol) markedly inhibits VSMCs migration and invasion (*27,28*).

Serum pharmacology is generally accepted as a standardized experimental method for use of TCM in *in vitro* experiments. Serum containing BYHWD (BYHWS) has been developed and described as an *in vitro* model of BYHWD treatment (*29,30*). To determine the role of BYHWS in the regulation of age-associated VSMCs migration and invasion, we induced human VSMC senescence by Ang II treatment and cultured VSMC in the presence or absence of BYHWS. We then assessed the consequences of invasion and migration capacities, MMP-2 expression and change of SIRT1 signaling.

2. Materials and Methods

2.1. *Animals and preparation of drug-containing serum*

Male Sprague-Dawley (SD) rats, aged 6-8 weeks, were purchased from Guangdong Medical Laboratory Animal Center (Guangzhou, China). All rats were caged under conditions of temperature control with water and food *ad libitum*. The experimental procedures and protocols were approved by the Institutional Animal Care and Use Committee of Guangdong Pharmaceutical University.

BYHWD was composed of *Huangqi* (Radix Astragali seu Hedysari), *Danggui* (Radix Angelica sinensis), *Chishao* (Radix Paeoniae Rubra), *Chuanxiong* (Rhizoma Ligustici Chuanxiong), *Honghua* (Flos Carthami), *Taoren* (Semen Persicae) and *Dilong* (Pheretima). The components were purchased from the First Affiliated Hospital of Guangdong Pharmaceutical University (Guangzhou, China) and mixed in a ratio of 120:6:4.5:3:3:3:3 (dry weight). BYHWD was boiled and concentrated to a final concentration of 1 g/mL (equivalent to dry weight of raw materials). The 28 SD rats were then randomly divided into 2 groups: control group (*n* = 12) and BYHWD group (*n* = 16). BYHWD (18.5 g/Kg, equivalent to adult human dose) was intragastricly administrated for 7 days (twice per day) according to previous reports (*30,31*). Control group was treated with distilled water correspondingly. After the rat was fasted for 12 h and received the last administration of medicine for 90 min, abdominal aortic blood was collected. Blood samples were allowed to clot for 2 h at 4°C and then centrifuged at 1,500 ×g for 20 min. The serum was filtered and stored at -20°C after inactivation at 56°C for 30 min. Serum containing BYHWD and control was defined as BYHWS and CS.

2.2. *Cell culture*

Human aorta VSMCs (HA-VSMCs), obtained from ATCC (CRL-1999, Manassas, VA, USA), were cultured in F-12K medium (ATCC) containing 0.05 mg/mL ascorbic acid, 0.01 mg/mL insulin, 0.01 mg/mL transferrin, 10 ng/mL sodium selenite, 0.03 mg/mL endothelial cell growth supplement (ECGS), 10 mM hydroxyethyl piperazine ethanesulfonic acid (HEPES) and 10 mM 2-[Tris(hydroxymethyl)-methylamino]-ethanesulfonic acid (TES), and supplemented with 10% fetal bovine serum (FBS, Gibco, Thermo Fisher Scientific, Inc., Waltham, MA, USA), 10% BYHWS or 10% CS. Cells were incubated in humidified 95% O_2 air and 5% CO_2 atmosphere at 37°C. Medium was renewed every 2 to 3 days. HA-VSMCs were cultured, passaged (less than passage 5) and treated with or without Ang II (100 nM, R&D research Inc., Minneapolis, MN, USA) for 72 h to induce senescence.

2.3. *SIRT1 siRNA silence*

HA-VSMCs were transfected with either si-SIRT1 (5 nM, AM 16708) or scrambled siRNA (Silencer Select SiRNA, 40 nM, AM 4635) (Ambion, Carlsbad, CA, USA) using Lipofectamine RNAiMAX Reagent (Invitrogen; Thermo Fisher Scientific, Inc., Waltham, MA, USA) for 6 h following manufacturer's instructions. The final concentration of si-SIRT1 and scrambled siRNA were 50 nM.

2.4. *Lentiviral activation particles transduction*

HA-VSMCs were seeded at 1×10^5 cells per well in 6-well plates and incubated with complete medium (10% FBS) overnight at 37°C. Transduction was carried out with complete medium containing 3 μg/mL Polybrene (sc-134220, Santa Cruz Biotechnology, Inc., Dallas, TX, USA). Then 10 μL of SIRT1 lentiviral activation particles (sc-400085-LAC, Santa Cruz Biotechnology, Inc.) and 10 μL of control lentiviral activation particles (sc-437282, Santa Cruz Biotechnology, Inc.) were added to the culture, followed by incubation overnight. The culture medium was then removed and replaced with appropriate treatment.

2.5. *Senescence-associated β-galactosidase (SA β-gal) Assay*

HA-VSMCs in 6-well plates were washed twice in PBS, fixed for 5 min in 4% paraformaldehyde in PBS, and stained with SA β-gal (C0602, Beyotime Biotechnology, Shanghai, China) according to the manufacturer's instructions. The percentage of SA β-gal-expressing cells was examined in 4 randomly selected fields under the microscope (Leica Microsystems GmbH, Wetlzar, Germany).

2.6. *Wound healing migration*

HA-VSMCs were seeded into 24-well plates with inserts in wells (CytoSelect, CBA-120-T, Neobioscience Biotechnology, Shenzhen, China) and grown to confluence. The monolayer cells then generated a 0.9mm "wound field" by carefully removing inserts. The cells were allowed to heal for 48 h. Cell stain solution was added to each well for 15 min and the wounded areas were viewed through a microscope. Quantitative analysis of the cell percent closure was performed using ImageJ software version 1.37 (National Institutes of Health, Bethesda, MA, USA). The level of wound-healing percent closure was evaluated by calculating the percentage of the repopulated cell surface area divided by the cell free area at the initial state. Average data were from at least three independent experiments. Appropriate intervention was performed prior to seeding.

2.7. *Invasion assay*

Serum-induced invasion movement was assessed using modified Boyden chambers equipped with 8μm pore-size polycarbonate filters (PFA8, Neuro probe, Gaithursburg, MD, USA). The upper compartment was coated with BD Matrigel (356234, Solasrbio Science & Technology Co., Ltd., Shanghai, China) to form a matrix barrier. In total, 2×10^5 cells were suspended in serum-free F-12K complete medium following appropriate treatment and added to the upper chamber. The lower chamber was filled with F-12K complete medium containing 10% FBS, 10% BYHWS or 10% CS as chemoattractant. After a 4 h incubation period at 37°C, the cells that had crossed the basement membrane and migrated to the lower side of the filter were fixed and stained with hematoxylin and eosin (Solasrbio Science & Technology Co., Ltd.). Four random fields were counted at 400× magnification for each filter.

2.8. *Western blotting analysis*

Western blot was performed according to our previous method (*32*). Briefly, whole-cell lysates were prepared and quantified. Proteins were then separated by 4-12% sodium dodecyl sulfate polyacrylamide gel electrophoresis (SDS-PAGE) (Bio-Rad Laboratories, Inc., Hercules, CA, USA) under reducing conditions and transferred onto polyvinylidene difluoride membranes. The transferred membranes were immunoblotted overnight at 4°C in phosphate buffer solution (PBS) containing primary antibodies to SIRT1 (04-1557, mouse anti-human monoclonal antibody, 1:1,000, EMD Millipore, Billerica, MA, USA), MMP-2 (AF902, goat anti-human polyclonal antibody, 1:500, R&D research Inc.), β-actin (cs-376421, mouse anti-human monoclonal antibody, 1:5,000, Santa Cruz Biotechnology, Inc.) after blocking nonpecific binding. The membranes were then incubated with horseradish peroxidase-conjugated anti-mouse/goat immunoglobulin G (BA1050 and BA1060, 1:2,000, Wuhan Boster Biological Technology, Ltd., Wuhan, China) at room temperature for 2 h. The density of the visualized bands was quantified using an image analyzer (model GS-700, Bio-Rad Laboratories, Inc.). β-actin was used as the loading control.

2.9. *Gelatin zymography*

HA-VSMCs were treated and cell supernatant was resolved onto 10% Novex gelatin zymogram gels (Invitrogen; Thermo Fisher Scientific, Inc.), run at 90 V for 3 h at 4°C. The gels were incubated in Novex zymogram renature buffer (Invitrogen; Thermo Fisher Scientific, Inc.) at room temperature for 30 min and then transferred to Novex zymogram developing buffer (Invitrogen; Thermo Fisher Scientific, Inc.) at 37°C overnight. The gels were photographed after staining with 0.2% Coomassie blue and quantified using ImageJ (National Institutes of Health).

2.10. *Statistical Analysis*

All results were presented as mean ± standard error of the mean. All experiments were repeated independently 3 times. Statistical comparisons of multiple groups were made *via* an ANOVA, followed by Bonferroni post hoc test. The differences between two groups using Student's *t* tests were two-sided. All statistical analyses
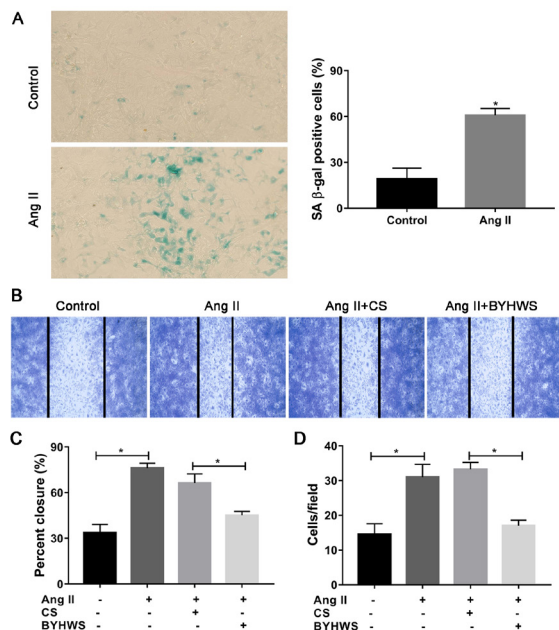
were performed using GraphPad Prism version 4.00 for windows (GraphPad Software, San Deigo, CA, USA). *P* < 0.05 was defined as statistical significance.

3. Results

3.1. *BYHWS inhibited the migration and invasion of senescent HA-VSMC*

Previous studies have shown that Ang II is an inductive agent of VSMC premature senescence (*18,19*). In this study, SA β-gal activity was measured first in HA-VSMC grown in the presence of Ang II. Cellular premature senescence induced by Ang II is shown in Figure 1A, among which the percentage of SA β-gal-positive cells was significantly increased (*p* < 0.05). To determine whether BYHWS can affect age-associated migration and invasion of VSMC *in vitro*, wound-healing and invasion assays were performed in HA-VSMC cultured by treatment with BYHWS. In contrast to control cells, the administration of Ang II significantly promoted the migration of HA-VSMCs to the wounded surface (Figure 1B and 1C). In addition, the invasion of HA-VSMCs was significantly enhanced in the presence of Ang II

compared to that of the control cells (*p* < 0.05) (Figure 1D). However, when HA-VSMCs in the presence of rat sera were analyzed, we found that the migration and invasion of Ang II-induced senescent cells cultured in 10% BYHWS were significantly decreased compared to those of cells grown in 10% CS (*p* < 0.05) (Figure 1B-1D), indicating that BYHWS inhibited migration and invasion of Ang II-induced senescent HA-VSMC.

3.2. *BYHWS reduced MMP-2 production and secretion in senescent HA-VSMC*

Since MMP-2 is a senescence marker and a key regulator in the migration and invasion of VSMCs (*2,3,22,25*), we conducted Western blotting and gelatin zymography detection to assess the effects of BYHWS on MMP-2 expression. As shown in Figure 2, Ang II treatment led to a significant increase of MMP-2 protein expression and induced its activation. Nevertheless, the treatment with serum containing BYHWD significantly reduced the expression and activation of MMP-2 protein, compared to that treated with medium containing 10% CS (*p* < 0.05) (Figure 2A and 2B).

3.3. *BYHWS delayed the down-regulation of SIRT1 protein in senescent HA-VSMCs*

A low SIRT1 level contributed to not only an acceleration of cellular senescence but also increased capacity for cellular migration and invasion (*25-28,33*). Thus we measured the levels of SIRT1 protein in the Ang II-induced HA-VSMCs. As shown in Figure 3, the amount of SIRT1 protein in HA-VSMCs progressively declined with Ang II treatment. Specifically, a 60% reduction in SIRT1 protein level was observed in Ang II-induced cells. Of note, in the Ang II-induced model,

Figure 1. BYHWS inhibited the migration and invasion of senescent HA-VSMC. (A) Representative photomicrographs and average data of SA β-gal staining in HA-VSMC with and without Ang II treatment. Scale bar indicates 50μm. *p* < 0.05 compared with control. **(B)** Representative photomicrographs of wound healing assay in HA-VSMC cultured without Ang II or with Ang II treatment in media containing 10% CS or 10% BYHWS. Original magnification ×40. **(C)** Average data of wound healing assay in HA-VSMC cultured without Ang II or with Ang II treatment in media containing 10% CS or 10% BYHWS. *p* < 0.05 in comparison between two groups. **(D)** Average data of invasion analysis of HA-VSMC cultured without Ang II or with Ang II treatment in media containing 10% CS or 10% BYHWS. *p* < 0.05 in comparison between two groups. Ang II, angiotensin II; CS, serum containing vehicle; BYHWS, serum containing Buyang Huanwu decoction.

Figure 2. BYHWS reduced MMP-2 expression in senescent HA-VSMC. (A) Representative immunoblots and average data of MMP-2 protein from HA-VSMCs without Ang II or with Ang II treatment in media containing 10% CS or 10% BYHWS. *p* < 0.05 in comparison between two groups. **(B)** Gelatin zymograms of cell supernatant from HA-VSMCs without Ang II or with Ang II treatment in media containing 10% CS or 10% BYHWS. *p* < 0.05 in comparison between two groups. Ang II, angiotensin II; CS, serum containing vehicle; BYHWS, serum containing Buyang Huanwu decoction.
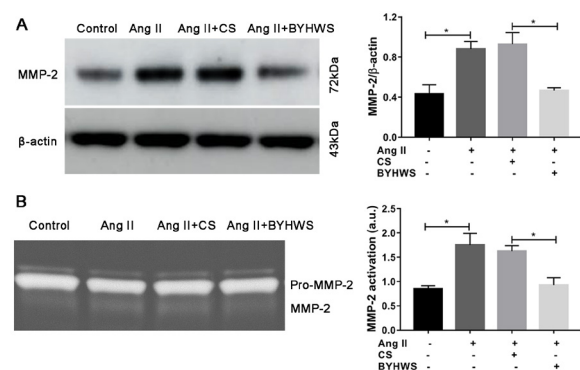
the SIRT1 protein levels in 10% BYHWS-treated cells were much higher than those found in 10% CS-treated cells. These results indicated that the administration of BYHWS significantly prevented the down-regulation of

age-associated SIRT1 caused by Ang II.

3.4. SIRT1 over-expression decreased the capacity of cell migration and invasion, as well as MMP-2 activation in senescent HA-VSMCs

To investigate the effects of SIRT1 on VSMC migration and invasion, and MMP-2 secretion, SIRT1 over-expression was conducted by transduction, and SIRT1 levels were significantly increased in SIRT1 over-expressed HA-VSMCs compared to negative lentiviral and controls ($p < 0.05$) (Figure 4A). Remarkably, the over expression of SIRT1 in senescent HA-VAMCs significantly reduced migratory and invasive capacity and MMP-2 activation compared to those of control cells ($p < 0.05$) (Figure 4B-4D).

3.5. SIRT1 was required for BYHWS's effects on the migration and invasion of senescent HA-VSMCs

We finally investigated the involvement of SIRT1 in the protective effect of BYHWS towards senescent HA-VSMC. Western blot analysis showed that after transfection of HA-VSMCs with si-SIRT1, the expression of SIRT1 protein was statistically down-regulated by approximately 45% compared to SIRT1 levels in cells
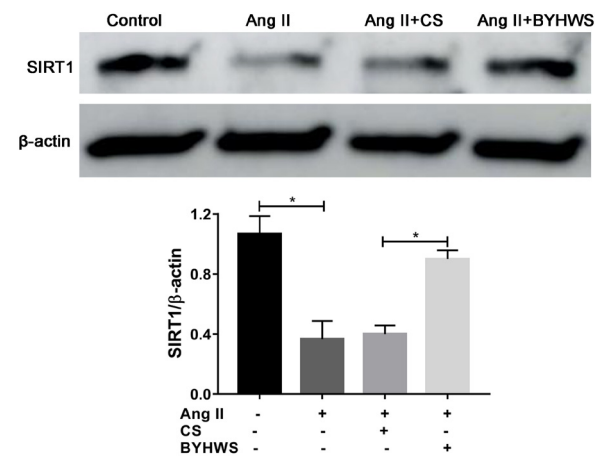
Figure 3. SIRT1 protein decreased in HA-VSMCs with Ang II-induced senescence and BYHWS retarded this effect. Representative immunoblots and average data of SIRT1 protein from HA-VSMCs without Ang II or with Ang II treatment in media containing 10% CS or 10% BYHWS. *$p < 0.05$ in comparison between two groups. Ang II, angiotensin II; CS, serum containing vehicle; BYHWS, serum containing Buyang Huanwu decoction.
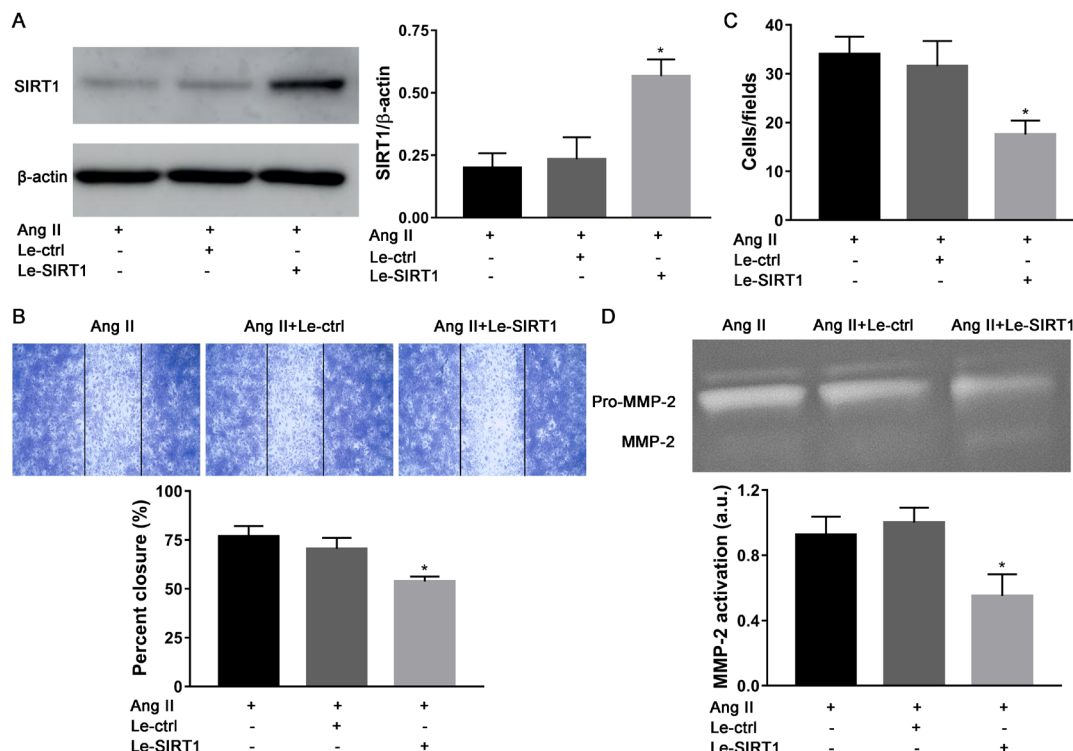
Figure 4. Over-expression of SIRT1 decreased cellular invasion and MMP-2 activation in HA-VSMCs with Ang II-induced senescence. (A) Representative immunoblots and average data of SIRT1 protein in senescent HA-VSMC transduced with Le-SIRT1 or Le-ctrl. *$p < 0.05$ compared with Ang II control. **(B)** Representative average invasion analysis of senescent HA-VSMC transduced with Le-SIRT1 or Le-ctrl. *$p < 0.05$ compared with Ang II control. **(C)** Representative average invasion analysis of HA-VSMC transduced with Le-SIRT1 or Le-ctrl. *$p < 0.05$ compared with Ang II control. **(D)** Gelatin zymograms of cell supernatant from senescent HA-VSMCs transduced with Le-SIRT1 or Le-ctrl. *$p < 0.05$ compared with Ang II control group. Ang II, angiotensin II; Le-ctrl, control lentiviral activation particles; Le-SIRT1, SIRT1 lentiviral activation particles. Ang II control group, AngII+, Le-ctrl-, Le-SIRT1-.

transfected with a negative control siRNA ($p < 0.05$) (Figure 5A). In wound healing and Boyden chamber assays, the decrease of SIRT1 expression dramatically increased the capacity of migration and invasion of senescent HA-VSMCs (Figure 5B and 5C). Moreover, si-SIRT1 also partially counteracted the inhibitory effect of BYHWS on cell migration and invasion (Figure 5B-5D). Similarly, transfection of si-SIRT1 in senescent HA-VAMCs further significantly increased MMP-2 protein and activation, and statistically abolished the protective effects of BYHWS with inhibition of MMP-2 expression

($p < 0.05$) (Figure 5E and 5F). These data suggested that BYHWS inhibited the migration and invasion of HA-VSMCs, *via* SIRT1 expression in Ang II-treated HA-VSMCs.

4. Discussion

The study of cellular processes of age-associated migration and invasion in organisms subjected to BYHWD regimens is experimentally challenging. Here, we aimed to determine the effects of BYHWS
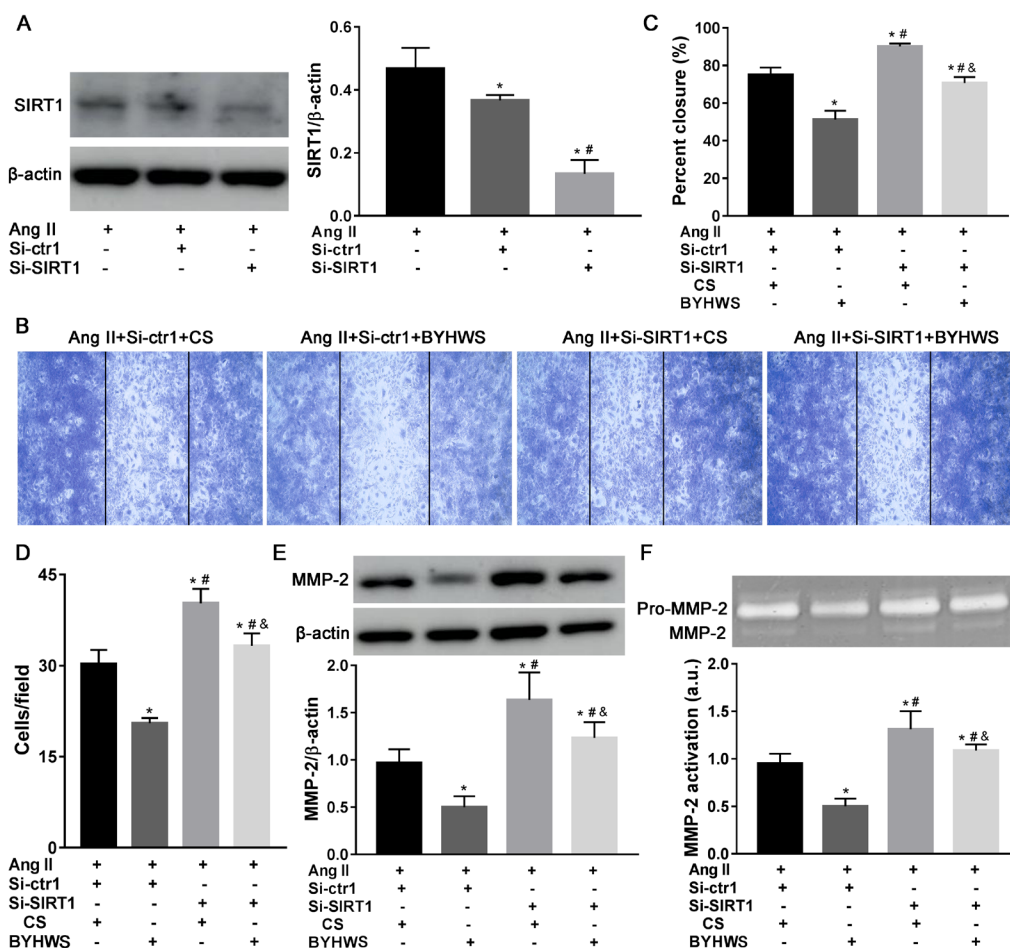
Figure 5. BYHWS modulated HA-VSMCs migration and invasion in a SIRT1-dependent manner. (A) Representative immunoblots and average data of SIRT1 protein in senescent HA-VSMC transfected with si-SIRT1 or si-ctrl. *$p < 0.05$ compared with Ang II control group. *$p < 0.05$ compared with Si-ctrl group. **(B)** Representative photomicrographs and average data of wound healing assay in HA-VSMC transfected with si-SIRT1 or si-ctrl, and then treated with Ang II in media containing 10% CS or 10% BYHWS . Original magnification ×40. *$p < 0.05$ compared with 10% CS control group. #$p < 0.05$ compared with 10% BYHWS group. &$p < 0.05$ compared with 10% CS + Si-SIRT1 group. **(C)** Representative average invasion analysis of HA-VSMC transfected with si-SIRT1 or si-ctrl, and then treated with Ang II in media containing 10% CS or 10% BYHWS. *$p < 0.05$ compared with 10% CS control group. #$p < 0.05$ compared with 10% BYHWS group. &$p < 0.05$ compared with 10% CS + Si-SIRT1 group. **(D)** Representative immunoblots and average data of MMP-2 protein from HA-VSMCs transfected with si-SIRT1 or si-ctrl, and then treated with Ang II in media containing 10% CS or 10% BYHWS. *$p < 0.05$ compared with 10% CS control group. #$p < 0.05$ compared with 10% BYHWS group. &$p < 0.05$ compared with 10% CS + Si-SIRT1 group. **(E)** Representative immunoblots and average data of MMP-2 protein from HA-VSMCs transfected with si-SIRT1 or si-ctrl, and then treated with Ang II in media containing 10% CS or 10% BYHWS. *$p < 0.05$ compared with 10% CS control group. #$p < 0.05$ compared with 10% BYHWS group. &$p < 0.05$ compared with 10% CS + Si-SIRT1 group. **(F)** Gelatin zymograms of cell supernatant from HA-VSMCs transfected with si-SIRT1 or si-ctrl, and then treated with Ang II in media containing 10% CS or 10% BYHWS. *$p < 0.05$ compared with 10% CS control group. #$p < 0.05$ compared with 10% BYHWS group. &$p < 0.05$ compared with 10% CS + Si-SIRT1 group. Ang II, angiotensin II; CS, serum containing vehicle; BYHWS, serum containing Buyang Huanwu decoction; si-ctrl, scrambled siRNA silence; si-SIRT1, SIRT1 siRNA silence. Ang II control group, Ang II+, Si-ctrl-, Si-SIRT1-. Si-ctrl group, Ang II+, Si-ctrl+, Si-SIRT1-. 10% CS control group, AngII+, Si-ctrl+, Si-SIRT1-, 10% CS+, 10% BYHWS-. 10% BYHWS group, AngII+, Si-ctrl+, Si-SIRT1-, 10% CS-, 10% BYHWS+. 10% CS + si SIRT1 group, AngII+, Si-ctrl-, Si-SIRT1+, 10% CS+, 10% BYHWS-.

on this cellular process *in vitro* using Ang II-induced senescent HA-VSMCs. Our results clearly showed that BYHWS could significantly delay age-associated increased migration and invasion of these cells, which was accompanied with reduced MMP-2 expression. In addition, we also identified SIRT1 as a pivotal factor in modulating BYHWS's effects on age-associated HA-VSMC responses.

Arterial aging is a cornerstone of systemic aging (*2,3,17*). The increase of intima thickness is nearly linearly associated with age mainly due to the migration and invasion of VSMCs from the arterial media to the intimal (*2,3,34*). While cumulative studies demonstrated that the capacity of migration and invasion was decreased in senescent VSMCs (*35,36*). Here, we used a model of HA-VSMC senescence induced by Ang II and verified that senescent HA-VSMCs enhanced migration and invasion, which was in agreement with previous reports regarding increasing migratory and invasive capacities in senescent rat VSMCs (*24,37*). Furthermore, it has been shown that Ang II can stimulate VSMC migration and invasion measured by a wound healing approach and Boyden chamber assay (*20,21*).

The precise roles mediating aging and age-associated events related with BYHWD are not fully understood. TCM of Qi-tonifying and stasis- eliminating may play a role in delaying aging, mainly due to the well-known theory that "Qi deficiency and blood stasis" is essential for human aging (*38*). In terms of vascular aging, it has been proved that TCM based on invigorating Qi and activating blood had effects on delaying VSMC senescence and lowering age-associated increase of VSMC proliferation (*6*). As a classic TCM formulation of invigorating Qi and activating blood, BYHWD can be used to treat many disorders with Qi deficiency and blood stasis, which is likely to target the specific pathogenesis of vascular diseases (*11*). BYHWD was previously shown to inhibit aortic intimal hyperplasia and cellular proliferation in cultured VSMC (*15,16*). In the current study we demonstrated for the first time that BYHWS treatment inhibited the migration and invasion of senescent HA-VSMCs. However, similar inhibition was not observed in CS-treated senescent HA-VSMCs. Other beneficial effects of BYHWD appear to promote the migration of neural precursor cells to ischemic brain areas, thus facilitating its neuroprotective effect (*39*). Under this condition, cellular migration is a nonpathogenic process for tissue repair in response to ischemic injury, which is different than the age-increased pathological process.

Uncontrolled MMPs, potently activated by Ang II, can cleave both cellular basement membrane and elastin fibers around VSMCs, which results in degradation of extracellular matrix, enabling VSMCs to migration, invasion and proliferation with advanced aging. In cultured VSMCs, both MMP-2 and MMP-9 are related to the migration and invasion of VSMCs (*2,3,22*). It has

been shown that MMP-9 is less important than MMP-2 in triggering intimal thickening in coronary artery rings *ex vivo* (*40*). Moreover, MMP-2 expression becomes increased within aging arterial walls, particularly in the thickened intima of different species including humans (*2,3,22,23*). Here, we showed that the administration of Ang II in HA-VSMCs enhanced MMP-2 expression whereas BYHWS inhibited this promoting effect. These results indicate that BYHWS treatment might retard age-associated migration and invasion through inhibition of MMP-2 in HA-VSMCs.

SIRT1 (member of the sirtuin family) is a nicotinamide adenosine dinucleotide (NAD)-dependent deacetylase that removes acetyl groups from various proteins. It has been implicated that Sirt1 can impact a wide array of proteins, such as peroxisome proliferator-activated receptor-gamma and its coactivator-1alpha, forkhead transcriptional factors, AMP-activated protein kinase, NF-kappaB and protein tyrosine phosphatase involved in cardiovascular and metabolic diseases, through regulating metabolic and physiologic processes including stress resistance, metabolism, apoptosis and energy balance (*41-43*). Notably, in the cardiovascular system, activation of SIRT1 can not only protect against oxidative stress at the cellular level, but can also elevate survival at the systemic level to reduce the risk of coronary heart disease and cerebrovascular disease (*42*). In the present study, SIRT1 levels *in vitro* as HA-VSMCs were decreased and senescence was induced. This is consistent with previous studies concerning the reduction of SIRT1 levels in senescent human VSMCs, endothelial cells and fibroblasts (*25,44,45*). Interestingly, when these senescent HA-VSMCs were cultured in the presence of BYHWS, much higher SIRT1 was induced than the same cells cultured in CS. Therefore, BYHWS protects cells against the decrease of SIRT1 associated with the senescence process. Although a study has reported that BYHWS is involved in a neuron protective role through suppression of the P53 pathway (*46*), to our knowledge, no previous studies have investigated whether BYHWS directly influences SIRT1 expression. It has been demonstrated that SIRT1's predominate function is in delaying aging and suppressing arterial remodeling (*26,27,33*). Our further experiments revealed that down regulation of SIRT1 levels by siRNA-knockdown elevated cellular migration/invasion and MMP-2, leading to enhancement in senescent HA-VSMCs. Of note, the suppression of SIRT1 reversed BYHWS-mediated inhibition of MMP-2 levels and the migration/invasion in senescent HA-VSMCs. Conversely, over-expression of SIRT1 in senescent HA-VSMCs resulted in reduced expression of MMP2 and was also consistent with concomitant decreases in cellular migration and invasion. Cumulative evidence unraveled that SIRT1 plays a pivotal role in the treatment of cardiovascular disease, through which, hydroxytyrosol, mitochondrial aldehyde dehydrogenase (ALDH2), and sulforaphane (SFN)

showed great promise for providing protection (47-50). Our data suggest that BYHWS regulation of cellular migration/invasion and MMP-2 expression in HA-VSMCs is dependent on activation of SIRT1. However, *in vitro* experiments are still required to investigate the effect of BYHWS in clinical practice, and the therapeutic value of combined use of BYHWS, ALDH2, SFN, *etc.* for instance, and requires further evaluation.

5. Conclusion

This study demonstrated that treatment with BYHWS in senescent HA-VSMCs resulted in *i*) reduced capacity of migration and invasion, *ii*) decreased MMP-2 expression, and *iii*) sustained the increase of SIRT1 levels. Our data also showed that modulation of SIRT1 levels by either knockdown or over-expression of this protein promoted or inhibited age-associated VSMC migration and invasion. Moreover, BYHWS has an effect on age-associated VSMC responses in a SIRT1-dependent manner.

Acknowledgements

References

1. Harvey A, Montezano AC, Touyz RM. Vascular biology of ageing-Implications in hypertension. J Mol Cell Cardiol. 2015; 83:112-121.
2. Wang M, Jiang L, Monticone RE, Lakatta EG. Proinflammation: The key to arterial aging. Trends Endocrinol Metab. 2014; 25:72-79.
3. Zhang G, Liu Z, Cui G, Wang X, Yang Z. MicroRNA-486-5p targeting PIM-1 suppresses cell proliferation in breast cancer cells. Tumor Biology. 2014; 35:11137.
4. Lakatta EG. So! What's aging? Is cardiovascular aging a disease? J Mol Cell Cardiol. 2015; 83:1-13.
5. Nilsson PM. Early vascular aging (EVA): Consequences and prevention. Vascular health and risk management. 2008; 4:547-552.
6. Tao LL, Lei Y, Wang GL, Zhu LQ, Wang Y. Effect of extracts from Radix Ginseng, Radix Notoginseng and Rhizoma Chuanxiong on delaying aging of vascular smooth muscle cells in aged rats. Chin J Integr Med. 2012; 18:582-590.
7. Ge X, Chen S, Liu M, Liang T, Liu C. Evodiamine Attenuates PDGF-BB-Induced Migration of Rat Vascular Smooth Muscle Cells through Activating PPARgamma. Int J Mol Sci. 2015; 16:28180-28193.
8. Hwang SM, Lee YJ, Lee YP, Yoon JJ, Lee SM, Cha JD, Choi KM, Kang DG, Lee HS. Anti-Proliferative Effect of an Aqueous Extract of Prunella vulgaris in Vascular Smooth Muscle Cells. Evid Based Complement Alternat Med. 2013; 2013:936463.
9. Shih HC, Chang KH, Chen FL, Chen CM, Chen SC, Lin YT, Shibuya A. Anti-aging effects of the traditional Chinese medicine bu-zhong-yi-qi-tang in mice. Am J Chin Med. 2000; 28:77-86.
10. Zhang W, Gao K, Liu J, Zhao H, Wang J, Li Y, Murtaza G, Chen J, Wang W. A review of the pharmacological mechanism of traditional Chinese medicine in the intervention of coronary heart disease and stroke. Afr J Tradit Complement Altern Med. 2013; 10:532-537.
11. Li JH, Liu AJ, Li HQ, Wang Y, Shang HC, Zheng GQ. Buyang huanwu decoction for healthcare: Evidence-based theoretical interpretations of treating different diseases with the same method and target of vascularity. Evid Based Complement Alternat Med. 2014; 2014:506783.
12. Jin Y, Dong L, Wu C, Qin J, Li S, Wang C, Shao X, Huang D. Buyang Huanwu Decoction fraction protects against cerebral ischemia/reperfusion injury by attenuating the inflammatory response and cellular apoptosis. Neural Regen Res. 2013; 8:197-207.
13. Liu Y, Lin R, Shi X, Fang Z, Wang W, Lin Q, Zhang J, Zhang H, Ji Q. The roles of buyang huanwu decoction in anti-inflammation, antioxidation and regulation of lipid metabolism in rats with myocardial ischemia. Evid Based Complement Alternat Med. 2011; 2011:561396.
14. Ren J, Lin C, Liu J, Xu L, Wang M. Experimental study on Qi deficiency and blood stasis induced by muti-factor stimulation in rats. Zhongguo Zhong Yao Za Zhi. 2011; 36:72-76. (in Chinese)
15. Chen G, Wu L, Deng CQ. The effects of BuYang HuanWu Decoction and its effective components on proliferation-related factors and ERK1/2 signal transduction pathway in cultured vascular smooth muscle cells. J Ethnopharmacol. 2011; 135:7-14.
16. Wu L, Zhang W, Li H, Chen BY, Zhang GM, Tang YH, He FY, Deng CQ. Inhibition of aortic intimal hyperplasia and cell cycle protein and extracellular matrix protein expressions by BuYang HuanWu Decoction. J Ethnopharmacol. 2009; 125:423-435.
17. Wang M, Khazan B, Lakatta EG. Central Arterial Aging and Angiotensin II Signaling. Curr Hypertens Rev. 2010; 6:266-281.
18. Kunieda T, Minamino T, Nishi J, Tateno K, Oyama T, Katsuno T, Miyauchi H, Orimo M, Okada S, Takamura M, Nagai T, Kaneko S, Komuro I. Angiotensin II induces premature senescence of vascular smooth muscle cells and accelerates the development of atherosclerosis *via* a p21-dependent pathway. Circulation. 2006; 114:953-960.
19. Zhao L, Li AQ, Zhou TF, Zhang MQ, Qin XM. Exendin-4 alleviates angiotensin II-induced senescence in vascular smooth muscle cells by inhibiting Rac1 activation *via* a cAMP/PKA-dependent pathway. Am J Physiol Cell Physiol. 2014; 307:C1130-1141.
20. Li Y, Wang N, Chen C, He D, Yang J, Zeng C. Inhibitory effect of D3 dopamine receptor on migration of vascular smooth muscle cells induced by synergistic effect of angiotensin II and aldosterone. Clin Exp Hypertens. 2015; 37:288-293.
21. Pantan R, Tocharus J, Phatsara M, Suksamrarn A, Tocharus C. Synergistic effect of atorvastatin and cyanidin-3-glucoside against angiotensin II-mediated vascular smooth muscle cell proliferation and migration through MAPK and PI3K/Akt pathways. Arch Pharm Res. 2016.
22. Wang M, Kim SH, Monticone RE, Lakatta EG. Matrix metalloproteinases promote arterial remodeling in aging, hypertension, and atherosclerosis. Hypertension. 2015; 65:698-703.

23. Wang M, Zhang J, Spinetti G, Jiang LQ, Monticone R, Zhao D, Cheng L, Krawczyk M, Talan M, Pintus G, Lakatta EG. Angiotensin II activates matrix metalloproteinase type II and mimics age-associated carotid arterial remodeling in young rats. Am J Pathol. 2005; 167:1429-1442.

24. Fu Z, Wang M, Gucek M, *et al.* Milk fat globule protein epidermal growth factor-8: A pivotal relay element within the angiotensin II and monocyte chemoattractant protein-1 signaling cascade mediating vascular smooth muscle cells invasion. Circ Res. 2009; 104:1337-1346.

25. de Cabo R, Liu L, Ali A, Price N, Zhang J, Wang M, Lakatta E, Irusta PM. Serum from calorie-restricted animals delays senescence and extends the lifespan of normal human fibroblasts *in vitro*. Aging (Albany NY). 2015; 7:152-166.

26. Baur JA, Ungvari Z, Minor RK, Le Couteur DG, de Cabo R. Are sirtuins viable targets for improving healthspan and lifespan? Nat Rev Drug Discov. 2012; 11:443-461.

27. Li L, Zhang HN, Chen HZ, *et al.* SIRT1 acts as a modulator of neointima formation following vascular injury in mice. Circ Res. 2011; 108:1180-1189.

28. Lin YC, Chen LH, Varadharajan T, Tsai MJ, Chia YC, Yuan TC, Sung PJ, Weng CF. Resveratrol inhibits glucose-induced migration of vascular smooth muscle cells mediated by focal adhesion kinase. Molecular nutrition & food research. 2014; 58:1389-1401.

29. Lou L, Zhou J, Liu Y, Wei YI, Zhao J, Deng J, Dong B, Zhu L, Wu A, Yang Y, Chai L. Chlorogenic acid induces apoptosis to inhibit inflammatory proliferation of IL-6-induced fibroblast-like synoviocytes through modulating the activation of JAK/STAT and NF-kappaB signaling pathways. Experimental and therapeutic medicine. 2016; 11:2054-2060.

30. Yu P, Guan L, Zhou L, Guo J, Guo R, Lin R, Ding W, Li X, Liu W. Upregulation of glutamate metabolism by BYHWD in cultured astrocytes following oxygen-glucose deprivation/reoxygenation in part depends on the activation of p38 MAPK. Exp Ther Med. 2017; 13:3089-3096.

31. Zhou YC, Liu B, Li YJ, Jing LL, Wen G, Tang J, Xu X, Lv ZP, Sun XG. Effects of buyang huanwu decoction on ventricular remodeling and differential protein profile in a rat model of myocardial infarction. Evidence-based complementary and alternative medicine : eCAM. 2012; 2012:385247.

32. Zhang L, Wu SZ, Ruan YJ, Hong L, Xing XW, Lai WY. Testosterone therapy delays cardiomyocyte aging *via* an androgen receptor-independent pathway. Braz J Med Biol Res. 2011; 44:1118-1124.

33. Zhang MJ, Zhou Y, Chen L, Wang X, Pi Y, Long CY, Sun MJ, Chen X, Gao CY, Li JC, Zhang LL. Impaired SIRT1 promotes the migration of vascular smooth muscle cell-derived foam cells. Histochem Cell Biol. 2016; 146:33-43.

34. Schmidt-Trucksass A, Grathwohl D, Schmid A, Boragk R, Upmeier C, Keul J, Huonker M. Structural, functional, and hemodynamic changes of the common carotid artery with age in male subjects. Arterioscler Thromb Vasc Biol. 1999; 19:1091-1097.

35. Thompson AM, Wagner R, Rzucidlo EM. Age-related loss of SirT1 expression results in dysregulated human vascular smooth muscle cell function. Am J Physiol Heart Circ Physiol. 2014; 307:H533-541.

36. Zhao W, Zheng XL, Peng DQ, Zhao SP. Myocyte enhancer factor 2A regulates hydrogen peroxide-induced senescence of vascular smooth muscle cells *via* microRNA-143. J Cell Physiol. 2015; 230:2202-2211.

37. Wang M, Spinetti G, Monticone RE, Zhang J, Wu J, Jiang L, Khazan B, Telljohann R, Lakatta EG. A local proinflammatory signalling loop facilitates adverse age-associated arterial remodeling. PLoS One. 2011; 6:e16653.

38. Liu LY, Sun ZQ, Xiang H. Studies on neuro-immunologic regulation of senile rats by using the principle of replenishing qi and promoting blood circulation. Zhongguo Zhong Xi Yi Jie He Za Zhi. 1997; 17:616-619. (in Chinese)

39. Kong X, Su X, Zhu J, Wang J, Wan H, Zhong M, Li L, Lin N. Neuroprotective effect of buyang huanwu decoction on rat ischemic/reperfusion brain damage by promoting migration of neural precursor cells. Rejuvenation Res. 2014; 17:264-275.

40. Louis SF, Zahradka P. Vascular smooth muscle cell motility: From migration to invasion. Exp Clin Cardiol. 2010; 15:e75-85.

41. Pillarisetti S. A review of Sirt1 and Sirt1 modulators in cardiovascular and metabolic diseases. Recent patents on cardiovascular drug discovery. 2008; 3:156-164.

42. Chong ZZ, Wang S, Shang YC, Maiese K. Targeting cardiovascular disease with novel SIRT1 pathways. Future cardiology. 2012; 8:89-100.

43. Ma L, Li Y. SIRT1: Role in cardiovascular biology. Clinica chimica acta; international journal of clinical chemistry. 2015; 440:8-15.

44. Gorenne I, Kumar S, Gray K, Figg N, Yu H, Mercer J, Bennett M. Vascular smooth muscle cell sirtuin 1 protects against DNA damage and inhibits atherosclerosis. Circulation. 2013; 127:386-396.

45. Ota H, Akishita M, Eto M, Iijima K, Kaneki M, Ouchi Y. Sirt1 modulates premature senescence-like phenotype in human endothelial cells. J Mol Cell Cardiol. 2007; 43:571-579.

46. Qu HD, Tong L, Shen JG. Effect of buyang huanwu decoction drug serum on expression of p53 and p21 genes in cultured rat's cerebral cortical neuron after hypoxia *in vitro*. Zhongguo Zhong Xi Yi Jie He Za Zhi. 2004; 24:133-135. (in Chinese)

47. Wang W, Jing T, Yang X, He Y, Wang B, Xiao Y, Shang C, Zhang J, Lin R. Hydroxytyrosol regulates the autophagy of vascular adventitial fibroblasts through the SIRT1-mediated signaling pathway. Canadian journal of physiology and pharmacology. 2018; 96:88-96.

48. Wang S, Wang C, Turdi S, Richmond KL, Zhang Y, Ren J. ALDH2 protects against high fat diet-induced obesity cardiomyopathy and defective autophagy: Role of CaM kinase II, histone H3K9 methyltransferase SUV39H, Sirt1, and PGC-1alpha deacetylation. International journal of obesity. 2018.

49. Han D, Wang J, Ma S, Chen Y, Cao F. SIRT1 as a Promising Novel Therapeutic Target for Myocardial Ischemia Reperfusion Injury and Cardiometabolic Disease. Current drug targets. 2017; 18:1746-1753.

50. Li YP, Wang SL, Liu B, Tang L, Kuang RR, Wang XB, Zhao C, Song XD, Cao XM, Wu X, Yang PZ, Wang LZ, Chen AH. Sulforaphane prevents rat cardiomyocytes from hypoxia/reoxygenation injury *in vitro via* activating SIRT1 and subsequently inhibiting ER stress. Acta pharmacologica Sinica. 2016; 37:344-353.

Original Article

Cinobufacini inhibits epithelial-mesenchymal transition of human hepatocellular carcinoma cells through c-Met/ERK signaling pathway

Fanghua Qi[1], Jinjing Wang[2], Lin Zhao[1], Pingping Cai[1], Wei Tang[3], Zhixue Wang[1,*]

[1] *Department of Traditional Chinese Medicine, Shandong Provincial Hospital affiliated to Shandong University, Ji'nan, China;*
[2] *Shandong University of Traditional Chinese Medicine, Ji'nan, China;*
[3] *Hepato-Biliary-Pancreatic Surgery Division, Department of Surgery, Graduate School of Medicine, the University of Tokyo, Tokyo, Japan.*

Summary   Cinobufacini, an aqueous extract from the skins and parotid venom glands of the toad *Bufo bufo gargarizans* Cantor, is a well known traditional Chinese medicine widely used in clinical cancer therapy in China. Its therapeutic effect is especially pronounced in liver cancer. However, the precise mechanisms induced by cinobufacini in human hepatocellular carcinoma (HCC) cells are still not very clear. Here, we investigated the effects and mechanisms of cinobufacini on inhibiting HepG2 cells invasion and metastasis. Epithelial-mesenchymal transition (EMT) is identified as an important initiation step for HCC metastasis. After the HepG2 cells were treated with different concentrations of cinobufacini, the expression of EMT related E-cadherin was increased while N-cadherin and Vimentin were decreased, and the expression of EMT related transcription factors Snail and Twist were decreased. Moreover, the phosphorylation of c-Met was inhibited by cinobufacini, and the expression of MEK1/2 and ERK1/2, the downstream kinase of the signal transduction pathway activated by c-Met, also decreased in a dose-dependent manner with cinobufacini. In addition, after the cells were treated with different concentrations of cinobufacini, there was a significant decrease in MMP-2 and MMP-9 expression in HepG2 cells. In conclusion, the current study suggested cinobufacini could prevent HepG2 cells migration and invasion *via* inhibiting EMT through c-Met/ERK signaling pathway, which might provide experimental evidence for cinobufacini treatment of HCC.

Keywords: Cinobufacini, hepatocellular carcinoma (HCC), invasion and metastasis, epithelial-mesenchymal transition (EMT), c-Met/ERK signaling pathway

1. Introduction

Hepatocellular carcinoma (HCC) is the fifth most common cancer worldwide with over 740,000 new cases per year and the second leading cause of cancer-related deaths worldwide (*1,2*). At present, resection and transplantation are still the available curative treatments, but are hampered because of their high recurrence rates and development of metastasis (*3*). Epithelial-mesenchymal transition (EMT) is an important biological process in the progression of malignant tumors. The cancer cells undergoing EMT lose their adhesion molecules such as E-cadherin, and gain mesenchymal cell markers, such as N-cadherin, Vimentin, alpha smooth muscle actin (α-SMA), fibronectin, and collagen I, which will enhance cells migration and invasion (*4*). These characteristic markers are modulated transcriptionally by several key transcription factors including Snail, Slug, Zeb, Twist and so forth (*5*). Accumulating data suggested that EMT was identified as the important initiation step for HCC metastasis (*5*). Therefore, to reduce the morbidity

and mortality rates of HCC, prevention of EMT is important for the inhibition of tumor metastasis and the molecular targets in the pathway of EMT have received great attention in HCC treatment.

c-Met, also called tyrosine-protein kinase Met or hepatocyte growth factor (HGF) receptor, is widely expressed by epithelial cells, endothelial cells, neurons, hepatocytes, and hematopoietic cells (7). HGF, the known ligand of c-Met, induces c-Met dimerization and activation, leading to stimulation of multiple downstream signaling pathways, including the MEK/ERK and PI-3K pathways, STAT3, RAC1, and the NF-KB pathway (8). This plays several causal roles in cancer progression, including the induction of EMT (9). Inhibitors of c-Met/HGF signaling have demonstrated antitumor potential in preclinical and clinical models of HCC (10). c-Met inhibitors have shown signs of efficacy in the treatment of HCC, particularly against c-Met positive tumors (11). Our previous basic studies showed that c-Met inhibitor SU11274 could neutralize the activation of HCC cell growth resulting from the addition of des-γ-carboxyprothrombin (DCP) by inhibiting the phosphorylation of c-Met and ERK (12). Moreover, clinical studies indicated that some encouraging phase II data on two c-MET inhibitors, tivantinib and cabozantinib, has led to phase III trials (13). Taken together, c-Met is a therapeutically relevant target in HCC, with important roles in tumor proliferation, motility, and invasion. It should be of significance to further investigate the mechanisms of c-Met on metastasis and EMT in HCC cells, which will be better for HCC treatment.

In recent years, many traditional Chinese medicines have been shown to have potent anti-cancer effects and have attracted considerable interest as potential candidates for the development of novel cancer therapeutics (14). Cinobufacini is a water-soluble extract from the skins and parotid venom glands of the toad *Bufo bufo gargarizans* Cantor. It composes a variety of bufadienolide cardiotonic steroids, such as bufalin, cinobufagin, resibufogenin, and telocinobufagin, which are the major active components (15). In 2005, cinobufacini was approved by the Chinese State Food and Drug Administration (SFDA) and then wildly accepted to treat patients with cancers at oncologic clinics in China (16). Clinical studies have suggested that cinobufacini used alone or in combination with other chemotherapeutic agents had significant activity against cancers, such as HCC, pancreatic cancer, non-small cell lung cancer, and gallbladder carcinoma (17,18). Experimental studies have indicated that cinobufacini has a significant apoptosis-inducing effect on a number of cancer cells. Our previous studies suggested that cinobufacini leads to apoptosis of HCC cells in a dose-dependent manner through the mitochondria- and Fas-mediated pathways (19,20).

According to previous studies, cinobufacini plays significant roles on HCC treatment. However, there are few studies on the effect and mechanism of cinobufacini on metastasis and EMT in HCC cells. Therefore, the aim of the present study was to clarify the possible signal pathway and related molecular mechanisms by which cinobufacini inhibited EMT in the HCC cell line HepG2.

2. Materials and Methods

2.1. Preparation of cinobufacini

The detailed preparation process of cinobufacini was described in previous studies (19). Cinobufacini, an aqueous extract from the skin and parotid venom glands of the toad *Bufo bufo gargarizans* Cantor, was obtained from Anhui Jinchan Biochemical Co., Ltd., Anhui, China. The extraction process was as follows: *Bufo bufo gargarizans* Cantor skins (20 g) were boiled with distilled water twice, and the resulting decoction was mixed and filtered using filter paper. Then, the filtered solution was collected, concentrated, lyophilized, and extracted two more times with ethanol. Finally, the decoction was concentrated to 1mL. In this study, various concentrations of cinobufacini were prepared by diluting the stock solution (20 g/mL) with serum-free DMEM medium.

2.2. Cells

The HCC cell line HepG2 was purchased from the European Collection of Animal Cell Cultures (ECACC, Salisbury, UK). HepG2 cells were cultured in high glucose DMEM supplemented with 10% fetal bovine serum (FBS; Gibco-BRL, Gaithersburg, MD, USA), 100 U/mL of penicillin and 100 g/mL of streptomycin in a humidified atmosphere with 5% CO_2 in air at 37°C.

2.3. Cell viability assay

Cells in the logarithmic growth phase were plated at a density of $6×10^4$ cells/mL in 96-well plates. Twenty-four hours later, the cells were incubated with various concentrations of cinobufacini (0, 0.005, 0.01, 0.05, 0.1, and 0.5 mg/mL). At times of 24, 48, and 72 h after addition of cinobufacini, cell viability was analyzed using a cell counting kit-8 (CCK-8) protocol ((Dojindo Molecular Technologies Inc. Shanghai, China). The absorbance value (OD) of each well was measured at 450 nm. All experiments were performed at least in triplicate on three separate occasions.

2.4. Quantitative real-time RT-PCR assay

Following previous studies, quantitative real-time RT-PCR was used to detect the mRNA expression of EMT

Table 1. Specific primer sequences for Snail, Twist and GAPDH

Gene	Forward primer (From 5' to 3')	Reverse primer (From 5' to 3')
Snail	GCTCCCTCTTCCTCTCCATACC	AAGTCCTGTGGGGCTGATGT
Twist	CAGCTACGCCTTCTCGGTCT	CTGTCCATTTTCTCCTTCTCTGG
GAPDH	GCACCGTCAAGGCTGAGAAC	TGGTGAAGACGCCAGTGGA

related transcription factors Snail and Twist (*21*). First, after cells were treated with specified concentrations of cinobufacini for 24h, total RNA was prepared by using TRIzol reagent (Grand Island, NY, USA) according to the manufacturer's instructions. (Grand Island, NY, USA). In the current study, relative mRNA expression levels for the target genes were determined by using glyceraldehyde 3-phosphate dehydrogenase (GAPDH) as a normalization control. Specific primer sequences of the target genes and GAPDH were designed by TaKaRa (TaKaRa Bio Inc., Dalian, China) as shown in Table 1. Afterwards, according to the protocol of SYBR Premix Ex Taq™ kit (TaKaRa Bio Inc., Dalian, China), amplification of target genes and GAPDH were conducted using ABI Prism 7500 Detection System (Applied Biosystems, Inc., USA). Analysis of relative genes expression was performed by the comparative $2^{-\Delta\Delta CT}$ method.

### 2.5. *Western blot analysis*

After cells were treated with specified concentrations of cinobufacini for 24h, total cell lysates and cytosolic fractions were prepared as previously described (*22*). Thirty micrograms of total cellular proteins were resolved by sodium dodecyl sulfate polyacrylamide gel electrophoresis (SDSPAGE) and transferred onto polyvinylidene fluoride (PVDF) transfer membranes by Western blotting. The results were quantified using Image J (National Institutes of Health, Bethesda, MD, USA). The following antibodies were used: c-Met and MMP-9 (Proteintech, Wuhan, China); p-c-Met and MMP-2 (Abcom, UK); N-cadherin, Vimentin, GAPDH and β-actin (Servicebio, Wuhan, China); E-cadherin and MEK1/2 (Affinity Biosciences, Cincinnati, OH, USA); and ERK1/2 (Cell Signaling Technology, Boston, MA, USA).

2.6. *Statistical analysis*

All experiments were performed in triplicate and the results were analyzed by ANOVA (one-way analysis of variance) using GraphPad Prism 4, followed by Student's *t*-test using Microsoft Office Excel software. $p < 0.05$ was indicative of significant difference.

3. Results

3.1. *Effects of cinobufacini on the proliferation of hepatocellular carcinoma cells*
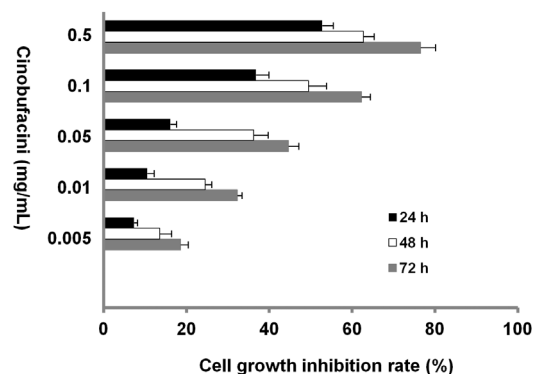
Figure 1. Growth inhibition effects of cinobufacini on HepG2 cells. Cells were treated with different concentrations of cinobufacini (0, 0.005, 0.01, 0.05, 0.1, and 0.5 mg/mL) for 24 h, 48 h and 72 h, and the cell viability was determined by CCK-8 assay. The results are expressed as percentage of cell growth relative to untreated control cells

The anti-proliferation effect of cinobufacini on HCC cells HepG2 was estimated by CCK-8 assay. As shown in Figure 1, cinobufacini had a significant inhibitive effect on HepG2 cells. The viability of HepG2 cells treated by various concentrations of cinobufacini was detected at different times, respectively. After treatment with 0.1 mg/mL cinobufacini for 24 h, 48h and 72h, the growth inhibition rates of HepG2 cells were 36.8%, 49.5%, and 62.3% respectively. These results indicated that cinobufacini had a significant growth inhibiting effect on HepG2 cells in a dose- and time-dependent manner.

3.2. *Effects of cinobufacini on EMT of hepatocellular carcinoma cells*

To explore the effect of cinobufacini on EMT of hepatocellular carcinoma cells, EMT related markers E-cadherin, N-cadherin, and Vimentin were detected by Western blot analysis, and EMT transcription factors Snail and Twist were detected by quantitative real-time RT-PCR assay. As shown in Figure 2A, after treatment with or without cinobufacini (0.01, 0.05 and 0.1 mg/mL) for 24 h, there were dose-dependent increases in E-cadherin protein expression and decreases in N-cadherin and Vimentin protein expression in HepG2 cells. Moreover, the mRNA expressions of Snail and Twist were decreased after treatment with or without cinobufacini (0.01, 0.05 and 0.1 mg/mL) for 24 h (Figure 2B). These results indicated that cinobufacini
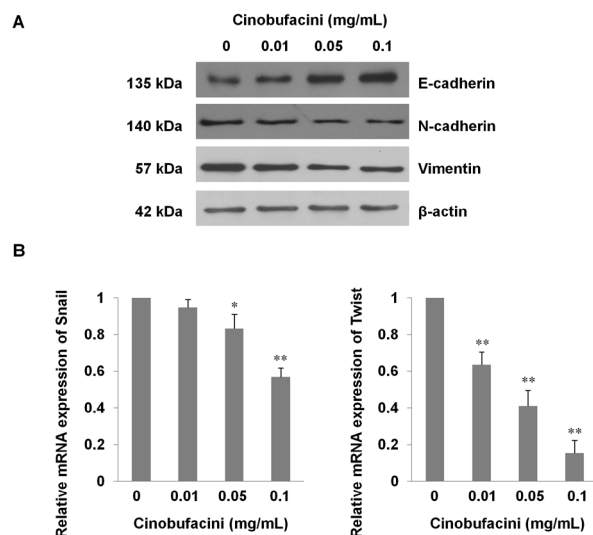
Figure 2. Effects of cinobufacini on EMT of hepatocellular carcinoma cells. (A) The protein expressions of EMT related markers E-cadherin, N-cadherin and Vimentin were detected by Western blot analysis. Afte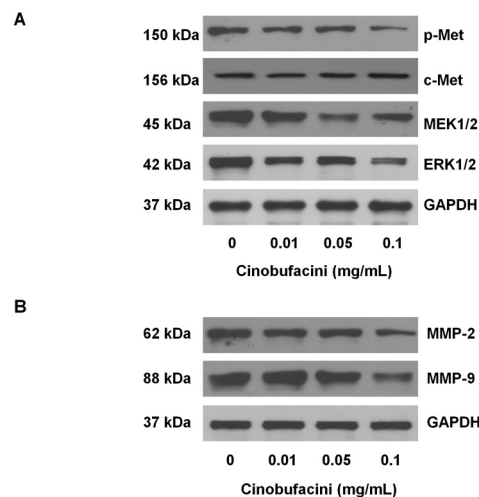r the HepG2 cells were treated with different concentrations of cinobufacini (0, 0.01, 0.05, and 0.1 mg/mL) for 24 h, the expression of E-cadherin was increased while N-cadherin and Vimentin were decreased. **(B)** The mRNA expression of EMT transcription factors Snail and Twist were detected by quantitative real-time RT-PCR assay. After the HepG2 cells were treated with different concentrations of cinobufacini (0, 0.01, 0.05, and 0.1 mg/mL) for 24 h, the mRNA expression of Snail and Twist were decreased. *$p < 0.05$, **$p < 0.01$ *vs.* untreated controls.

had a significant effect on inhibiting of EMT of HepG2 cells.

3.3. Cinobufacini inhibits EMT of hepatocellular carcinoma cells through c-Met /ERK signaling pathway in hepG2 cells

c-Met was reported to play important roles in cancer progression, including the induction of EMT (*9*). MEK/ERK is one of the definite downstream targets of c-Met receptor. Inhibition of c-Met/ ERK signaling pathway has proven to be an efficient way to attenuate tumor proliferation, motility, and invasion in HCC (*11,12*). Here we investigated the effect and mechanism of Cinobufacini on EMT of hepatocellular carcinoma cells by Western blot analysis. We found that c-Met/ ERK signaling pathway was inhibited after treatment with cinobufacini. As shown in Figure 3A, the protein expression of phosphorylated-c-Met (p-c-Met) gradually decreased in a dose-dependent manner with cinobufacini, while the protein expression of c-Met did not change significantly with the addition of cinobufacini. Furthermore, the protein expression of MEK1/2 and ERK1/2, the downstream kinase of the signal transduction pathway activated by c-Met, also decreased in a dose-dependent manner with cinobufacini. These results suggest that cinobufacini could inhibit EMT of hepatocellular carcinoma cells through c-Met/ERK signaling pathway.

Figure 3. Cinobufacini inhibits invasion and metastasis of HCC cells through c-Met /ERK signaling pathway in hepG2 cells. (A) The protein expression of p-c-Met, c-Met, MEK1/2 and ERK1/2 were detected by Western blot analysis. The expression of p-c-Met gradually decreased in a dose-dependent manner with cinobufacini, while the expression of c-Met did not change significantly. The protein expression of MEK1/2 and ERK1/2 decreased in a dose-dependent manner with cinobufacini. **(B)** The protein expression of MMP-2 and MMP-9 were detected by Western blot analysis. After the HepG2 cells were treated with different concentrations of cinobufacini (0, 0.01, 0.05, and 0.1 mg/mL) for 24 h, the expression of E-cadherin was decreased.

3.4. Cinobufacini inhibits cell migration and invasion by regulating MMP-2 and MMP-9 in hepatocellular carcinoma cells

MMP-2 and MMP-9 are factors, which have been proven to play significant function in tumor metastasis (*23*). Thus, the expression of MMP-2 and MMP-9 were examined to further determine the mechanism by which cinobufacini inhibited migration and invasion in hepatocellular carcinoma cells. Here the protein expression of MMP-2 and MMP-9 were detected by Western blot analysis. As shown in Figure 3B, after treatment with or without cinobufacini (0.01, 0.05 and 0.1 mg/mL) for 24 h, there were dose-dependent decreases in MMP-2 and MMP-9 protein expression in HepG2 cells. These results indicated that cinobufacini could inhibit cell invasion and metastasis by regulating MMP-2 and MMP-9 in hepatocellular carcinoma cells.

4. Discussion

Cinobufacini, a well-known traditional Chinese medicine, is widely used to treat a variety of cancers in clinical cancer therapy in China. Its therapeutic effect is especially pronounced in liver cancer (*15*). The antitumor effects of cinobufacini mainly include inhibiting cancer cell proliferation and differentiation, inducing apoptosis, and enhancing immune responses against cancer (*24*). Recently, an experimental study

showed cinobufacini could prevent cell migration and invasion of human breast carcinoma MDA-MB-231 cells into a model stromal tissue, which indicated cinobufacini might possess cancer cell migration preventing activity in addition to cell toxicity such as apoptosis-inducing activity (*25*). However, there are few studies about the effects of cinobufacini on inhibiting HCC cells invasion and metastasis. Here, we investigated the effects and mechanisms of cinobufacini on inhibiting HepG2 cells migration and invasion. We found that cinobufacini could prevent HepG2 cells invasion and metastasis *via* inhibiting EMT through c-Met/ERK signaling pathway.

Previous studies demonstrated that EMT activation in cancer cells contributed to tumor invasion and metastasis in various types of cancer, including HCC, resulting in aggressive cancer progression. EMT is the conversion of epithelial cells to mesenchymal cells, in which cells undergo physiological or pathological changes including the loss of cell polarity and cell-cell adhesion as well as the acquisition of migratory and invasive properties. The classical EMT is featured with the loss of epithelial markers, such as E-cadherin and the up-regulation of mesenchymal markers, such as Vimentin and N-cadherin. These characteristic markers are modulated transcriptionally by several key transcription factors including Snail and Twist (*5*). Snail is a zinc-finger transcription factor that is known as an essential player in the aggressive phenotype of the EMT. Snail binds to the E-boxes of the human Ecadherin promoter and represses E-cadherin expression (*26*). Recently, the basic helix-loop-helix transcription factor Twist has been added to the list of developmental genes with a key role in E-cadherin repression and EMT induction (*27*). Lee *et al*. found that overexpression of Twist was correlated with HCC metastasis and its expression was negatively correlated with E-cadherin expression by tissue microarray (*28*). Moreover, Twist was able to suppress E-cadherin expression and induce EMT changes in metastatic HCC cell lines, which was correlated with increased HCC cell invasiveness. These findings indicated that EMT was associated with HCC metastasis and therefore inhibition of EMT might be a novel approach for HCC treatment. Here we found that after treatment with or without cinobufacini for 24 h, there were dose-dependent increases in E-cadherin protein expression and decreases in N-cadherin and Vimentin protein expression in HepG2 cells. Moreover, the mRNA expression of Snail and Twist were decreased after treatment with or without cinobufacini. Our findings indicated that cinobufacini could prevent HepG2 cells invasion and metastasis by inhibiting EMT with the expression of EMT and transcription factors reversed.

The phosphorylation of c-Met and subsequent activation of various downstream signal transduction pathways may play a significant role in the progression
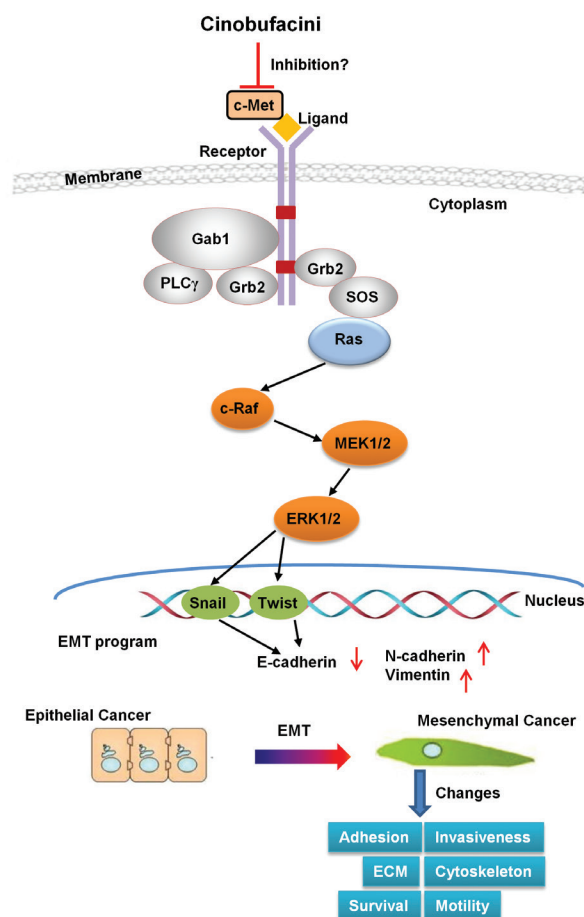
Figure 4. Cinobufacini might prevent HCC cells invasion and metastasis *via* inhibiting EMT through c-Met/ERK signaling pathway.

of HCC including cell proliferation and invasion (*12*). Once c-Met binds to its ligand HGF, it is dimerized and activated, leading to stimulation of multiple downstream signaling pathways, including the MEK/ERK and PI-3K pathways, STAT3, RAC1, and the NF-KB pathway (*8*). The ERK pathway has significant roles in cell proliferation, cell survival and metastasis. Deregulation of the ERK pathway has been implicated in multiple types of human cancers, including HCC (*29*). Previous studies have established a critical role for receptor tyrosine kinase signaling and ERK pathway in EMT (*30*). In HepG2 and Huh7 HCC cell lines, HGF-induced EMT phenotypes are significantly inhibited by the Raf inhibitor sorafenib and the MEK inhibitor U0126, but not the PI3K inhibitor wortmannin (*31*). This finding suggests that the Raf-ERK-MAPK pathway mediates the signal between c-MET activation and EMT induction in HCC cell lines. Therefore, c-Met/ERK signaling pathway might be an important pathway in EMT of HCC cells and inhibiting this pathway might be significant for preventing EMT and migration and invasion. Here we found that the phosphorylation of c-Met was inhibited by cinobufacini. Furthermore, the

expression of MEK1/2 and ERK1/2, the downstream kinase of the signal transduction pathway activated by c-Met, also decreased in a dose-dependent manner with cinobufacini. These findings suggested that cinobufacini could inhibit EMT of HCC cells through c-Met/ERK signaling pathway.

MMPs are major proteolytic enzymes that are important in the degradation of the extracellular matrix thus influencing distinct cellular functions (*32*). MMPs contribute to the regulation of cancer cell invasion and tumor metastasis. Expression of various MMPs including MMP-1, MMP-2, MMP-9, MMP-12 and MMP-14 were implicated in regulating HCC tumor progression and prognosis. Here we found that after treatment with cinobufacini, there was a significant decrease in MMP-2 and MMP-9 expressions in HepG2 cells. These results indicated that cinobufacini could inhibit cell invasion and metastasis by regulating MMP-2 and MMP-9 in HCC cells.

5. Conclusion

In conclusion, the current study suggested cinobufacini could prevent HepG2 cells invasion and metastasis by inhibiting EMT through c-Met/ERK signaling pathway, which might provide experimental evidence for cinobufacini treatment of HCC (Figure 4).

Acknowledgments

References

1. Song PP, Cai YL, Tang HW, Li C, Huang JW. The clinical management of hepatocellular carcinoma worldwide: A concise review and comparison of current guidelines from 2001 to 2017. BioSci Trends. 2017; 11:389-398.

2. Torre LA, Bray F, Siegel RL, Ferlay J, Lortet-Tieulent J, Jemal A. Global cancer statistics, 2012. CA Cancer J Clin. 2015; 65:87-108.

3. Forner A, Llovet JM, Bruix J. Hepatocellular carcinoma. Lancet. 2012; 379:1245-1255.

4. Singh M, Yelle N, Venugopal C, Singh SK. EMT: Mechanisms and therapeutic implications. Pharmacol Ther. 2018; 182:80-94.

5. Nieto MA, Huang RY, Jackson RA, Thiery JP. EMT: 2016. Cell. 2016; 166:21-45.

6. Davis FM, Stewart TA, Thompson EW, Monteith GR. Targeting EMT in cancer: Opportunities for pharmacological intervention. Trends Pharmacol Sci. 2014; 35:479-488.

7. Fasolo A, Sessa C, Gianni L, Broggini M. Seminars in clinical pharmacology: An introduction to MET inhibitors for the medical oncologist. Ann Oncol. 2013; 24:14-20.

8. Giordano S, Columbano A. Met as a therapeutic target in HCC: Facts and hopes. J Hepatol. 2014; 60:442-452.

9. Eder JP, Vande Woude GF, Boerner SA, LoRusso PM. Novel therapeutic inhibitors of the c-Met signaling pathway in cancer. Clin Cancer Res 2009; 15:2207-2214.

10. Bouattour M, Raymond E, Qin S, Cheng AL, Stammberger U, Locatelli G, Faivre S. Recent developments of c-Met as a therapeutic target in hepatocellular carcinoma. Hepatology. 2018; 67:1132-1149.

11. Bladt F, Friese-Hamim M, Ihling C, Wilm C, Blaukat A. The c-Met inhibitor MSC2156119J effectively inhibits tumor growth in liver cancer models. Cancers (Basel). 2014; 6:1736-1752.

12. Inagaki Y, Qi F, Gao J, Qu X, Hasegawa K, Sugawara Y, Tang W, Kokudo N. Effect of c-Met inhibitor SU11274 on hepatocellular carcinoma cell growth. Biosci Trends. 2011; 5:52-56.

13. Lee JJX, Chan JJ, Choo SP. Clinical Development of c-MET Inhibition in Hepatocellular Carcinoma. Diseases. 2015; 3:306-324.

14. Qi F, Zhao L, Zhou A, Zhang B, Li A, Wang Z, Han J. The advantages of using traditional Chinese medicine as an adjunctive therapy in the whole course of cancer treatment instead of only terminal stage of cancer. Biosci Trends. 2015; 9:16-34.

15. Qi F, Li A, Inagaki Y, Kokudo N, Tamura S, Nakata M, Tang W. Antitumor activity of extracts and compounds from the skin of the toad *Bufo bufo gargarizans* Cantor. Int Immunopharmacol. 2011; 11:342-349.

16. Qi F, Li A, Inagaki Y, Gao J, Li J, Kokudo N, Li XK, Tang W. Chinese herbal medicines as adjuvant treatment during chemo- or radio-therapy for cancer. Biosci Trends. 2010; 4:297-307.

17. Xia J, Inagaki Y, Gao J, Qi F, Song P, Han G, Sawakami T, Gao B, Luo C, Kokudo N, Hasegawa K, Sakamoto Y, Tang W. Combination of cinobufacini and doxorubicin increases apoptosis of hepatocellular carcinoma cells through the Fas- and mitochondria-mediated pathways. Am J Chin Med. 2017; 45(7):1537-1556.

18. Meng Z, Yang P, Shen Y, Bei W, Zhang Y, Ge Y, Newman RA, Cohen L, Liu L, Thornton B, Chang DZ, Liao Z, Kurzrock R. Pilot study of huachansu in patients with hepatocellular carcinoma, nonsmall-cell lung cancer, or pancreatic cancer. Cancer. 2009; 115:5309-5318.

19. Qi F, Li A, Zhao L, Xu H, Inagaki Y, Wang D, Cui X, Gao B, Kokudo N, Nakata M, Tang W. Cinobufacini, an aqueous extract from *Bufo bufo gargarizans* Cantor, induces apoptosis through a mitochondria-mediated pathway in human hepatocellular carcinoma cells. J Ethnopharmacol. 2010; 128:654-661.

20. Qi F, Li A, Inagaki Y, Xu H, Wang D, Cui X, Zhang L, Kokudo N, Du G, Tang W. Induction of apoptosis by cinobufacini preparation through mitochondria- and Fas-mediated caspase-dependent pathways in human hepatocellular carcinoma cells. Food Chem Toxicol. 2012; 50:295-302.

21. Yin Y, Qi F, Song Z, Zhang B, Teng J. Ferulic acid combined with astragaloside IV protects against vascular endothelial dysfunction in diabetic rats. Biosci Trends. 2014; 8:217-226.

22. Qi F, Inagaki Y, Gao B, Cui X, Xu H, Kokudo N, Li A, Tang W. Bufalin and cinobufagin induce apoptosis of human hepatocellular carcinoma cells *via* Fas- and mitochondria-mediated pathways. Cancer Sci. 2011; 102:951-958.

23. Daniele A, Abbate I, Oakley C, Casamassima P, Savino E,

Casamassima A, Sciortino G, Fazio V, Gadaleta-Caldarola G, Catino A, Giotta F, De Luca R, Divella R. Clinical and prognostic role of matrix metalloproteinase-2, -9 and their inhibitors in breast cancer and liver diseases: A review. Int J Biochem Cell Biol. 2016; 77(Pt A):91-101.

24. Wei X, Si N, Zhang Y, Zhao H, Yang J, Wang H, Wang L, Han L, Bian B. Evaluation of bufadienolides as the main antitumor components in cinobufacini injection for liver and gastric cancer therapy. PLoS One. 2017; 12:e0169141.

25. Nakata M, Mori S, Kamoshida Y, Kawaguchi S, Fujita-Yamaguchi Y, Gao B, Tang W. Toad skin extract cinobufatini inhibits migration of human breast carcinoma MDA-MB-231 cells into a model stromal tissue. Biosci Trends. 2015; 9:266-269.

26. Zucchini-Pascal N, Peyre L, Rahmani R. Crosstalk between beta-catenin and snail in the induction of epithelial to mesenchymal transition in hepatocarcinoma: Role of the ERK1/2 pathway. Int J Mol Sci. 2013; 14:20768-20792.

27. Zou H, Feng X, Cao JG. Twist in hepatocellular carcinoma: Pathophysiology and therapeutics. Hepatol Int. 2015; 9:399-405.

28. Lee TK, Poon RT, Yuen AP, Ling MT, Kwok WK, Wang XH, Wong YC, Guan XY, Man K, Chau KL, Fan ST. Twist overexpression correlates with hepatocellular carcinoma metastasis through induction of epithelial-mesenchymal transition. Clin Cancer Res. 2006; 12:5369-5376.

29. Roux PP, Blenis J. ERK and p38 MAPK-activated protein kinases: A family of protein kinases with diverse biological functions. Microbiol Mol Biol Rev. 2004; 68:320-344.

30. McCubrey JA, Steelman LS, Chappell WH, Abrams SL, Wong EW, Chang F, Lehmann B, Terrian DM, Milella M, Tafuri A, Stivala F, Libra M, Basecke J, Evangelisti C, Martelli AM, Franklin RA. Roles of the Raf/MEK/ERK pathway in cell growth, malignant transformation and drug resistance. Biochim Biophys Acta. 2007; 1773:1263-1284.

31. Nagai T, Arao T, Furuta K, Sakai K, Kudo K, Kaneda H, Tamura D, Aomatsu K, Kimura H, Fujita Y, Matsumoto K, Saijo N, Kudo M, Nishio K. Sorafenib inhibits the hepatocyte growth factor-mediated epithelial mesenchymal transition in hepatocellular carcinoma. Mol Cancer Ther. 2011; 10:169-177.

32. Egeblad M, Werb Z. New functions for the matrix metalloproteinases in cancer progression. Nat Rev Cancer. 2002; 2:161-174.

33. Mckenna GJ, Chen Y, Smith RM, Meneghetti A, Ong C, McMaster R, Scudamore CH, Chung SW. A role for matrix metalloproteinases and tumor host interaction in hepatocellular carcinomas. Am J Sur. 2002; 183:588-594.

Original Article

Bi-specific ligand-controlled chimeric antigen receptor T-cell therapy for non-small cell lung cancer

Wenqi Chu[1,§], Yixiong Zhou[2,§], Qi Tang[1], Min Wang[1], Yongjia Ji[1], Jingjing Yan[1], Dan Yin[1], Shuye Zhang[1], Hongzhou Lu[1,3,*], Jiayin Shen[1,*]

[1] *Shanghai Public Health Clinical Center & Institutes of Biomedical Sciences, Fudan University, Shanghai, China;*
[2] *Shanghai 9th People's Hospital, Shanghai Jiao Tong University School of Medicine, Shanghai, China;*
[3] *Department of Infectious Diseases, Huashan Hospital Affiliated to Fudan University, Shanghai, China.*

Summary   **Our goal is to develop a switch-controlled approach to enable better control of reactivity and safety of chimeric antigen receptor (CAR)-T therapy for non-small-cell lung cancer (NSCLC). Lentiviral transduction was performed to generate anti-FITC CAR-T cells and target cells stably expressing either isoform of the folate receptor. Colorimetric-based cytotoxic assay, enzyme-linked immunosorbent assay, and multiparametric flow cytometry analysis were used to evaluate the specificity and activity of CAR-T cells *in vitro*. Human primary T cells stably expressing the fully human anti-FITC CAR were generated. Anti-FITC CAR-T cells displayed antigen-specific and folate-FTIC dependent reactivity against engineered A549-FRα and THP-1-FRβ. The selective activation and proliferation of anti-FITC CAR-T cells *in vitro* stringently relied on the co-existence of folate-FITC and FR-expressing target cells and was dose-titratable with the folate-FITC switch. The excellent *in vitro* efficacy and specificity of an adaptor-controlled CAR-T therapy to target both tumor cells and tumor-associated macrophages in NSCLCs were validated.**

Keywords: Non-small cell lung cancer, chimeric antigen receptor T cell, folate receptor, folate-FITC

1. Introduction

Lung cancer continues to be one of the most commonly diagnosed cancer types and the leading cause of cancer deaths in both United States and China (*1,2*). Non-small-cell lung cancer (NSCLC) accounts for 80% to 85% of all lung cancer cases (*3*). Although giant steps have been made in targeted chemotherapy and immunotherapy of NSCLC, the 5-year survival rate remains below 20% (*3,4*). Therefore, the development of new and more effective therapies for NSCLC is imperative.

Recently, chimeric antigen receptor (CAR)-T

cell therapy has had great success in treatment of hematologic malignancies, most notably in B cell acute lymphoblastic leukemia (B-ALL) with up to a 90% complete remission rate (*5*). With FDA approval of Kymriah for certain pediatric and young adult patients with a form of acute lymphoblastic leukemia (ALL) (*6*), we entered a new frontier in medical innovation with the ability to genetically reprogram patients-derived T lymphocytes to attack a deadly cancer. For the treatment of NSCLC, an appropriate target is the folate receptor α (FRα), a glycosylphosphatidylinositol (GPI)-anchored cell surface protein, which binds and mediates the uptake of free folic acid as well as its drug conjugates with high affinity and specificity (*7*). Numerous studies have confirmed elevated expression of FRα in over 70% of lung adenocarcinomas and about 10% of squamous cell carcinomas by using different clones of anti-FRα antibodies (*8-12*). Notably, a high concordance of FRα expression was not only observed between biopsy and primary tumor but also seen between distant metastases of NSCLC and their corresponding local tumors (*9*).

Address correspondence to:
Dr. Jiayin Shen and Dr. Hongzhou Lu, Shanghai Public Health Clinical Center Affiliated to Fudan University, 2901 Caolang Road, Jin Shan District, Shanghai, 201508, P.R.China.
E-mail: shenjiayin@shaphc.org or luhongzhou@fudan.edu.cn

In contrast, the low to negligible distribution of FRα in normal human tissues is restricted to the apical (luminal) surface of cells, which reside in the bronchial epithelium, renal tubules and choroid plexus (*13,14*). Consequently, six folate-targeted drugs are currently undergoing human clinical trials (*15-19*), and one folate-vinca alkaloid conjugate (EC145) has even advanced to phase IIb clinical trials for targeted therapy of NSCLC (*18,19*). Thus, FRα has not only become an established NSCLC marker, but it could also act as a promising target for adoptive CAR-T therapy for this cancer.

However, normal tissue toxicity is an issue, which needs to be addressed especially when expression of tumor-associated antigen targeted by CAR-T is generally less restricted (*20-24*). Several strategies have been proposed to minimize CAR-T therapy-related toxicities, including the use of kill switches (*25*), splitting the chimeric receptor (*26*), and antibody-based intercellular switches to mediate the formation of immunological synapses between CAR-T cells and target cells (*27-31*).

In recognition of the fact that over 70% of lung adenocarcinomas expressing FRα also contain tumor-associated macrophages (TAMs) with high expressing levels of FRβ (*10*), we herein describe an approach using fluorescein isothiocyanate (FITC) conjugated with folate (folate-FITC) as an intermediary "switch" to induce the assembly of a pseudoimmunological synapse between anti-FITC CAR-T cells and target cells expressing either FRα or FRβ. We demonstrate potent antigen-specific and dose-dependent *in vitro* efficacies of anti-FITC CAR-T cells against both FRα-positive NSCLC cell lines and macrophage cell lines expressing the β isoform of FR. Moreover, the activation and proliferation of anti-FITC CAR-T cell was strictly dependent on the presence of the bi-specific switch molecule folate-FITC. These results suggest that CAR-T cells could be exploited to target both tumor and the tumor microenvironment in NSCLC patients by using our approach.

2. Materials and Methods

2.1. *Generation of CAR-T cells*

The human anti-FITC scFv (*31*) gene was synthesized by GENEWIZ and cloned into a lentiviral vector (LV-vector) containing a CD8α hinge and transmembrane region, and 41BB and CD3ζ signaling domains. Lentiviruses were produced in HEK293T cells, and transduction of human primary T cells was performed as previously described (*31*). Briefly, 8×10^6 HEK293T cells were seeded per 10-cm tissue dish 24 hours before transfection. Cells were transfected with anti-FITC CAR plasmid and viral packaging vectors using Lipofectamine® 2000 reagent (Thermo Fisher Scientific, Waltham, MA). Supernatants were harvested 48h later. Viral particles were concentrated using an Amicon®Ultra

100K device (Merk Millipore, Worcester, MA), titrated, and stored at -80°C until use. All plasmids were purified using Endo-free Maxi prep kits (Qiagen, Valencia, CA). Peripheral blood mononuclear cells (PBMCs) were obtained from healthy volunteer donors using Ficoll-Hypaque Solution (GE Healthcare, Chicago, IL). Isolated PBMCs were transferred into complete medium (CM) (AIM-V, 5% human serum AB, 1% pen-strep media) (Thermo Fisher Scientific, Waltham, MA) and incubated at 37°C for 3 hours. Suspension cells were collected and activated with anti-CD3/CD28 beads (Thermo Fisher Scientific, Waltham, MA). Activated T cells were transduced with lentivirus after 24 hours of activation in the presence of 10 μg/mL protamine sulfate (Sigma-Aldrich, St. Louis, MO). T cells were then expanded in CM with 300 IU/mL of recombinant human interleukin-2 (rhIL-2) (R&D Systems, Minneapolis, MN) after media replacement, maintaining a cell density of $0.5 - 2 \times 10^6$ cells/mL. Anti-FITC CAR expression was verified by flow cytometry using Alexa Fluor® 647 conjugated anti-human IgG F(ab')$_2$ antibodies (Jackson ImmunoResearch, West Grove, PA). Its binding capacity to FITC was also confirmed by using a FITC-labeled mouse IgG1 isotype control antibody (Biolegend, San Diego, CA) and folate-FITC (AdooQ, Nanjing, Jiangsu). Non-transduced T cells or T cells transduced with lentivirus expressing green fluorescent protein (GFP) stained with corresponding reagents served as background controls.

2.2. *Cell lines*

HEK293T cell line, human lung adenocarcinoma cell line A549, a human monocytic cell line THP-1, immortalized human T lymphocyte cell line Jurkat, and the HL-60 (Human promyelocytic leukemia cells) cell line were purchased from American Type Culture Collection. A549 and THP-1 cells were transduced with lentiviral vectors encoding human FRα and FRβ gene, respectively, to generate cells stably expressing FRα (A549-FRα) and FRβ (THP-1-FRβ). The expression of human FRα and FRβ was confirmed by quantitative RT-PCR. Briefly, total RNA was extracted from the corresponding cell lines. Then cDNA was generated using the Reverse Transcription System (Promega, Fitchburg, WI) and added to SYBR Green PCR Master Mix with primers specific for human FRα or FRβ, in triplicate. The relative human FRα or FRβ messenger RNA (mRNA) copy number was calculated using the standard curve method and the real-time PCR system (Bio-Rad Laboratories, Hercules, CA). A549-FRα and THP-1-FRβ cells were maintained in folate-deficient RPMI 1640 media with 10% fetal bovine serum and antibiotics. A549, THP-1, Jurkat and HL60 cells were cultured in complete media prepared with RPMI1640. HEK293T cells were cultured in complete media prepared with DMEM. All reagents were purchased

from Thermo Fisher Scientific (Waltham, MA).

2.3. Colorimetric-based cytotoxic assays

Anti-FITC or GFP CAR T cells were co-cultured with target cells at indicated E:T (effector-to-target) ratios in 96-well round bottom plates with 100 µL/well of complete media (folate-deficient RMPI 1640, 5% fetal bovine serum, 1% pen-strep media) containing different concentrations of folate-FITC. After incubation at 37℃ for 24 hours, cytotoxicity towards target cells was determined by measuring the amount of lactate dehydrogenase (LDH) released into culture media using CytoTox-96 nonradioactive cytotoxicity assay kit (Promega, Fitchburg, WI). The percent lytic activity was calculated with the following formula: (values used represent absorbance at 490 nM) % Cytotoxicity = 100 × [((Target cells + Effector cells + folate-FITC) - (Target cells + Effector cells only)) / ((Maximum target cell lysis) – (Target cells only))].

2.4. T cell activation assay

Anti-FITC or GFP CAR T cells were co-cultured with target cells as described above. Supernatants were harvested, and IFN-γ released by T cells was quantified by enzyme-linked immunosorbent assay (ELISA) using Human IFN-gamma Quantikine ELISA Kit (BD Biosciences, San Jose, CA). The expression level of T cell activation markers, CD25 and CD69, were analyzed by flow cytometry using anti-CD25 (BD Biosciences, San Jose, CA) and anti-CD69 (eBioscience, San Diego, CA). After being co-cultured with target cells for 5 hours, the ability of CAR-T cells to secrete cytolytic granules was visualized by CD107a staining using anti-CD107a antibody (eBioscience, San Diego, CA).

2.5. T cell proliferation assay

Anti-FITC CAR-T cells were pre-labeled with 5 mM PKH26 (Sigma-Aldrich, St. Louis, MO) according to the manufacturer's protocol. Anti-FITC CAR-T cells were cocultured with target cells at an effector to target cell ratio (E:T ratio) of 1 to 1 in triplicate in 96-well round bottom plates in 200 µL of complete media (folate-deficient RMPI 1640, 5% fetal bovine serum, 1% pen-strep media) containing different concentrations of folate-FITC. After a 3-day incubation in the presence of folate-FITC, cells were stained and analyzed for PKH26 distribution.

2.6. Statistical analysis

The data are reported as mean ± SD. Statistical analysis was performed using Student's t test or Mann-Whitney test. Statistical significance and EC_{50} values were calculated using GraphPad Prism 5.0. $P < 0.05$ was considered significant.

3. Results

3.1. Generation of anti-FITC CART cells

Recently, a proof-of-concept study demonstrated that the efficacy of FITC-conjugated anti-CD19 Fab directed anti-FITC CAR-T against human CD19^{+} B-acute lymphoblastic leukemia line was comparable to the current FDA-approved CTL019 therapy (Kymirah®) both *in vitro* and *in vivo* (*31*). More importantly, it has been reported that folate-FITC, a FRα-targeted optical contrast agent also known as EC17 (*32*), was 100% accurate in identifying lung adenocarcinomas with very limited toxicities in a phase I clinical trial of targeted intraoperative molecular imaging for surgical resection (*33*). Therefore, we plan to evaluate if folate-FITC would be able to elicit a specific reactivity of anti-FITC CAR-T cells against FRα-expressing lung cancer cells (Figure 1A). To create a FITC-specific CAR, a fully human anti-FITC scFv clone (*31*) was subcloned into a lentiviral vector containing a second-generation CAR (from N-terminus: anti-FITC scFv, CD8α hinge and transmembrane domain, the cytoplasmic domains of 4-1BB and CD3ζ), using GFP CAR as a control (Figure 1B). Lentiviral particles were produced in HEK293T cells and used to transduce Jurkat cells. A transduction efficiency of 69.3% was observed by flow cytometry after staining for scFv surface expression using mouse anti-human IgG, F(ab')₂ polyclonal antibody (Figure 1C, left panel). To further confirm that the anti-FITC scFv was properly folded on the cell surface and retained its affinity for FITC, a flow cytometry binding assay was performed using folate-FITC and a commercially available FITC-labeled mouse IgG1 isotype control antibody. Similar to the transduction efficiency measured as stated above, we observed the binding of FITC anti-mouse IgG antibody (62.7% positive) (Figure 1C, middle panel) and folate-FITC (64.7% positive) (Figure 1C, right panel) to Jurkat cells.

3.2. Anti-FITC CAR-T cells display antigen-specific and switch-dependent reactivity against engineered A549-FRα

To evaluate the ability of folate-FITC to redirect the anti-FITC CAR-T cells toward FRα-positive NSCLC cells, we first engineered A549, an FR-negative human lung adenocarcinoma cell line, to constitutively overexpress human FRα (A549-FRα). Surface expression of functional FRα was assessed, by labeling with folate-FITC, using flow cytometry (Figure 1D), and the selective expression of FRα but not FRβ mRNA was confirmed with quantitative RT-PCR (Figure 1E). Moreover, results from Western Blot with anti-human FRβ polyclonal antibody also demonstrated that A549-
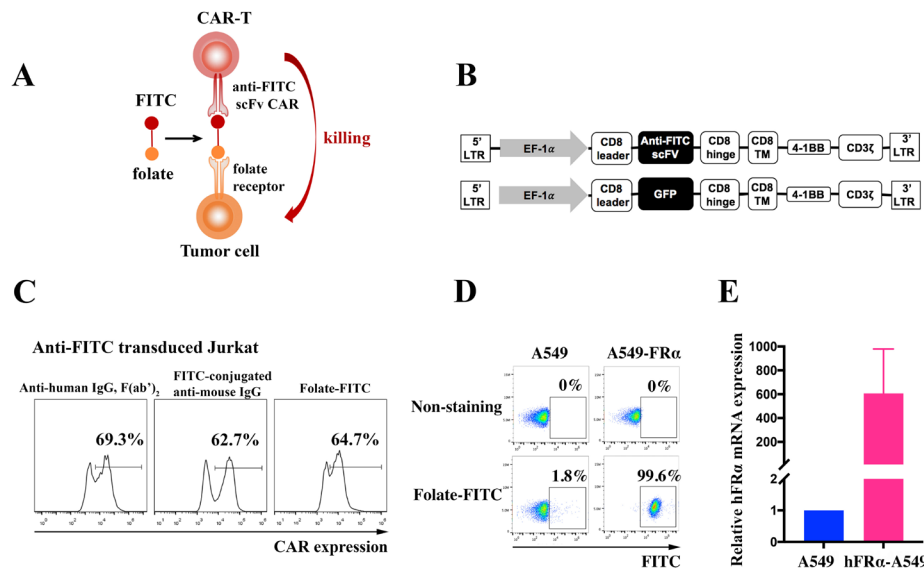
Figure 1. Schematic representation of the killing mechanism, lentivirial vector and CAR-modified Jurkat cells, and engineered A549-FRα cell line. (A) Schematic diagram of folate-FITC mediated CAR-T cytotoxicity to tumor cells. **(B)** Anti-FITC and GFP CAR lentiviral construct. **(C)** Anti-FITC CAR expression on Jurkat cells was assessed by staining with AlexaFlour647® mouse anti-human IgG F(ab')₂ antibody (Jackson ImmunoResearch, West Grove, PA), a FITC-conjugated anti-mouse IgG1 isotype control antibody (Biolegend, San Diego, CA), or folate-FITC (AdooQ, Nanjing, Jiangsu). **(D)** Assessment of folate-FITC binding to A549 and A549-FRα cell lines by flow cytometry. **(E)** Relative FRα mRNA expression was confirmed using quantitative RT-PCR. Indicated mRNA expression is shown relative to A549. Results shown represent findings observed in three independent experiments.
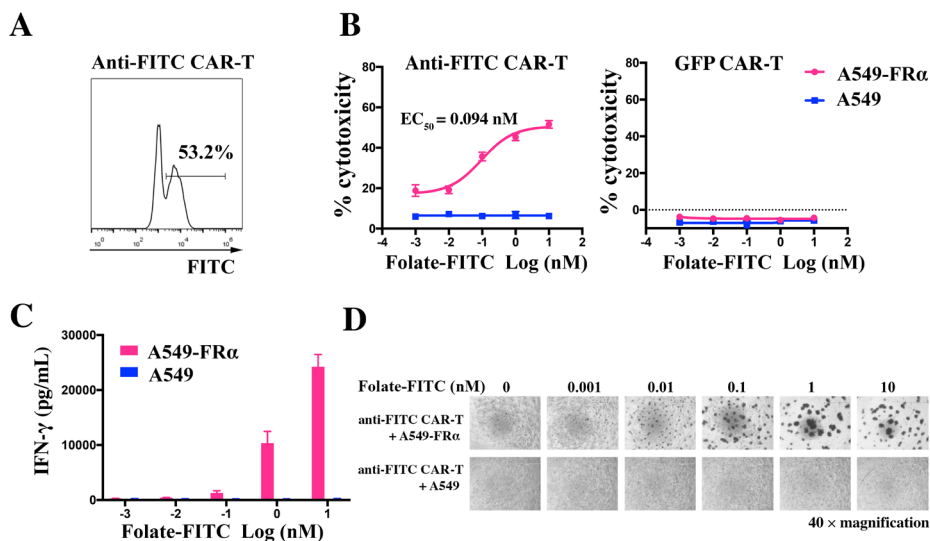
Figure 2. Folate-FITC can specifically and dose-dependently redirect anti-FITC CAR-T cells to target A549-FRα cells. (A) Anti-FITC CAR expression on human T cells was detected by a FITC-conjugated anti-mouse IgG1 isotype control antibody. **(B)** 24 hours co-culture of anti-FITC CAR-T or GFP CAR-T cells with A549 and A549-FRα cells in the presence of serial dilutions of folate-FITC at an effector to target cell ratio of 5:1 (5×10^4 to 1×10^4 cells per well). Cytolytic activity was determined by measuring the amount of LDH released into culture media using CytoTox 96 Nonradioactive cytotoxicity assay kit (Promega). Each concentration was carried out in triplicate and error bars represent SD. **(C)** Quantification of IFN-γ levels in cultures at a E:T ratio of 5:1 by ELISA. Error bars represent SD derived from triplicate samples. **(D)** Microscopic images of cytotoxicity assay at a E:T ratio of 5:1.

FRα cells do not express FRβ (data not shown). Then, lentiviral particles were used to transduce activated peripheral human blood mononuclear cells (PBMCs), and 7 days post viral transduction, more than 50% of the primary human T cells expressed CAR as determined by flow cytometry after labeling with folate-FITC (Figure 2A).

As shown in Figure 2B, at an effector to target cell ratio (E:T ratio) of 5 to 1 in folate-deficient media, highly potent cytotoxic activity of anti-FITC CAR-T cells was induced by folate-FITC ($EC_{50} = 0.094 \pm 0.116$ nM) against A549-FRα. These results were reproducible across multiple T cell donors with similar efficacies. In contrast, folate-FITC did not induce lytic activity towards A549-FRα cells in the presence of GFP CAR-T cells (Figure 2B, right panel). Furthermore, no significant

A

B

C
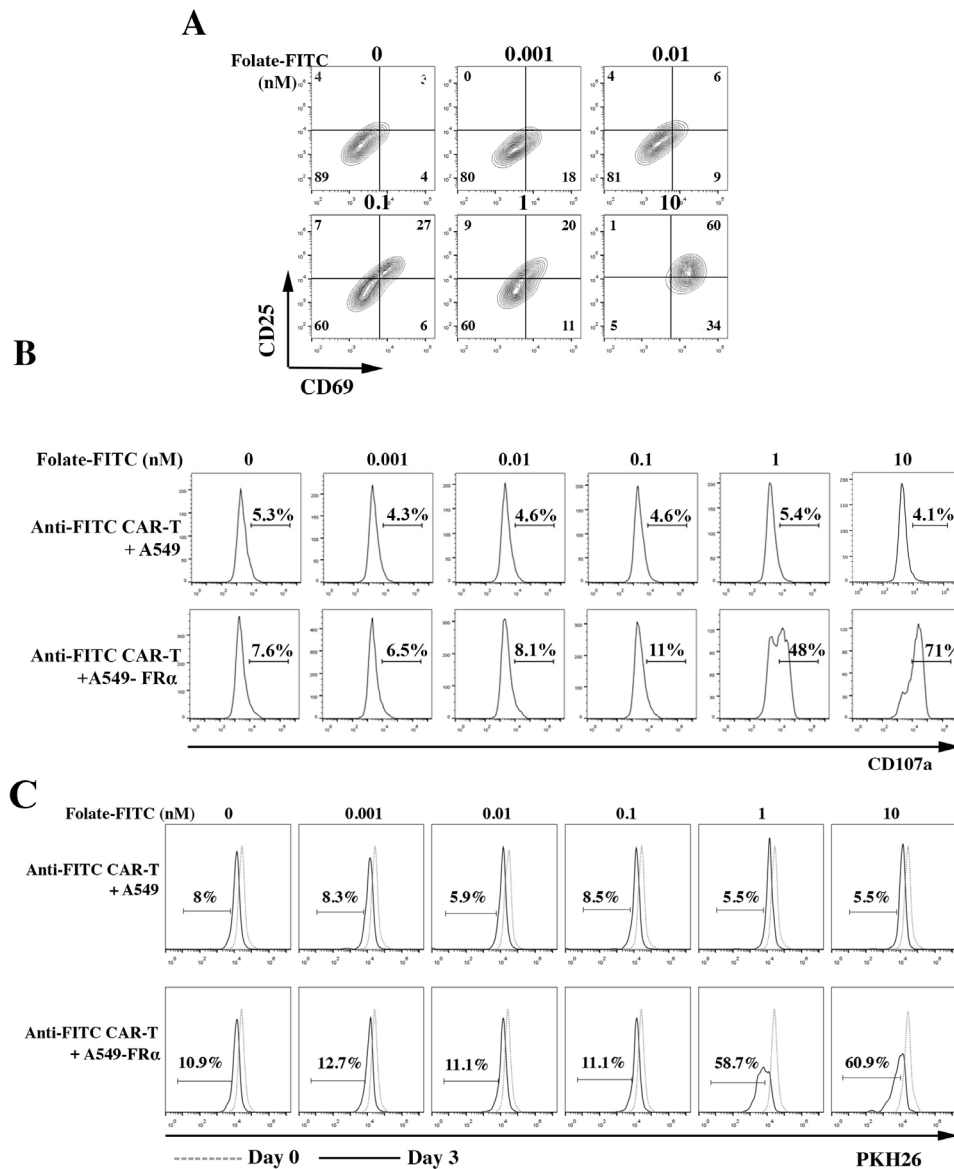
Figure 3. Activation, degranulation and proliferation of anti-FITC CAR-T cells co-cultured with A549-FRα in the presence of Folate-FITC. (A) Folate-FITC dependent titratable activation of anti-FITC CAR-T cells. Anti-FITC CAR-T cells (5×10^4 cells) were co-cultured with A549- FRα cells (1×10^4 cells) for 24 h with serial dilutions of folate-FITC, and subsequently stained with AlexaFlour647 mouse anti-human IgG F(ab′)₂ antibody followed by PE-conjugated anti-CD25 (BD Biosciences, San Jose, CA) and FITC-conjugated anti-CD69 antibody (eBioscience, San Diego, CA). **(B)** Folate-FITC dependent degranulation of Anti-FITC CAR-T cells. Anti-FITC CAR-T cells (1×10^5 cells) were co-cultured with A549 and A549-FRα cells (1×10^5 cells) in the presence of folate-FITC and PE-conjugated anti-human CD107a antibody (eBioscience, San Diego, CA). After 5 hours of co-culture, CD107a surface expression was measured following the staining of AlexaFlour647 mouse anti-human IgG F(ab′)2 antibody. **(C)** Folate-FITC dependent proliferation of Anti-FITC CAR-T cells. Anti-FITC CAR-T cells were pre-labeled with 5 mM PKH26 (Sigma-Aldrich, St. Louis, MO) according to the manufacturer's protocol. Anti-FITC CAR T cells (1×10^4 cells) were co-cultured with A549 and A549-FRα cells (1×10^4 cells). After 3-day incubation in the presence of folate-FITC, cells were stained and analyzed for PKH26 distribution.

cytotoxic activity was observed with FRα-negative A549 cells at concentrations of folate-FITC up to 10 nM, demonstrating the high selectivity of folate-FITC and anti-FITC CAR-T cells. The amount of IFN-γ released from anti-FITC CAR-T cells after 24-hour co-culture with A549-FRα was positively correlated with the dose of folate-FITC put into the assay media (Figure 2C). Moreover, formation of aggregates, indicative of cross-linking between T cells and target cells, was visible in cocultures of anti-FITC CAR-T cells and A549-FRα cells with folate-FTIC, but not in any other controls (Figure

2D). Overall, our findings demonstrate that folate-FITC, as a bispecific small molecule, can specifically and dose-dependently redirect anti-FITC CAR-T cells to target FRα-positive cells.

3.3. *Folate-FITC mediates activation and proliferation of FITC-specific CAR-T for A549-FRα*

Next, we confirmed the stringent dependence of anti-FITC CAR-T cell activation on folate-FITC by monitoring their expression of cell surface activation

Figure 4. Folate-FITC can specifically and dose-dependently redirect anti-FITC CAR-T cells to target FRβ-positive cells.
(A) Assessment of folate-FITC binding to HL60, THP-1 and THP-1-FRβ cell lines by flow cytometry. **(B)** Relative FRβ mRNA expression was confirmed using quantitative RT-PCR. Indicated mRNA expression is shown relative to HL60. Res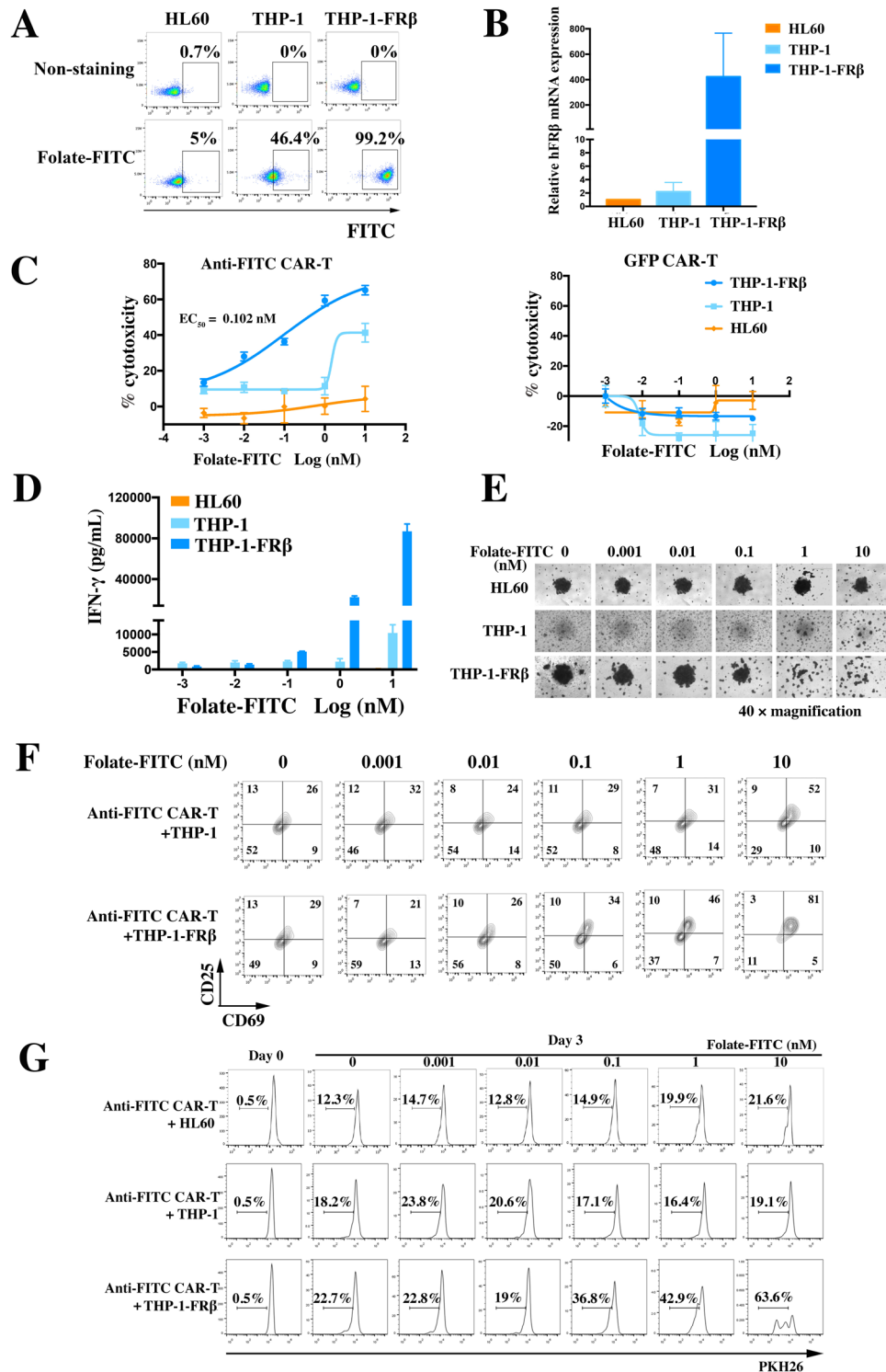ults shown represent findings observed in three experiments. **(C)** 24 hours co-culture of anti-FITC CAR-T or GFP CAR-T cells with HL60, THP-1 and THP-1-FRβ cells in the presence of serial dilutions of folate-FITC at an effector to target cell ratio of 2:1 (4×10^4 to 2×10^4 cells per well). Cytolytic activity was determined by measuring the amount of LDH released into culture media using CytoTox 96 Nonradioactive cytotoxicity assay kit (Promega). Each concentration was carried out in triplicate and error bars represent SD. **(D)** Quantification of IFN-γ levels in cultures at a E:T ratio of 2:1 by ELISA. Error bars represent SD derived from triplicate samples. **(E)** Microscopic images of cytotoxicity assay at a E:T ratio of 2:1. **(F)** Titratable activation of anti-FITC CAR-T cells co-cultured with THP-1-FRβ at a E:T ratio of 2:1 in the presence of Folate-FITC. CD25 and CD69 expression was measured following the staining of AlexaFlour647 mouse anti-human IgG F(ab′)₂ antibody. **(G)** Folate-FITC dependent proliferation of Anti-FITC CAR-T cells. Anti-FITC CAR-T cells were pre-labeled with 5 mM PKH26 (Sigma-Aldrich, St. Louis, MO). Anti-FITC CAR T cells (1×10^4 cells) were co-cultured with HL60, THP-1 and THP-1-FRβ cells (1×10^4 cells). After 3-day incubation in the presence of folate-FITC, cells were stained and analyzed for PKH26 distribution.

markers, CD25 and CD69, after 24-hour co-culture with A549-FRα cells. As expected, the increase of CD25 and CD69 expression levels on anti-FITC CAR-T cells was correlated with the concentration of folate-FITC in the assay media (Figure 3A). Degranulation, as quantified by increased cell surface CD107a expression, is an established surrogate for T-cell lytic function. After 5-hour co-culture, we observed specific degranulation in anti-FITC CAR-T cells only in the presence of A549-FRα, and surface mobilization of CD107a was also dependent on the concentration of folate-FITC (Figure 3B). Besides, folate-FITC dependent proliferation of anti-FITC CAR-T cells was also confirmed by detecting the PKH26 dilution of PKH26 labelled anti-FITC CAR-T cells after 3-day co-culture with A549-FRα cells (Figure 3C).

3.4. *Anti-FITC CAR-T cells exhibit specific cytotoxicity against FRβ-positive macrophage cell line*

To evaluate the ability of folate-FITC to redirect the anti-FITC CAR-T cells toward FRβ-positive macrophage cells, we first engineered THP-1-FRβ cell line, which stably overexpresses human FRβ. Surface expression of functional FRβ on THP-1 and THP-1-FRβ was assessed by labeling with folate-FITC using flow cytometry (Figure 4A). FRβ mRNA expression on THP-1 and THP-1-FRβ were measured by quantitative RT-PCR (Figure 4B). Both quantitative RT-PCR and Western Blot were performed to show that THP-1 and THP-1-FRβ do not express FRα. Besides, protein level of FRβ on THP-1 and THP-1-FRβ was also measured by Western Blot with anti-human FRβ polyclonal antibody (data not shown).

As shown in Figure 4C, at an effector to target cell ratio (E:T ratio) of 2 to 1 in folate-deficient media, highly potent cytotoxic activity of anti-FITC CAR-T cells was induced by folate-FITC ($EC_{50} = 0.102 \pm 0.272$ nM) against THP-1-FRβ. Notably, anti-FITC CAR-T cells also exhibited specific reactivity against endogenous FRβ on THP-1 cells in the presence of 10 nM Folate-FITC. In contrast, no lytic activity of GFP CAR-T cells was induced towards THP-1 and THP-1-FRβ by Folate-FITC. For all the cytotoxicity experiments, HL60 cells were used as a control because none of the HL60 cells expressed FRβ as determined by both folate-FITC binding and quantitative RT-PCR (Figure 4A, 4B and 4C). These results were reproducible across multiple T cell donors with similar efficacies. Herein, the cytolytic effect of anti-FITC CAR-T on target cells was FRβ dependent and relied on the concentration of Folate-FITC. The amount of IFN-γ released from anti-CAR-T cells after 24-hour co-culture with THP-1-FRβ was positively correlated with the dose of folate-FITC in the assay media (Figure 4D). The reduction of cell aggregation in the bottom indicated the lytic reactivity of T cells to target cells, which was

visible in co-cultures of anti-FITC CAR T cells and THP-1-FRβ cells with 1 nM and 10 nM folate-FTIC. Meanwhile, cell aggregation in co-cultures of anti-FITC CAR T cells and THP-1 cells with 10 nM folate-FTIC was also visible though slightly decreased (Figure 4E). Overall, our findings demonstrate that folate-FITC, as a bispecific small molecule, can redirect anti-FITC CAR-T cells to target FRβ-positive cells in an antigen-specific and dose-dependent manner. In addition, cell surface expression of CD25 and CD69 were detected after 24-hour co-culture with THP-1 and/or THP-1-FRβ cells to confirm the strict dependence of anti-FITC CAR-T cell activation on folate-FITC. As expected, the increase of CD25 and CD69 expression levels on anti-FITC CAR-T cells was not only correlated with concentration of folate-FITC in the assay media but also correlated with relevant surface expression levels of FRβ in target cells (Figure 4F). Furthermore, folate-FITC dependent proliferation of anti-FITC CAR-T cells was also confirmed by detecting the PKH26 dilution of PKH26 labelled anti-FITC CAR-T cells after 3-day co-culture with THP-1-FRβ cells (Figure 4G).

4. Discussion

The morbidity and mortality of lung cancer both rank first in all malignancies worldwide, and NSCLC is the most common form of lung cancer. Although targeted therapy such as epidermal growth factor receptor (EGFR) tyrosine kinase inhibitors (TKI) and activated lymphocyte kinase (ALK)-TKI can prolong the survival of NSCLC patients with such mutations, drug resistance almost inevitably occurs (*4*). In recent years, immunotherapy, a promising field that harnesses the power of the immune system as a therapeutic agent, has been revolutionizing the lung cancer treatment paradigm. Unfortunately, checkpoint blockade therapy using PD-L1/PD-1 antibodies like Nivolumab and Pembrolizumab only works in a small percentage of NSCLC patients (*34*). Another potentially more potent approach being investigated is adoptive transfer of chimeric antigen receptor T-Cell (CAR-T) with high binding affinity and specificity to the tumor associated antigen (TAA). CAR-T cell immunotherapy has shown tremendous success in the treatment of acute lymphocytic leukemia (ALL) and refractory large B-cell lymphoma demonstrated by the FDA approval of Kymriah and YESCARTA, respectively (*35,36*). However, there are several obstacles to overcome in the process of translation of CAR T-cell therapy to solid tumors.

First and foremost, an ideal tumor specific antigen target is required for generating high affinity scFv, which is the most commonly used ectodomain for CAR. Previous studies have proved that FRα is highly expressed in NSCLC cells and to a large extent in lung adenocarcinoma (*8-10*). Moreover, several studies have

found that its expression levels are associated with tumor stage and survival in lung adenocarcinoma (*11-13*). With the advent of targeted therapies towards FRα for NSCLC treatment and with several such agents, i.e. folate-conjugated small molecule drug and humanized anti-FRα monoclonal antibody, in late stage clinical development (*15-18*), FRα has long been appreciated as a promising target for NSCLC therapy.

Another limitation endowed with current approved CAR-T therapy is treatment-related toxicities. Although the safety and efficiency of Kymriah and YESCARTA were both demonstrated in multicenter clinical trials, unique acute toxicities, which can be severe or even fatal, have been brought to the forefront. The two most commonly observed toxicities with CAR-T therapy are cytokine release syndrome (CRS), which is triggered by the activation and proliferation of CAR-T cells causing high fever, flu-like symptoms, and/or multi-organ toxicity; and a CAR-T cell-related encephalopathy syndrome (CRES), which can sometimes lead to lethal cerebral edema.

Besides administration of anti-IL-6 antibodies and steroids, various strategies are being pursued to rein in the side effects of engineered T cells. One approach to mitigate adverse effects is by incorporating an inducible safety switch into the T-cell product. Mechanisms which are being explored include: inducible caspase 9 system where a small molecule (AP1903) drug dimerizes caspase-9 pro-molecules so that apoptotic pathways in CAR-T cells are activated (*25,37*); transducing genes for CD20 or EGFR so that antibody therapy with rituximab or cetuximab respectively depletes CAR-T cells; HSV thymidine kinase incorporation so that the pro-drug ganciclovir leads to elimination of CART cells (*38*); transient CAR expression by using mRNA (*39*). Undoubtedly, these methods would improve our ability to manage toxicity when it occurs, but they would also affect the persistence of CAR-Ts. Therefore, engineering CAR-Ts to further improve specificity to avoid "on-target, off-tumor" effects is another way that has been proceeding. One such solution would be requiring CAR-Ts to recognize combinatorial antigens by using a synthetic NOTCH receptor for one antigen which then drives the inducible expression of another CAR specific antigen, so that target cell must express two antigens to 'arm and activate' the CAR-Ts (*40*). Other strategies have looked to the use of 'tumor sensing' where T cells are transduced with a CAR that only provides suboptimal activation after binding to its antigen, but a chimeric co-stimulatory receptor that recognizes a second antigen leads to full activation (*41*). Lastly, using a CAR-T that requires a small molecule drug to activate an 'ON-switch' so that antigen binding and intracellular signaling components only assemble in its presence is an interesting approach (*42*). While such approaches have shown improved specificity in preclinical settings, several immunotherapy groups are

also working to develop a new generation of therapies that are inherently safer, yet just as efficacious. One of these technologies uses an intermediate bispecific molecule as a "switch" to redirect the specificity of CAR-Ts and control their activation, expansion, and termination. Unlike conventional CAR-T cells, the scFv portion of the CAR is not raised against any TAA, thus, these CAR-T cells do not recognize endogenous antigen or normal tissue. However, in the presence of an adaptor molecule that is recognized by the CAR extracellular domain and binds specifically to a TAA, CAR-T cells can be redirected specifically to target cancer cells. Moreover, the activity of these CAR-T cells can be regulated in a switch dose-dependent manner. More recently, proof-of-principle studies have been achieved using FITC-, biotin-, or peptide-tagged antibodies (*27-31*).

In this study, we generated CAR T-cells that express a fully humanized scFv for FITC with high affinity. Their potent antigen-specific and folate-FITC dependent *in vitro* cytotoxicity against a FRα-positive cancer cell line was demonstrated. Moreover, the activity, cytokine release ability, activation phenotype and proliferation of anti-FITC CAR-T cells could be controlled or titrated based on the dosage of folate-FITC. Furthermore, we demonstrate that this approach is readily adaptable to target FRβ on a macrophage cell line using the same anti-FITC CAR-T cells.

Folate-FITC, also known as EC17, has been evaluated clinically for use in image-guided surgery for NSCLCs and displayed almost exclusively grade I/II toxicity (*43*). Moreover, its safety has also been approved in a phase I clinical trial for kidney cancer (*44,45*). One additional advantage of using folate-FITC as a switch is the high affinity and specificity of folate, the endogenous ligand, to FRα. In addition to safety, it has been reported that folate-FITC was extremely accurate in identified pulmonary adenocarcinomas in clinical settings (*33*), which further corroborates its specificity. Therefore, the use of folate-FITC as an adaptor to redirect the reactivity of CAR-T cells almost certainly would reduce the potential for off-target cross-reactivity of CAR.

Among the four isoforms of FRs, two forms (FRα and FRβ) bind folate with high affinity ($K_d \sim 1nM$) (*14*). Previous studies showed that over 70% of human lung adenocarcinomas contain FRβ-positive tumor associated macrophages in regions with high immune cell infiltration (*10,33*). With the ability to use folate-FITC to target FRβ-expressing macrophages in the immunotherapy of rheumatoid arthritis that has been demonstrated in animal models, it has been suggested that folate-FITC might likewise efficiently bind to FRβ-expressing TAMs accumulated in the tumor mass of human lung adenocarcinomas. More importantly, higher abundance of TAMs in the stroma of lung adenocarcinoma was observed in patients with more

progressive disease, poorer prognosis, and a lower response rate of targeted chemotherapy (*46,47*). Given that folate-FITC directed anti-FITC CAR-T cells could effectively kill not only FRα-positive tumor cells but also FRβ-expressing macrophages, this strategy might be feasible to improve the of immunosuppressive tumor microenvironment.

Admittedly, there are several limitations to our study. First, given the exploratory nature of this initiative study, the *in vivo* efficacy of folate-FITC controlled anti-FITC CAR-T therapy towards FRα-positive NSCLCs has not been assessed. Second, the plasma clearance half-life of the folate-FITC is relatively short. After a single *i.v.* or *s.c.* injection of ^{3}H-folate-FITC (500 nmol/kg), the majority of radioactivity was cleared from the mouse plasma within 1 to 2 hours (*48*). This may affect the *in vivo* persistence of anti-FITC CAR-T cells. However, the pre-clinical potency of recruiting cytotoxic T cells to FRα-positive ovarian cancer cells for lysis using conjugates of folate and anti-CD3 Fab is promising, even if the serum half-life of folate-conjugate anti-CD3 Fab (a single *i.v.* dose of 1mg/kg) in mouse was about 60 minutes (*49*). In addition, in one previous study, we did not observe a significant difference between Fab and IgG switch mediated cytotoxicity against CD19$^+$ B cell malignance in animal studies. In contrast, Fab-based switch enabled better temporal control over the reactivity due to its shorter pharmacokinetic half-life (*50*). Third, not all NSCLCs, especially squamous cell carcinomas, express FRα. Therefore, use of folate-FITC as a switch is not applicable to other NSCLCs when FRα overexpression is not present. Nevertheless, this shortcoming may also be compensated by the other aspect of this switch-base using the CAR-T strategy. By simply conjugating FITC into another antibody or ligand that targets another well-established NSCLC-specific antigen, the anti-FITC CAR-T cells are readily available to attack those tumor antigen escape variants (*31,50*).

5. Conclusion

We established that *in vitro* anti-FITC CAR-T cell activity can be controlled with a switch, *i.e.* folate-FITC. This bispecific chemical ligand mediated anti-FRα-positive lung cancer cell activity, activation, proliferation and cytokine release ability of CAR-T cells was dose-titratable with a folate-FITC switch. We have also demonstrated that use of folate-FITC as a switch intermediate allows one to target both tumor and tumor-associated macrophages with a single CAR construct. Future studies need to be performed to evaluate the *in vivo* feasibility of this approach.

Acknowledgements

References

1. Siegel RL, Miller KD, Jemal A. Cancer Statistics, 2017. CA Cancer J Clin. 2017; 67:7-30.
2. Chen W, Zheng R, Baade PD, Zhang S, Zeng H, Bray F, Jemal A, Yu XQ, He J. Cancer statistics in China, 2015. CA Cancer J Clin. 2016; 66:115-132.
3. Ettinger DS, Wood DE, Aisner DL, *et al.* Non-Small Cell Lung Cancer, Version 5.2017, NCCN Clinical Practice Guidelines in Oncology. J Natl Compr Canc Netw. 2017; 15:504-535.
4. Heigener DF, Reck M. Lung cancer in 2017: Giant steps and stumbling blocks. Nat Rev Clin Oncol. 2018; 15:71-72.
5. Maude SL, Frey N, Shaw PA, *et al.* Chimeric antigen receptor T cells for sustained remissions in leukemia. N Engl J Med. 2014; 371:1507-1517.
6. Morrow T. Novartis's Kymriah: Harnessing Immune System Comes With Worry About Reining in Costs. Manag Care. 2017; 26:28-30.
7. Leamon CP, Low PS. Delivery of macromolecules into living cells: A method that exploits folate receptor endocytosis. Proc Natl Acad Sci U S A. 1991; 88:5572-5576.
8. Christoph DC, Reyna-Asuncion B, Hassan B, Tran C, Maltzman JD, O'Shannessy DJ, Gauler TC, Wohlschlaeger J, Schuler M, Eberhardt WE, Hirsch FR. Assessment of folate receptor-alpha and epidermal growth factor receptor expression in pemetrexed-treated non-small-cell lung cancer patients. Clin Lung Cancer. 2014; 15:320-330 e321-323.
9. Boogerd LS, Boonstra MC, Beck AJ, Charehbili A, Hoogstins CE, Prevoo HA, Singhal S, Low PS, van de Velde CJ, Vahrmeijer AL. Concordance of folate receptor-alpha expression between biopsy, primary tumor and metastasis in breast cancer and lung cancer patients. Oncotarget. 2016; 7:17442-17454.
10. Shen J, Hu Y, Putt KS, Singhal S, Han H, Visscher DW, Murphy LM, Low PS. Assessment of folate receptor alpha and beta expression in selection of lung and pancreatic cancer patients for receptor targeted therapies. Oncotarget. 2018; 9:4485-4495.
11. Iwakiri S, Sonobe M, Nagai S, Hirata T, Wada H, Miyahara R. Expression status of folate receptor alpha is significantly correlated with prognosis in non-small-cell lung cancers. Ann Surg Oncol. 2008; 15:889-899.
12. O'Shannessy DJ, Yu G, Smale R, Fu YS, Singhal S, Thiel RP, Somers EB, Vachani A. Folate receptor alpha expression in lung cancer: Diagnostic and prognostic significance. Oncotarget. 2012; 3:414-425.
13. Weitman SD, Lark RH, Coney LR, Fort DW, Frasca V, Zurawski VR, Jr., Kamen BA. Distribution of the folate receptor GP38 in normal and malignant cell lines and tissues. Cancer Res. 1992; 52:3396-3401.
14. Xia W, Low PS. Folate-targeted therapies for cancer. J

Med Chem. 2010; 53:6811-6824.

15. Lorusso PM, Edelman MJ, Bever SL, Forman KM, Pilat M, Quinn MF, Li J, Heath EI, Malburg LM, Klein PJ, Leamon CP, Messmann RA, Sausville EA. Phase I study of folate conjugate EC145 (Vintafolide) in patients with refractory solid tumors. J Clin Oncol. 2012; 30:4011-4016.

16. Fisher RE, Siegel BA, Edell SL, Oyesiku NM, Morgenstern DE, Messmann RA, Amato RJ. Exploratory study of 99mTc-EC20 imaging for identifying patients with folate receptor-positive solid tumors. J Nucl Med. 2008; 49:899-906.

17. Konner JA, Bell-McGuinn KM, Sabbatini P, Hensley ML, Tew WP, Pandit-Taskar N, Vander Els N, Phillips MD, Schweizer C, Weil SC, Larson SM, Old LJ. Farletuzumab, a humanized monoclonal antibody against folate receptor alpha, in epithelial ovarian cancer: A phase I study. Clin Cancer Res. 2010; 16:5288-5295.

18. Edelman MJ, Harb WA, Pal SE, Boccia RV, Kraut MJ, Bonomi P, Conley BA, Rogers JS, Messmann RA, Garon EB. Multicenter trial of EC145 in advanced, folate-receptor positive adenocarcinoma of the lung. J Thorac Oncol. 2012; 7:1618-1621.

19. Guertin AD, O'Neil J, Stoeck A, *et al*. High Levels of Expression of P-glycoprotein/Multidrug Resistance Protein Result in Resistance to Vintafolide. Mol Cancer Ther. 2016; 15:1998-2008.

20. Tey SK. Adoptive T-cell therapy: Adverse events and safety switches. Clin Transl Immunology. 2014; 3:e17.

21. Morgan RA, Yang JC, Kitano M, Dudley ME, Laurencot CM, Rosenberg SA. Case report of a serious adverse event following the administration of T cells transduced with a chimeric antigen receptor recognizing ERBB2. Mol Ther. 2010;18:843-851.

22. Parkhurst MR, Yang JC, Langan RC, *et al*. T cells targeting carcinoembryonic antigen can mediate regression of metastatic colorectal cancer but induce severe transient colitis. Mol Ther. 2011;19:620-626.

23. Lamers CH, Sleijfer S, van Steenbergen S, van Elzakker P, van Krimpen B, Groot C, Vulto A, den Bakker M, Oosterwijk E, Debets R, Gratama JW. Treatment of metastatic renal cell carcinoma with CAIX CAR-engineered T cells: Clinical evaluation and management of on-target toxicity. Mol Ther. 2013; 21:904-912.

24. Linette GP, Stadtmauer EA, Maus MV, *et al*. Cardiovascular toxicity and titin cross-reactivity of affinity-enhanced T cells in myeloma and melanoma. Blood. 2013; 122:863-871.

25. Di Stasi A, Tey SK, Dotti G, *et al*. Inducible apoptosis as a safety switch for adoptive cell therapy. N Engl J Med. 2011; 365:1673-1683.

26. Wilkie S, van Schalkwyk MC, Hobbs S, Davies DM, van der Stegen SJ, Pereira AC, Burbridge SE, Box C, Eccles SA, Maher J. Dual targeting of ErbB2 and MUC1 in breast cancer using chimeric antigen receptors engineered to provide complementary signaling. J Clin Immunol. 2012; 32:1059-70.

27. Tamada K, Geng D, Sakoda Y, Bansal N, Srivastava R, Li Z, Davila E. Redirecting gene-modified T cells toward various cancer types using tagged antibodies. Clin Cancer Res. 2012; 18:6436-6445.

28. Urbanska K, Lanitis E, Poussin M, Lynn RC, Gavin BP, Kelderman S, Yu J, Scholler N, Powell DJ Jr. A universal strategy for adoptive immunotherapy of cancer through use of a novel T-cell antigen receptor. Cancer Res. 2012;

72:1844-1852.

29. Kudo K, Imai C, Lorenzini P, Kamiya T, Kono K, Davidoff AM, Chng WJ, Campana D. T lymphocytes expressing a CD16 signaling receptor exert antibody-dependent cancer cell killing. Cancer Res. 2014; 74:93-103.

30. Kim MS, Ma JS, Yun H, Cao Y, Kim JY, Chi V, Wang D, Woods A, Sherwood L, Caballero D, Gonzalez J, Schultz PG, Young TS, Kim CH. Redirection of genetically engineered CAR-T cells using bifunctional small molecules. J Am Chem Soc. 2015;137:2832-2835.

31. Ma JS, Kim JY, Kazane SA, *et al*. Versatile strategy for controlling the specificity and activity of engineered T cells. Proc Natl Acad Sci U S A. 2016; 113:E450-458.

32. van Dam GM, Themelis G, Crane LM, Harlaar NJ, Pleijhuis RG, Kelder W, Sarantopoulos A, de Jong JS, Arts HJ, van der Zee AG, Bart J, Low PS, Ntziachristos V. Intraoperative tumor-specific fluorescence imaging in ovarian cancer by folate receptor-α targeting: First in-human results. Nat Med. 2011; 17:1315-1319.

33. Predina JD, Newton AD, Keating J, Dunbar A, Connolly C, Baldassari M, Mizelle J, Xia L, Deshpande C, Kucharczuk J, Low PS, Singhal S. A Phase I Clinical Trial of Targeted Intraoperative Molecular Imaging for Pulmonary Adenocarcinomas. Ann Thorac Surg. 2018; 105:901-908.

34. Morgensztern D, Herbst RS. Nivolumab and Pembrolizumab for Non-Small Cell Lung Cancer. Clin Cancer Res. 2016; 22:3713-3717.

35. Prasad V. Immunotherapy: Tisagenlecleucel - the first approved CAR-T-cell therapy: Implications for payers and policy makers. Nat Rev Clin Oncol. 2018; 15:11-12.

36. Yip A, Webster RM. The market for chimeric antigen receptor T cell therapies. Nat Rev Drug Discov. 2018; 17:161-162.

37. Zhou X, Dotti G, Krance RA, *et al*. Inducible caspase-9 suicide gene controls adverse effects from alloreplete T cells after haploidentical stem cell transplantation. Blood. 2015; 125:4103-4013.

38. Casucci M, Hawkins RE, Dotti G, Bondanza A. Overcoming the toxicity hurdles of genetically targeted T cells. Cancer Immunol Immunother. 2015; 64:123-130.

39. Riet T, Holzinger A, Dörrie J, Schaft N, Schuler G, Abken H. Nonviral RNA transfection to transiently modify T cells with chimeric antigen receptors for adoptive therapy. Methods Mol Biol. 2013; 969:187-201.

40. Roybal KT, Williams JZ, Morsut L, Rupp LJ, Kolinko I, Choe JH, Walker WJ, McNally KA, Lim WA. Engineering T Cells with Customized Therapeutic Response Programs Using Synthetic Notch Receptors. Cell. 2016;167:419-432.

41. Kloss CC, Condomines M, Cartellieri M, Bachmann M, Sadelain M. Combinatorial antigen recognition with balanced signaling promotes selective tumor eradication by engineered T cells. Nat Biotechnol. 2013; 31:71-75.

42. Wu CY, Roybal KT, Puchner EM, Onuffer J, Lim WA. Remote control of therapeutic T cells through a small molecule-gated chimeric receptor. Science. 2015; 350:aab4077.

43. Kennedy GT, Okusanya OT, Keating JJ, Heitjan DF, Deshpande C, Litzky LA, Albelda SM, Drebin JA, Nie S, Low PS, Singhal S. The Optical Biopsy: A Novel Technique for Rapid Intraoperative Diagnosis of Primary Pulmonary Adenocarcinomas. Ann Surg. 2015; 262:602-609.

44. Amato RJ, Shetty A, Lu Y, Ellis PR, Mohlere V, Carnahan N, Low PS. A Phase I/Ib study of folate immune (EC90 vaccine administered with GPI-0100 adjuvant followed by EC17) with interferon-α and interleukin-2 in patients with renal cell carcinoma. J Immunother. 2014; 37:237-244.

45. Amato RJ, Shetty A, Lu Y, Ellis R, Low PS. A phase I study of folate immune therapy (EC90 vaccine administered with GPI-0100 adjuvant followed by EC17) in patients with renal cell carcinoma. J Immunother. 2013; 36:268-275.

46. Wang R, Zhang J, Chen S, Lu M, Luo X, Yao S, Liu S, Qin Y, Chen H. Tumor-associated macrophages provide a suitable microenvironment for non-small lung cancer invasion and progression. Lung Cancer. 2011; 74:188-196.

47. Chung FT, Lee KY, Wang CW, Heh CC, Chan YF, Chen HW, Kuo CH, Feng PH, Lin TY, Wang CH, Chou CL, Chen HC, Lin SM, Kuo HP. Tumor-associated macrophages correlate with response to epidermal growth factor receptor-tyrosine kinase inhibitors in advanced non-small cell lung cancer. Int J Cancer. 2012;131:E227-35.

48. Lu Y, Xu LC, Parker N, Westrick E, Reddy JA, Vetzel M, Low PS, Leamon CP. Preclinical pharmacokinetics, tissue distribution, and antitumor activity of a folate-hapten conjugate-targeted immunotherapy in hapten-immunized mice. Mol Cancer Ther. 2006; 5:3258-3267.

49. Kularatne SA, Deshmukh V, Gymnopoulos M, *et al*. Recruiting cytotoxic T cells to folate-receptor-positive cancer cells. Angew Chem Int Ed Engl. 2013; 52:12101-12104.

50. Rodgers DT, Mazagova M, Hampton EN, *et al*. Switch-mediated activation and retargeting of CAR-T cells for B-cell malignancies. Proc Natl Acad Sci U S A. 2016;113:E459-68.

Original Article

Long non-coding RNA Linc00312 modulates the sensitivity of ovarian cancer to cisplatin *via* the Bcl-2/Caspase-3 signaling pathway

Chuanqi Zhang, Min Wang*, **Cong Shi, Fanli Shi, Cheng Pei**

Department of Gynecology and Obstetrics, Shengjing Hospital Affiliated of China Medical University, Shenyang, Liaoning, China;

Summary	Chemotherapy is one of the main treatments for ovarian cancer (OC). Cisplatin combined with paclitaxel is a commonly used chemotherapy regimen. However, effective cancer therapy is hindered by a patient's resistance to cisplatin. The mechanism that potentially leads to that resistance is unclear. The current study examined the mechanism by which Linc00312 is involved in resistance to cisplatin in OC. Quantitative real-time PCR (RT-qPCR) was used to test for expression of Linc00312 in freshly frozen tissue samples of OC and in SKOV3 and SKOV3/DDP cells. In situ hybridization was performed to examine the distribution of Linc00312 expression in paraffin-embedded histological sections that were sensitive or resistant to cisplatin. The cell counting kit-8 assay was used to detect cell viability. Flow cytometry was used to measure cell apoptosis. RT-qPCR was performed to confirm changes in expression of MDR1, MRP1, Bcl-2, Bax, Caspase-3, and Caspase-9 mRNA. Levels of MDR1, Bcl-2, Bax, Caspase-3, and Caspase-9 protein were detected with Western blotting. Experiments indicated that the expression of Linc00312 decreased significantly in SKOV3/DDP cells compared to that in SKOV3 cells. Upregulation of Linc00312 can considerably increase the sensitivity of SKOV3/DDP cells to cisplatin, while down-regulation of Linc00312 has the exact opposite effect in SKOV3 cells. Linc00312 enhanced the sensitivity of SKOV3/DDP cells to cisplatin by promoting cell apoptosis *via* the Bcl-2/Caspase-3 signaling pathway. These findings suggest that Linc00312 may be a promising clinical strategy for the treatment of drug-resistant OC.

Keywords: Linc00312, cisplatin, chemosensitivity, ovarian cancer, cell apoptosis

1. Introduction

Ovarian cancer (OC) is one of the most common threats to women's health worldwide; OC has a high incidence and mortality, so molecular biomarkers for OC need to be identified and the pathogenesis of OC needs to be determined in order to devise an effective therapy (*1*). Numerous studies have established that long non-coding RNAs (LncRNAs) are widespread and potent regulators of diseases, so LncRNAs could serve as biomarkers and targets in OC.

LncRNAs, a class of RNA longer than 200 nucleotides that cannot encode proteins, are mRNA-like transcripts that have been increasingly identified as the key regulators in the tumorigenesis and progression of various human cancers (*2*). Thus, investigating the roles and potential mechanisms of LncRNAs in tumorigenic driver pathways is of considerable interest (*3*). One such LncRNA is Linc00312. Linc00312 is transcribed from the genomic region of chromosome 3p25.3, and Linc00312 has been found to be significantly dysregulated in a wide range of diseases, such as non-small cell lung cancer (*4*), bladder cancer (*5*), thyroid cancer (*6*) and nasopharyngeal carcinoma (*7*). Furthermore, Linc00312 plays a vital role in cell proliferation (*8*), cell apoptosis, differentiation, and metastasis (*7*) by interacting with particular microRNAs

Table 1. The primers for RT-qPCR

Name	Sequence (from 5' to 3'), Sense	Sequence (from 5' to 3'), Antisense
Linc00312	TCTGGCTGTTGTTGTGTTGGA	GCTTATTGGCTTGGTTCGCT
MDR1	GACCGGACATCCCAGTGCTT	TGTGCTCGGAGCCACTGAAC
MRP1	TCTACCTCCTGTGGCTGAATCTG	CCGATTGTCTTTGCTCTTCATG
Bcl-2	AAGAGCAGACGGATGGAAAAAGG	GGGCAAAGAAATGCAAGTGAATG
Bax	CTGAGCGAGTGTCTCAAGCG	CCCCAGTTGAAGTTGCCGTC
Caspase-3	GGGATCGTTGTAGAAGTCTAA	CGGCCTCCACTGGTATT
Caspase-9	CCAGACCAGTGGACATT	CTCCATGCTCAGGATGTAA
Gapdh	CAGGAGGCATTGCTGATGAT	GAAGGCTGGGGCTCATTT

or target genes.

However, there is no evidence to prove whether Linc00312 is connected to drug resistance, especially in OC. This study is the first to describe the functions of Linc00312 in the sensitivity of OC to cisplatin.

2. Materials and Methods

2.1. *Patient samples*

Freshly frozen tissue samples of serous epithelial ovarian carcinoma (EOC) from chemosensitive patients ($n = 60$) and chemoresistant patients ($n = 60$) were retrospectively collected at Liaoning Cancer Hospital and Institute from 2014 to 2016. Paraffin-embedded histological sections came from 15 patients in each group from 2013 to 2015. All patients underwent tumor excision, followed by 6-8 cycles of chemotherapy with cisplatin and paclitaxel. In accordance with NCCN guidelines, the chemoresistant group responded to initial chemotherapy but failed to respond during later chemotherapy or within 6 months of the conclusion of chemotherapy. The chemosensitive group were patients with recurrence after 12 months or with no recurrence after chemotherapy. Clinical information including age, stage of surgery, tumor grade, pathological subtype, and lymph node metastasis was obtained from medical records. This study was approved by the Ethics Committee of China Medical University's Shengjing Hospital.

2.2. *Cell lines and culture*

The human ovarian cancer cell line SKOV3 were purchased from the Cell Culture Collection of Shanghai. Cisplatin-resistant SKOV3/DDP cells were obtained from the Chinese Academy of Medical Sciences and Peking Union Medical College, Beijing, China. Cells were cultured in Iscove's modified Dulbecco's medium (IMDM; Hyclone, Logan, Utah, USA) supplemented with 10% fetal bovine serum (Australian FBS; Cellmax Cell Technology Co., Ltd, Lanzhou, China) and 1% penicillin/streptomycin (HyClone) in a humidified incubator at 37°C in an atmosphere of 5% CO_2. To maintain resistance, SKOV3/DDP cells were cultured in the presence of 1 μg/mL cisplatin (Meilune Biotechnology Co., Ltd., Dalian, China). Cells in the logarithmic phase of growth were used in all experiments.

2.3. *Cell transfection*

An Linc00312-overexpression plasmid and a control plasmid were purchased from Genechem Co., Ltd. (Shanghai, China). SiRNAs (GenePharma Co., Ltd., Shanghai, China) for Linc00312 and negative controls (NC) were synthesized. SKOV3 and SKOV3/DDP cells were counted and seeded in 6-well plates with antibiotic-free medium for 24 h to ensure 70% cell confluence on the day of transfection. Cells were transfected with Lipofectamine 3000 (Invitrogen; Thermo Fisher Scientific, Inc.) according to the manufacturer's instructions. RNA isolation was performed 48 h after transfection, and protein extraction was performed 72 h after transfection. SiRNA was transfected 3 times at a final concentration of 30 nM.

2.4. *Quantitative real-time PCR (RT-qPCR)*

Total RNA was extracted from tumor cells and tissues using TRIzol reagent (Invitrogen, Carlsbad, CA, USA), and 400ng of total RNA from each sample was converted to cDNA using the PrimeScriptVR RT Reagent Kit (Takara, Dalian, China). RT-qPCR was performed using SYBR Premix Ex Taq (Takara, Dalian, China) on the Stratagene Mx3000P Real-Time PCR System (Agilent Technologies, USA) according to the manufacturer's instructions. The primers for analysis are listed in Table 1. Gapdh mRNA served as an endogenous control, and relative levels of expression of other mRNAs were measured using the 2−ΔΔct method.

2.5. *Cell counting kit-8 assay (CCK-8 assay)*

SKOV3 cells and SKOV3/DDP cells were plated on 96-well plates at a density of $8×10^3$ cells/100 μL of medium per well. After transfection for 24 h, cisplatin was added to each well at a concentration of 0, 1, 2, 4, 8, 12, 16, 24, 32, or 60 μg/mL. Cells were incubated for 48 h. Cell viability was assessed using the CCK-8 assay (Dojindo Laboratories, Shanghai, China). After 1 h, the

absorbance of each well was measured at a wavelength of 450 nm using a spectrophotometer (XFLUOR4 Version: V 4.51). The 50% inhibitory concentration (IC_{50}) value for cisplatin treatment was estimated based on the viability curve.

2.6. Cell apoptosis assay

Cells were plated at a density of 2×10^5 cells/2 mL medium on 6-well plates for 24 h. After transfection for 24 h, cells were treated with 3 μg/mL cisplatin. After 48 h of treatment, cells were harvested and washed twice with cold PBS. Cell apoptosis was detected using the Annexin V-FITC Apoptosis Detection Kit (Yuheng Co., Ltd, Jiangsu, China). Cells were stained with 5 μL Annexin V and 2 μL PI in the binding buffer for 15 min in the dark and then subjected to flow cytometry (BD FACSDiva TM Fusion).

2.7. Western blot analysis

Whole-cell lysates were prepared and quantified and then protein was separated on 10% SDS-PAGE gel. Protein was harvested using RIPA lysis buffer (Beyotime, China), diluted with loading buffer containing SDS (Beyotime, China), and denatured at 100°C for 5 min. After electrophoresis, protein (30 μg) was transferred to PVDF membranes (Millipore, Boston, MA, USA) and then blocked with 5% BSA. The membranes were incubated overnight with primary antibodies from Wanleibio (Shenyang, China) against MDR1 (1:500, Rabbit), Bcl-2 (1:500, Rabbit), Bax (1:500, Rabbit), Caspase-3 (1:1,000, Rabbit), Caspse-9 (1:1,000, Rabbit), and Gapdh (1:1,000, Mouse) as a visual loading control. After membranes were incubated with the secondary antibody (1:4,000, EarthOx, San Francisco, CA, USA), protein signals were detected using enhanced chemiluminescence (ECL, Amersham, Germany).

2.8. In situ hybridization (ISH)

The Linc00312 probes were 5'-CTTGACATCTTAGAAG ATTAAAGGT TATTT AAAGTTGTTG-3', 5'-ATT ACCATCCTTATTTATTTTAATGCTCAAATTGT CCCAA-3', and 5'-TGCAATGGCATGGCTGTTGG TCATTCACATCTCTCTCTGT-3' (Boster Biological Technology Co. Ltd., Wuhan, China). Five-μm-thick paraffin-embedded sections were incubated for 30 min ahead of schedule. The sections were then procedurally dewaxed, rehydrated, and immersed in 3% H_2O_2 at 42°C for 10 min to inactivate endogenous peroxidase activity. Fragments of mRNA nucleic acid were degraded with pepsin that was diluted with 3% citric acid at 42°C for 10 min. The slides were incubated with a prehybridization solution at 42°C for 2 hours and hybridized with an Linc00312 probe at 42°C in a wet box overnight. The next day, sections were washed with SSC, respectively

incubated with a blocking solution, biotinylated anti-mouse digoxin, SABC, and biotinylated peroxidase at 42°C, stained with DAB, and then counterstained with hematoxylin. Finally, tissues sections were dehydrated and mounted.

Two pathologists examined all of the sections and graded them independently. Five views were randomly selected at 400× magnification. A positive hybridization signal was identified by dark brown staining in the cytoplasm. Depending on the intensity of positive staining, staining was scored as follows: negative = 0, weak = 1, moderate = 2, and strong = 3. The proportion of stained cells was scored as < 10% = 1, 10-50% = 2, > 50% = 3. The final score was the product of the two aforementioned scores: 0:(−), 1-3: (+), 4-6: (++), and 7-9: (+++).

2.9. Statistical analysis

SPSS software Version 17.0 (IBM SPSS, Chicago, IL) was used for statistical analysis. The Student's two-tailed t-test was used to evaluate the statistical relevance between different groups. All data are expressed as the mean ± the standard deviation (SD). A value of $p < 0.05$ was considered statistically significant. All experiments were performed in triplicate.

3. Results

3.1. Downregulation of Linc00312 in chemo-resistant serous EOC tissues

In this study, the level of Linc00312 expression decreased significantly in OC chemo-resistant tissues according to RT-qPCR. The expression of Linc00312 in chemo-sensitive tissue samples was normalized as shown in Figure 1A. The level of expression was significantly lower in chemo-resistant tissues ($p < 0.01$). The localization of Linc00312 in cells was determined using ISH. Results indicated that Linc00312 was mainly localized in the cytoplasm (Figure 2), and the same trend was as was noted in RT-qPCR was evident (Table 2).

Receiver operating characteristics (ROC) curve analysis was performed to evaluate the accuracy with which patients with OC who were resistant to chemotherapy could be distinguished from those who were sensitive to chemotherapy. A cut-off value was obtained. An area under the curve (AUC) of 0.907 had a high discriminatory power (95% CI: 0.854-0.960, $p < 0.01$) (Figure 1B). When the cut-off point was 0.717, the chemo-resistance of OC was predicted with a sensitivity of 91.7% and a sensitivity of 80%. These results suggest that decreased expression of Linc00312 in patients with OC could serve as a biomarker with which to determine the chemo-resistant features of serous EOC.
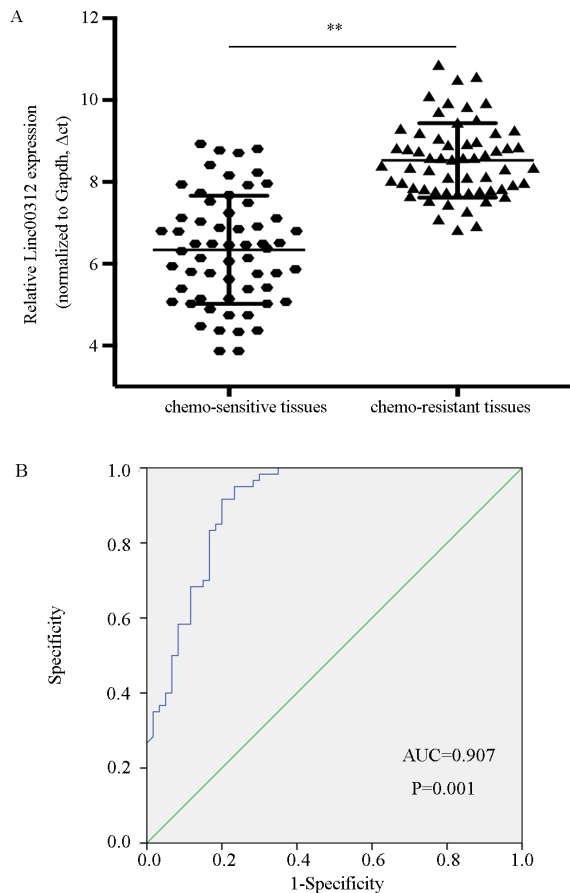
Figure 1. Linc00312 expression and ROC curve analysis in chemo-sensitive tissues and chemo-resistant tissues of freshly frozen tissue samples in serous epithelial ovarian carcinoma. (A) Levels of expression according to RT-qPCR. *******p* < 0.01 *vs.* chemo-sensitive tissues. **(B)** ROC curve for the value.
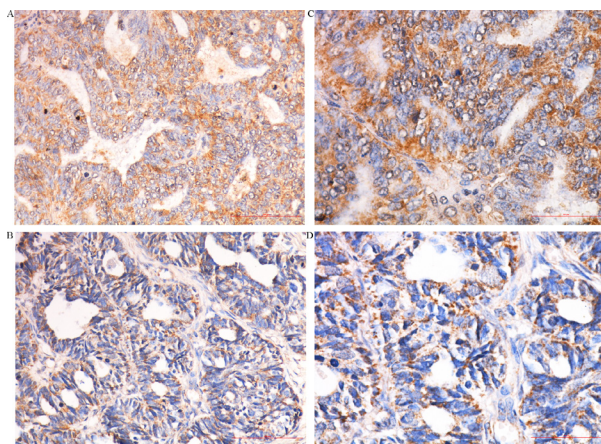
Figure 2. Expression of Linc00312 in paraffin-embedded histological sections of serous epithelial ovarian cancer by ISH. (A,C) chemosensitive tissue, A×200, C×400; **(B,D)** chemoresistant tissue, B×200, D×400.

3.2. Linc00312 reduces chemoresistance to cisplatin in SKOV3 and SKOV3/DDP cells

RT-qPCR results revealed that SKOV3/DDP cells had a lower level of Linc00312 expression than that in SKOV3 cells (*p* < 0.01, Figure 3A).
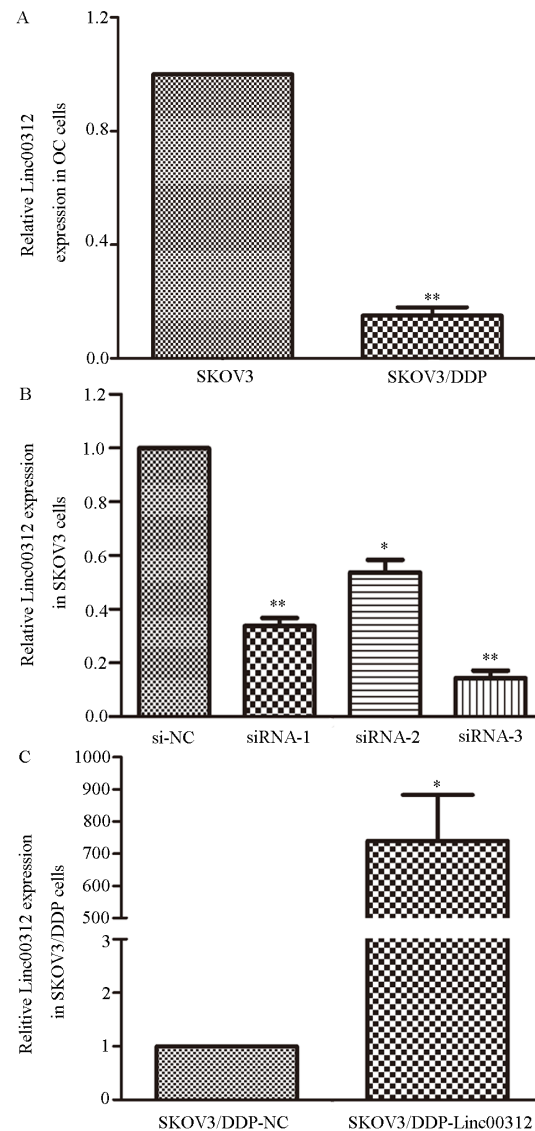
Figure 3. Expression of Linc00312 in cisplatin-sensitive and cisplatin-resistant ovarian cancer cell lines according to RT-RT-QPCR, normalized to Gapdh. (A) Level of Linc00312 mRNA in SKOV3 and SKOV3/DDP cells, *******p* < 0.01 *vs.* SKOV3 cell group. **(B)** The level of Linc00312 mRNA transfected with Linc00312 siRNA in SKOV3 cells, ******p* < 0.05 and *******p* < 0.01 *vs.* si-NC group. **(C)** Expression of Linc00312 in SKOV3/DDP cells transfected with an overexpression plasmid, ******p* < 0.05 *vs.* SKOV3/DDP NC group.

Table 2. The expression of Linc00312 in different ovarian cancer tissues

Group	N	Linc00312 expression				High cases (N)	High cases Rates (%)	P
		-	+	++	+++			
Sensitivity	15	0	8	6	1	7	46.7	
Resistance	15	0	11	4	0	4	26.7	0.0437*

*Sensitivity *vs.* resistance, *P = 0.0437

To further investigate the effect of Linc00312 on cell proliferation and cisplatin resistance, siRNA was transfected into SKOV3 cells and GV146-Linc00312 into SKOV3/DDP cells (Figures 3B and C). Cells were treated with different concentrations of cisplatin. Inhibition rates and IC_{50} values were determined with a CCK-8 assay. After treatment with cisplatin, the rate of inhibition of SKOV3-siRNA cells decreased significantly compared to that in SKOV3-NC cells ($p < 0.05$, Figure 4A). The rate of inhibition of SKOV3/DDP cells with GV146-Linc00312 increased markedly

($p < 0.05$, Figure 4B). In SKOV3 cells transfected with siRNA, the IC_{50} of cisplatin was 6.308 ± 0.299 µg/mL , which was higher th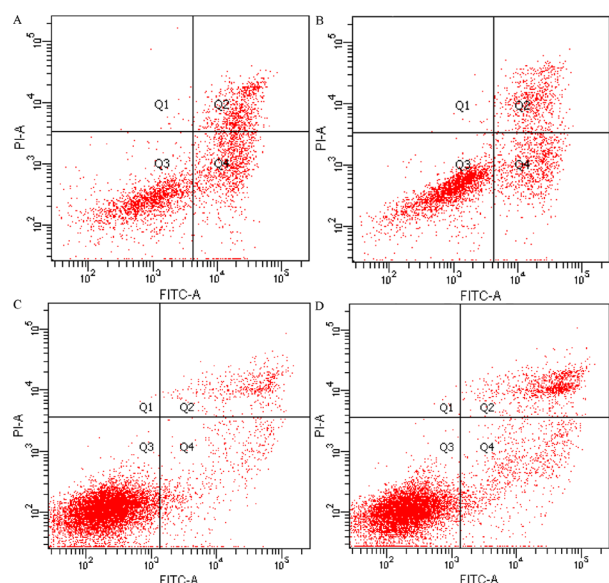an 4.297 ± 0.148 µg/mL in control SKOV3 cells. The IC_{50} of cisplatin decreased to 4.609 ± 0.551 µg/mL in SKOV3/DDP cells transfected with GV146-Linc00312 in comparison to that in control SKOV3/DDP cells (8.817 ± 0.988 µg/mL) ($p < 0.01$, Figure 4C). These results indicate that Linc00312 acted as a key factor for the chemoresistance of SKOV3/DDP cells to cisplatin.

3.3. *Linc00312 suppresses chemoresistance to cisplatin through activation of cell apoptosis*

Resistance to apoptosis is one of the key reasons for a poor response to cisplatin, so the current authors hypothesized that Linc00312 might be involved in cisplatin resistance through activation of cell apoptosis. After transfection, cells were exposed to 3 µg/mL cisplatin for 48 h. Flow cytometry analysis indicated that suppressing Linc00312 expression in SKOV3 cells decreased cell apoptosis in an inverse manner (17.4000 ± 0.55678 *vs.* 21.0667 ± 1.65630, $p < 0.05$, Figures 5A and B, Figure 6) and that overexpression of Linc00312 in SKOV3/DDP cells increased cell apoptosis (10.3667 ± 0.92916 *vs.* 6.6333 ± 0.45092, $p < 0.01$, Figures 5C and D, Figure 6).

3.4. *Linc00312 activates the Bcl-2/Caspase-3 apoptotic signaling pathway*

As mentioned earlier, the overexpression of Linc00312 promoted sensitivity to cisplatin and increased the rate of inhibition of SKOV3/DDP cells, resulting in

Figure 4. The rate of inhibition and the IC_{50} of cisplatin in ovarian cancer cells. (A) The rate of inhibition of SKOV3 cells after si-Linc00312 transfection, *$p < 0.05$ *vs.* SKOV3 NC group. **(B)** The rate of inhibition of SKOV3/DDP cells after GV146-Linc00312 transfection, *$p < 0.05$ and **$p < 0.01$ *vs.* SKOV3/DDP NC group. **(C)** The IC_{50} of cisplatin in SKOV3 cells transfected with Linc00312 siRNA and SKOV3/DDP cells transfected with an overexpression plasmid, **$p < 0.01$ *vs.* si-NC, ##$p < 0.01$ *vs.* GV146-NC.

Figure 5. Effect of Linc00312 siRNA and an overexpression plasmid on the ratio of apoptosis of SKOV3 and SKOV3/ DDP cells after exposure to cisplatin. The ratio of apoptosis of **(A)** SKOV3 si-NC, **(B)** SKOV3 si-Linc00312, **(C)** SKOV3/ DDP GV146-NC, and **(D)** SKOV3/DDP GV146-Linc00312.
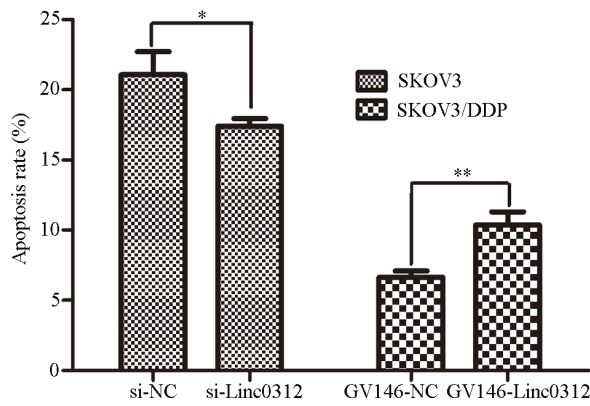
Figure 6. Column chart of the ratio of apoptosis in SKOV3 and SKOV3/DDP cells. *$p < 0.05$ vs.* si-NC group and ***$p < 0.01$ vs.*GV146-NC group.

significantly increased cell apoptosis. To explore the signaling pathway for this response, the mRNA of drug resistance-related genes (MDP1 and MRP1) and apoptosis genes (Bcl-2, Bax, Caspase-3, and Caspase-9) was detected with RT-qPCR after transfecting cells with Linc00312 siRNA and an overexpression plasmid. When SKOV3 cells were transfected with siRNA, the expression of MDR1, MRP1, and Bcl-2 mRNA increased while the expression of Bax, Caspase-3, and Caspase-9 mRNA was lower than that in SKOV3 NC cells ($p < 0.05$, Figure 7A). When GV146-Linc00312 was transfected into SKOV3/DDP cells, the reverse trend was evident ($p < 0.05$, Figure 7B). Western blotting was used to detect levels of MDR1, Bcl-2, Bax, Caspase-3, and Caspase-9 protein, and results revealed
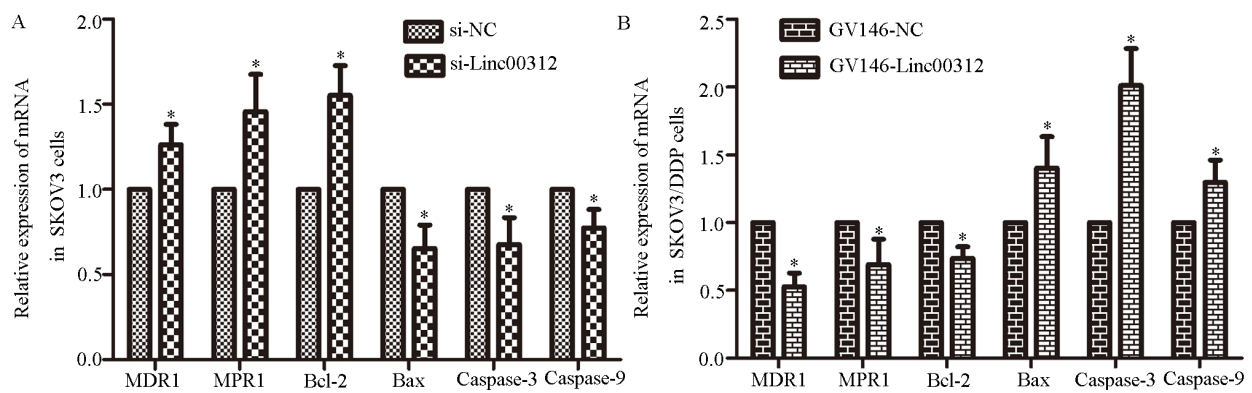
Figure 7. Levels of mRNA expression of several genes in (A) SKOV3 cells, *$p < 0.05$ vs.* si-NC group, and **(B)** SKOV3/DDP cells, *$p < 0.05$ vs.* GV146-NC group.
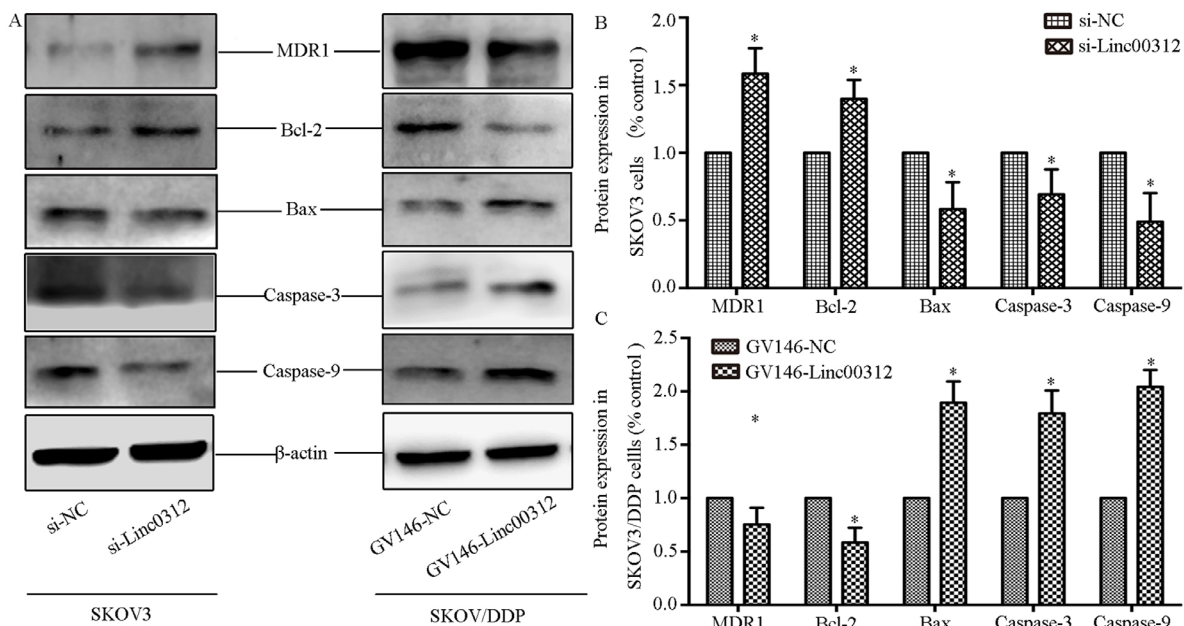
Figure 8. Levels of expression of MDR1, Bcl-2, Bax, Caspase-3, and Caspase-9 protein in SKOV3 and SKOV3/DDP cells. (A) Respective Western blots of protein expression in SKOV3 cells transfected with Linc00312 siRNA or SKOV3/DDP cells transfected with a GV146 plasmid. The column chart shows quantified expression in SKOV3 cells **(B)** and SKOV3/DDP cells **(C)**. *$p < 0.05$ vs.* si-NC group or GV146-NC group.

the same trends as were noted in levels of mRNA ($p <$ 0.05, Figure 8).

4. Discussion

OC is frequently treated with chemotherapy with cisplatin and paclitaxel, and primary chemotherapy is successful for 80-90% of patients (9). However, patients eventually become resistant to cisplatin, so chemoresistance significantly hampers chemotherapy for OC and patient prognosis (10).

According to recent studies, Linc00312 plays a key role as a tumor suppressor gene. It is down-regulated in several cancer tissues compared to normal tissues, including non-small cell lung cancer (4), bladder cancer (5), thyroid cancer (6), and nasopharyngeal carcinoma (7). At present, however, the expression of Linc00312 and its possible role in chemoresistance in OC has not been studied. The current study found that the expression of Linc00312 was much lower in 60 samples of serous EOC chemo-resistant tissues than that in 60 samples of chemo-sensitive tissues according to RT-qPCR. Furthermore, Linc00312 was mainly localized in the cytoplasm of serous EOC epithelial cells, and its expression according to ISH followed the same trend as that according to RT-qPCR. The ROC curve implied that Linc00312 could be a potential marker with which to distinguish chemo-resistant serous EOC from chemo-sensitive serous EOC.

SKOV3 and SKOV3/DDP cell lines were used to examine Linc00312 expression in cisplatin-resistant OC *via in vitro* experiments. The restoration of Linc00312 sensitized SKOV3/DDP cells to cisplatin and enhanced cisplatin-mediated apoptosis. Inversely, restraining Linc00312 decreased the responsiveness of SKOV3 cells to chemotherapy. This indicated that Linc00312 may be a promising marker for the identification of chemotherapy-resistant and sensitive OC and a biomarker for use in patients who have been diagnosed with OC and who are receiving platinum-based chemotherapy.

To ascertain the possible mechanism for this phenomenon, siRNA was transfected into SKOV3 cells and an overexpressed plasmid was transfected into SKOV3/DDP cells. Knockdown of Linc00312 promoted the resistance of OC cells to cisplatin by suppressing cell proliferation and inducing apoptosis, whereas overexpression of Linc00312 sensitized OC cells to cisplatin.

Multi-drug resistance (MDR) is mainly due to ATP-binding cassette transporters, and this phenomenon explains why few patients with cancer respond well to chemotherapy drugs (11). Multidrug resistance 1 (MDR1) and multidrug resistance protein 1 (MRP1) are two well-known transporters (12) that are involved in cisplatin-induced resistance (13). The over-expression of MDR1 and MRP1 inhibit intracellular drug accumulation and catalyze energy-dependent drug efflux in different malignancies (14,15), such as OC (16).

Most chemotherapies kill cancer cells mainly by promoting cell apoptosis, and fewer cells are apoptotic when they are chemoresistant. Bcl-2 is mainly located in the mitochondria and rough endoplasmic reticulum, and it participates in the cell apoptosis intrinsic pathway by inhibiting the oligomerization of Bax to prolong the life cycle of cells (17). Bcl-2 overexpression induces the immortalization of damaged cells, it promotes tumor development, and it regulates cell proliferation and apoptosis (18). Bax induces the permeabilization of the outer mitochondrial membrane and it then activates the caspase family to form an apoptotic signaling pathway (19,20). The current results indicated that underexpression of Linc00312 increased the expression of Bcl-2 and decreased the expression of Bax, Caspase-3, and Caspase-9, while overexpression of Linc00312 had the opposite effect on expression of the those genes. These results indicate that Linc00312 acted *via* the bcl-2/caspase-3 pathway in OC cells.

According to previous studies, the most common way in which LncRNA functions is through competing endogenous RNA (ceRNA) during the transcription and post-transcriptional stages. LncRNA absorbs cytoplasmic miRNAs like a sponge and reduces their abundance, keeping miRNAs from repressing target proteins in various cancers (21). This is also an effective regulative pathway that is correlated with chemotherapy resistance and that has been found in OC (22,23). In addition, Linc00312 has been found to act as a sponge and down-regulate miR-197-3p, thereby inhibiting the invasion and migration of cancer cells (5,6). Therefore, Linc00312 may adsorb another miRNA and thus allow the expression of a target protein to increase. This in turn activates the Bcl-2/Caspase-3 signaling pathway and it promotes cell apoptosis in OC. This point will be studied further in the future.

In summary, this study found that the expression of Linc00312 decreased significantly in chemo-resistant serous EOC tissues compared to chemo-sensitive tissues. Moreover, results indicated that Linc00312 inhibited cell proliferation and promoted cell apoptosis in SKOV3 and SKOV3/DDP cells. Linc00312 decreases Bcl-2 expression and increases Bax expression, thus activating the Bcl-2/Caspase-3 signaling pathway to promote cell apoptosis, and this counteracts chemo-resistance to cisplatin. Thus, Linc00312 may be a potential target for treatment of cisplatin-resistant OC.

References

1. Cortez AJ, Tudrej P, Kujawa KA, Lisowska KM. Advances in ovarian cancer therapy. Cancer Chemother Pharmacol. 2018; 81:17-38.
2. Mercer TR, Mattick JS. Structure and function of long noncoding RNAs in epigenetic regulation. Nat Struct Mol Biol. 2013; 20:300-307.
3. Huarte M. The emerging role of lncRNAs in cancer. Nat Med. 2015; 21:1253-1261.
4. Tan Q, Yu Y, Li N, Jing W, Zhou H, Qiu S, Liang C, Yu M, Tu J. Identification of long non-coding RNA 00312 and 00673 in human NSCLC tissues. Mol Med Rep. 2017; 16:4721-4729.
5. Wang YY, Wu ZY, Wang GC, Liu K, Niu XB, Gu S, Meng JS. LINC00312 inhibits the migration and invasion of bladder cancer cells by targeting miR-197-3p. Tumour Biol. 2016; 37:14553-14563.
6. Liu K, Huang W, Yan DQ, Luo Q, Min X. Overexpression of long intergenic noncoding RNA LINC00312 inhibits the invasion and migration of thyroid cancer cells by down-regulating microRNA-197-3p. Biosci Rep. 2017; 37.
7. Zhang W, Huang C, Gong Z, *et al*. Expression of LINC00312, a long intergenic non-coding RNA, is negatively correlated with tumor size but positively correlated with lymph node metastasis in nasopharyngeal carcinoma. J Mol Histol. 2013; 44:545-554.
8. Zhu Q, Lv T, Wu Y, Shi X, Liu H, Song Y. Long non-coding RNA 00312 regulated by HOXA5 inhibits tumour proliferation and promotes apoptosis in Non-small cell lung cancer. J Cell Mol Med. 2017; 21:2184-2198.
9. Wilson MK, Friedlander ML, Joly F, Oza AM. A Systematic Review of Health-Related Quality of Life Reporting in Ovarian Cancer Phase III Clinical Trials: Room to Improve. Oncologist. 2018; 23:203-213.
10. Zhao H, Bi T, Qu Z, Jiang J, Cui S, Wang Y. Expression of miR-224-5p is associated with the original cisplatin resistance of ovarian papillary serous carcinoma. Oncol Rep. 2014; 32:1003-1012.
11. Wu X, Gu J, Wu TT, Swisher SG, Liao Z, Correa AM, Liu J, Etzel CJ, Amos CI, Huang M, Chiang SS, Milas L, Hittelman WN, Ajani JA. Genetic variations in radiation and chemotherapy drug action pathways predict clinical outcomes in esophageal cancer. J Clin Oncol. 2006; 24:3789-3798.
12. Wang TH, Wan JY, Gong X, Li HZ, Cheng Y. Tetrandrine enhances cytotoxicity of cisplatin in human drug-resistant esophageal squamous carcinoma cells by inhibition of multidrug resistance-associated protein 1. Oncol Rep. 2012; 28:1681-1686.
13. Florea AM, Busselberg D. Cisplatin as an anti-tumor drug: Cellular mechanisms of activity, drug resistance and induced side effects. Cancers (Basel). 2011; 3:1351-1371.
14. Zou W, Ma X, Hua W, Chen B, Cai G. Caveolin-1 mediates chemoresistance in cisplatin-resistant ovarian cancer cells by targeting apoptosis through the Notch-1/Akt/NF-kappaB pathway. Oncol Rep. 2015; 34:3256-3263.
15. He SM, Li R, Kanwar JR, Zhou SF. Structural and functional properties of human multidrug resistance protein 1 (MRP1/ABCC1). Curr Med Chem. 2011; 18:439-481.
16. Stordal B, Hamon M, McEneaney V, Roche S, Gillet JP, O'Leary JJ, Gottesman M, Clynes M. Resistance to paclitaxel in a cisplatin-resistant ovarian cancer cell line is mediated by P-glycoprotein. PloS One. 2012; 7:e40717.
17. Li Z, Qu L, Zhong H, Xu K, Qiu X, Wang E. Low expression of Mig-6 is associated with poor survival outcome in NSCLC and inhibits cell apoptosis *via* ERK-mediated upregulation of Bcl-2. Oncol Rep. 2014; 31:1707-1714.
18. Guo Q, Dong B, Nan F, Guan D, Zhang Y. 5-Aminolevulinic acid photodynamic therapy in human cervical cancer *via* the activation of microRNA-143 and suppression of the Bcl-2/Bax signaling pathway. Mol Med Rep. 2016; 14:544-550.
19. Zhang R, Shi H, Ren F, Li X, Zhang M, Feng W, Jia Y. Knockdown of MACC1 expression increases cisplatin sensitivity in cisplatin-resistant epithelial ovarian cancer cells. Oncol Rep. 2016; 35:2466-2472.
20. Feng X, Liu N, Deng S, Zhang D, Wang K, Lu M. miR-199a modulates cisplatin resistance in ovarian cancer by targeting Hif1alpha. Onco Targets Ther. 2017; 10:5899-5906.
21. Qi H, Wen B, Wu Q, Cheng W, Lou J, Wei J, Huang J, Yao X, Weng G. Long noncoding RNA SNHG7 accelerates prostate cancer proliferation and cycle progression through cyclin D1 by sponging miR-503. Biomed Pharmacother. 2018; 102:326-332.
22. Enling L, Zheng L, Yuxiu Z, Ruoran M, Dehua W. Overexpression of long non-coding RNA PVT1 in ovarian cancer cells promotes cisplatin resistance by regulating apoptotic pathways. Int J Clin Exp Med. 2015; 8:20565-20572.
23. Ju X, Yu H, Liang D, Jiang T, Liu Y, Chen L, Dong Q, Liu X. LDR reverses DDP resistance in ovarian cancer cells by affecting ERCC-1, Bcl-2, Survivin and Caspase-3 expressions. Biomed Pharmacother. 2018; 102:549-554.

Original Article

Detection of chromosome abnormalities using current noninvasive prenatal testing: A multi-center comparative study

Yan Du[1,2,3,§]**, Jing Lin**[1,3,4,§]**, Likun Lan**[5]**, Ying Dong**[6]**, Jun Zhu**[7]**, Wen Jiang**[8]**, Xinyao Pan**[1,3,4]**, Youhui Lu**[1,3,4]**, Dajin Li**[1,3,4]**, Ling Wang**[1,3,4,*]

[1] *Laboratory for Reproductive Immunology, Hospital & Institute of Obstetrics and Gynecology, Shanghai Medical College, Fudan University, Shanghai, China;*
[2] *Office of Clinical Epidemiology, Obstetrics and Gynecology Hospital of Fudan University, Shanghai, China;*
[3] *The Academy of Integrative Medicine of Fudan University, Shanghai, China;*
[4] *Shanghai Key Laboratory of Female Reproductive Endocrine-related Diseases, Shanghai, China;*
[5] *Second Affiliated Hospital of Hexi University, Gansu, China;*
[6] *Putuo District Institute of Maternity and Child Health of Shanghai, Shanghai, China;*
[7] *Department of Obstetrics and Gynecology, Wenling People's Hospital, Wenzhou Medical University, Zhejiang, China;*
[8] *Department of Obstetrics and Gynecology, Zhoushan Maternity and Child Healthcare Hospital, Zhejiang, China.*

| Summary | Noninvasive prenatal testing (NIPT) is increasingly recognized and utilized in the antenatal care field. In the current study, we aimed to evaluate the clinical application and compare test outcomes of two generations of currently used NIPT techniques for detecting fetal chromosome abnormalities in a high-risk prenatal population. A total of 7,252 pregnant women were included from twenty-one hospitals from January 2015 to September 2017. A maternal blood sample of each participant was collected for fetal DNA sequencing. Group I received a first generation NIPT sequencing technique to detect chromosome aneuploidies, and Group II received a second generation NIPT sequencing technique to detect subchromosome abnormalities. An abnormal NIPT result was reported in 0.90% (44/4,868) of the women in Group I and 2.68% (64/2,384) in Group II. In Group I, seventeen (17/37, 45.95%) women with suspected fetal aneuploidy received amniocentesis, which confirmed 100% (10/10) of positive trisomy 21 samples, 100% (1/1) of trisomy 18, 100% (1/1) of sex chromosome abnormality, 0% (0/2) of trisomy 16, 0% (0/2) of trisomy 13, and 0% (0/1) of trisomy 20 and 13. In Group II, aneuploidy accounted for 46.88% (30/64) of the abnormal results. Five underwent amniocentesis and three had an abnormal result, including two cases of trisomy 21 and one case of chromosome 5p deletion syndrome. Whereas one case of 46,XN,del(16q11.2-q22.3) and another case of 46,XN,dup(Xp22.31) were considered as normal. NIPT is a quick and reliable screening method for detecting fetal chromosome aneuploidies and subchromosome deletions/duplications. Challenges remain for the comprehensive clinical application of NIPT.

Keywords: Noninvasive prenatal testing (NIPT), prenatal testing, chromosome aneuploidies, subchromosome deletions/duplications |

1. Introduction

Prenatal testing is designed to acquire a fetal biological

Address correspondence to:
Dr. Ling Wang, Laboratory for Reproductive Immunology, Hospital & Institute of Obstetrics and Gynecology, Fudan University, 419 Fangxie Road, Shanghai 200011, China.
E-mail: Dr.wangling@fudan.edu.cn

and genetic profile and thus detect any potential genetic abnormalities of the fetus. Prenatal screening for fetal health assessment involves maternal serum biochemical markers and ultrasound scan, which have limitations such as the need to combine a series of markers or to be performed at different time points. Prenatal diagnosis, including amniocentesis and chorionic villus sampling, provides information about the fetal karyotype at a certain gestational window and has its clinical applicability; however, it can also cause risks for the fetus (*1*). With the advancement of highly accurate

noninvasive approaches, new options for prenatal testing become available.

Noninvasive prenatal testing (NIPT) which analyzes cell-free DNA (cfDNA) of fetal origin in maternal circulation for detection of fetal chromosome abnormalities in high-risk pregnancies has received widespread recognition and utilization since 2011 (*2*). NIPT offers high sensitivity and specificity for common fetal chromosome aneuploidies such as trisomy 21, 18, and 13. It has been proposed that the indication of NIPT can be expanded to all autosomes and even sub-chromosome deletions/duplications (*3*). It has also been recommended to incorporate cfDNA screening into current clinical prenatal practice as a screening alternative for various genetic conditions. Moreover, guidelines of the American College of Medical Genetics and Genomics (ACMG) have suggested that NIPT may replace conventional screening of common aneuploidies for women across the maternal age spectrum (*4*).

NIPT marks a revolution in prenatal screening and opens up new possibilities, but it has certain limitations, including coverage of only the most common trisomies, the possibility of both false-positive and false-negative results, and occurrence of test failure (*5*). Despite the above mentioned limitations, NIPT is likely to be increasingly adopted as part of prenatal practice. So far, there are two generations of sequencing techniques of NIPT. The first generation NIPT sequencing mainly detects chromosome aneuploidies, while the second generation NIPT sequencing can also detect subchromosome abnormalities. The most important differences between the first and second generation NIPT sequencing techniques are the length of sequencing reads and depth of coverage. The first generation NIPT sequencing technique for chromosome aneuploidies is based on reads up to 1,000 bp, while the size of reads for the second generation NIPT sequencing technique is up to 400 bp. Therefore, we investigated the clinical application and compared the outcomes of the two NIPT techniques for direct detection of fetal chromosome aneuploidies or subchromosome deletions/duplications in women with high-risk pregnancies.

2. Materials and Methods

2.1. *Participant recruitment*

A total of 7,252 pregnant women were included from January 13th, 2015 to September 30th, 2017 from the following twenty-one hospitals: Zhoushan Maternity and Child Healthcare Hospital, International Peace Maternity and Child Health Hospital, Renji Hospital of Shanghai Jiaotong University School of Medicine, Obstetrics and Gynecology Hospital of Fudan University, Shanghai First Maternity and Infant Hospital, Shanghai First People's Hospital, Shanghai Sixth People's Hospital, Shanghai Eighth People's

Hospital, Shanghai Ninth People's Hospital, Changning Maternity and Infant Health Hospital, Putuo Maternity and Infant Health Hospital, Jiading Maternity and Infant Health Hospital, Hongkou Maternity and Infant Health Hospital, Maternity and Infant Health Hospital of Pudong New District, Shanghai Pudong Hospital, Shanghai Institute of Planned Parenthood Research Hospital, Zhongshan Hospital, Yueyang Hospital, Shuguang Hospital, Minhang District Central Hospital, and Jinshan Hospital. Maternal characteristics that were important risk indicators of fetal chromosome aneuploidy included advanced maternal age, personal history of abnormal gestation and birth, family history of chromosome aneuploidy, positive serum marker screening, and abnormal fetal ultrasound findings. The participants received either the first generation (Group I) or the second generation (Group II) NIPT sequencing technique. Peripheral venous blood of each participating pregnant woman was collected. The study protocol was approved by the institutional review board of Zhoushan Maternity and Child Healthcare Hospital. Informed consent was obtained from all participants.

2.2. *cfDNA preparation and sequencing*

Five to 10 mL of the maternal blood sample was collected and the plasma was separated from peripheral blood cells. Using the QIAamp DSP DNA Blood Mini Kit (Qiagen), cfDNA from 600 μL of maternal plasma was extracted following the manufacturer's protocol. DNA fragments were obtained with the NEBNext dsDNA Fragmentase (New England Biolabs). Fetal Chromosome Aneuploid (T21, T18, and T13) Detection Kit (CapitalBio Corporation) was utilized for library construction, library quality control, and library amplification following the manufacturer's protocol. DNA sequencing was performed using the BioelectronSeq 4000 Semiconductor Sequencing System (CapitalBio Corporation) according to the manufacturer's instructions.

2.3. *Statistical analysis*

Age was compared using Student's *t* test as a continuous variable between the two Groups. The obtained reads were aligned to the human genomic reference sequences (hg19) using the BWA algorithm. Unmapped reads or those with multiple primary alignment records were filtered by FLAG field in the alignment file with an in-house Perl script. An integrated three-step process [LOESS regression (*6*), intrarun normalization (*7*), and linear model regression (*8*)] was applied to eliminate the effect of GC bias. A Z score was calculated to identify fetuses with trisomy 21, 18, 13, or sex chromosome aneuploidies. A cutoff value of Z score > 3 was set to determine whether the ratio of chromosome 21, 18, or 13 was increased and hence fetal trisomy 21, 18, or 13 was

present. Then the Z scores for each 1 Mb region were combined and a Stouffer's Z-score method was adopted to improve the accuracy for detection of subchromosome abnormalities. A Stouffer's Z score > 5 was determined as microduplication, whereas a Stouffer's Z score < -5 was classified as microdeletion.

3. Results

3.1. Study participants

A total of 7,252 pregnant women were included in this study and received either the first generation (Group I) or the second generation (Group II) NIPT sequencing technique. Group I contained 4,868 pregnant women, using the first generation NIPT sequencing technique to detect chromosome aneuploidies. Group II included 2,384 women, using the second generation NIPT sequencing technique to detect subchromosome abnormalities. The percentage of pregnant women receiving second generation NIPT sequencing technique (Group II) increased significantly from the year 2015 to 2017 (Figure 1).

### 3.2. Detection of fetal aneuploidies in Group I

An abnormal NIPT result (aneuploidy detected or "unclassified" result) was reported in 0.90% (44/4,868) of the women in Group I. Table 1 presents detailed information of abnormal NIPT results in Group I.

We detected fifteen candidate samples with trisomy 21 (15/44, 34.09%), five with trisomy 13 (5/44, 11.36%), three with trisomy 20 (3/44, 6.81%), three with trisomy 18 (3/44, 6.81%), three with trisomy 16 (1/44, 6.81%), one with trisomy 15 (3/44, 2.27%), one with trisomy 9 (1/44, 2.27%), one with trisomy 7 (1/44, 2.27%), one with trisomy 20 and 13 (1/44, 2.27%), two with 45,X (2/44, 4.55%), one with 47,XXX (1/44, 2.27%), one with unclassified sex chromosome abnormality (1/44, 2.27%), four samples with microdeletion (4/44, 9.09%), and three with microduplication (3/44, 6.82%). Seventeen (17/37, 45.95%) women with suspected fetal aneuploidy received amniocentesis, which confirmed 100% (10/10) of positive trisomy 21 samples, 100% (1/1) of trisomy 18, 100% (1/1) of sex chromosome abnormality, 0% (0/2) of trisomy 16, 0% (0/2) of trisomy 13, and 0% (0/1) of trisomy 20 and 13.

3.3. Detection of fetal subchromosome abnormalities in Group II

Sixty-four of the 2,384 (64/2,384, 2.68%) women in Group II who received second generation NIPT sequencing technique to detect subchromosome abnormalities were screen-positive.

Table 2 presents detailed information of abnormal NIPT results in Group II. Aneuploidy accounted for
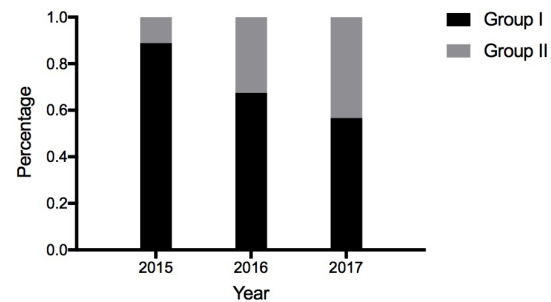
Figure 1. Percentages of pregnant women receiving first (Group I) and second (Group II) generation NIPT sequencing techniques each year, 2015-2017.

Table 1. Detailed information of abnormal NIPT results in Group I

Abnormal NIPT results	N	% of patients with abnormal results
Aneuploidy		
47,XN,+7	1	2.27%
47,XN,+9	1	2.27%
47,XN,+13	5	11.36%
47,XN,+15	1	2.27%
47,XN,+16	3	6.82%
47,XN,+18	3	6.82%
47,XN,+20	3	6.82%
47,XN,+21	15	34.09%
48,XN,+13,+20	1	2.27%
45,X	2	4.55%
47,XXX	1	2.27%
Unclassified sex chromosome abnormality	1	2.27%
Deletion		
46,XN,del(3)	1	2.27%
46,XN,del(4q34.1-q35.1)	1	2.27%
46,XN,del(10)	1	2.27%
46,XN,del(20)	1	2.27%
Duplication		
46,XN,dup(3q26.1-q29)	1	2.27%
46,XN,dup(7)	1	2.27%
46,XN,dup(15)	1	2.27%

NIPT, noninvasive prenatal testing.

46.88% (30/64) of the abnormal results, followed by twenty-five cases of subchromosome duplication (25/64, 39.06%), seven cases of subchromosome deletion (7/64, 10.94%), and two cases of both duplication and deletion (2/64, 3.13%). Of all screen-positive women in Group II, five (5/64, 7.81%) underwent amniocentesis and three of them had abnormal results, including two cases of trisomy 21 and one case of chromosome 5p deletion syndrome (Cri-du-chat syndrome). However, one case of 46,XN,del(16q11.2-q22.3) and another case of 46,XN,dup(Xp22.31) were considered as normal according to the results of amniocentesis.

3.4. Comparison between Group I and Group II

The average maternal age of Group I was 32 years (range: 17-54 years), and the average gestational age

Table 2. Detailed information of abnormal NIPT results in Group II

Abnormal NIPT results	N	% of patients with abnormal results
Aneuploidy		
47,XN,+10	1	1.56%
47,XN,+11	2	3.13%
47,XN,+13	5	7.81%
47,XN,+14	1	1.56%
47,XN,+16	1	1.56%
47,XN,+18	3	4.69%
47,XN,+21	13	20.31%
48,XXY,+8	1	1.56%
45,X	3	4.69%
Deletion		
46,XN,del(5p15.31-15.2)	1	1.56%
46,XN,del(7q21.3-q31.2)	1	1.56%
46,XN,del(15q21.3)	1	1.56%
46,XN,del(16q11.2-q22.3)	1	1.56%
46,XN,del(17p12)	2	3.13%
46,XN,del(18p11.32)	1	1.56%
Duplication		
46,XN,dup(1q44)	1	1.56%
46,XN,dup(2q13)	1	1.56%
46,XN,dup(2q22.3-q23.1)	1	1.56%
46,XN,dup(2q37.1-q37.2)	1	1.56%
46,XN,dup(2p24.3)	1	1.56%
46,XN,dup(4q21.1-q21.21)	1	1.56%
46,XN,dup(4q35.2)	1	1.56%
46,XN,dup(5q14.3)	1	1.56%
46,XN,dup(6p12.1)	1	1.56%
46,XN,dup(7q11.22-q11.23)	1	1.56%
46,XN,dup(10p14)	1	1.56%
46,XN,dup(12q21.1)	1	1.56%
46,XN,dup(14q31.3)	1	1.56%
46,XN,dup(16q23.3-q24.1)	1	1.56%
46,XN,dup(17q12)	1	1.56%
46,XN,dup(20p12.1)	1	1.56%
46,XN,dup(22q11.23)	2	3.13%
46,XN,dup(Xp21.3)	1	1.56%
46,XN,dup(Xp22.31)	6	9.38%
Deletion and duplication		
46,XN,dup(1q41-q44), del(13q32.3-q34)	1	1.56%
46,XN,dup(7p21.3), del(19q13.2-q13.31)	1	1.56%

NIPT, noninvasive prenatal testing.

was 17^{+1} weeks (range: 6^{+0}–36^{+6} weeks). The mean maternal age of Group II was 33 years (range: 12-47 years), with a corresponding gestational age of 15^{+3} weeks (range 4^{+0}–34^{+6} weeks). There was no age difference ($P = 0.20$) between the two groups. However, the gestational age was significantly earlier in Group II compared to that in Group I ($P < 0.001$). NIPT was most actively selected at the 13th and the 9th weeks of gestation in Group I and II, respectively. The peak age range to receive NIPT in both groups was around 27-30 and 34-37 years, respectively. Figure 2A and 2B present the distribution of age and gestational week of the two groups.

The average maternal age was 33.2 years and the average gestational age was 16^{+5} weeks among 44 NIPT-positive women in Group I. The average maternal age and average gestational age of 64 NIPT-positive

women in Group II was 33.8 years and 14^{+4} weeks, respectively. There was no age difference ($P = 0.64$) of NIPT-positive women between the two groups. However, the gestational age was significantly earlier for NIPT-positive women in Group II compared to that in Group I ($P < 0.007$). Figure 3A and 3B show the distribution of maternal age and gestational age among NIPT-positive women in Group I and Group II, respectively.

Figure 4 shows the NIPT process and results.

4. Discussion

The rate of abnormal NIPT result was 0.90% (44/4,868) in Group I and 2.68% (64/2,384) in Group II. Our results showed that aneuploidy accounted for 84.09% (37/44) of the abnormal results in Group I, and 46.88% (30/64) in Group II. Notably, subchromosome deletions/duplications comprised a higher percentage of abnormal NITP results in Group II (34/64, 53.13%) compared to Group I (7/44, 15.91%), which could be explained by the fact that the second generation sequencing technique offered a higher throughput and more sensitive platform to generate accurate data and unexpected DNA variation, thus increasing the screen-positive rate and the detection rate of subchromosome abnormalities. The reported screen-positive rate varied according to the technique selected and population studied. The Harmony test conducted in Belgium and the Netherlands reported a screen-positive rate of 1.9% (57/3,000) of pregnancies (*9*).

The performance of the laboratory developed NIPT technology was evaluated using fetal karyotype results obtained from invasive approaches in singleton pregnancies as the gold standard. Of screen-positive women in Group I, 38.64% (17/44) received invasive diagnostic testing and 70.59% (12/17) of those tested had an abnormal result. Amniocentesis confirmed ten positive trisomy 21 samples, one positive trisomy 18, and one positive sex chromosome abnormality; while two cases of trisomy 16, two cases of trisomy 13, and one case of trisomy 20 and 13 were considered as normal. In Group II, five (5/64, 7.81%) women underwent amniocentesis and three had an abnormal result. Two cases of trisomy 21 and one case of Cri-du-chat syndrome were confirmed by amniocentesis, whereas one case of 46,XN,del(16q11.2-q22.3) and another case of 46,XN,dup(Xp22.31) were considered as normal. Previous studies have reported that NIPT could be successfully validated for common aneuploidies in singleton pregnancies; and the detection rates were 99.7% for trisomy 21, 98% for trisomy 18, and 99% for trisomy 13 with a combined false-positive rate (FPR) of 0.13% (*10*), and the detection rate for subchromosome abnormalities was 71.8% (*11*). Another study using NIPT to identify common aneuploidies reported that the sensitivity and specificity were
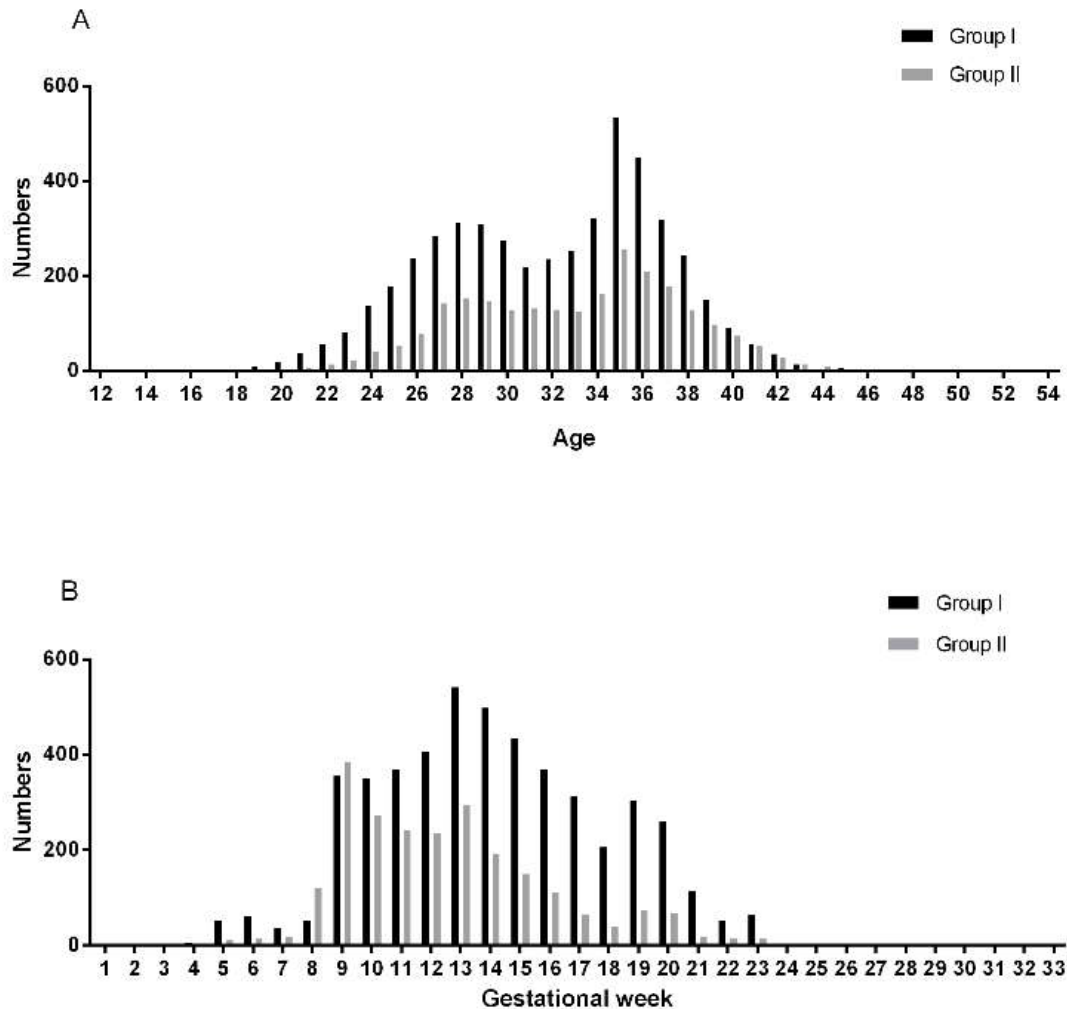
Figure 2. Distribution of maternal age and gestational week of all participants in Group I (*n* = 4,868) and Group II (*n* = 2,384). A: age; **B:** gestational week.
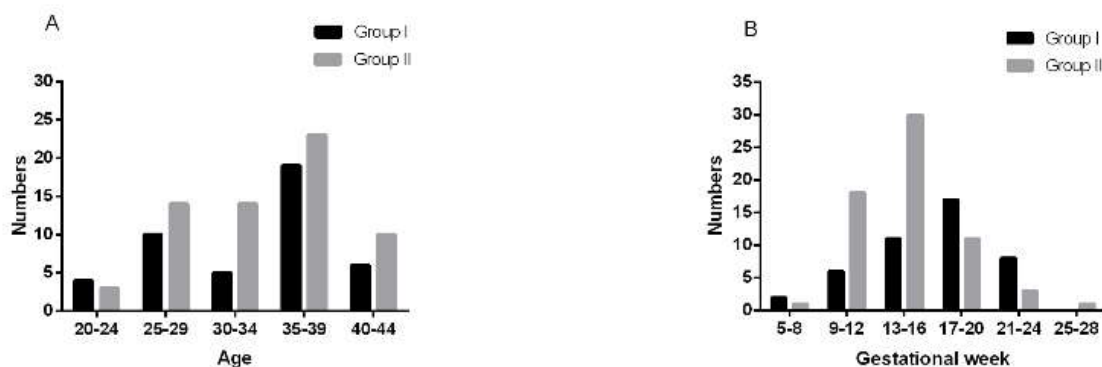
Figure 3. Distribution of NIPT-positive women by maternal age and gestational age in Group I (*n* = 44) and Group II (*n* = 64). A: age; **B:** gestational week.

99.94% and 99.46% for trisomy 21, 100% and 99.24% for trisomy 18, and 100% and 100% for trisomy 13, respectively (*12*). Data from a large referral genetic diagnostic laboratory in the United States showed that the positive predictive values (PPV) were 84% for trisomy 21, 76% for trisomy 18, 45% for 13, 50% for

trisomy X, 26% for monosomy X, and 0% to 21% for microdeletion syndromes (*13*). In line with the above findings, our results also demonstrated that NIPT has better performance when screening for trisomy 21 than other aneuploidies, while the FPR is higher and the PPV is lower when NIPT is used to screen for
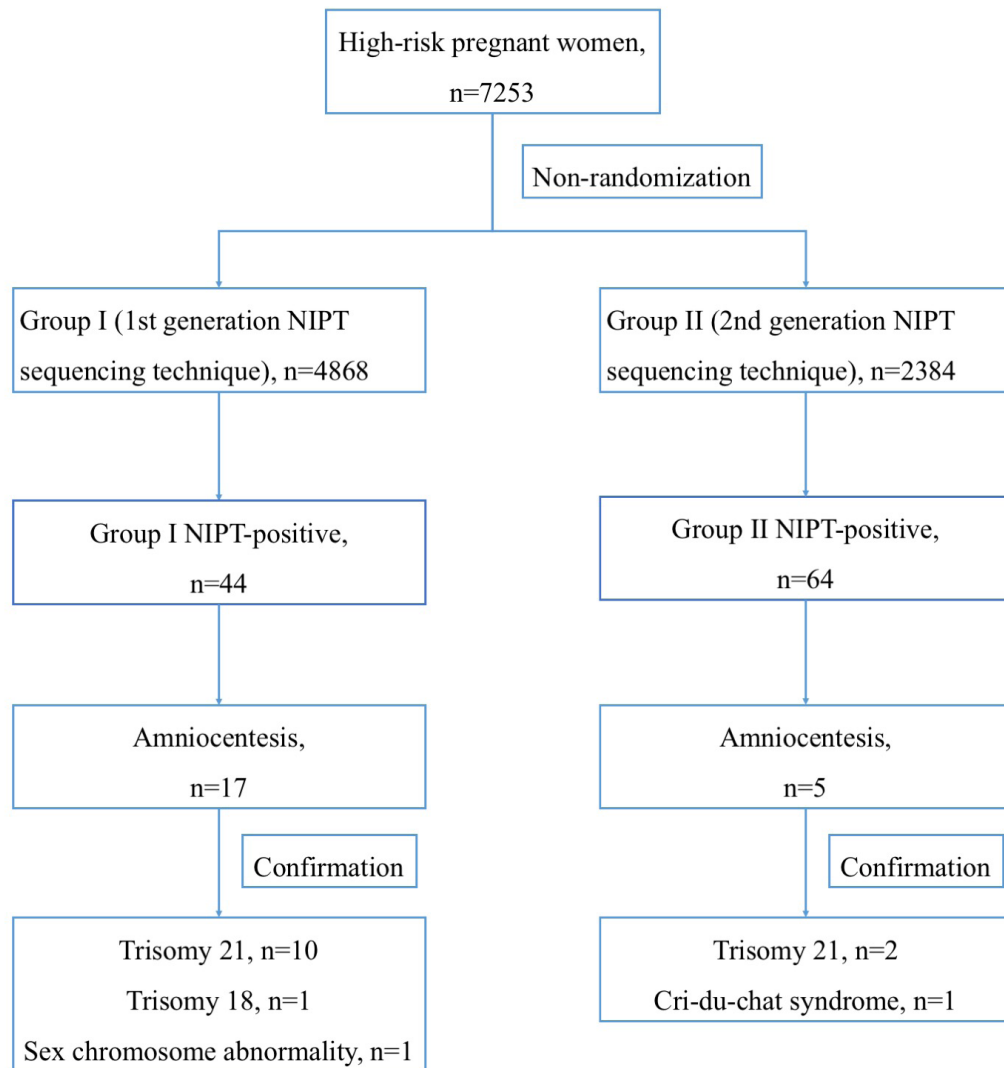
Figure 4. Flow chart of NIPT process and results.

subchromosome abnormalities.

Compared with traditional screening methods and invasive approaches, cfDNA-based NIPT detects the core pathology of chromosome abnormalities instead of epiphenomenon. In addition, NIPT also has minimal risks of fetal losses compared to invasive procedures. It is estimated that the implementation of NIPT as a second step screening procedure in high-risk pregnancies would lead to a 10.2% increase in detected Down syndrome cases and a 96.3% decrease in fetal losses (*14*). However, NIPT needs to be implemented in combination with other prenatal tests to avoid certain limitations.

NIPT is selected mainly for reassurance by low-risk pregnant women in the clinical setting (*15*). Studies have shown that introduction of NIPT as a second-tier screen was not associated with a decrease of invasive testing in the high-risk population (*16*). Furthermore, NIPT could detect unconfirmed results or variants of unknown clinical significance, ranging from relatively healthy

newborns to those associated with fetal abnormality or pregnancy complication (*17*). With the increasing utilization of the second generation NIPT sequencing technique as seen in our study, how to decrease FPR and increase PPV becomes an important issue to avoid unnecessary stress for pregnant women.

From the biological perspective, fetoplacental mosaicism is one of the underlying causes of false-positives and false-negatives in NIPT, since cfDNA originates from the mother and the placenta (trophoblasts) rather than from the fetus proper (*18*). Other causes of false positive or negative results include: pregnancy with twins or triplets; women with chromosome disorders, malignancy, or previous treatments such as transplant, stem-cell treatment, immune therapy, blood transfusion, and *in vitro* fertilization-embryo transfer; the interference of fetal balanced translocation, mosaic trisomy; and inappropriate collection, transferring, and handling of the samples (*5*). Meanwhile, studies have shown that approximately 15% of chromosome abnormalities

would not be identified by NIPT among those high-risk women with abnormalities who pursued prenatal diagnostic testing (*16*). Moreover, NIPT cannot be used to screen for the broad term of "any genetic condition", such as cleft palette, deafness, neural tube defects, or autism. Recently some researchers have suggested expanding the indication of NIPT to all autosomes and even subchromosome deletion/duplication syndromes (*3*). However, the majority of published consensus or recommendations from the professional societies are not in favor of the clinical implementation of NIPT to detect fetal microdeletions (*19*).

On the technological side, there are several features of the sequencing platform that restrict the extensive application of NIPT, which include high test price, requirement of fetal fraction above the threshold, test failure after repeated sampling, difficulties to detect small aberrations, and high false positive rate (*20*). Moreover, standard infrastructure, innovative algorithm, as well as personnel expertise are required for subsequent data analysis (*21*).

In conclusion, NIPT is increasingly recognized and accepted in the antenatal care field, because of the cost reduction and repertoire expansion to add subchromosome abnormalities besides the originally included trisomy 21, 18, 13, and sex chromosome aneuploidies. With the expanding availability of NIPT, health providers are challenged to educate patients about the benefits, limitations, costs, risks, results, and follow-up options of NIPT for adequate informed consent. Our study provided further evidence to support the utilizations and benefits of the cell-free fetal DNA screening technology. It is crucial to improve the laboratory standards for testing and reporting, execute pre- and post-test counseling, identify clearer indicators for invasive testing, and perform continuous evaluation in order to comprehensively establish the clinical application of NIPT.

Acknowledgements

References

1. Wilson RD, Gagnon A, Audibert F, Campagnolo C, Carroll J. Prenatal diagnosis procedures and techniques to obtain a diagnostic fetal specimen or tissue: Maternal and fetal risks and benefits. J Obstet Gynaecol Can. 2015; 37:656-668.

2. Benn P, Borrell A, Cuckle H, Dugoff L, Gross S, Johnson JA, Maymon R, Odibo A, Schielen P, Spencer K, Wright D, Yaron Y. Prenatal detection of Down syndrome using massively parallel sequencing (MPS): A rapid response statement from a committee on behalf of the Board of the International Society for Prenatal Diagnosis, 24 October 2011. Prenat Diagn. 2012; 32:1-2.

3. Helgeson J, Wardrop J, Boomer T, Almasri E, Paxton WB, Saldivar JS, Dharajiya N, Monroe TJ, Farkas DH, Grosu DS, McCullough RM. Clinical outcome of subchromosomal events detected by whole-genome noninvasive prenatal testing. Prenat Diagn. 2015; 35:999-1004.

4. Gregg AR, Skotko BG, Benkendorf JL, Monaghan KG, Bajaj K, Best RG, Klugman S, Watson MS. Noninvasive prenatal screening for fetal aneuploidy, 2016 update: A position statement of the American College of Medical Genetics and Genomics. Genet Med. 2016; 18:1056-1065.

5. Harraway J. Non-invasive prenatal testing. Aust Fam Physician. 2017; 46:735-739.

6. Alkan C, Kidd JM, Marques-Bonet T, Aksay G, Antonacci F, Hormozdiari F, Kitzman JO, Baker C, Malig M, Mutlu O, Sahinalp SC, Gibbs RA, Eichler EE. Personalized copy number and segmental duplication maps using next-generation sequencing. Nat Genet. 2009; 41:1061-1067.

7. Jiang F, Ren J, Chen F, *et al*. Noninvasive Fetal Trisomy (NIFTY) test: An advanced noninvasive prenatal diagnosis methodology for fetal autosomal and sex chromosomal aneuploidies. BMC Med Genomics. 2012; 5:57.

8. Chen EZ, Chiu RW, Sun H, *et al*. Noninvasive prenatal diagnosis of fetal trisomy 18 and trisomy 13 by maternal plasma DNA sequencing. PLoS One. 2011; 6:e21791.

9. Willems PJ, Dierickx H, Vandenakker E, Bekedam D, Segers N, Deboulle K, Vereecken A. The first 3,000 non-invasive prenatal tests (NIPT) with the Harmony test in Belgium and the Netherlands. Facts Views Vis Obgyn. 2014; 6:7-12.

10. Gil MM, Accurti V, Santacruz B, Plana MN, Nicolaides KH. Analysis of cell-free DNA in maternal blood in screening for aneuploidies: Updated meta-analysis. Ultrasound Obstet Gynecol. 2017; 50:302-314.

11. Yin AH, Peng CF, Zhao X, *et al*. Noninvasive detection of fetal subchromosomal abnormalities by semiconductor sequencing of maternal plasma DNA. Proc Natl Acad Sci U S A. 2015; 112:14670-14675.

12. Liao C, Yin AH, Peng CF, *et al*. Noninvasive prenatal diagnosis of common aneuploidies by semiconductor sequencing. Proc Natl Acad Sci U S A. 2014; 111:7415-7420.

13. Petersen AK, Cheung SW, Smith JL, Bi W, Ward PA, Peacock S, Braxton A, Van Den Veyver IB, Breman AM. Positive predictive value estimates for cell-free noninvasive prenatal screening from data of a large referral genetic diagnostic laboratory. Am J Obstet Gynecol. 2017; 217:691.

14. Okem ZG, Orgul G, Kasnakoglu BT, Cakar M, Beksac MS. Economic analysis of prenatal screening strategies for Down syndrome in singleton pregnancies in Turkey. Eur J Obstet Gynecol Reprod Biol. 2017; 219:40-44.

15. Manegold-Brauer G, Berg C, Flock A, Ruland A, Gembruch U, Geipel A. Uptake of non-invasive prenatal testing (NIPT) and impact on invasive procedures in a tertiary referral center. Arch Gynecol Obstet. 2015; 292:543-548.

16. Maxwell S, Dickinson JE, Murch A, O'Leary P. The potential impact of NIPT as a second-tier screen on the outcomes of high-risk pregnancies with rare chromosomal abnormalities. Aust N Z J Obstet Gynaecol. 2015; 55:420-426.

17. Neofytou MC, Tsangaras K, Kypri E, Loizides C, Ioannides M, Achilleos A, Mina P, Keravnou A, Sismani C, Koumbaris G, Patsalis PC. Targeted capture enrichment assay for non-invasive prenatal testing of large and small size sub-chromosomal deletions and duplications. PLoS One. 2017; 12:e0171319.

18. Taglauer ES, Wilkins-Haug L, Bianchi DW. Review: Cell-free fetal DNA in the maternal circulation as an indication of placental health and disease. Placenta. 2014; 35 Suppl:S64-S68.

19. ACOG. Committee opinion No. 640: Cell-free DNA screening for fetal aneuploidy. Obstet Gynecol. 2015.

20. Liu L, Li K, Fu X, Chung C, Zhang K. A forward look at noninvasive prenatal testing. Trends Mol Med. 2016; 22:958-968.

21. Allyse M, Minear MA, Berson E, Sridhar S, Rote M, Hung A, Chandrasekharan S. Non-invasive prenatal testing: A review of international implementation and challenges. Int J Womens Health. 2015; 7:113-126.

325

Brief Report

pH-Dependent exhibition of hemolytic activity by an extract of *Hypsizygus marmoreus* fruiting bodies

Kohsuke Saito[1], Syohto Hazama[1], Yoshiki Oda[2], Munehiro Nakata[1],*

[1] *Department of Applied Biochemistry, Tokai University, Hiratsuka, Kanagawa, Japan;*
[2] *Technology Joint Management Office, Research Promotion Division, Tokai University, Hiratsuka, Kanagawa, Japan.*

Summary	The current study found that an extract from the fruiting bodies of the edible mushroom *Hypsizygus marmoreus* exhibited hemolytic activity against sheep red blood cells when its pH was lowered. Although hemolytic activity was not detected when an extract had a neutral pH, an extract with a low pH exhibited potent hemolytic activity. The maximal hemolytic activity was exhibited by an extract with a pH of 5.5. A heat-treated extract did not exhibit hemolytic activity before its pH was lowered, and that activity was inhibited in the presence of PMSF and EDTA. The turbidity of the extract increased during lowering of its pH, and the precipitate fraction exhibited hemolytic activity. Fractionation by a modified Bligh and Dyer method and TLC analyses suggested that a hemolytic compound in the extract might be a type of lipid. These results suggest that a hemolytic lipid-like compound in an extract of *H. marmoreus* fruiting bodies may be released by a non-active precursor substance(s) through metalloenzyme(s) while the extract has a low pH.

Keywords: Hemolysis, hemolysin, *Hypsizygus marmoreus*, mushroom

1. Introduction

Higher Basidiomycetes mushrooms contain biologically active compounds in their fruiting bodies (*1,2*). Extracts prepared from the fruiting bodies of various mushrooms have been found to contain substances that act against red blood cells (RBCs) (*3,4*). These substances include hemolytic proteins (hemolysins), which cause the lysis of RBCs, and carbohydrate-binding proteins (lectins), which cause RBC agglutination. The carbohydrate-binding specificity of mushroom lectins has been ascertained, but few studies have examined mushroom hemolysins. Nonetheless, some mushroom hemolysins have been reported to assume an oligomeric structure, resulting in holes in the membrane of RBCs (*5*) similar to those created by the membrane attack complex of the complement system (*6,7*) or perforin produced by natural killer T cells (*8,9*). However, the physiological

significance of hemolysins or cell membrane disruption in the life cycle of basidiomycetes has yet to be determined.

Hypsizygus marmoreus (buna-shimeji or brown beech mushroom) is an edible mushroom. Although a lectin from the mushroom (*H. marmoreus* lectin) has been identified (*10*), hemolysins from the mushroom and the mushroom's hemolytic activity have not been described. The current study examined the hemolytic activity of an extract of *H. marmoreus* fruiting bodies during lowering of its pH.

2. Materials and Methods

2.1. *Fruiting bodies and reagents*

Fruiting bodies of *H. marmoreus* were purchased from a local market. Excised fruiting bodies were freeze-dried and stored at –30°C until use. Sheep blood was obtained from Nippon Bio-Supp Center, Tokyo, Japan. Phenylmethylsulfonyl fluoride (PMSF) and leupeptin were from MP Bio Japan, Tokyo, Japan, and ethylenediaminetetraacetic acid (EDTA) was from Dojindo Laboratories, Kumamoto, Japan. All chemicals used were of analytical grade.

Address correspondence to:
Dr. Munehiro Nakata, Department of Applied Biochemistry, Tokai University, Hiratsuka, Kanagawa 259-1292, Japan.
E-mail: nak@tsc.u-tokai.ac.jp

2.2. *Extract preparation and adjustment of its pH*

Pieces of freeze-dried fruiting bodies of *H. marmoreus* were grinded and sonicated 10 times for 2 sec in 10 mM phosphate buffer (pH 7.3). The homogenate was centrifuged at 12,000 rpm for 30 min. The supernatant obtained was used as an extract.

The extract was mixed with an equal volume of a 0.1 M buffer at a pH range of 3.0-10.0 and incubated at 37°C for 30 min. The following buffers were used: a citrate buffer with a pH of 3.0 or 4.0, an acetate buffer with a pH of 5.0 or 5.5, a phosphate buffer with a pH of 6.0, 7.0, or 8.0, and a carbonate buffer with a pH of 9.0 or 10.0. The turbidity of the mixture was measured at 660 nm using a UV-Vis spectrophotometer (UVmini 1240; Shimadzu, Kyoto, Japan).

Inhibition of the hemolytic activity of an extract was examined while lowering its pH in the presence of 10 mM EDTA, PMSF, or 20 μg/mL of leupeptin. Effects of divalent metal ions were also examined using various metal chlorides at a concentration of 20 mM in the presence of 10 mM EDTA.

2.3. *Assay of hemolytic activity*

Sheep RBCs were used to determine hemolytic activity. The cells were washed with phosphate-buffered saline (PBS) three times. A suspension of sheep RBCs (0.1 mL) was mixed with 1.9 mL of distilled water in order to cause osmotic lysis, and absorbance was measured at 541 nm. PBS was added to the suspension so that the absorbance at 541 nm would be 0.500.

A reaction mixture (2 mL) containing 0.1 mL of suspended sheep RBCs prepared as described above, PBS, and a sample was incubated at 37°C for 10 min. A positive control was prepared by mixing 0.1 mL of suspended sheep RBCs with 1.9 mL of distilled water, and a negative control was prepared by similarly mixing the sheep RBCs with PBS. After centrifugation at 2,200 rpm for 5 min at 4°C, the absorbance of the supernatant was measured at 541 nm. One hundred percent lysis was defined as the absorbance of the supernatant obtained from osmotically lysed cells (the positive control) (*11*). One unit was defined as the amount of a hemolytic compound causing 50% hemolysis.

2.4. *Fractionation by a modified Bligh and Dyer method*

Pieces of freeze-dried fruiting bodies of *H. marmoreus* (54 g) were used to obtain the hemolytic compound. An extract prepared as described above was treated with 0.1 M acetate buffer (pH 5.5) and incubated at 37°C for 30 min. After centrifugation at 12,000 rpm for 20 min, the precipitate was dissolved in ethanol. A fat-soluble fraction was obtained with a modified solvent system using the Bligh and Dyer method (*12*) with ethanol instead of methanol. The sample dissolved in ethanol

was mixed with one part chloroform and 0.9 parts distilled water. After vigorous vortexing, the mixture was centrifuged. The lower layer was mixed with the upper layer of a mixture of chloroform/ethanol/water (1:1:0.9, v/v) followed by vortexing and centrifugation again. The resulting lower layer was evaporated under reduced pressure and the resulting residue was dissolved in ethanol.

2.5. *Thin layer chromatography (TLC)*

TLC was performed with TLC plates (Merck, Kenilworth, NJ, USA) and chloroform/methanol/water (60:35:6, v/v) as a development solvent. Lpids were detected with primulin staining and iodine vapor (*13-16*). TLC plates were also subjected to a hemolysis assay to detect hemolytic compounds as described elsewhere (*17*).

2.6. *Data analysis*

Data were analyzed using Student's *t*-test with the software StatMate III (ATMS, Tokyo, Japan). A p value less than 0.05 was considered significant.
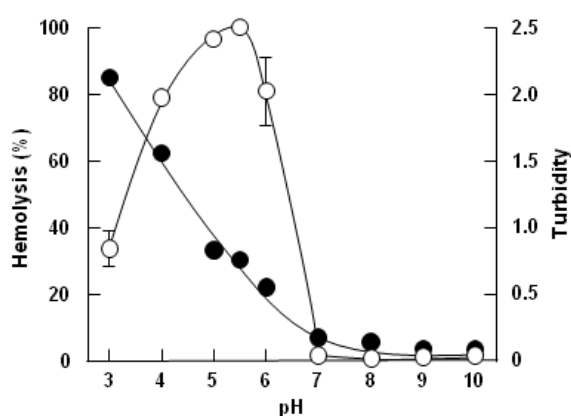
3. Results and Discussion

In preliminary experiments, hemolytic activity was detected in an acid-treated extract of *H. marmoreus* fruiting bodies but not in a neutral extract (Data not shown). Therefore, the relationship between the exhibition of hemolytic activity and the pH of the extract was examined. When the pH of the extract was adjusted at 37°C for 30 min, hemolytic activity was noted in acidic extracts but not in neutral or basic extracts (Figure 1). The maximal hemolytic activity was exhibited by an extract with a pH of 5.5.

Extracts with a low pH exhibited hemolytic activity and also had increased turbidity (Figure 1). A turbid extract with a pH of 5.5 was centrifuged at 12,000 rpm for 20 min in order to separate the supernatant and precipitate fractions. Potent hemolytic activity was exhibited by the precipitate fraction that was dissolved in ethanol (data not shown). In contrast, hemolytic activity was not detected in the supernatant fraction while potent hemagglutinating activity was noted (data not shown). This may have been caused by *H. marmoreus* lectin (*10*). This finding suggests that a water-insoluble hemolytic compound is present in the extract during its incubation at a low pH.
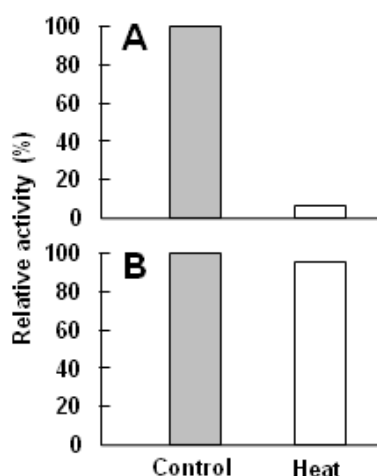
The effect of heat on the exhibition of hemolytic activity was examined. A boiled extract did not exhibit hemolytic activity or an increase in turbidity when its pH was 5.5 (Figure 2A). In contrast, the precipitate fraction that was obtained from an extract with a pH of 5.5 retained sufficient hemolytic activity even if the fraction was heat-treated (Figure 2B). These results

suggest that the hemolytic compound is heat-stable and that heat-labile metabolism may account for the hemolytic activity exhibited by the compound.

The effect that inhibitors had on the generation of the hemolytic compound was examined. Extracts were prepared with a neutral pH in the presence of inhibitors and then their pH was lowered to 5.5. As shown in Figure 3, hemolytic activity during lowering of the pH was prevented by PMSF and the divalent cation chelator EDTA but not by leupeptin. Hemolytic activity inhibited by EDTA markedly returned in the presence of Ca^{2+}, though other cations failed to sufficiently restore that activity (Figure 3B).

To characterize the nature of the hemolytic compound, the precipitate fraction obtained from an extract with a pH of 5.5 was further fractionated using a modified Bligh-Dyer method as described in the Materials and Methods. As shown in Figure 4A, potent hemolytic activity was detected in the lower
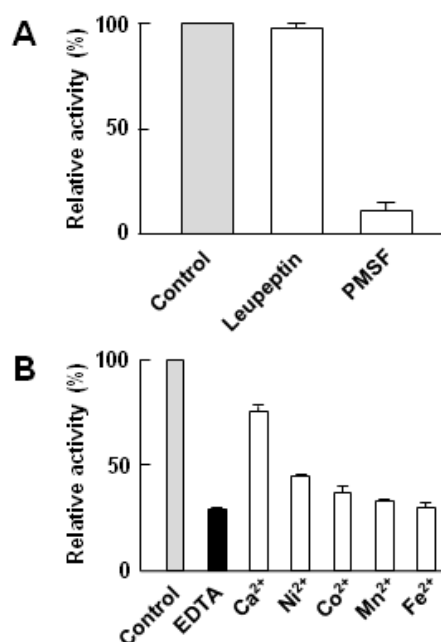

Figure 1. Effect of pH on the exhibition of hemolytic activity by and the turbidity of an extract of *H. marmoreus* fruiting bodies. An extract was incubated at 37°C for 30 min at the pH indicated. The hemolytic activity of aliquots was measured (open circle) and turbidity was determined (closed circle) as described in the Materials and Methods.
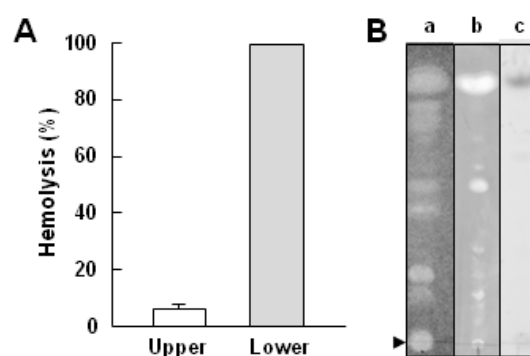

Figure 3. Effect of inhibitors of hemolytic activity on extracts with a low pH. (A) Extracts prepared at a pH of 7.3 were separately pretreated with or without 10 mM PMSF and 20 µg/mL of leupeptin. **(B)** Extracts were pretreated with or without 10 mM EDTA followed by incubation with 20 mM of the metal ions indicated. The pretreated extracts were incubated at a pH of 5.5 and then subjected to a hemolytic assay.

Figure 2. Effect of heat-treatment on the hemolytic activity of extracts before or after lowering pH. An extract prepared at a pH of 7.3 was boiled for 10 min and then its pH was lowered to 5.5 **(A)** or its pH was lowered to 5.5 and then it was boiled **(B)**. The samples were subjected to a hemolytic assay. Controls were produced by omitting boiling.

Figure 4. Fractionation of hemolytic activity using a modified Bligh and Dyer method and TLC. (A) A precipitate fraction was fractionated by using a modified Bligh and Dyer method as described in the Materials and Methods. Upper and lower layer fractions dissolved in water and ethanol, respectively, were subjected to a hemolysis assay. **(B)** The lower layer fraction was developed on TLC plates using a solvent system of chloroform/methanol/water (60:35:6, v/ v). Detection was performed by primulin staining (lane a), a hemolysis assay (lane b), and iodine vapor (lane c). An arrowhead indicates the origin.

layer (lipid fraction) but not in the upper layer (aqueous fraction), suggesting that the hemolytic component is a type of lipid. Primulin staining after TLC development revealed that the lower layer fraction contained various components (Figure 4B, lane a). A hemolysis assay of TLC plates revealed hemolytic activity at several places on the plate (Figure 4B, lane b). Potent activity was noted at the same site where a spot was produced by iodine vapor (Figure 4B, lane c). These results suggest that the hemolytic compound in an extract of *H. marmoreus* fruiting bodies with a low pH may be a lipid-like substance.

Proteinous hemolysins have been found in various mushrooms, including aegerolysin in *Agrocybe aegerita* (*18*), flammutoxin in *Flammulina velutipes* (*19*), pleurotolysin and ostreolysin in *Pleurotus ostreatus* (*11,20*), erylysins in *P. eryngii* (*21*), nebrodeolysin in *P. nebrodensis* (*22*), schizolysin in *Schzophyllum commune* (*23*), and volvatoxin in *Volvarilla volvacea* (*24*). These hemolysins were active when the first extract was adjusted to a neutral pH with buffers. However, a proteinous hemolysin from *H. marmoreus* has yet to be described. Lowering of the pH of an extract of *H. marmoreus* was essential for it to exhibit hemolytic activity (Figure 1), which presumably explains why this activity was not been noted thus far.

That said, the hemolytic compound found in the current study may be a lipid-like substance but not a proteinous hemolysin as has been found in various mushrooms. Some lipids such as fatty acids are known to non-specifically damage cells by disrupting their membrane structure. In fact, the compound found in the current study non-specifically caused hemolysis of rabbit and horse RBCs as well as sheep RBCs (data not shown).

Hemolytic activity was not detected in an extract heated before its pH was lowered, but activity was detected in a heat-stable extract after its pH was lowered (Figure 2). Therefore, a non-active precursor substance(s) may be present in fruiting bodies and a heat-labile enzyme(s) may cause that precursor(s) to release a heat-stable hemolytic compound. Since hemolytic activity was inhibited in the presence of EDTA and that activity resumed with the addition of Ca^{2+} (Figure 3B), enzyme action is presumably Ca^{2+}-dependent. In addition, PMSF (a known serine protease inhibitor) was an effective inhibitor of hemolytic activity during lowering of the extract's pH (Figure 3A). However, leupeptin (a competitive inhibitor of serine protease) did not inhibit hemolytic activity (Figure 3A). Therefore, a metalloenzyme possessing a catalytically active serine residue in its active site, but not serine protease, might be responsible for the formation of a hemolytic compound. The structure of the hemolytic lipid-like compound(s) and the precursor(s) and the enzymes in *H. marmoreus* fruiting bodies need to be studied further.

The role of mushroom hemolysins is somewhat unclear. Since hemolysins influence the cell membrane structure and lyse cells, hemolysins may provide protection from outside factors or participate in the fusion of mycelia in the life cycle of basidiomycetes (*3*). The hemolytic lipid-like compound found in the current study is not thought to exist as a free active substance in the fruiting bodies of *H. marmoreus*. If hemolytic activity is regulated in the life cycle of *H. marmoreus*, the current study might provide new evidence of the physiological role of hemolytic components in basidiomycetes.

In conclusion, a non-active precursor substance(s) may release a hemolytic lipid-like compound from an extract of *H. marmoreus* fruiting bodies through metalloenzyme(s) while the extract has a low pH.

References

1. Wasser SP, Weis AL. Medicinal properties of substances occurring in higher basidiomycetes mushrooms: Current perspectives. Int J Med Mushrooms. 1999; 1:31.
2. Wasser SP. Medicinal mushroom science: Current perspectives, advances, evidences, and challenges. Biomed J. 2014; 37:345-356.
3. Nayak AP, Green BJ, Beezhold DH. Fungal hemolysins. Med Mycol. 2013; 51:1-16.
4. Hassan MA, Rouf R, Tiralongo E, May TW, Tiralongo J. Mushroom lectins: Specificity, structure and bioactivity relevant to human disease. Int J Mol Sci. 2015; 16:7802-7838.
5. Sepčić K, Berne S, Rebolj K, Batista U, Plemenitas A, Sentjurc M, Macek P. Ostreolysin, a pore-forming protein from the oyster mushroom, interacts specifically with membrane cholesterol-rich lipid domains. FEBS Lett. 2004; 575:81-85.
6. McCormack R, de Armas L, Shiratsuchi M, Podack ER. Killing machines: Three pore-forming proteins of the immune system. Immunol Res. 2013; 57:268-278.
7. Merle NS, Church SE, Fremeaux-Bacchi V, Roumenina LT. Complement system Part I - Molecular mechanisms of activation and regulation. Front Immunol. 2015; 6:262.
8. Voskoboinik I, Whisstock JC, Trapani JA. Perforin and granzymes: Function, dysfunction and human pathology. Nat Rev Immunol. 2015; 15:388-400.
9. Gilbert RJ. Protein-lipid interactions and non-lamellar lipidic structures in membrane pore formation and membrane fusion. Biochim Biophys Acta. 2016;1858:487-499.
10. Suzuki T, Abe T, Umehara K, Choi J-H, Hirai H, Dohra H, Kawagishi H. Purification and characterization of a lectin from the mushroom *Hypsizigus marmoreus*. Mycoscience. 2015; 56:359-363.
11. Tomita T, Noguchi K, Mimuro H, Ukaji F, Ito K, Sugawara-Tomita N, Hashimoto Y. Pleurotolysin, a novel sphingomyelin-specific two-component cytolysin from the edible mushroom *Pleurotus ostreatus*, assembles into a transmembrane pore complex. J Biol Chem. 2004; 279:26975-26982.
12. Bligh EG, Dyer WJ. A rapid method of total lipid extraction and purification. Can J Biochem Physiol. 1959; 37:911-917.

13. Vioque E, Holman RT. Characterization of the ketodienes formed in the oxidation of linoleate by lipoxidase. Arch Biochem Biophys. 1962; 99:522-528.

14. Feizi T, Stoll MS, Yuen CT, Chai W, Lawson AM. Neoglycolipids: probes of oligosaccharide structure, antigenicity, and function. Methods Enzymol. 1994; 230:484-519.

15. Zarzycki PK, Bartoszuk MA, Radziwon AI. Optimization of TLC detection by phosphomolybdic acid staining for robust quantification of cholesterol and bile acids. J Planar Chromatogr. 2006; 19:52-57.

16. Fuchs B, Süss R, Teuber K, Eibisch M, Schiller J. Lipid analysis by thin-layer chromatography--a review of the current state. J Chromatogr A. 2011; 1218:2754-2774.

17. Sharma OP, Kumar N, Singh B, Bhat TK. An improved method for thin layer chromatographic analysis of saponins. Food Chem. 2012; 132:671-674.

18. Berne S, Krizaj I, Pohleven F, Turk T, Macek P, Sepcić K. Pleurotus and Agrocybe hemolysins, new proteins hypothetically involved in fungal fruiting. Biochim Biophys Acta. 2002; 1570:153-159.

19. Bernheimer AW, Oppenheim JD. Some properties of flammutoxin from the edible mushroom *Flammulina velutipes*. Toxicon. 1987; 25:1145-1152.

20. Sepcić K, Berne S, Potrich C, Turk T, Macek P, Menestrina G. Interaction of ostreolysin, a cytolytic protein from the edible mushroom *Pleurotus ostreatus*, with lipid membranes and modulation by lysophospholipids. Eur J Biochem. 2003; 270:1199-1210.

21. Shibata T, Kudou M, Hoshi Y, Kudo A, Nanashima N, Miyairi K. Isolation and characterization of a novel two-component hemolysin, erylysin A and B, from an edible mushroom, *Pleurotus eryngii*. Toxicon. 2010; 56:1436-1442.

22. Lv H, Kong Y, Yao Q, Zhang B, Leng FW, Bian HJ, Balzarini J, Van Damme E, Bao JK. Nebrodeolysin, a novel hemolytic protein from mushroom Pleurotus nebrodensis with apoptosis-inducing and anti-HIV-1 effects. Phytomedicine. 2009; 16:198-205.

23. Han CH, Zhang GQ, Wang HX, Ng TB. Schizolysin, a hemolysin from the split gill mushroom *Schizophyllum commune*. FEMS Microbiol Lett. 2010; 309:115-121.

24. Weng YP, Lin YP, Hsu CI, Lin JY. Functional domains of a pore-forming cardiotoxic protein, volvatoxin A2. J Biol Chem. 2004; 279:6805-6814.

Brief Report

An ethanolic extract of the aerial part of *Siegesbeckia orientalis* L. inhibits the production of inflammatory mediators regulated by AP-1, NF-κB and IRF3 in LPS-stimulated RAW 264.7 cells

Hui Guo[1], Yi Zhang[1], Brian Chiyan Cheng[1], Xiuqiong Fu[1], Peili Zhu[1], Jiali Chen[1], Yuencheung Chan[1], Chengle Yin[1], Yaping Wang[1], Muhammadjahangir Hossen[1], Aftab Amin[1], Anfernee Kaiwing Tse[1], Zhi-ling Yu[1,2,*]

[1] *Centre for Cancer and Inflammation Research, School of Chinese Medicine, Hong Kong Baptist University, Hong Kong, China;*
[2] *Research and Development Centre for Natural Health Products, HKBU Shenzhen Research Institute and Continuing Education, Shenzhen, China.*

Summary   Herba Siegesbeckiae (HS, the dried aerial part of *Siegesbeckia orientalis* L.) is a commonly used traditional Chinese medicinal herb for treating inflammatory diseases. HS has been reported to exert anti-inflammatory effects by inhibiting the MAPKs and NF-κB pathways, the downstream effectors of TLR4 signalling. This study aims to further investigate the involvement of TLR4 signalling cascades in the effects of an ethanolic extract of HS (HS for short) on inflammatory mediators in murine macrophages. HS was extracted using 50% ethanol. Lipopolysaccharide (LPS)-stimulated RAW264.7 macrophages were used as the cell model. ELISA was used to detect cytokine/chemokine secretion. Real time-PCR and immunoblotting were used to examine mRNA and protein levels, respectively. We observed that HS dose-dependently inhibited the secretion of PGE_2, MCP-1, MIP-1α and RANTES, and down-regulated mRNA levels of iNOS, COX-2, IL-1β, IL-6, TNF-α, mPGES-1, MCP-1, MIP-1α and RANTES in LPS-stimulated RAW264.7 cells. HS did not affect the protein levels of TAK1, TBK1, PI3K, Akt, IKK, c-Jun, c-Fos and IRF3, while, dose-dependently decreased levels of their phosphorylated forms. The protein levels of IRAK1 and IRAK4 were upregulated, while those of TRAF6 and TRAF3 were downregulated by HS. Moreover, the nuclear protein levels of AP-1, NF-κB and IRF3 were dose-dependently decreased by HS. These results indicate that suppression of the IRAK4/MAPKs/AP-1, IRAK4/MAPKs/NF-κB, IRAK4/PI3K/NF-κB and TRAF3/TBK1/IRF3 pathways is associated with the inhibitory effects of HS on inflammatory mediators in LPS-stimulated RAW264.7 cells. This study provides a pharmacological basis for the clinical application of this herb in the treatment of inflammatory disorders.

Keywords: Herba Siegesbeckiae, *Siegesbeckia orientalis*, Inflammation mediators, AP-1, NF-κB, IRF3, RAW 264.7 macrophages

1. Introduction

Herba Siegesbeckiae (HS, *Xixiancao* in Chinese), as a medicinal herb, was first documented in the Newly Revised Materia Medica (*Xinxiu Bencao*), issued in

A.D. 659 in the Tang Dynasty of China. It functions to eliminate wind-dampness and relieve joint pain (*1,2*). In the 2015 edition of Chinese Pharmacopeia, it is recorded that the aerial parts of three *Siegesbeckia* genus plants *Siegesbeckia pubescens* Makino, *S. orientalis* L. and *S. glabrescens* Makino are used as HS (*3*). In the clinic, HS is widely prescribed to treat inflammatory diseases such as furuncle, arthritis and gout (*4*). Some preparations made solely from this herb are commercially available (*e.g. Xixian* Pill/ Tablet) in China and European countries. Of these

*Address correspondence to:
Dr. Zhiling Yu, School of Chinese Medicine, Hong Kong Baptist University, Kowloon Tong, Hong Kong SAR 999077, China.
E-mail: zlyu@hkbu.edu.hk

preparations, the patent drug Joint and Muscle Relief Tablets™ produced by Phynova is the first traditional Chinese medicine licensed under the Traditional Herbal Medicinal Products Directive in the United Kingdom (*5*). Although there is no contention regarding the use, and efficacy, of HS in the treatment of inflammatory disorders, the mode and mechanism of action of this herb are poorly understood.

Pharmacological studies have demonstrated that HS possesses anti-inflammatory effects in animal models, such as xylene-induced ear edema in mice; cotton-ball-induced granuloma (*6*), collagenase-induced paw edema (*7*) and urate-induced synovitis in rats (*4*); as well as rheumatoid arthritis induced by mixed arthrogen monoclonal antibody in mice (*8*). *In vitro* studies have shown that HS inhibits inflammatory mediators by suppressing the MAPK- and NF-κB-pathways in LPS-stimulated RAW264.7 cells (*9*). Kirenol, a natural compound occuring in HS, has been reported to inhibit NF-κB activity and exert anti-inflammatory effects in collagen-induced arthritic rats (*10*). However, these mechanistic studies do not address whether HS/kirenol affect(s) molecular events upstream and/or downstream of NF-κB and MAPKs, which are downstream effectors of troll-like receptor 4 (TLR4). TLR4 is part of a receptor complex that recognizes and responds to the bacteria lipopolysaccharide (LPS) ligand (*11,12*). TLR4 signalling pathway activation has been implicated in inflammatory disorders. TLR4 signalling activates transcription factors such as NF-κB, AP-1 and IRF3. These proteins are key inflammatory response mediators (*13*). In this study we found that inhibition of the IRAK4/MAPKs/AP-1, IRAK4/MAPKs/NF-κB, IRAK4/PI3K/NF-κB and TRAF3/TBK1/IRF3 pathways is associated with the inhibitory effects of HS on inflammatory mediators in LPS-stimulated RAW264.7 cells. These novel findings provide additional justification for the clinical application of HS in the treatment of inflammatory disorders.

2. Materials and Methods

2.1. Reagents and materials

LPS from Escherichia coli O55:B5, dimethyl sulfoxide (DMSO), 3-(4,5-dimethylthiazol-2-yl)-2,5-diphenyltetrazolium bromide (MTT) and Griess reagent were obtained from Sigma Chemicals Ltd. (St. Louis, MO, USA). Penicillin, streptomycin, Dulbecco's Modified Eagle Medium (DMEM) and foetal bovine serum (FBS) were purchased from Hyclone (Logan, UT, USA). Cyclooxygenase-2 (COX-2), Inducible nitric oxide synthase (iNOS), TNF receptor associated factor protein 3 (TRAF3), IKKα/β, PI3K, phospho-PI3K p85 (Tyr458)/p55 (Tyr199), phospho-IKKα/β (Ser176/180), IκBα, phospho-IκBα (Ser32), NF-κB p50, IFN regulatory factor 3 (IRF3), phospho-IRF3 (Ser396), extracellular signal-regulated kinase (ERK), phospho-

ERK (Thr202/Tyr204), c-Jun N-terminal kinase (JNK), phospho-JNK (Thr183/Tyr185), p38 mitogen-activated protein kinase (p38), phospho-p38 (Thr180/Tyr182), TGFβ-activated kinase 1 (TAK1), phospho-TAK1 (Ser412), interleukin-1 receptor-associated kinase 1 (IRAK1), IRAK4, TANK-binding kinase 1 (TBK1), phospho-TBK1 (Ser172) and GAPDH monoclonal antibodies were obtained from Cell Signalling Technology (Boston, MA, USA). TNF receptor associated factor protein 6 (TRAF6), Akt, phospho-Akt (Ser473), NF-κB p65, phospho-NF-κB p65 (Ser536), c-Jun, phosphor-c-Jun (Ser63), Pol II (H-224) antibodies were obtained from Santa Cruz Biotechnology (Santa Cruz, CA, USA). Acetonitrile (ACN, HPLC grade) was obtained from RCI Labscan Limited (Thailand). A Milli-Q system (Millipore, MA, USA) was used to prepare ultra-pure water for HPLC analyses. Ethanol (absolute) was from Merck (Darmstadt, Germany). Other materials used in bioassays were from Life Technologies Inc. (GIBICO, USA).

2.2. Herbal materials

Three *Siegesbeckia* genus plants are used as origins of HS in China. However, HS derived from *S. orientalis* is the most commonly used. In this study, we used the dried aerial part of *S. orientalis*, which originates in Hubei province, China (Longitudes: 108–116°E, latitudes: 29–33°N). The herb was purchased from the Hubei Shen Nong Traditional Chinese Medicine Co. Ltd and authenticated by Professor Hubiao Chen (Hong Kong Baptist University, HKBU). A voucher specimen (No.20141101) has been deposited at the School of Chinese Medicine, HKBU.

HS is traditionally used in the forms of decoction (extraction using water) and pill made from herb powder, suggesting that the bioactive components of HS may be polar and/or non-polar. Previously, we extracted the herb with three different solvents including water, 50% ethanol and 95% ethanol; and compared the inhibitory effect of the three extracts on NO production in LPS-stimulated RAW 264.7 cells. Results indicated that the extract prepared with 50% ethanol possesses the most potent inhibitory effect on NO production (*14*). Thus, we used 50% ethanol to extract the herb in this work. HS (10 g) was grounded and macerated for 1 h with 100 mL of 50% ethanol at room temperature (25 ± 2°C), and then extracted by refluxing twice for 1 h each. The extracts were filtered and combined after cooling; the filtrate and washings were combined and then concentrated by rotary evaporation under reduced pressure to remove the solvent. The concentrated extracts were rapidly frozen at −80°C, and then dried in a freeze-dryer (Virtis freeze mobile, Virtis Co., Gardiner, USA). The yield of the extract (HS for short) was 18.03%. To prepare the sample solution for bioassays, HS was freshly dissolved in DMSO, filtered

with a syringe filter (0.22 μm), and then diluted with cell culture medium to various concentrations.

For the quality control of the prepared HS, HPLC analyses were performed on an Agilent 1260 series HPLC-DAD system using a previously described method (*15*) with some modifications. The separation was conducted on an Alltima™ C-18 analytical column (250 mm × 4.6 mm I.D., 5 μm) with a gradient mobile phase of solvent A (ultra-pure water) and solvent B (acetonitrile). The HPLC elution profile was as follows: 0-6 min, 30% B; 6-20 min, 30-45% B; 20-30 min, 45% B. The flow rate was maintained at 1.0 mL/min and the column temperature was set at 25°C. The chromatograms were monitored with the DAD detector at a wavelength of 215 nm. Each sample of 20 μL was injected for analysis.

2.3. Cell culture

The RAW267.4 murine macrophage cell line (ATCC TIB-71) was obtained from the American Type Culture Collection (Manassas, VA, USA). The cells were cultured in DMEM at 37°C with 5% CO_2 in a humidified incubator. Heat inactivated FBS (5%) and penicillin/ streptomycin antibiotic cocktail (1%) were included in the culture (*16*).

2.4. Cell viability assay

RAW264.7 cells were seeded in 96-well plates (5×10^3 cells/well) and allowed to adhere overnight. The cells were treated with HS at indicated concentrations for 1h, and further treated in the presence or absence of LPS (100 ng/mL) for another 24 h. The final concentration of DMSO in the cell culture medium was less than 0.05% (v/v). Cell viability was evaluated using the MTT assay as described (*17*).

2.5. Enzyme-linked immunosorbent assay (ELISA)

RAW264.7 cells were seeded in 24-well plates (1.5×10^5 cells/well) and allowed to adhere overnight. The cells were treated with indicated concentrations (μg/mL) of HS for 1 h, and then in the presence or absence of LPS (100 ng/mL) for another 24 h. ELISA kits purchased from eBioscience (San Diego, CA, USA) were used to determine PGE_2, MCP-1, MIP-1α, IL-1, IL-6, TNF-α and RANTES in the supernatants of the cell cultures following manufacturer's instructions (*18*).

2.6. Nitric oxide (NO) production measurement

The supernatant of cultured RAW 264.7 cells obtained in Section 2.5 was used to measure NO production by determining the accumulated nitrite formed using the Griess reagent according to manufacturer's instructions (Sigma) (*19*).

2.7. Real-time polymerase chain reaction analysis

RAW264.7 cells were seeded in 6-well plates (1.0×10^5 cells/mL) and allowed for adhere over night. After pretreatment with HS (80 μg/mL) for 1 h, the cells were incubated in the presence or absence of LPS (100 ng/mL) for another 16 h. Trizol reagent (Invitrogen, USA) was used to prepare total RNA. Five μg of RNA was used for reverse transcription by oligo-dT using the SuperScript II Reverse Transcription Kit (Invitrogen, USA). The following primers were used: iNOS (Sense 5'-AGCAACTACTGCTGGTGGTG-3' and anti-sense 5'-TCTTCAGAGTCTGCCCATTG-3'), COX-2 (Sense 5'-CTGGAACATGGACTCACTCAGTTTG-3' and anti-sense 5'-AGGCCTTTGCCACTGCTTGT-3'), IL-1β (Sense 5'-GAAGAAGAGCCCATCCTCTG-3' and anti-sense 5'-TCATCTCGGAGCCTGTAGTG-3'), IL-6 (Sense 5'-AGTCCGGAGAGGAGACTTCA-3' and anti-sense 5'-ATTTCCACGATTTCCCAGAG-3'), TNF-α (Sense 5'-ATGAGAAGTTCCCAAATGGC-3' and anti-sense 5'-CTCCACTTGGTGGTTTGCTA-3'), mPGES-1 (Sense 5'-ATGAGGCTGCGGAAGAAGG-3' and anti-sense 5'-GCCGAGGAAGAGGAAAGGATAG-3'), MCP-1 (Sense 5'-AATGCTAACGCCACCGAGAG-3' and anti-sense 5'-CCTTGTTCTGCTCCTCATAGTCC-3'), MIP-1α (Sense 5'-CCCAGCCAGGTGTCATTTTCC-3' and anti-sense 5'-GCATTCAGTTCCAGGTCAGTG-3'), RANTES (Sense 5'-CATATGGCTCGGACACCA-3' and anti-sense 5'-ACACACTTGGCGGTTCCT-3'), GAPDH (Sense 5'-GGCCTTCCGTGTTCCTACC-3' and anti-sense 5'-TGCCTGCTTCACCACCTTC-3'); Real-time PCR analysis was conducted using SYBR green reaction mixture in the ABI 7500 Fast Real-time PCR System (Applied Biosystems, USA) (*20*).

2.8. Western blotting

RAW 264.7 cells were seeded in 60-mm-diameter culture dishes (2×10^5 cells/mL) and allowed to adhere overnight. The cells were treated with HS at indicated concentrations for 1 h, and then in the presence or absence of LPS (100 ng/mL) for indicated periods (30, 60 min; or 24 h). Cell total extract, cytosolic fraction and nuclear fraction were prepared, respectively. Soluble lysates were immunoblotted with the designated antibodies, and signals were detected by ECL detection reagents (Amersham Biosciences, USA) (*21*).

2.9. Statistical analysis

Data were presented as the mean ± SD of at least three triplicate determinations. Statistical differences were determined using one-way ANOVA followed by Tukey's multiple comparisons test. GraphPad Prism 5.0 (GraphPad Software, San Diego, CA) was used for statistical analyses. $P < 0.05$ was considered to be statistically significant.

3. Results and Discussion

In clinic, HS is commonly prescribed for treating hypertension, malaria, neurasthenia, hepatitis, and inflammatory diseases such as rheumatic arthritis and gout. Phytochemical investigations revealed that this herb contains various types of compounds such as diterpenoids, sesquiterpenoids and flavonoids. Diterpenoids are reported as being major bioactive components of HS (*22*). Kirenol and darutigenol are two diterpenoids abundant in HS. Kirenol has been shown to inhibit NF-κB activity and exert anti-inflammatory effects in collagen-induced arthritic rats (*10*). In this study, the HPLC chromatogram showed that kirenol and darutigenol were present in HS (Figure 1). The mean contents of kirenol and darutigenol in HS were 0.51% and 0.22%, respectively. Further studies are required to identify the anti-inflammatory compounds in HS.

Previous studies indicated that the MAPKs and NF-κB signalling pathways play essential roles in the inhibitory effects of HS on inflammatory mediators (*9,20*). MAPKs and NF-κB are components of TLR4 signalling cascades. We believe that inhibition of TLR4 signalling pathways contributes to the inhibitory effects of HS on inflammatory mediators.

In this work, LPS-stimulated RAW264.7 macrophage cells were used as the TLR4-activated cell model to investigate the inhibitory effect of HS on inflammatory mediators. To determine sub-lethal concentrations of HS, MTT assays were first conducted. In the presence or absence of 100 ng/mL of LPS, the viability of RAW264.7 cells was not significantly altered during a 24-h treatment with up to 120 μg/mL of HS (Figure 2A). HS concentrations of 20, 40 and 80 μg/mL were used in subsequent assays.

TLR4 transduces signals through the MyD88-dependent and MyD88-independent pathways, which are mainly mediated by the activation of transcription factors NF-κB, AP-1 and IRF3. Upon LPS stimulation, NF-κB and AP-1 are activated *via* the MyD88-dependent pathway, and IRF3 is activated *via* the MyD88-independent pathway in macrophages (*13*). We have determined the effect of HS on pro-inflammatory mediators regulated by the three transcription factors in LPS-induced RAW264.7 cells, and observed that HS concentration-dependently reduced the production of PGE$_2$ (regulated by NF-κB), MCP-1, MIP-1α (regulated by AP-1), and RANTES (regulated by IRF3) (Figure 2B), and lowered mRNA levels of iNOS, COX-2, IL-1β, IL-6, TNF-α, mPGES-1, MCP-1, MIP-1α and RANTES (Figure 2C). Additionally, HS inhibited other NF-κB-regulated inflammatory mediators that have previously been reported (*9,20*). These mediators have been examined (Supplementary Figure 1S, *http://www.biosciencetrends.com/action/getSupplementalData.php?ID=26*) and discussed in the subsequent sections.

We determined the effect of HS on the nuclear localization of transcription factors NF-κB, AP-1 and IRF3 in LPS-induced RAW264.7 cells. Our results indicate that the nuclear protein levels of NF-κB subunits (p65 and p50), AP-1 subunits (c-Jun and c-Fos) and IRF3 were markedly increased upon LPS stimulation. HS concentration-dependently reversed the increment (Figure 3A). Moreover, LPS-induced down-regulation of p65, p50, c-Jun and c-Fos in the cytoplasm was dose-dependently inhibited by HS (Figure 3B). Cytoplasmic IRF3 levels were not significantly altered by the treatments (data not shown). These results demonstrate that HS inhibits the production of pro-inflammatory mediators regulated by NF-κB, AP-1 and IRF3, suggesting that both MyD88-dependent and MyD88-independent pathways are involved in the anti-inflammatory effects of HS.

Upon activation of MyD88-dependent signalling, MyD88 recruits IRAK4, thereby allowing the association of IRAK1. The TLR4 receptor complex-associated IRAK1 is phosphorylated by IRAK4, which in turn promotes the autophosphorylation and dissociation of IRAK1 from the receptor complex. Subsequently, IRAK1 interacts with TAK1-TAB1-TAB2 kinase complex-associated TRAF6. This interaction leads to the ubiquitylation of TRAF6, which induces the activation of TAK1 (*23*). The activated TAK1 induces the phosphorylation of MAPKs and IKK, leading to the activation of transcription factors NF-kB and AP-1 (*24,25*). Upon activation of the MyD88-independent pathway, the TRAF3/TBK1 complex is activated, resulting in the phosphorylation and nuclear localization of IRF3 (*26*). Our results showed that HS inhibited LPS-induced degradation of IRAK1 and IRAK4, concentration-dependently lowered protein levels of TRAF6, TRAF3, and phosphorylated forms of TAK1 and TBK1 (Figure 4A). These data further suggest the involvement of both MyD88-dependent and MyD88-independent pathways in the effects of HS.

Activation of IKK kinase initiates the phosphorylation and degradation of IκBα resulting in the release of p50-p65 for nuclear translocation, and the eventual mediation of NF-κB-dependent transcriptional activity (*27*). Studies have demonstrated that the PI3K/Akt pathway can regulate NF-κB signalling positively or negatively (*28,29*). Our results showed that HS concentration-dependently inhibited the phosphorylation of MAPKs (JNK, ERK and p38), IκBα and NF-κB p65. HS also inhibited the protein expression of iNOS and COX-2, the secretion of cytokines (IL-1β, IL-6 and TNF-α) and the production of NO in a concentration-dependent manner (Supplementary Figure 1S, *http://www.biosciencetrends.com/action/getSupplementalData.php?ID=26*). These results are consistent with observations in previous reports (*9,20*) and thus confirm the involvement of MAPKs and NF-κB signalling in the effects of HS. Our results also showed that HS concentration-dependently inhibited
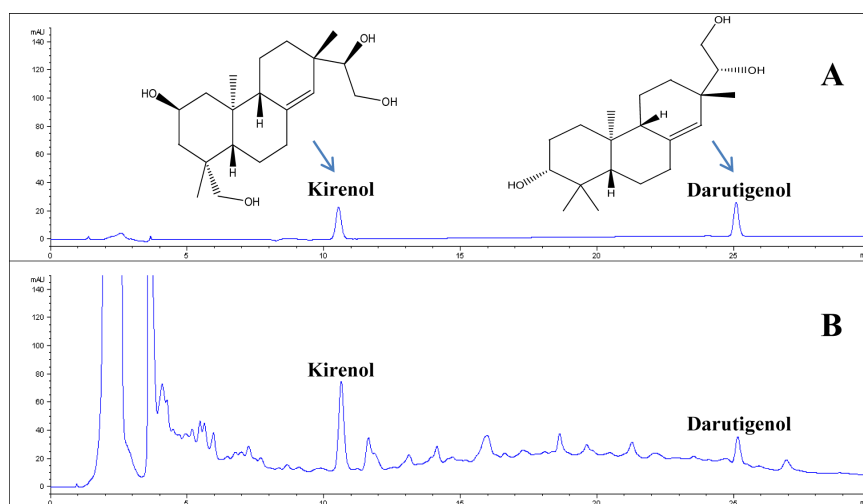
Figure 1. HPLC analyses of HS and mixed standards (kirenol and darutigennol) (A. Mixed standards; B. HS sample).
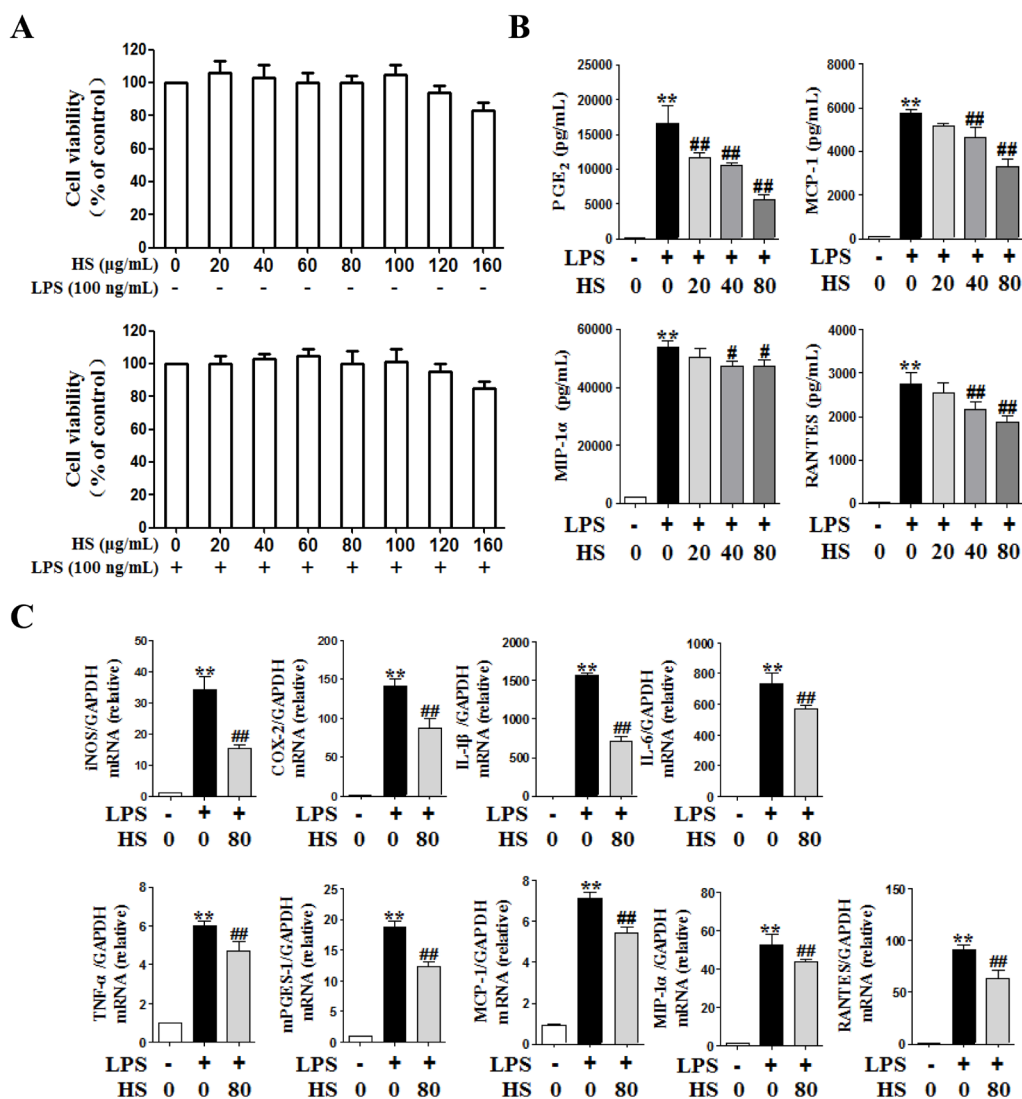
Figure 2. HS inhibited inflammatory mediators in LPS-stimulated RAW 264.7 cells. (A) Effects of HS on the cell viability in the absence (upper panel) or presence of LPS (lower panel). **(B)** HS reduced the production of PGE_2, MCP-1, MIP-1α and RANTES. **(C)** HS decreased mRNA levels of iNOS, COX-2, IL-1β, IL-6, TNF-α, mPGES-1, MCP-1, MIP-1α and RANTES in LPS-stimulated RAW 264.7 cells. Data are shown as mean ± SD from tree independent experiments. $**P < 0.01$ *vs.* value in corresponding control; $^{\#\#}P < 0.01$, $^{\#}P < 0.05$ *vs.* value in cells treated with LPS alone.
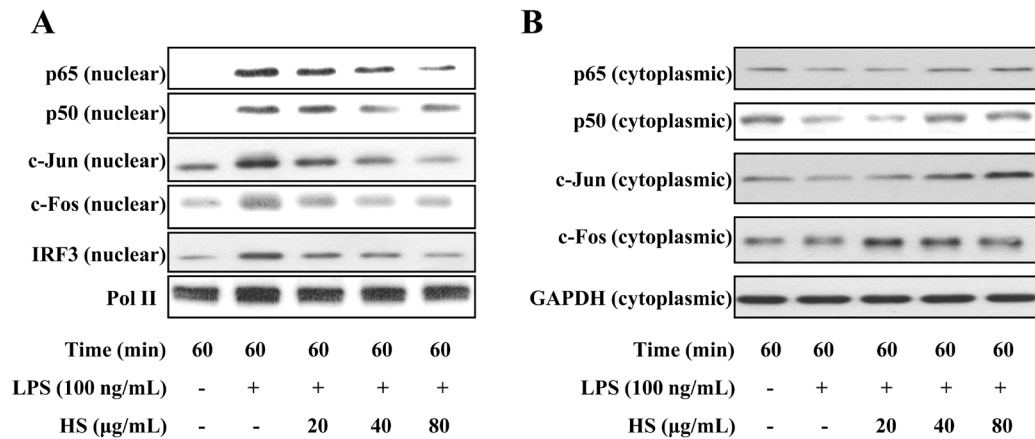
Figure 3. Effects of HS on the nuclear localization of the three transcription factors in LPS-induced RAW264.7 cells. (A) HS decreased nuclear protein levels of NF-κB subunits (p65 and p50), AP-1 subunits (c-Jun and c-Fos) and IRF3. **(B)** HS inhibited down-regulation of cytoplasmic protein levels of p65, p50, c-Jun and c-Fos. Results of a typical experiment from three independent ones are shown.
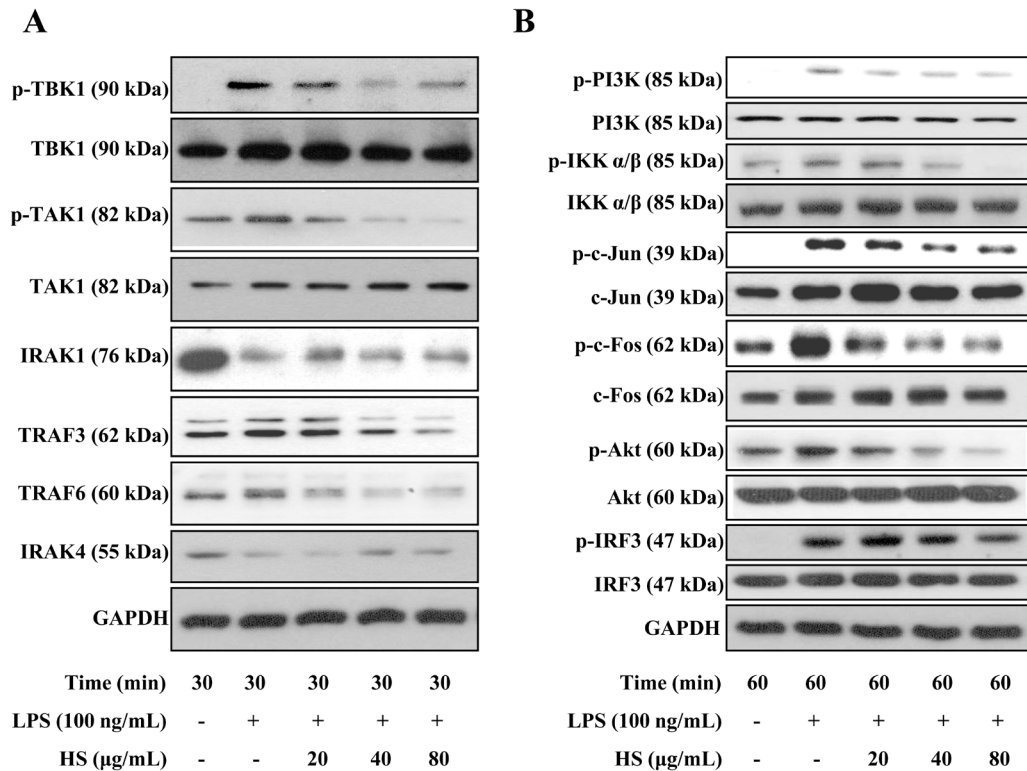
Figure 4. Effects of HS on molecules involved in the TLR4 signaling pathways in LPS-stimulated RAW 264.7 cells. (A) Effects of HS on protein levels of TRAF6, TRAF3, IRAK1, IRAK4, phospho-TAK1, TAK1, phospho-TBK1 and TBK1. **(B)** Effects of HS on protein levels of phosphorylated and nonphosphorylated forms of PI3K, Akt, IKK, c-Jun, c-Fos and IRF3. Results of a typical experiment from three independent ones are shown.

LPS-induced phosphorylation of PI3K, Akt, IKK, c-Jun, c-Fos and IRF3 (Figure 4B). These findings support the involvement of the MyD88-dependent pathways of MAPKs/AP-1 and PI3K/Akt, and the MyD88-independent pathway TBK1/IRF3 in the effects of HS. As stated previously, the role of Akt signalling in NF-κB activation is still controversial. Further studies are needed to delineate the inhibitory effect of HS on the Akt/NF-κB pathway.

Although we examined the proteins levels of TLR4, MyD88 and TRAM (data not shown) following HS treatment, we did not observe any significant changes. Previous studies suggest that some agents can alter the interaction between TLR4 receptor complex and LPS by competitively binding to the extracellular domain of TLR4 (*30*). Therefore, further studies are needed to determine the possible abrogation of LPS-TLR4 interaction by HS in RAW264.7 cells.

4. Conclusion

In this study, our results indicate that inhibition of the IRAK4/MAPKs/AP-1, IRAK4/MAPKs/NF-κB, IRAK4/PI3K/NF-κB and TRAF3/TBK1/IRF3 pathways is associated with the inhibitory effects of HS on inflammatory mediators in LPS-stimulated RAW264.7 cells. Therefore, not only do our experiments support the use of HS as a medicinal herb in the treatment of various inflammatory conditions, they also provide a novel pharmacological and mechanistic insight into the fundamentals of its activity. However, additional studies are warranted to further explore the molecular mechanism of action and identify the bioactive components of HS.

Acknowledgements

References

1. Wang JP, Zhou YM, Ye YJ, Shang XM, Cai YL, Xiong CM, Wu YX, Xu HX. Topical anti-inflammatory and analgesic activity of kirenol isolated from Siegesbeckia orientalis. J Ethnopharmacol. 2011; 137:1089-1094.
2. Wang LL, Hu LH. Chemical constituents of Siegesbeckia orientalis L. J Integr Plant Biol. 2006; 48:991-995.
3. The State Pharmacopoeia Commission of PR China. Chinese Pharmacopoeia. China Medical Science and Technology Press, Beijing, China, 2015; Part I:pp.368. (in Chinese)
4. Nguyen TD, Thuong PT, Hwang IH, Hoang TK, Nguyen MK, Nguyen HA, Na M. Anti-Hyperuricemic, Anti-Inflammatory and Analgesic Effects of Siegesbeckia orientalis L. Resulting from the Fraction with High Phenolic Content. BMC Complement Altern Med. 2017; 17:191.
5. Phynova. Phynova Joint and Muscle Relief Tablets™. *https://www.phynova.com/products/phynova-joint-and-muscle-relief-tablets/* (accessd March 01, 2018).
6. Liu DY, Hu HH. Experimental Research on anti-inflammation of processed Herba Siegesbeckiae. Lishenzhen medicine and materia medica research. 2008; 19:668-669.
7. Huh JE, Baek YH, Lee JD, Choi DY, Park DS. Therapeutic effect of Siegesbeckia pubescens on cartilage protection in a rabbit collagenase-induced model of osteoarthritis. J Pharmacol Sci. 2008; 107:317-328.
8. Fu XC, Jiang FP, Fan JZ, Bai HB. Extract of Herba Siegesbeckiae on mouse rheumatoid arthritis induced by anthrogen-CIA monoclonal antibody. Zhejiang Da Xue Xue Bao Yi Xue Ban. 2013; 42:556-560. (in Chinese)
9. Hong YH, Weng LW, Chang CC, Hsu HF, Wang CP, Wang SW, Houng JY. Anti-inflammatory effects of Siegesbeckia orientalis ethanol extract in in vitro and in vivo models. Biomed Res Int. 2014; 2014:329712.
10. Wang ZM, Zhu SG, Wu ZW, Lu Y, Fu HZ, Qian RQ. Kirenol upregulates nuclear annexin-1 which interacts with NF-kappaB to attenuate synovial inflammation of collagen-induced arthritis in rats. J Ethnopharmacol. 2011; 137:774-782.
11. Aminlari A, Richard KD, Zhang HY, O'Donnell DP, Wang GS, Alarcon WH, Steinstraesser L, Wang SC, Remick DG, Su GL. LPS activation of kupffer cells is mediated by toll like receptor 4 (TLR 4). Hepatology. 1999; 30:374a-374a.
12. Panzer S. Differential response to LPS isotypes induced platelet activation mediated by Toll-like receptor (TLR)-4. Clin Immunol. 2013; 146:13-14.
13. Lu YC, Yeh WC, Ohashi PS. LPS/TLR4 signal transduction pathway. Cytokine. 2008; 42:145-151.
14. Guo H, Zhang Y, Cheng BC, Lau MY, Fu XQ, Li T, Su T, Zhu PL, Chan YC, Tse AK, Yi T, Chen HB, Yu ZL. Comparison of the chemical profiles and inflammatory mediator-inhibitory effects of three Siegesbeckia herbs used as Herba Siegesbeckiae (Xixiancao). BMC Complement Altern Med. 2018; 18:141.
15. Yan DX, Wang YJ, Duan Q, Zhang XM, Zhao HQ. Simultaneous Determination of Kirenol and Darutigenol in Herba Siegesbeckiae by RP-HPLC. Chinese Pharmaceutical Journal. 2010; 45:945-948. (in Chinese)
16. Su T, Bai JX, Chen YJ, Wang XN, Fu XQ, Li T, Guo H, Zhu PL, Wang Y, Yu ZL. An Ethanolic Extract of Ampelopsis Radix Exerts Anti-colorectal Cancer Effects and Potently Inhibits STAT3 Signaling In Vitro. Front Pharmacol. 2017; 8:227.
17. Gerlier D, Thomasset N. Use of Mtt Colorimetric Assay to Measure Cell Activation. J Immunol Methods. 1986; 94:57-63.
18. Du J, Cheng BCY, Fu XQ, Su T, Li T, Guo H, Li SM, Wu JF, Yu H, Huang WH, Cao H, Yu ZL. In vitro assays suggest Shenqi Fuzheng Injection has the potential to alter melanoma immune microenvironment. J Ethnopharmacol. 2016; 194:15-19.
19. Green LC, Wagner DA, Glogowski J, Skipper PL, Wishnok JS, Tannenbaum SR. Analysis of nitrate, nitrite, and [15N]nitrate in biological fluids. Anal Biochem. 1982; 126:131-138.
20. Su T, Yu H, Kwan HY, Ma XQ, Cao HH, Cheng CY, Leung AK, Chan CL, Li WD, Cao H, Fong WF, Yu ZL. Comparisons of the chemical profiles, cytotoxicities and anti-inflammatory effects of raw and rice wine-processed Herba Siegesbeckiae. J Ethnopharmacol. 2014; 156:365-369.
21. Cheng BC, Yu H, Su T, Fu XQ, Guo H, Li T, Cao HH, Tse AK, Kwan HY, Yu ZL. A herbal formula comprising Rosae Multiflorae Fructus and Lonicerae Japonicae Flos inhibits the production of inflammatory mediators and the IRAK-1/TAK1 and TBK1/IRF3 pathways in RAW 264.7 and THP-1 cells. J Ethnopharmacol. 2015; 174:195-199.
22. Huo L, Jiang Z, Li H, Wang M, Ye X, Ji B, Guo X. Simultaneous determination of seven major diterpenoids in Siegesbeckia pubescens Makino by high-performance liquid chromatography coupled with evaporative light scattering detection. J Sep Sci. 2012; 35:2585-2591.
23. Akira S, Takeda K. Toll-like receptor signalling. Nat Rev Immunol. 2004; 4:499-511.

24. Hipskind RA, Bilbe G. MAP kinase signaling cascades and gene expression in osteoblasts. Front Biosci. 1998; 3:d804-816.

25. Schulze-Osthoff K, Ferrari D, Riehemann K, Wesselborg S. Regulation of NF-κB Activation by MAP Kinase Cascades. Immunobiology. 1997; 198:35-49.

26. Kim SS, Lee KG, Chin CS, Ng SK, Pereira NA, Xu S, Lam KP. DOK3 is required for IFN-beta production by enabling TRAF3/TBK1 complex formation and IRF3 activation. J Immunol. 2014; 193:840-848.

27. Cianciulli A, Calvello R, Porro C, Trotta T, Salvatore R, Panaro MA. PI3k/Akt signalling pathway plays a crucial role in the anti-inflammatory effects of curcumin in LPS-activated microglia. Int Immunopharmacol. 2016; 36:282-290.

28. Bauerfeld CP, Rastogi R, Pirockinaite G, Lee I, Huttemann M, Monks B, Birnbaum MJ, Franchi L, Nunez G, Samavati L. TLR4-Mediated AKT Activation Is MyD88/TRIF Dependent and Critical for Induction of Oxidative Phosphorylation and Mitochondrial Transcription Factor A in Murine Macrophages. J Immunol. 2012; 188:2847-2857.

29. Luyendyk JP, Schabbauer GA, Tencati M, Holscher T, Pawlinski R, Mackman N. Genetic analysis of the role of the PI3K-Akt pathway in lipopolysaccharide-induced cytokine and tissue factor gene expression in monocytes/macrophages. J Immunol. 2008; 180:4218-4226.

30. Brodsky I, Medzhitov R. Two modes of ligand recognition by TLRs. Cell. 2007; 130:979-981.

Communication

The proangiogenic role of polymorphonuclear myeloid-derived suppressor cells in mice infected with *Echinococcus granulosus*

Jianhai Yin, Yujuan Shen, Aiping Yu, Congshan Liu, Jiaqing Yao, Wenci Gong, Jianping Cao*

National Institute of Parasitic Diseases, Chinese Center for Disease Control and Prevention, Chinese Center for Tropical Diseases Research, WHO Collaborating Centre for Tropical Diseases, National Center for International Research on Tropical Diseases, Ministry of Science and Technology, Key Laboratory of Parasite and Vector Biology, Ministry of Health, Shanghai, China.

Summary　　　The aim of this study was to first evaluate the proangiogenic activity of polymorphonuclear myeloid-derived suppressor cells (PMN-MDSC) in mice infected with *Echinococcus granulosus*. PMN-MDSCs derived from experimentally infected mice were collected and cultured *in vitro*, and their effect on angiogenesis was investigated using a human umbilical vein endothelial cell (HUVEC) tube-formation assay stimulated with the supernatant by microscope and the Angiogenesis module of the software NIH Image J. In addition, the expression levels of several functional factors related to proangiogenic activity were analyzed. The results showed that vascular endothelial growth factor (VEGF) was increased in the serum from infected mice, and the PMN-MDSCs expressed VEGF directly. The culture supernatant from PMN-MDSCs significantly promoted HUVECs to form tubes. VEGF mRNA was higher and soluble fms-like tyrosine kinase-1 levels were lower, in PMN-MDSCs from infected mice than in those from control mice. In conclusion, host angiogenesis in mice infected with *E. granulosus* appeared to be promoted by PMN-MDSCs. Other specific angiogenic factors derived from PMN-MDSCs and parasites in the microenvironment of infection foci should be clarified in further studies, in order to provide more information for the prophylaxis and treatment of echinococcosis.

Keywords: Polymorphonuclear myeloid-derived suppressor cells, proangiogenic, *Echinococcus granulosus*, vascular endothelial growth factor, soluble fms-like tyrosine kinase-1

1. Introduction

The circulatory system, consisting of the cardiovascular and lymphatic systems, transports circulating nutrients, oxygen, hormones, growth factors, and their metabolites to tissues and cells. Angiogenesis, the growth of new capillary blood vessels in the body, is an important physiological process (*1*). It is highly regulated by a precise balance of growth and inhibitory factors produced in healthy tissues (*2,3*). However, abnormal blood vessel growth due to the imbalance of these factors is related to many deadly and debilitating pathological conditions, including cancer, diabetic ulcers, and rheumatoid arthritis (*1,4*). More and more diseases are being reported to have angiogenesis as an underlying mechanism.

Vascular endothelial growth factor (VEGF) is considered to be the strongest stimulator of angiogenesis (*5*). It promotes the proliferation and migration of endothelial cells, antagonizes cell apoptosis and promotes differentiation through activating intracellular tyrosine kinase, and finally directly forms blood vessels. Moreover, VEGF can also initiate the proteolytic enzyme system to participate in the degradation of extracellular matrix and promote the formation of new blood vessels (*6*). In addition, VEGF may increase vascular permeability resulting in plasma protein extravasation, participate in the formation of vascular basement membrane and extracellular matrix, and provide support for endothelial cell migration and blood vessel growth (*7*).

*Address correspondence to:
Dr. Jianping Cao, National Institute of Parasitic Diseases, Chinese Center for Disease Control and Prevention, Chinese Center for Tropical Diseases Research, WHO Collaborating Centre for Tropical Diseases, National Center for International Research on Tropical Diseases, Ministry of Science and Technology, Key Laboratory of Parasite and Vector Biology, Ministry of Health, Shanghai 200025, China.
E-mail: caojp@yahoo.com

In contrast, soluble fms-like tyrosine kinase-1 (sFlt-1) is a tyrosine kinase protein that disables proteins that cause blood vessel growth (*8,9*).

The growth, maturation, and reproduction of parasites in a host are inseparable from nutrient supply and metabolite excretion, both of which depend on the circulatory system (*10*). Angiogenesis in a host during a parasitic infection can be activated by various factors produced by the parasites themselves. For example, echinococcosis caused by *Echinococcus multilocularis* produces tumor-like infiltrative growth in the host liver, and causes the development of hydatid cysts wrapped by granulation tissues, with abundant new vessels visible (*11*). This is partially attributed to the glucose phosphate isomerase expressed by *E. multilocularis*, which is not only essential for the growth, development, infiltration, and metastasis of *E. multilocularis*, but also plays a potential role in host angiogenesis (*12*).

In addition to parasite-derived factors, parasite-infected hosts can also produce factors that promote angiogenesis in the host. Myeloid-derived suppressor cells (MDSC) including polymorphonuclear MDSCs (PMN-MDSC) and monocytic MDSCs (M-MDSC) are activated and enriched during parasitic infections, and play an important role in immunosuppression (*13*). These cells have a proangiogenic role in the processes of tumor growth, invasion and metastasis (*14-16*), but whether they function similarly during parasitic infection is unclear. It has been reported that MDSCs secrete angiogenic factors such as VEGF and/or directly differentiate into vascular endothelial cells to promote host angiogenesis, which is beneficial to tumor development. In our previous studies, we found that hydatid cysts of *Echinococcus granulosus* promoted the formation of tubes by human umbilical vein endothelial cells (HUVEC) *in vitro* (*17*). We also found that MDSCs were significantly enriched in the spleen and peripheral blood of BALB/c mice infected with *E. granulosus*, and played an immunosuppressive role (*18*). Moreover, M-MDSCs from the spleen of BALB/c mice infected with *E. granulosus* could significantly promote HUVECs into forming tubes.

We therefore investigated the potential proangiogenic role of PMN-MDSCs from the spleen of BALB/c mice infected with *E. granulosus* using the tube formation assay and analysis of key angiogenic factors. To our knowledge, this is the first time this has been investigated, and the results have important implications for the prophylaxis and treatment of echinococcosis.

2. Angiogenesis caused by *E. granulosus* infection

Host angiogenesis caused by parasite infection is an extremely complicated process that is not only affected by parasitic factors; host response to infection is also important (*10*). In general, the exchange of angiogenic factors between parasite and host plays an important
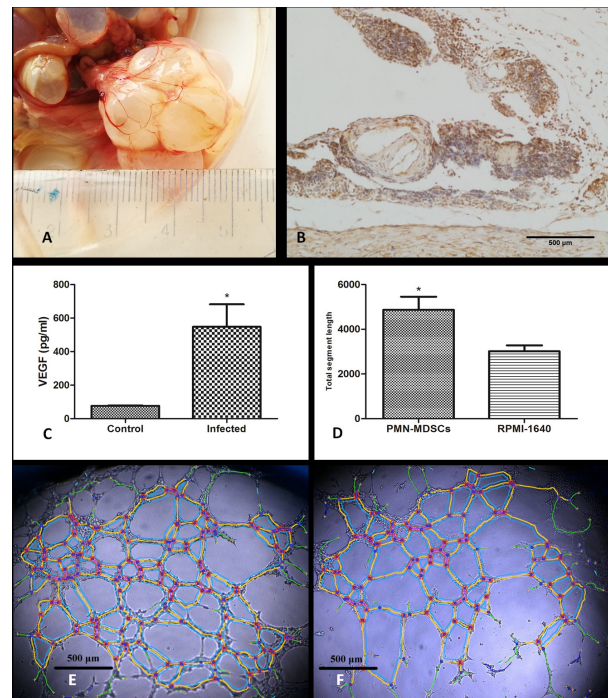
Figure 1. Angiogenesis casused by *E. granulosus*. (A) New blood vessels wrapped around the hydatid cysts isolated from mice infected with *Echinococcus granulosus*. (scale: cm) **(B)** CD31 was highly expressed in the tissues surrounding the hydatid cysts using immunohistochemical staining. **(C)** Higher level of VEGF in serum from mice infected with *E. granulosus* compared with controls (*n* = 7, each) detected by ELISA. **(D)** Total tube segment length induced by supernatant of PMN-MDSCs from infected mice was higher than that from controls. **(E)** HUVEC tube formation induced by the supernatant from PMN-MDSCs from infected mice. **(F)** HUVEC tube formation induced by RPMI-1640. **p* < 0.05.

role. In this study, around 2,000 live protoscoleces from sheep liver hydatid cysts were injected intraperitoneally into each BALB/c mouse (aged 4 weeks), and it was clear that new blood vessels were wrapped around the outside of cysts developed 8 months post infection through visual observation (Figure 1A). Meanwhile, CD31 was highly expressed in these tissues using immunohistochemistry (Figure 1B), suggesting that the host cells stimulated by this parasite have a tendency to differentiate into endothelial cells, thereby possessing the potential for the tube formation that is necessary for angiogenesis.

It has been reported that the supernatant from hydatid cysts isolated from mice infected with *E. granulosus* significantly induced HUVEC tube formation *in vitro* (*17*), suggesting that parasite-derived angiogenic factors are involved in the regulation of host angiogenesis. In the current study, a significantly higher level of VEGF was found in serum from mice infected with *E. granulosus* (548.100 ± 134.200 pg/mL) than in serum from control mice (76.950 ± 2.760 pg/mL; $t = 4.109$, $p = 0.001$) by Enzyme-linked immunosorbent assay according to the instructions of Mouse VEGF ELISA Kit (RayBiotech, USA) (Figure 1C). It is therefore likely that this increased level of VEGF could boost host angiogenesis.

3. PMN-MDSCs promotes angiogenesis

MDSCs are enriched in peripheral blood and spleen during infection with *E. granulosus*, especially in the period of chronic infection (*18*). We showed that M-MDSCs may have a proangiogenic role using the HUVEC tube formation assay and transcriptome analyses. In the present study, PMN-MDSCs were isolated from spleens of BALB/c mice infected with *E. granulosus* after 8 months post-infection and normal control mice (*n* = 7, each) using a mouse Myeloid-Derived Suppressor Cell Isolation Kit (Miltenyi Biotec, Germany) and flow cytometry (purity higher than 90%) (*18*), VEGF was detected by Mouse VEGF ELISA Kit (RayBiotech, USA) in the supernatant of PMN-MDSCs from mice infected with *E. granulosus* (5.444 ± 1.191 pg/mL) at a density of 10^6 cells/well in 24-well plates with Roswell Park Memorial Institute (RPMI)-1640 medium (Gibco, USA) containing 100 U/mL penicillin and 100 U/mL streptomycin incubating at 37°C in a 5% CO_2/95% air atmosphere for 24 h, but it couldn't be detected in the culture supernatant of PMN-MDSCs from control mice.

An *in vitro* tube formation assay was used to evaluate the effect of PMN-MDSCs on HUVECs differentiation on a Matrigel matrix (BD Biosciences, USA). In brief, 100 μL of HUVECs (3-5 passages) at a density of 3×10^5 cells/mL per well of 96-well plates were stimulated with 100 μL PMN-MDSC culture supernatant from infected mice, or RPMI-1640 medium with 100 U/mL penicillin and 100 U/mL streptomycin as a control. After 3 h of incubation at 37°C in 5% CO_2/95% air, the total segment length of tube-like structures in three random fields per well was quantified using the angiogenesis module of the NIH ImageJ software. As a result, HUVEC tube formation was much greater with the supernatant (4873 ± 586.1) than control group (3015 ± 269.3) ($t = 2.685$, $p = 0.025$) (Figure 1D-1F). Moreover, analysis of the transcriptional expression of VEGF (forward: 5′-GAGTACCCCGACGAGATAGA-3′, reverse: 5′-GGCTTTGGTGAGGTTTGAT-3′) and sFlt-1 (forward: 5′-GGGAAGACATCCTTCGGAAGA-3′, reverse: 5′-TCCGAGAGAAAATGGCCTTTT-3′) genes by quantitative real-time PCR showed that the expression of VEGF mRNA was higher in the PMN-MDSCs of *E. granulosus*-infected mice than in those of normal control mice ($t = 13.81$, $p < 0.001$) (Figure 2A), and that the expression of sFlt-1 mRNA ($t = 7.550$, $p = 0.026$) was downregulated (Figure 2B).

In conclusion, host angiogenesis in mice infected with *E. granulosus* appeared to be promoted by PMN-MDSCs, as shown by their high expression of VEGF, promotion of tube formation in the *in vitro* HUVEC assay, and significantly higher expression of VEGF mRNA and lower expression of sFlt-1 mRNA. Taken together, it suggests that MDSCs, including M-MDSCs and PMN-MDSCs, from mice infected with *E. granulosus* play a role in host angiogenesis. Furthermore,
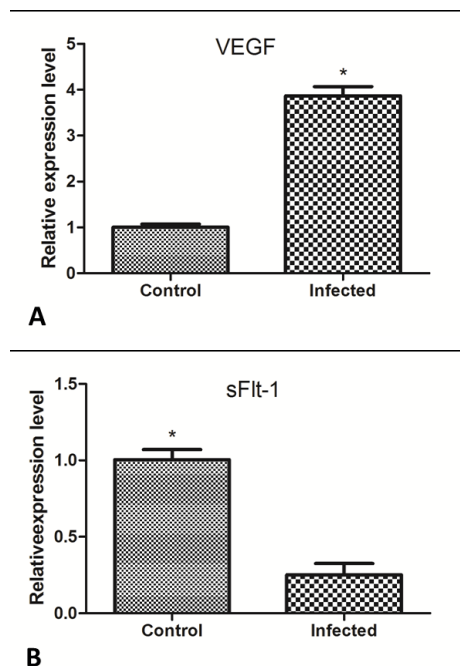
Figure 2. The relative mRNA expression levels of target genes. (A) VEGF mRNA was expressed more highly in PMN-MDSCs from mice infected with *E. granulosus* than in normal control mice. **(B)** sFlt-1 mRNA was expressed at a lower level in PMN-MDSCs from mice infected with *E. granulosus* than in controls. *p < 0.05.

other angiogenic factors in addition to VEGF derived from host cells (such as MDSCs) and pathogens (such as *E. granulosus*) in the microenvironment of local lesions should be clarified in future studies. This would provide ideas for the further study of host angiogenesis induced by *E. granulosus* infection.

Acknowledgements

References

1. Carmeliet P. Angiogenesis in life, disease and medicine. Nature. 2005; 438:932-936.
2. Semenza GL. Vasculogenesis, angiogenesis, and arteriogenesis: Mechanisms of blood vessel formation and remodeling. J Cell Biochem. 2007; 102:840-847.
3. Carmeliet P. Mechanisms of angiogenesis and arteriogenesis. Nat Med. 2000; 6:389-395.
4. Polverini PJ. Angiogenesis in health and disease: Insights into basic mechanisms and therapeutic opportunities. J Dent Educ. 2002; 66:962-975.
5. Carmeliet P. VEGF as a key mediator of angiogenesis in cancer. Oncology. 2005; 69 Suppl 3:4-10.
6. McColl BK, Stacker SA, Achen MG. Molecular regulation of the VEGF family -- inducers of angiogenesis

and lymphangiogenesis. APMIS. 2004; 112:463-480.
7. Melgar-Lesmes P, Tugues S, Ros J, Fernandez-Varo G, Morales-Ruiz M, Rodes J, Jimenez W. Vascular endothelial growth factor and angiopoietin-2 play a major role in the pathogenesis of vascular leakage in cirrhotic rats. Gut. 2009; 58:285-292.
8. Maynard SE, Min JY, Merchan J, Lim KH, Li J, Mondal S, Libermann TA, Morgan JP, Sellke FW, Stillman IE, Epstein FH, Sukhatme VP, Karumanchi SA. Excess placental soluble fms-like tyrosine kinase 1 (sFlt1) may contribute to endothelial dysfunction, hypertension, and proteinuria in preeclampsia. J Clin Invest. 2003; 111:649-658.
9. Kendall RL, Thomas KA. Inhibition of vascular endothelial cell growth factor activity by an endogenously encoded soluble receptor. Proc Natl Acad Sci U S A. 1993; 90:10705-10709.
10. Dennis RD, Schubert U, Bauer C. Angiogenesis and parasitic helminth-associated neovascularization. Parasitology. 2011; 138:426-439.
11. Guerret S, Vuitton DA, Liance M, Pater C, Carbillet JP. *Echinococcus multilocularis*: Relationship between susceptibility/resistance and liver fibrogenesis in experimental mice. Parasitol Res. 1998; 84:657-667.
12. Stadelmann B, Spiliotis M, Muller J, Scholl S, Muller N, Gottstein B, Hemphill A. *Echinococcus multilocularis* phosphoglucose isomerase (EmPGI): A glycolytic enzyme involved in metacestode growth and parasite-host cell interactions. Int J Parasitol. 2010; 40:1563-1574.
13. Van Ginderachter JA, Beschin A, De Baetselier P, Raes G. Myeloid-derived suppressor cells in parasitic infections. Euro J Immunol. 2010; 40:2976-2985.
14. Gabrilovich DI. Myeloid-derived suppressor cells. Cancer Immunol Res. 2017; 5:3-8.
15. Kumar V, Patel S, Tcyganov E, Gabrilovich DI. The nature of myeloid-derived suppressor cells in the tumor microenvironment. Trends Immunol. 2016; 37:208-220.
16. Binsfeld M, Muller J, Lamour V, De Veirman K, De Raeve H, Bellahcene A, Van Valckenborgh E, Baron F, Beguin Y, Caers J, Heusschen R. Granulocytic myeloid-derived suppressor cells promote angiogenesis in the context of multiple myeloma. Oncotarget. 2016; 7:37931-37943.
17. Yin JH, Shen YJ, Yu AP, Cao JP. *In vitro* pro-angiogenic activity of *Echinococcus granulosus* hydatid cysts from experimentally infected mice. Chin J Schisto Contrl. 2017; 29:320-323. (in Chinese)
18. Pan W, Zhou HJ, Shen YJ, Wang Y, Xu YX, Hu Y, Jiang YY, Yuan ZY, Ugwu CE, Cao JP. Surveillance on the status of immune cells after Echinnococcus granulosus protoscoleces infection in Balb/c mice. PloS One. 2013; 8:e59746.

BST
BioScience Trends

Guide for Authors

1. Scope of Articles

BioScience Trends is an international peer-reviewed journal. BioScience Trends devotes to publishing the latest and most exciting advances in scientific research. Articles cover fields of life science such as biochemistry, molecular biology, clinical research, public health, medical care system, and social science in order to encourage cooperation and exchange among scientists and clinical researchers.

2. Submission Types

Original Articles should be well-documented, novel, and significant to the field as a whole. An Original Article should be arranged into the following sections: Title page, Abstract, Introduction, Materials and Methods, Results, Discussion, Acknowledgments, and References. Original articles should not exceed 5,000 words in length (excluding references) and should be limited to a maximum of 50 references. Articles may contain a maximum of 10 figures and/or tables.

Brief Reports definitively documenting either experimental results or informative clinical observations will be considered for publication in this category. Brief Reports are not intended for publication of incomplete or preliminary findings. Brief Reports should not exceed 3,000 words in length (excluding references) and should be limited to a maximum of 4 figures and/or tables and 30 references. A Brief Report contains the same sections as an Original Article, but the Results and Discussion sections should be combined.

Reviews should present a full and up-to-date account of recent developments within an area of research. Normally, reviews should not exceed 8,000 words in length (excluding references) and should be limited to a maximum of 100 references. Mini reviews are also accepted.

Policy Forum articles discuss research and policy issues in areas related to life science such as public health, the medical care system, and social science and may address governmental issues at district, national, and international levels of discourse. Policy Forum articles should not exceed 2,000 words in length (excluding references).

Case Reports should be detailed reports of the symptoms, signs, diagnosis, treatment, and follow-up of an individual patient. Case reports may contain a demographic profile of the patient but usually describe an unusual or novel occurrence. Unreported or unusual side effects or adverse interactions involving medications will also be considered. Case Reports should not exceed 3,000 words in length (excluding references).

News articles should report the latest events in health sciences and medical research from around the world. News should not exceed 500 words in length.

Letters should present considered opinions in response to articles published in BioScience Trends in the last 6 months or issues of general interest. Letters should not exceed 800 words in length and may contain a maximum of 10 references.

3. Editorial Policies

Ethics: BioScience Trends requires that authors of reports of investigations in humans or animals indicate that those studies were formally approved by a relevant ethics committee or review board.

Conflict of Interest: All authors are required to disclose any actual or potential conflict of interest including financial interests or relationships with other people or organizations that might raise questions of bias in the work reported. If no conflict of interest exists for each author, please state "There is no conflict of interest to disclose".

Submission Declaration: When a manuscript is considered for submission to BioScience Trends, the authors should confirm that 1) no part of this manuscript is currently under consideration for publication elsewhere; 2) this manuscript does not contain the same information in whole or in part as manuscripts that have been published, accepted, or are under review elsewhere, except in the form of an abstract, a letter to the editor, or part of a published lecture or academic thesis; 3) authorization for publication has been obtained from the authors' employer or institution; and 4) all contributing authors have agreed to submit this manuscript.

Cover Letter: The manuscript must be accompanied by a cover letter signed by the corresponding author on behalf of all authors. The letter should indicate the basic findings of the work and their significance. The letter should also include a statement affirming that all authors concur with the submission and that the material submitted for publication has not been published previously or is not under consideration for publication elsewhere. The cover letter should be submitted in PDF format. For example of Cover Letter, please visit http://www.biosciencetrends.com/downcentre.php (Download Centre).

Copyright: A signed JOURNAL PUBLISHING AGREEMENT (JPA) form must be provided by post, fax, or as a scanned file before acceptance of the article. Only forms with a hand-written signature are accepted. This copyright will ensure the widest possible dissemination of information. A form facilitating transfer of copyright can be downloaded by clicking the appropriate link and can be returned to the e-mail address or fax number noted on the form (Please visit Download Centre). Please note that your manuscript will not proceed to the next step in publication until the JPA Form is received. In addition, if excerpts from other copyrighted works are included, the author(s) must obtain written permission from the copyright owners and credit the source(s) in the article.

Suggested Reviewers: A list of up to 3 reviewers who are qualified to assess the scientific merit of the study is welcomed. Reviewer information including names, affiliations, addresses, and e-mail should be provided at the same time the manuscript is submitted online. Please do not suggest reviewers with known conflicts of interest, including participants or anyone with a stake in the proposed research; anyone from the same institution; former students, advisors, or research collaborators (within the last three years); or close personal contacts. Please note that the Editor-in-Chief may accept one or more of the proposed reviewers or may request a review by other qualified persons.

Language Editing: Manuscripts prepared by authors whose native language is not English should have their work proofread by a native English speaker before submission. If not, this might delay the publication of your manuscript in BioScience Trends.

The Editing Support Organization can provide English proofreading, Japanese-English translation, and Chinese-English translation services to authors who want to publish in BioScience Trends and need assistance before submitting a manuscript. Authors can visit this organization directly at http://www.iacmhr.com/iac-eso/support.php?lang=en. IAC-ESO was established to facilitate manuscript preparation by researchers whose native language is not English and to help edit works intended for international academic journals.

4. Manuscript Preparation

Manuscripts should be written in clear, grammatically correct English and submitted as a Microsoft Word file in a single-column format. Manuscripts must be paginated and typed in 12-point Times New Roman font with 24-point line spacing. Please do not embed figures in the text. Abbreviations should be used as little as possible and should be explained at first mention unless the term is a well-known abbreviation (*e.g.* DNA). Single words should not be abbreviated.

Title Page: The title page must include 1) the title of the paper (Please note the title should be short, informative, and contain the major key words); 2) full name(s) and affiliation(s) of the author(s), 3) abbreviated names of the author(s), 4) full name, mailing address, telephone/fax numbers, and e-mail address of the corresponding author; and 5) conflicts of interest (if you have an actual or potential conflict of interest to disclose, it must be included as a footnote on the title page of the manuscript; if no conflict of

interest exists for each author, please state "There is no conflict of interest to disclose"). Please visit Download Centre and refer to the title page of the manuscript sample.

Abstract: The abstract should briefly state the purpose of the study, methods, main findings, and conclusions. For article types including Original Article, Brief Report, Review, Policy Forum, and Case Report, a one-paragraph abstract consisting of no more than 250 words must be included in the manuscript. For News and Letters, a brief summary of main content in 150 words or fewer should be included in the manuscript. Abbreviations must be kept to a minimum and non-standard abbreviations explained in brackets at first mention. References should be avoided in the abstract. Key words or phrases that do not occur in the title should be included in the Abstract page.

Introduction: The introduction should be a concise statement of the basis for the study and its scientific context.

Materials and Methods: The description should be brief but with sufficient detail to enable others to reproduce the experiments. Procedures that have been published previously should not be described in detail but appropriate references should simply be cited. Only new and significant modifications of previously published procedures require complete description. Names of products and manufacturers with their locations (city and state/country) should be given and sources of animals and cell lines should always be indicated. All clinical investigations must have been conducted in accordance with Declaration of Helsinki principles. All human and animal studies must have been approved by the appropriate institutional review board(s) and a specific declaration of approval must be made within this section.

Results: The description of the experimental results should be succinct but in sufficient detail to allow the experiments to be analyzed and interpreted by an independent reader. If necessary, subheadings may be used for an orderly presentation. All figures and tables must be referred to in the text.

Discussion: The data should be interpreted concisely without repeating material already presented in the Results section. Speculation is permissible, but it must be well-founded, and discussion of the wider implications of the findings is encouraged. Conclusions derived from the study should be included in this section.

Acknowledgments: All funding sources should be credited in the Acknowledgments section. In addition, people who contributed to the work but who do not meet the criteria for authors should be listed along with their contributions.

References: References should be numbered in the order in which they appear in the text. Citing of unpublished results, personal communications, conference abstracts, and theses in the reference list is not recommended but these sources may be mentioned in the text. In the reference list, cite the names of all authors when there are fifteen or fewer authors; if there are sixteen or more authors, list the first three followed by *et al.* Names of journals should be abbreviated in the style used in PubMed. Authors are responsible for the accuracy of the references. Examples are given below:

Example 1 (Sample journal reference):
Inagaki Y, Tang W, Zhang L, Du GH, Xu WF, Kokudo N. Novel aminopeptidase N (APN/CD13) inhibitor 24F can suppress invasion of hepatocellular carcinoma cells as well as angiogenesis. Biosci Trends. 2010; 4:56-60.

Example 2 (Sample journal reference with more than 15 authors):
Darby S, Hill D, Auvinen A, *et al.* Radon in homes and risk of lung cancer: Collaborative analysis of individual data from 13 European case-control studies. BMJ. 2005; 330:223.

Example 3 (Sample book reference):
Shalev AY. Post-traumatic stress disorder: diagnosis, history and life course. In: Post-traumatic Stress Disorder, Diagnosis, Management and Treatment (Nutt DJ, Davidson JR, Zohar J, eds.). Martin Dunitz, London, UK, 2000; pp. 1-15.

Example 4 (Sample web page reference):
Ministry of Health, Labour and Welfare of Japan. Dietary reference intakes for Japanese. *http://www.mhlw.go.jp/houdou/2004/11/h1122-2a.html* (accessed June 14, 2010).

Tables: All tables should be prepared in Microsoft Word or Excel and should be arranged at the end of the manuscript after the References section. Please note that tables should not in image format. All tables should have a concise title and should be numbered consecutively with Arabic numerals. If necessary, additional information should be given below the table.

Figure Legend: The figure legend should be typed on a separate page of the main manuscript and should include a short title and explanation. The legend should be concise but comprehensive and should be understood without referring to the text. Symbols used in figures must be explained.

Figure Preparation: All figures should be clear and cited in numerical order in the text. Figures must fit a one- or two-column format on the journal page: 8.3 cm (3.3 in.) wide for a single column, 17.3 cm (6.8 in.) wide for a double column; maximum height: 24.0 cm (9.5 in.). Please make sure that the symbols and numbers appeared in the figures should be clear. Please make sure that artwork files are in an acceptable format (TIFF or JPEG) at minimum resolution (600 dpi for illustrations, graphs, and annotated artwork, and 300 dpi for micrographs and photographs). Please provide all figures as separate files. Please note that low-resolution images are one of the leading causes of article resubmission and schedule delays. All color figures will be reproduced in full color in the online edition of the journal at no cost to authors.

Units and Symbols: Units and symbols conforming to the International System of Units (SI) should be used for physicochemical quantities. Solidus notation (*e.g.* mg/kg, mg/mL, mol/mm^2/min) should be used. Please refer to the SI Guide www.bipm.org/en/si/ for standard units.

Supplemental data: Supplemental data might be useful for supporting and enhancing your scientific research and BioScience Trends accepts the submission of these materials which will be only published online alongside the electronic version of your article. Supplemental files (figures, tables, and other text materials) should be prepared according to the above guidelines, numbered in Arabic numerals (*e.g.*, Figure S1, Figure S2, and Table S1, Table S2) and referred to in the text. All figures and tables should have titles and legends. All figure legends, tables and supplemental text materials should be placed at the end of the paper. Please note all of these supplemental data should be provided at the time of initial submission and note that the editors reserve the right to limit the size and length of Supplemental Data.

5. Submission Checklist

The Submission Checklist will be useful during the final checking of a manuscript prior to sending it to BioScience Trends for review. Please visit Download Centre and download the Submission Checklist file.

6. Online Submission

Manuscripts should be submitted to BioScience Trends online at http://www.biosciencetrends.com. The manuscript file should be smaller than 5 MB in size. If for any reason you are unable to submit a file online, please contact the Editorial Office by e-mail at office@biosciencetrends.com.

7. Accepted Manuscripts

Proofs: Galley proofs in PDF format will be sent to the corresponding author via e-mail. Corrections must be returned to the editor (proof-editing@biosciencetrends.com) within 3 working days.

Offprints: Authors will be provided with electronic offprints of their article. Paper offprints can be ordered at prices quoted on the order form that accompanies the proofs.

Page Charge: Page charges will be levied on all manuscripts accepted for publication in BioScience Trends ($140 per page for black white pages; $340 per page for color pages). Under exceptional circumstances, the author(s) may apply to the editorial office for a waiver of the publication charges at the time of submission.

(*Revised February 2013*)

JOURNAL PUBLISHING AGREEMENT (JPA)

Manuscript No.:

Title:

Corresponding Author:

The International Advancement Center for Medicine & Health Research Co., Ltd. (IACMHR Co., Ltd.) is pleased to accept the above article for publication in BioScience Trends. The International Research and Cooperation Association for Bio & Socio-Sciences Advancement (IRCA-BSSA) reserves all rights to the published article. Your written acceptance of this JOURNAL PUBLISHING AGREEMENT is required before the article can be published. Please read this form carefully and sign it if you agree to its terms. The signed JOURNAL PUBLISHING AGREEMENT should be sent to the BioScience Trends office (Pearl City Koishikawa 603, 2-4-5 Kasuga, Bunkyo-ku, Tokyo 112-0003, Japan; E-mail: **office@biosciencetrends.com**; Tel: **+81-3-5840-8764**; Fax: **+81-3-5840-8765**).

1. Authorship Criteria

As the corresponding author, I certify on behalf of all of the authors that:

1) The article is an original work and does not involve fraud, fabrication, or plagiarism.

2) The article has not been published previously and is not currently under consideration for publication elsewhere. If accepted by BioScience Trends, the article will not be submitted for publication to any other journal.

3) The article contains no libelous or other unlawful statements and does not contain any materials that infringes upon individual privacy or proprietary rights or any statutory copyright.

4) I have obtained written permission from copyright owners for any excerpts from copyrighted works that are included and have credited the sources in my article.

5) All authors have made significant contributions to the study including the conception and design of this work, the analysis of the data, and the writing of the manuscript.

6) All authors have reviewed this manuscript and take responsibility for its content and approve its publication.

7) I have informed all of the authors of the terms of this publishing agreement and I am signing on their behalf as their agent.

2. Copyright Transfer Agreement

I hereby assign and transfer to IACMHR Co., Ltd. all exclusive rights of copyright ownership to the above work in the journal BioScience Trends, including but not limited to the right 1) to publish, republish, derivate, distribute, transmit, sell, and otherwise use the work and other related material worldwide, in whole or in part, in all languages, in electronic, printed, or any other forms of media now known or hereafter developed and the right 2) to authorize or license third parties to do any of the above.

I understand that these exclusive rights will become the property of IACMHR Co., Ltd., from the date the article is accepted for publication in the journal BioScience Trends. I also understand that IACMHR Co., Ltd. as a copyright owner has sole authority to license and permit reproductions of the article.

I understand that except for copyright, other proprietary rights related to the Work (*e.g.* patent or other rights to any process or procedure) shall be retained by the authors. To reproduce any text, figures, tables, or illustrations from this Work in future works of their own, the authors must obtain written permission from IACMHR Co., Ltd.; such permission cannot be unreasonably withheld by IACMHR Co., Ltd.

3. Conflict of Interest Disclosure

I confirm that all funding sources supporting the work and all institutions or people who contributed to the work but who do not meet the criteria for authors are acknowledged. I also confirm that all commercial affiliations, stock ownership, equity interests, or patent-licensing arrangements that could be considered to pose a financial conflict of interest in connection with the article have been disclosed.

Corresponding Author's Name (Signature):

Date:

BioScience Trends (www.biosciencetrends.com)

Pearl City Koishikawa 603, 2-4-5 Kasuga, Bunkyo-ku, Tokyo 112-0003, Japan; E-mail: office@biosciencetrends; Tel: +81-3-5840-8764; Fax: +81-3-5840-8765